

# **Deformations in Concrete Cantilever Bridges: Observations and Theoretical Modelling**

Peter F. Takács

Doctoral Thesis

Department of Structural Engineering  
The Norwegian University of Science and Technology  
Trondheim, Norway

March 2002



## **Abstract**

The thesis deals with the deformation problem of segmental, cast-in-place concrete cantilever bridges. This type of bridge has shown some propensity to develop larger deflections than those were predicted in the design calculation. Excessive deflections may lead to deterioration of aesthetics, serviceability problems and eventually early reconstruction of the bridge. Also in the construction stages the deflections have to be properly compensated to achieve the smooth camber in the completed bridge deck.

Deformation prediction in concrete cantilever bridges is not as reliable as it would be necessary due to several factors. The high degree of uncertainty in creep and shrinkage prediction in concrete constitutes the major difficulty. Other factors are the complex segmental construction procedure and the sensitivity of the deformations to variations in the construction schedule, the uncertainty in estimating the frictional loss of prestress and relaxation in the prestressing tendons and uncertainty in estimating model parameters such as temperature and relative humidity.

The doctoral study was initiated with the objective to improve deformation prediction in segmentally cast concrete cantilever bridges and to establish guidelines for deformation analysis based on advanced numerical methods.

A database on observed deformations in three modern long span concrete cantilever bridges in Norway has been established. Two of the bridges were partly constructed from lightweight aggregate concrete. The deformations have been monitored since the construction stages up to the present time. The measurements cover the construction stages and the service life of 14, 8 and 3 years, respectively for the three bridges. The measured deformations are deflections in the superstructure and in one of the bridges, also strain measurements in the piers and the superstructure.

A sophisticated numerical model was created for deformation analysis. The numerical model realistically simulates the segmental construction procedure and the entire life span of the bridge. The effects of the segmental construction method, temporarily supports and constraints and changes in the structure system during construction are taken into account. The model considers the different concrete age from segment to segment, the sequential application of permanent loads and prestressing and the effect of temporary loads. The prestressing tendons are individually modelled with their true profile taking into account the variation of the effective prestressing force along the length of the tendon and with time.

The finite element model consists of beam elements which are based on an advanced beam element formulation. The beam model was verified against a robust two-and-a-half dimensional shell model concerning its general performance and some specific issues. The comparison confirmed the accuracy of the beam model.

Existing experimental data on creep and shrinkage in lightweight aggregate concrete and high strength concrete were evaluated in comparison with theoretical models. The main focus was on the CEB-FIP Model Code 1990 and its subsequent extensions. The findings were considered in the numerical studies.

Deformations of the three bridges were computed. The CEB-FIP Model Code 1990 material model was used for concrete for the most part. The elastic moduli were taken from test results where they were available. The creep coefficient and the shrinkage strain of the lightweight aggregate concrete were assumed equal to those of normal density concrete of the same strength. The agreement between the calculated and the measured deformations were satisfactory in view of the large uncertainty involved in theoretical prediction. While moderate differences were observed in most cases, no clear overall tendency toward under- or overestimation was found. In subsequent numerical studies, the sensitivity of the deformations to variations in various model parameters was investigated. The B3 model was compared to the CEB-FIP Model Code 1990 in the analysis of one of the bridges, where the latter model showed somewhat better agreement with the measurements.

The last part of the work concerned a robust probabilistic analysis which was based on a Monte Carlo simulation. The objective of the probabilistic analysis was to estimate the statistical properties of the deformation responses. With the distribution function of a given deformation response being known, the confidence limit for the deformation can be determined. It is recommended to design the bridge for the long-time deflection which represents a certain confidence limit (*e.g.* the 95 % confidence limit) of the response rather than its mean. Such way the risk that the bridge will suffer intolerable deflection over its life span can be minimised.

## Acknowledgement

The work which constitutes this doctoral thesis was carried out at the Department of Structural Engineering, the Norwegian University of Science and Technology (NTNU) between 1998 and 2002.

The study was implemented within the framework of the CMC (Computational Mechanics in Civil Engineering) SIP-Programme which is a five year long research programme at SINTEF and NTNU, financed by the Norwegian Research Council (NFR). The programme provided the financial support for this doctoral study which I highly appreciate.

I want to express my sincere gratitude to my supervisor, Professor Terje Kanstad for his professional support and encouragement and for providing me a pleasant working environment. I am very grateful for the opportunity for doing my research work at the department.

I am also very grateful to Professor Kalle Høiseith for the opportunity for participating in the CMC Programme.

I want to acknowledge the help of the Norwegian Public Road Administration offices for providing the measurements on the bridges. I would like to specially thank Svein Rosseland for his effort to conduct the measurements on Stolma Bridge.

I am grateful to all my colleagues in the concrete group at the Department of Structural Engineering for the pleasant and friendly environment which I had the privilege to be part of.

Finally I would like to thank my parents who have always been very supportive and caring. Knowing that I always have a place to go home is important for my peace of mind.



# Contents

Abstract.....	i
Acknowledgement .....	iii
Contents.....	v
Chapter 1 Introduction.....	1
1.1 Background .....	1
1.2 Objective and scope of the study.....	3
1.3 Organisation of the thesis.....	3
Chapter 2 Deformation Problem in Concrete Cantilever Bridges .....	5
2.1 Introduction .....	5
2.2 Long span concrete cantilever bridges .....	6
2.3 Description of the studied bridges.....	8
2.3.1 Norddalsfjord Bridge.....	8
2.3.2 Støvset Bridge .....	9
2.3.3 Stolma Bridge.....	11
2.4 The deformation problem .....	12
2.5 A review on research works on the deformation problem .....	16
Chapter 3 Material Models for Time-dependent Analysis .....	17
3.1 Introduction .....	17
3.2 Creep and shrinkage models .....	18
3.2.1 Modulus of elasticity.....	19
3.2.2 CEB-FIP Model Code 1990 .....	21
3.2.3 The 1999 update of the CEB-FIP Model Code 1990.....	30
3.2.4 Norwegian Standard (NS 3473).....	34
3.2.5 B3 model .....	34
3.2.6 Uncertainty in creep and shrinkage prediction.....	35
3.2.7 Creep and shrinkage models in comparison.....	36
3.3 Material model for reinforcing and prestressing steel.....	41
Chapter 4 Lightweight Aggregate Concrete .....	45
4.1 Introduction .....	45
4.2 Prediction models for creep and shrinkage in LWAC.....	47
4.2.1 Modulus of elasticity.....	47
4.2.2 Creep .....	47
4.2.3 Shrinkage.....	48

4.3	Experimental results in comparison with theoretical models.....	48
4.3.1	Modulus of elasticity .....	49
4.3.2	Creep.....	50
4.3.3	Shrinkage .....	55
4.4	Conclusions .....	56
<b>Chapter 5</b>	<b>Experimental Results on High Strength Concrete .....</b>	<b>57</b>
5.1	Introduction.....	57
5.2	Experimental results from SINTEF.....	59
5.2.1	Description of the experiments .....	59
5.2.2	Elastic modulus .....	61
5.2.3	Creep.....	62
5.2.4	Shrinkage .....	64
5.3	Experimental results from <i>Persson</i> .....	64
5.3.1	Description of the experiments .....	65
5.3.2	Experimental creep data in comparison with theoretical models .....	66
5.4	Conclusions .....	71
<b>Chapter 6</b>	<b>Mathematical Modelling of Viscoelasticity .....</b>	<b>73</b>
6.1	Introduction.....	73
6.2	Viscoelastic models.....	74
6.2.1	Basic viscoelastic models.....	75
6.2.2	Maxwell and Kelvin Chain models .....	78
6.3	Rate-type constitutive relations .....	80
6.3.1	Formulation with the relaxation function.....	80
6.3.2	Formulation with the creep function.....	81
6.4	Determination of the chain parameters .....	82
6.4.1	Curve fitting.....	83
6.4.2	Ageing chain.....	83
<b>Chapter 7</b>	<b>Numerical Model and Simulation.....</b>	<b>85</b>
7.1	Introduction.....	85
7.2	Geometrical model.....	86
7.2.1	Two dimensional beam model.....	86
7.2.2	Reinforcement and prestressing tendons.....	89
7.2.3	Verification of the <i>Mindlin</i> beam model and shear deformation.....	89
7.2.4	Effect of non-uniform creep and shrinkage over the cross-section .....	92
7.3	Modelling the effective prestressing force.....	98
7.3.1	Friction and anchor slip.....	99
7.3.2	Relaxation.....	103
7.3.3	Shortening of the concrete member .....	104
7.4	Modelling the segmental construction.....	104
<b>Chapter 8</b>	<b>Long-term Monitoring of Deformations .....</b>	<b>109</b>
8.1	Introduction.....	109
8.2	Methods of monitoring .....	110
8.2.1	Deformation control in the construction period .....	110



8.2.2	Long-term monitoring of the deflection by levelling.....	110
8.2.3	Strain measurements.....	111
8.3	Long-term deformations in the investigated bridges .....	111
8.3.1	Norrdalsfjord Bridge.....	112
8.3.2	Støvset Bridge .....	115
8.3.3	Stolma Bridge.....	117
Chapter 9	Numerical Studies .....	119
9.1	Introduction .....	119
9.2	Norrdalsfjord Bridge.....	120
9.3	Støvset Bridge .....	126
9.4	Stolma Bridge.....	128
9.5	Sensitivity of the deflections to variations in material models.....	131
9.6	Estimation error for the relative humidity and the temperature .....	132
9.7	Uncertainty in the long-term characteristics of LWAC .....	134
9.8	Calculated deflection, MC90 versus B3 model .....	136
9.9	Concluding remarks.....	138
Chapter 10	Probabilistic Deformation Modelling.....	141
10.1	Introduction.....	141
10.2	Statistical properties and definitions .....	142
10.2.1	Arithmetic mean .....	142
10.2.2	Standard deviation, variance and coefficient of variation.....	142
10.2.3	Standard error of the mean and the standard deviation .....	143
10.2.4	Confidence limit .....	144
10.2.5	Pearson Product Moment Correlation.....	145
10.3	Design criteria concerning deformations in concrete bridges .....	146
10.4	Monte Carlo simulation for probabilistic deformation analysis .....	147
10.4.1	Introduction.....	147
10.4.2	System parameters and their statistical properties .....	148
10.4.3	Latin hypercube sampling.....	152
10.4.4	Estimating the mean and the variance.....	155
10.4.5	Estimating the confidence limits.....	158
10.5	Simplified method.....	163
10.6	Conclusions .....	164
Chapter 11	Conclusions .....	167
11.1	Summary and conclusions .....	167
11.2	Suggestions for further research.....	170
References	.....	173
Appendix A	.....	179
Appendix B	.....	181
Appendix C	.....	187



# Chapter 1

## Introduction

### 1.1 Background

Concrete cantilever bridges built with the balanced cantilever method have become very popular due to the many advantages offered by the construction method and the structural form. Nowadays segmental, cast-in-place concrete cantilever bridges are routinely built in the 200 to 300 meter span range while the longest span of this type is 301 meter.

Segmentally cast concrete cantilever bridges often exhibit larger deflections than it was predicted in the design calculation. The excessive deflection can lead to the deterioration of the aesthetic of the bridge and may reach the level where serviceability and traffic safety are compromised. The many cases where long-term deflections significantly exceeded the expected deflections have made design engineers and researches aware of the deformation problem in this type of structure.

Deflections of the superstructure are large due to the slender and long free concrete span and the fact that the permanent loads are only partially compensated by the prestressing. The deformations are increasing with time over the entire life span of the bridge, although in a decreasing rate. The physical mechanisms which are responsible for the time dependent deformation increase in concrete are creep and shrinkage, where the former is stress dependent and the latter is stress independent. The creep and shrinkage characteristics are probably the most uncertain mechanical properties of the concrete. Despite the development of scientific knowledge on concrete creep and shrinkage which made enormous progress (*e.g.* Bazant 2001) from the seventies, the prediction models can be considered as not as reliable as it would be necessary (*fib* 2000a).

The uncertainty in creep and shrinkage prediction is even more pronounced with the introduction of high strength concrete and lightweight aggregate concrete. The notable increase in the potential span length of concrete cantilever bridges is largely attributable to the progress made in the research and application of these materials. On the other hand, little information exists on their long-term deformation characteristic and the theoretical models in their present state are controversial, particularly for lightweight aggregate concrete (Walraven 2000).

Beyond the uncertainty raised by creep and shrinkage in the deformation prediction, several other factors contribute to the problem. Relaxation in the prestressing steel is also a time dependent mechanism which causes slight reduction in the effective prestressing force. Besides relaxation, the loss of prestress due to friction is particularly significant in segmental construction as the result of additional unintended change in the tendon profile at the segment boundaries (Collins and Mitchell 1991). The latter emphasises the importance of the quality of workmanship.

The construction process is complex where deviation from the planned schedule may have significant influence on the structural responses. In the design phase it is hardly possible to foresee precisely the construction schedule and temporary effects on the bridge, let alone the changes made during the construction process.

The development of sophisticated numerical models and advanced computational methods and the enormous increase in the computational power of personal computers have enabled to address the most complex engineering problems effectively. Nevertheless, numerical models are time consuming and reasonable simplifications need to be made. To recognise which parameters and features are important and which are those that can be neglected are not instantly evident.

The recognition of the importance of the deformation problem in segmentally cast concrete cantilever bridges has generated interest for research on the subject since the nineties, *e.g.* (Kanstad 1993), (Favre *et al.* 1995), (Vitek 1997), (Vitek and Kristek 1999) and (Santos *et al.* 2001).

While it was often found that the observed deformations in the bridges are larger than they were predicted by the design calculation, no clear conclusions were reached about the reasons, beyond a series of assumptions and speculations. In fact, in most cases it is very difficult to pinpoint the exact reason due to the many uncertain factors which influence the deformation of the structure. Creep and shrinkage prediction models alone are marked with a considerably large statistical variation which is the inherent property of the existing prediction models. Acknowledging the inevitable statistical variation, one has to accept the fact that expected deflections will be exceeded in a number of cases. The statistical variation

therefore has to taken into consideration (Bazant and Baweja 1995) in order to minimise the risk of intolerable deformations.

## 1.2 Objective and scope of the study

The general objective of the study is to contribute to the improvement in deformation prediction in segmentally cast concrete cantilever bridges. My goal is to establish guidelines for the deformation analysis in this kind of structure and to recommend a methodology for numerical analysis.

The particular objectives are

- To evaluate existing creep and shrinkage models based on available experimental results on lightweight aggregate concrete and high strength concrete and if it is possible to utilise the findings in the models
- To set up a reliable numerical model for deformation analyses of concrete cantilever bridges taking advantage of existing advanced numerical techniques while keeping the model suitable for large-scale practical applications. To examine the effect of some of the simplifications which need to be made in the model
- To establish a database on observed deformations in modern long-span concrete cantilever bridges
- To evaluate the observed and calculated deformations
- To study the effect of the statistical uncertainty in creep and shrinkage prediction models on the deformations of the bridges. To investigate the effect of the variation in various model parameters. To study the influence of the model choice.

## 1.3 Organisation of the thesis

The doctoral thesis is organised in eleven chapters.

Following the introductory chapter, in Chapter 2 the deformation problem of segmentally cast concrete bridges is defined. The chapter also provides a brief review on the longest span concrete cantilever bridges in the world. The three bridges, Norddalsfjord Bridge, Støvset Bridge and Stolma Bridge which are involved in the study are described. A short review on similar research works is given.

Chapter 3 presents a review on material models for concrete, reinforcing steel and prestressing steel that are used for long-term deformation analysis. Different creep and shrinkage prediction models are reviewed with a main emphasis on the CEB-FIP Model Code 1990 which serves as the basic material model in this study.

In Chapter 4 experimental results on creep and shrinkage in lightweight aggregate concrete are discussed and evaluated in comparison with existing model formulations. The current approach to creep and shrinkage modelling is reviewed. The databank on experimental results consists of data from experimental programs which were carried out in the past 15 years in Norway.

Experimental results on creep and shrinkage in high strength concrete and high performance concrete are discussed and evaluated in Chapter 5. The experimental results which are utilised were carried out in 1987-90 in Norway and in 1991-96 in Sweden.

The mathematical algorithm for modelling aging viscoelastic behaviour in numerical analysis is described in Chapter 6. The rate type formulation is based on the Kelvin and Maxwell chain models.

Chapter 7 covers a series of issues concerning the numerical model and simulation used for the deformation analysis of segmental, cast-in-place concrete cantilever bridges. The geometrical model with the element formulation is described. The geometrical model for the conventional reinforcement and the prestressing tendons is presented together with the model for computing the effective prestressing force. The beam model is verified against a two-and-a-half dimensional shell model with the main focus being on the influence of shear deformation and the effect of non-uniform creep and shrinkage characteristics along the height of the box-girder. Finally the numerical simulation of the segmental construction process is described.

In Chapter 8 the established database on the measured deformations in Norddalsfjord Bridge, Støvset Bridge and Stolma Bridge is introduced. The database contains deflection and strain measurements in Norddalsfjord Bridge and deflection measurements in Støvset Bridge and Stolma Bridge. The measurements cover the construction periods and the service life of the completed bridges up till 2001.

In Chapter 9 various numerical studies on the investigated bridges are presented. The calculated deformations are evaluated in comparison with the observed deformations. The effect of the statistical uncertainty in creep and shrinkage prediction models are investigated in sensitivity studies. The effect of variation in various model parameters is also studied.

Chapter 10 presents a robust probabilistic method for deformation modelling. The probabilistic model is based on a Monte Carlo simulation. The statistical variation of the structural responses of Støvset Bridge are estimated.

Finally, in Chapter 11 the main conclusions of the study are presented along with recommendations for future work.

## Chapter 2

# Deformation Problem in Concrete Cantilever Bridges

*The chapter introduces the deformation problem of the segmentally cast concrete cantilever bridge which the doctoral study is aiming to investigate. Also description of the three bridges which are involved in the study is presented, followed by a short review on similar investigations by other researchers.*

### 2.1 Introduction

The segmentally cast concrete cantilever bridge has gained its popularity due to its elegant and slender appearance, clear and efficient structural form and cost-efficient construction method. Free and slender concrete spans, however, are subjected to large deformations which are also time-dependent. Prediction of the deformations with the required accuracy is essential for the successful erection of the superstructure as well as for the uncompromised state of the bridge through its entire life span.

Deformation prediction in concrete is marked with significant uncertainty, mainly due to the time-dependent deformation mechanisms known as creep and shrinkage. Even though the structural form of the cantilever bridge is simple and the structural system is transparent, the aforementioned material behaviour coupled with the staged construction process and complex loading history present a challenging task to the engineer. In the never-flagging endeavour of bridge engineering to build record breaking spans, the reliance on previous experiences with shorter spans can not remain unquestioned. With the introduction of high strength concrete and high strength lightweight aggregate concrete and with the increased geometrical dimensions, the “extrapolation of previous experiences” has to be taken with caution.

## 2.2 Long span concrete cantilever bridges

The segmental, cast-in-place concrete cantilever bridge has proven to be an ideal solution to bridge the numerous straits and fjords along the Norwegian coast. This type of bridge has been well established in the span length range of 200-300 meter where it presents a cost-effective alternative to the cable-stayed bridge and the suspension bridge. For the time being, the longest span of this type is the 301 meter long main span of Stolma Bridge.

The notable increase in the length of free concrete spans can be attributed to the advancement in concrete research, construction technology and the development of sophisticated design tools.

High strength concrete and high strength lightweight aggregate concrete are the cornerstones in the realisation of long free concrete spans. The dominant portion of the total load in this type of bridge is the dead weight of the structural concrete itself. With the increased strength to weight ratio the amount of prestressing and necessary counterweight ballast can be reduced considerably. In inverse, the span length can be increased with the same amount of prestressing and counterweight.

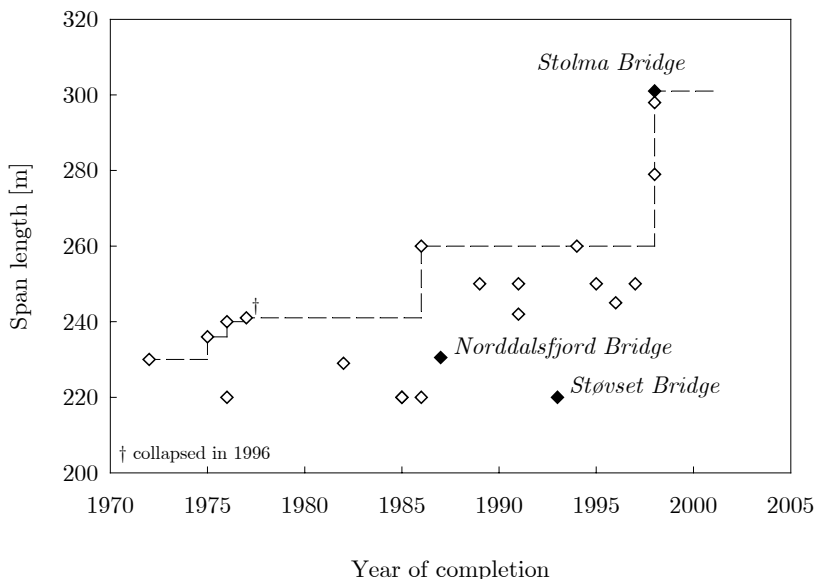


Figure 2.1 The longest span concrete cantilever bridges in the world (e.g. Brueckenweb databank)





Figure 2.2 Stolma Bridge, world record in free cantilevering

Figure 2.1 shows the longest free concrete spans and the year of completion for spans of 220 m and longer (also *vide* Table 2.1). The dashed line marks the progress in the world record for this type of bridge. The three bridges marked in the figure are involved in the present study. It is noteworthy that three of the five longest spans were built in Norway.

Table 2.1 Concrete cantilever bridges with the longest spans (*e.g.* *Brueckenweb* databank)

	Name	Country	Year of completion	Length of main span [m]
<b>1</b>	<b>Stolma Bridge</b>	<b>Norway</b>	<b>1998</b>	<b>301</b>
2	Raftsundet Bridge	Norway	1998	298
3	Boca Tigris 2	China	1998	279
4	Gateway Bridge	Australia	1986	260
5	Varodd Bridge	Norway	1994	260
6	Talübvergang Schottwien	Austria	1989	250
7	Ponte de São João	Portugal	1991	250
8	Skye Bridge	UK	1995	250
9	Confederation Bridge	Canada	1997	250
10	Huangshi Bridge	China	1996	245
11	Pont de Cheviré	France	1991	242
12	Koror-Babeldaob Bridget†	Palau	1977	241
13	Hamana Bridge	Japan	1976	240
14	Hikoshima Bridge	Japan	1975	236
<b>15</b>	<b>Norddalsfjord Bridge</b>	<b>Norway</b>	<b>1987</b>	<b>230.5</b>
...				
<b>22</b>	<b>Støvset Bridge</b>	<b>Norway</b>	<b>1993</b>	<b>220</b>

† collapsed in 1996

## 2.3 Description of the studied bridges

The three segmental, cast-in-place, prestressed concrete cantilever bridges involved in the study are *Norrdalsfjord Bridge* in Sogn and Fjordane county, *Støvset Bridge* in Nordland county and *Stolma Bridge* in Hordaland county.

All three bridges are consisting of three spans. The main spans are made continuous after the coupling and prestressed by continuity tendons. The main spans were constructed in free cantilevering while the side spans were constructed either in free cantilevering or on scaffolding. When *Norrdalsfjord Bridge* was completed in May 1987, its 230.5 meter long central span was the longest free concrete span in Europe. *Stolma Bridge* is the current world record holder among concrete cantilever bridges with its 301 meter long main span.

The concrete grade in the descriptions is given for the cube strength as required by the Norwegian Standard. The conversion between the characteristic cylinder and cube strength can be made according to the recommendation of the CEB-FIP Model Code 1990 as shown in Table 2.2. The grade in the table is given according to the cylinder strength.

Table 2.2 Characteristic strength values [MPa]

Concrete grade	C20	C30	C40	C50	C60	C70	C80
$f_{ck, cylinder}^1$	20	30	40	50	60	70	80
$f_{ck, cube}^2$	25	37	50	60	70	80	90

<sup>1</sup> cylinder 150/300

<sup>2</sup> cube 150/150/150

For lightweight aggregate concrete the grade refers to the cube strength too but the Norwegian Standard requires to specify the characteristic cylinder strength in addition.

### 2.3.1 Norrdalsfjord Bridge

*Norrdalsfjord Bridge* is situated on the western coast of Norway, northward from the city of Bergen. It was completed in 1987. The bridge has a total length of 397 meter and consists of three spans, 98 meter, 230.5 meter and 68.5 meter. The height of the box-girder varies from 3.0 m to 13.0 m. The thickness of the bottom slab varies from 730 mm at the piers to 220 mm at mid-span. The web thickness in the main span is 350 mm, 300 mm and 250 mm changing approximately in the thirds of the cantilevers.

The main span consists of 47 segments. The main part of the A1-A2 side span was built in free cantilevering while the A3-A4 side span was built entirely on scaffolding. The counterweight structures are filled with rock and they are supported on moveable bearings

in A1 and A4. The superstructure is supported by twin wall piers built on monolithic foundations. The twin wall pier in A2 has adequate flexibility to cope with the horizontal deformations between the piers. In the construction stage, temporary walls were added between the twin walls in A2 in order to form a box section which had the sufficient torsional stiffness to withstand the dynamic wind load in the free cantilever state. Before the cantilevers were connected in the main span the superstructure was lowered by 200 mm in A1 in order to create a balanced load distribution in the twin pier walls in A2.

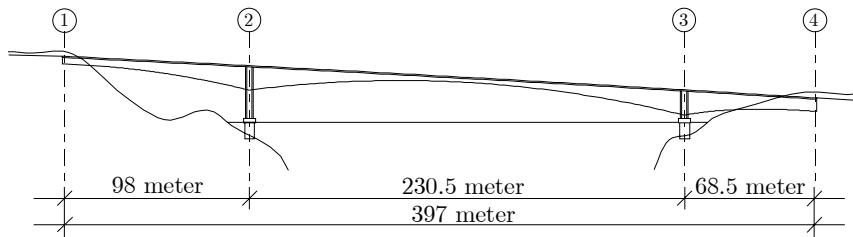


Figure 2.3 Norddalsfjord Bridge

The designed concrete strength was grade C45 for the superstructure and the piers and C35 for foundations.

### 2.3.2 Støvset Bridge

Støvset Bridge is situated on the northern coast of Norway, not far from the city of Bodø. It was completed in October 1993. The bridge has a total length of 420 meter and consists of three spans, 100 meter, 220 meter and 100 meter. The superstructure is a box-girder with variable height, 12.0 meter at the piers and 3.0 meter at mid-span and at the two ends of the side spans. The thickness of the bottom slab varies from 1000 mm at the piers to 250 mm at mid-span. The web thickness is 350 mm near the piers and 300 mm in-span.

The entire span was constructed in balanced free cantilevers. The central span consists of 45 segments while the two side spans consist of 20 segments each. 146 meter of the 220 meter long central span was made from lightweight aggregate concrete of grade LC55 and designed characteristic cylinder strength of 50 MPa. The rest part of the superstructure and the columns were made from normal weight concrete of grade C55. The concrete grade for the foundations was C45. The modulus of elasticity was measured in laboratory at the age of 28 days and it was found to be 28300 MPa for C55 and 22000 MPa for LC55. The density was 2420 kg/m<sup>3</sup> for C55 and 1940 kg/m<sup>3</sup> for LC55. The density of the lightweight aggregate concrete was also measured on drilled cores. The average initial density was determined as 1924 kg/m<sup>3</sup> while the oven-dry density was 1779 kg/m<sup>3</sup> (Heimdal 1997).

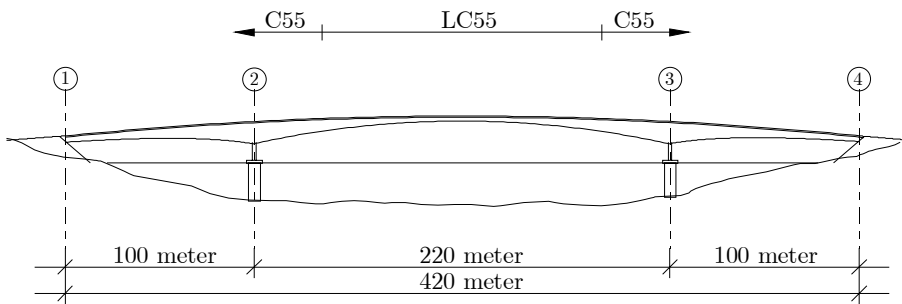


Figure 2.4 Støvset Bridge

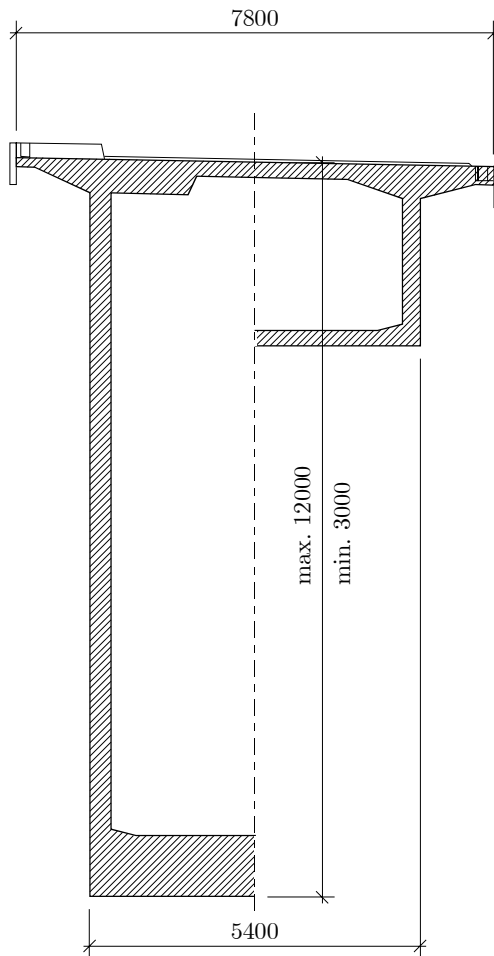


Figure 2.5 A typical arrangement of the box-girder, Støvset Bridge

The thickness of the pier is 1900 mm in A2 and 1500 mm in A3. To provide stability during construction temporary columns were placed at both sides of the piers at a distance of 3.3 m from the pier axes and supported on the pier foundations. In addition auxiliary piers were placed 30 m from the pier axes on the land side.

### 2.3.3 Stolma Bridge

Stolma Bridge is situated on the western coast of Norway, not far from the city of Bergen. The bridge was completed in 1998. The bridge has a total length of 467 meter and consists of three spans, 94 meter, 301 meter and 72 meter. The superstructure is a box-girder with variable height, 15.0 meter at the piers and 3.5 meter at mid-span. The thickness of the bottom slab varies from 1030 mm at the piers to 270 mm at mid-span. The web thickness varies in steps from 450 mm at the piers and 250 mm at mid-span.

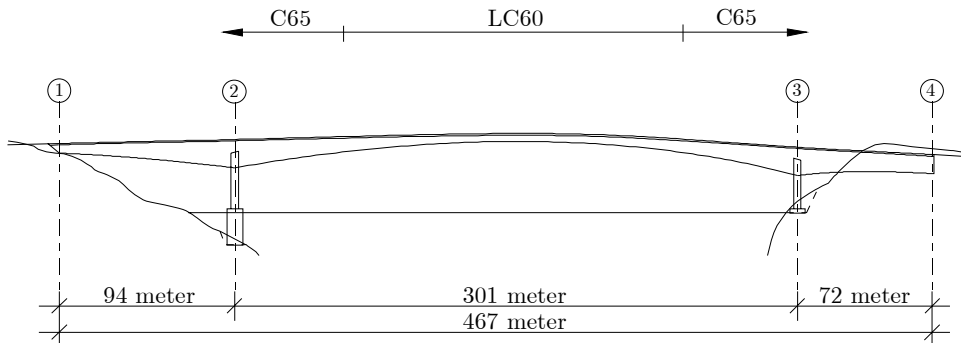


Figure 2.6 Stolma Bridge

The central span consists of 61 segments. The A1-A2 side was constructed partly in free cantilevering and partly in fixed formwork supported by temporary columns. The A3-A4 side span was constructed entirely in fixed formwork on abutments. 186 meter of the central span was made from high strength lightweight aggregate concrete of grade LC60. The rest part of the superstructure and the columns were made from normal density concrete of grade C65. The concrete grade for the foundations was C45. The modulus of elasticity was measured in laboratory at the age of 28 days; 22100 MPa for LC60 and 29500 MPa for C65. The designed density of the lightweight aggregate concrete was 1950 kg/m<sup>3</sup>. The density was determined as 1931 kg/m<sup>3</sup> after the removal of the formwork.

Figure 2.7 shows the arrangement of the box-girder cross-section in Stolma Bridge. All corners of the cross-section were rounded due to durability considerations. The bridge is located on the seashore in a very aggressive environment (Rosseland and Thorsen 2000).

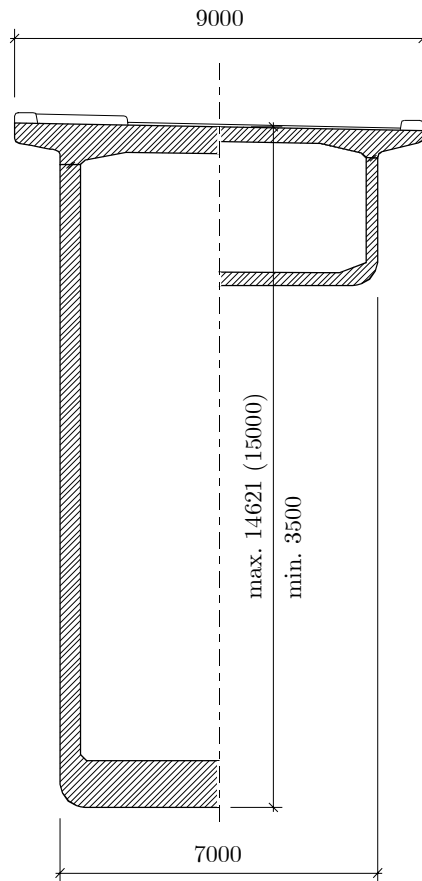


Figure 2.7 The box-girder of Stolma bridge

## 2.4 The deformation problem

Deformation prediction in segmentally cast concrete cantilever bridges is a serious concern. Deformations are significant and they are increasing virtually over the entire life span of the bridge. Inadequate consideration of deformations may compromise both the construction and the service life of bridges. The primary importance is to achieve the smooth camber in the bridge deck and to avoid sag at mid-span. The actual elevation of the deck remains of secondary importance as long as the deviation from the design elevation is relatively small and it does not compromise safety, functionality and aesthetic, in this order of importance (*vide* Figure 2.8). In this context, safety mainly concerns traffic safety, as excess deflection in this kind of structure normally does not influence the structural safety.

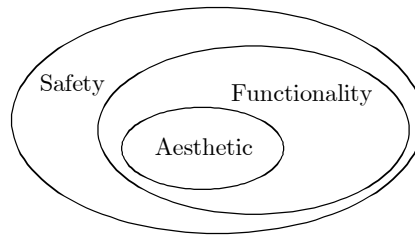


Figure 2.8 The trinity of bridge engineering

Excessive deflection in the completed bridge span may result in sag around the mid-span as it is illustrated in Figure 2.9. It may develop over a longer period of time as the result of underestimation of long-term deformations.



Figure 2.9 Excessive deflection in the completed bridge span

Large deviation from the expected deflection in the construction stage may jeopardise the smooth connection of the free cantilevers (*vide* Figure 2.10). A small difference in the elevation of the tip of the cantilevers is tolerable because measures are available which allow the elimination of small differences. The deviation can be corrected by adjustment with extra prestressing tendons, adjustment in the counterweight ballast or imposed deformations at the abutments by means of jacking. As an additional measure, the cantilevers in the same span are intentionally not erected simultaneously but with the difference of a number of segments (usually 4 to 8 segments). If the observed deflection in the firstly completed cantilever deviates from the expected value, the correction can be made by readjusting the prescribed over-height for the remaining segments in the other cantilever.

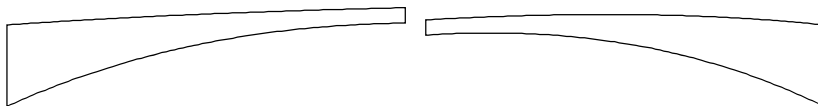


Figure 2.10 Vertical difference between the tip of the two cantilevers before the cantilevers are connected

Long-time deformation prediction in concrete cantilever bridges can be rather inaccurate as a result of several factors. Most importantly, creep and shrinkage modelling carry significant

uncertainty. The real governing mechanisms behind these phenomena are not yet fully understood. Significant scatter is observed in experimental data, at least from the standpoint of the current understanding and approach to modelling. Besides, experimental information on new materials such as high strength concrete and high strength lightweight aggregate concrete is insufficient.

Long-time prediction models for creep and shrinkage are developed and adjusted based on a wide range of experimental data with considerable heterogeneity in material properties and test conditions. Experiments are typically carried out on cylinders with diameter of 50-200 mm. The tests usually cover a time span of 1-12 months but in fact many of them are shorter than 3 months. Experimental results over longer period of time are scarce. The majority of the experimental data in existing databanks concerns normal concrete of strength not higher than 50 MPa. Thus, when the models which are developed on the basis of these experimental results are applied to modern long span concrete bridges, the prediction relies to a great extent on a series of extrapolations with regard to loading and drying time, material properties and geometrical dimensions (*vide* Figure 2.11).

Different long-time material models may exhibit large differences, thus the choice of the material model may considerably influence the prediction. It is still controversial whether concrete creep approaches a final asymptotic value. This discrepancy may result in considerable deviations between theoretical creep curves after a loading age of about 100-1000 days. Such differences well reflect the uncertainty of extrapolation and the conjectural nature of long-time prediction.

Significant progress has been made in the research on the creep and shrinkage properties of high strength concrete and lightweight aggregate concrete. The experimental evidence, however, is still very limited and existing information does not allow clear conclusions. In particular, the current formulations on the creep and shrinkage characteristics of LWAC can be seen as controversial (Walraven 2000).

The element size represents an other factor of uncertainty as dimensions of the bridge elements are significantly larger than those of the specimens in experiments. Little information exists on drying in large concrete members after long time. It is presumed that the drying process in bulk concrete may be slower than it is estimated based on tendencies observed in smaller specimens.

Experimental results on creep and shrinkage are marked with large scatter, at least from the perspective of existing approach in modelling. The creep compliance and the shrinkage strain given by the theoretical models are seen as the expected average value of the responses and the prediction is also characterised by the corresponding measure of variation. Consequently the structural response should be considered as a statistical variable rather than a deterministic value. The expected statistical variation has to be taken into



account in the structural design. The reported coefficient of variation is 20 % for the creep compliance and 35 % for the shrinkage strain for the CEB-FIP Model Code 1990 (CEB 1991). The same values are 23 % and 34 % for the B3 model (Bazant and Baweja 1995).

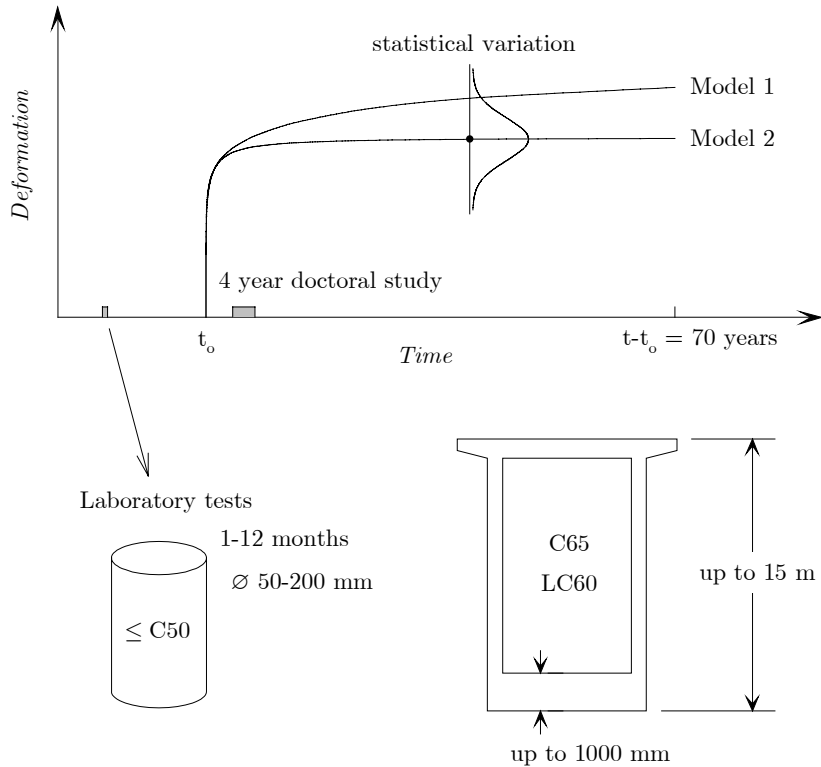


Figure 2.11 Prediction of the long-term deformation development in modern long span concrete bridges based on the extrapolation of observations in experiments

Beyond the uncertainties associated with the creep and the shrinkage characteristics in concrete, which are undoubtedly the biggest obstacle to the improvement in the accuracy of deformation prediction, there are further uncertainties contributing to the deformation problem in concrete cantilever bridges: relaxation in the prestressing steel, estimation of the effective prestressing force and sensitivity of the deformations to variations in construction schedule and procedure.

## 2.5 A review on research works on the deformation problem

The deformation problem in segmentally built concrete cantilever bridges has received considerable attention lately. Many bridges have been suffering from excessive deflections not only in Norway but in parts of the world as well. The numerous cases of impaired concrete cantilever bridges has led to the realisation that the problem needs to be studied. Moreover, the effective way to do so is if the theoretical investigation is based on measurements made on actual bridges and supported by relevant experimental data.

Kanstad (1993) demonstrated the use of advanced numerical techniques for the deformation problem. He calculated the deflections in Mjøsund Bridge which has a main span length of 185 m. Deflections in the early part of the construction were observed within  $\pm 10\%$  of the computed values when the MC90 creep and shrinkage model was used.

An observational investigation was carried out on deformations in concrete cantilever bridges by the CEB Task Group 2.4 "Serviceability Models" (Vitek *et al.* 1997). The investigation was initiated as a consequence of numerous reported cases where excessive deflection in the bridge span had been observed. Data on observed deflections in 27 bridges were collected; 26 bridges were from European countries and one bridge was from the US. The bridges were built between 1955 and 1993. The length of the main spans vary between 53 m and 195 m. The bridges are typically segmental, cast-in-place bridges. About half of them were constructed with continuous spans and the other half were constructed with a hinge close to the midspan. 5 bridges were built with precast segments. Unfortunately no predicted deformations were reported together with the observations. It would have been useful to look into the tendency in the accuracy of the predictions. Nevertheless, it is interesting to see that some of the bridges exhibited very significant deformation gradients even after 8-10 years. In fact there were two bridges where deformations were increasing at an almost constant rate from the completion of bridges up to the last reported measurements at the age of 16 and 20 years respectively.

The variability in creep and shrinkage properties was studied by Santos *et al.* (2001) in four concrete bridges in Portugal (among them is the *Ponte de São João*, *vide* Table 2.1). In addition to the measurements made on the bridges, instrumented concrete specimens were placed inside and outside the box-girders, thus exposing them to the same environmental conditions as the bridges themselves. The specimens were made of the same concrete as the bridges. Creep and shrinkage measurements in the specimens resulted in coefficient of variation as 10-20 % for creep and 10-20 % for shrinkage inside the box-girder and 20-30 % for shrinkage outside the box-girder.

## Chapter 3

# Material Models for Time-dependent Analysis

*Material models for time-dependent analysis of prestressed concrete structures are discussed. Creep and shrinkage models in the CEB-FIP Model Code 1990 and its 1999 update are reviewed. The chapter adverts briefly to Eurocode 2, the Norwegian Standard and Bazant's B3 model. Material models for prestressing steel and conventional steel are also reviewed.*

### 3.1 Introduction

In the present study the creep and shrinkage models presented in the CEB-FIP Model Code 1990 are used in the majority of the numerical analyses. The MC90 model will also be considered as a point of reference in several parametric and numerical studies when other models are involved. The CEB-FIP Model Code 1990 and its earlier version, the Model Code 1978 have had a considerable impact on the national design codes in many European countries and also served as the basic reference material for Eurocode 2 (CEN 1999). The Model Code was updated in 1999 (*fib* 1999) and it reflects the recent progress made in the research and the application of high strength concrete and high performance concrete. The review further adverts to the national design code of Norway (NS3473 1998) and the B3 model (Bazant and Baweja 1995).

The fact that creep and shrinkage models may exhibit significant differences reflects the general uncertainty associated with the phenomena. The large inherent scatter in experimental data, the relatively short loading or drying duration of experiments and the lack of sufficient understanding of the governing mechanisms are the main factors behind the uncertainty. Although attempts have been made to bring the models in line with

fundamental theoretical principles, the models are considered as largely empirical formulations which were developed based on the available experimental data.

A comprehensive set of guidelines and recommendations for formulation of creep and shrinkage models was created by the *RILEM Committee TC107* (Bazant *et al.* 1993). Naturally, Bazant's B3 model which was developed along these guidelines satisfies those requirements whereas the CEB-FIP Model Code 1990, Eurocode 2 and several of the national codes in European countries have conflicts with some of the requirements. On the other hand the latter models have the advantage of simplicity at the expense of "sophistication" and they are more suitable for practical applications.

### 3.2 Creep and shrinkage models

In the present study, concrete is considered as an ageing linear viscoelastic material. This assumption is very important as the condition of linearity is the point of departure for the numerical models in this work. The assumption of linear viscoelasticity is valid under the conditions as follow (Bazant 1982): (1) the concrete stress does not exceed forty percent of the mean compressive strength, (2) the strains do not decrease significantly, (3) no large increase in stress magnitude takes place long after the initial loading and (4) the concrete is not subjected to significant drying. These conditions are satisfied for the most part concerning the deformations of cantilever bridges within the scope of this thesis, although some conflict with the last criteria exists. The assumption of linear viscoelasticity implies that the linear superposition principle is applicable.

Two basic types of creep models can be distinguished: product models and summation models. The characteristic feature of the product model (also known as aging creep model) is that the formulation for the creep compliance contains the product of an ageing function which takes into account the effect of age at loading and a time development function which describes the development of creep with time under load. In the summation model creep is expressed as the sum of a term for reversible delayed elasticity and a term for irreversible flow. The models dealt with in this study are all product models. Even the B3 model is technically a product formulation, however, it separates the creep compliance into additive terms which are linked to different physical mechanisms.

The other characteristic feature of the present creep and shrinkage models is that the model parameters are associated with the cross-section and they are considered uniform over the cross-section area. The type of model is called engineering model (or cross-section model). In reality the effect of drying in a given point of the concrete member depends on its position within the cross-section (*i.e.* its distance from the surface) and consequently several related properties are varying across the cross-section area. Taking into account this non-uniform distribution is largely impractical for a global structural analysis. Therefore

these properties are taken with their average value and they are considered representative for the entire cross-section.

### 3.2.1 Modulus of elasticity

The modulus of elasticity is an input parameter to the creep compliance. It is defined as the tangent modulus of elasticity at the origin of the stress-strain diagram and can be estimated from the mean compressive cylinder strength and the concrete age. The tangent modulus is approximately equal to the secant modulus of unloading which is usually measured in tests. Formulas according to some relevant design codes are shown in Table 3.1 and they are illustrated in Figure 3.1. If the mean strength is not known, it can be estimated from the characteristic strength as

$$f_{cm} = f_{ck} + 8 \quad (3.1)$$

where

$f_{cm}$  is the mean concrete compressive strength at the age of 28 days [MPa],

$f_{ck}$  is the characteristic concrete compressive strength [MPa].

Table 3.1 Formulas for the modulus of elasticity at age of 28 days

Design code	Formula for $E_c$ [MPa]
CEB-FIP Model Code 1990	$E_c = 9980 (f_{cm})^{1/3}$ (3.2)
Eurocode 2	$E_c = 9500 (f_{cm})^{1/3}$ (3.3)
NS 3473 (Norwegian Standard)	$E_c = 9500 (f_{cm})^{0.3}$ (3.4)
ACI 318	$E_c = 4733 (f_{cm})^{0.5}$ (3.5)

$f_{cm}$  has to be given in MPa

Besides the concrete strength, the elastic modulus depends also on the type of the aggregate, the curing conditions and the test method. The influence of these factors are largely responsible for the significant scatter which can be observed when experimental values of the modulus of elasticity are plotted against the concrete strength. To take into account the type of the aggregate other than quartzitic aggregates CEB-FIP Model Code 1990 applies a coefficient to the original formula.

An important reason for the uncertainty is the lack of precise definition of what actually *instantaneous* is. The common argument (*e.g.* Bazant *et al.* 1993) reasons that since creep is

already significant after a very short load duration, the  $1/E$  response is inevitably an arbitrarily chosen point on the creep curve. On the other hand, it is also widely acknowledged that for a structural creep analysis it does not really matter what the instantaneous and creep deformations are as long as the sum of them gives the correct value. In other words the creep compliance,  $J$  is of primary importance rather than the elastic modulus,  $E$  and the creep coefficient,  $\phi$  on their own. Specifying the creep compliance eliminates the risk of combining non-corresponding values of the elastic modulus and the creep coefficient.

In the practical field, however, it is often difficult to comply with this principle. Test result on the elastic modulus is usually available for major structures but it is very rare that at least a short-term creep test is carried out. The design engineer then may face the dilemma – as the author of this thesis did – whether to utilise the laboratory test result on the elastic modulus and combine it with the theoretical value of the creep coefficient and thus risk incompatibility problem or to ignore the single measured elastic modulus due to the absence of the corresponding creep coefficient, keeping the creep compliance coherent but not taking advantage of the test result on the elastic modulus. Applying the measured elastic modulus may improve the deformation prediction or may corrupt it. A short-term creep test is therefore a recommended option for major structures. Under precise and careful implementation a creep test with a load duration as short as two days can be adequate to adjust the theoretical creep compliance with appreciable accuracy (Bazant *et al.* 1993b).

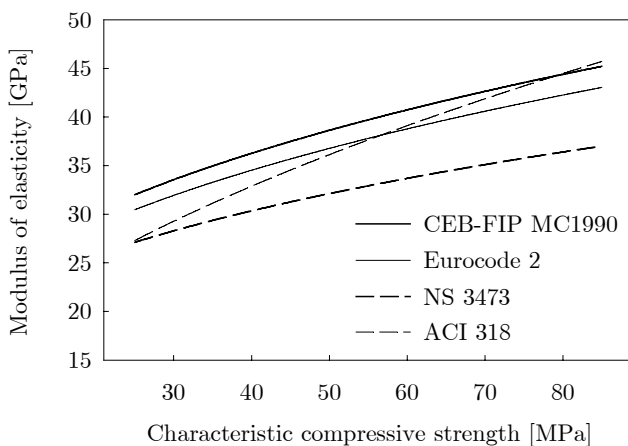


Figure 3.1 Modulus of elasticity according to different formulas (*vide* Table 3.1)

The effect of ageing on the elastic modulus can be taken into account with the time development function

$$E_c(t) = \beta_E(t) \cdot E_c \quad (3.6)$$

where

- $E_c(t)$  is the modulus of elasticity at the concrete age of  $t$  days [MPa],
- $\beta_E(t)$  is the time development function for the elastic modulus (*vide* Eq.(3.7)).

The time development function in the CEB-FIP Model Code 1990 is given as

$$\beta_E(t) = \left( \exp \left\{ s \left[ 1 - \left( \frac{28}{t} \right)^{0.5} \right] \right\} \right)^{0.5} \quad (3.7)$$

where

- $t$  is the concrete age [day],
- $s$  is a coefficient which depends on the cement type, 0.20 for rapid hardening high strength cement, 0.25 for normal and rapid hardening cement and 0.38 for slowly hardening cement.

### 3.2.2 CEB-FIP Model Code 1990

The equations presented here were published in final draft of the CEB-FIP Model Code 1990 (CEB 1991). The model is valid for normal density concrete with grade up to C80 and exposed to a mean relative humidity in the range of 40 to 100 percent. At the time when the code was prepared very limited information on concrete with a characteristic strength higher than 50 MPa were available and therefore the models should be used with caution in that strength range.

#### 3.2.2.1 Creep

The relationship between the total stress-dependent strain and the stress is described with the compliance function which is written as

$$J(t, t_o) = \frac{1}{E_c(t_o)} + \frac{\phi(t, t_o)}{E_c} \quad (3.8)$$

where

- $\phi(t, t_o)$  is the creep coefficient,
- $t_o$  is the age of concrete at loading [day],

$E_c$  is the modulus of elasticity at the age of 28 days according to Eq. (3.2) [MPa],  
 $E_c(t_o)$  is the modulus of elasticity at the age of loading,  $t_o$  according to Eq. (3.6) [MPa].

The creep coefficient is estimated from

$$\phi(t, t_o) = \phi_o \cdot \beta_c(t - t_o) \quad (3.9)$$

where

$\phi_o$  is the notional creep coefficient,  
 $\beta_c(t - t_o)$  is the time function to describe the development of creep with time.

The final value of the time function,  $\beta_c(t - t_o)$  is one which the function is approaching asymptotically. That implies that the creep compliance is approaching a final value with time. The existence of such a final value for creep is still controversial. From a practical perspective, however, this has little significance. After a load duration of about 70 years the rate of creep becomes very low and it is unlikely that considerable increase in creep will occur afterwards.

A convenient feature of this creep prediction model is that the input parameters are those which are easily accessible to the design engineer, even in the early phase of the design process; compressive strength, concrete age at loading, dimensions of the structural member, relative humidity of ambient environment and cement type (the latter in Eq. (3.7)).

The notional creep coefficient is estimated from

$$\phi_o = \phi_{RH} \cdot \beta(f_{cm}) \cdot \beta(t_o) \quad (3.10)$$

with

$$\phi_{RH} = 1 + \frac{1 - RH/100}{0.46(h/100)^{1/3}} \quad (3.11)$$

$$\beta(f_{cm}) = \frac{5.3}{(f_{cm}/10)^{0.5}} \quad (3.12)$$

$$\beta(t_o) = \frac{1}{0.1 + t_o^{0.2}} \quad (3.13)$$

where

$$h = 2A_c / u$$

$RH$  is the relative humidity of the ambient environment [%],

$h$  is the notional size of the structural member [mm],



- $A_c$  is the area of the cross-section of the structural member [mm<sup>2</sup>],  
 $u$  is the perimeter of the cross-section in contact with the atmosphere [mm],  
 $f_{cm}$  is the mean compressive strength of concrete at the age of 28 days [MPa],  
 $t_o$  is the age of concrete at loading [day].

The time development function for the creep coefficient is written as

$$\beta_c(t - t_o) = \left[ \frac{t - t_o}{\beta_H + t - t_o} \right]^{0.3} \quad (3.14)$$

with

$$\beta_H = 150 \left\{ 1 + \left( 1.2 \frac{RH}{100} \right)^{18} \right\} \frac{h}{100} + 250 \leq 1500 \quad (3.15)$$

The influence of the relative humidity and the notional size on the notional creep coefficient is illustrated in Figure 3.2 according to Eq. (3.11). The typical range for the relative humidity and the notional size for the bridges which are concerned in the present study are 60-90 % and 350-750 mm, respectively<sup>1</sup>.

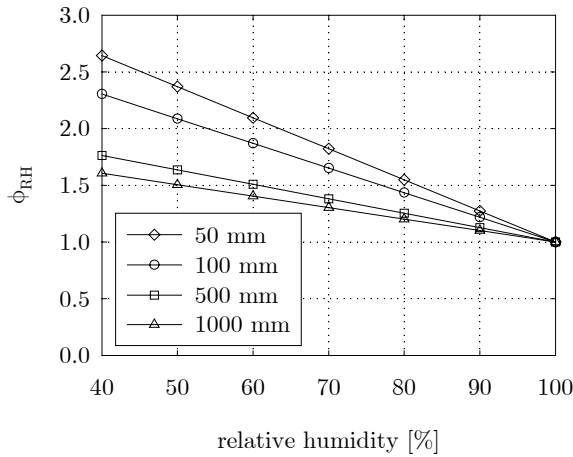


Figure 3.2 Influence of the notional size and the relative humidity on the notional creep coefficient

<sup>1</sup> These values are considered as the annual average relative humidity and the average notional size of the entire cross-section.

The CEB-FIP Model Code 1990 does not distinguish the basic creep component and the drying creep component *per se*. Nevertheless the second term in Eq. (3.11) can be interpreted as the drying creep term. If no moisture exchange with the atmosphere takes place that term is zero and therefore  $\phi_{RH}$  equals to one. Consequently the value of  $\phi_{RH}$  can be considered as the ratio of the total creep to the basic creep.

Figure 3.3 illustrates the influence of the concrete strength on the notional creep coefficient according to Eq. (3.12). The source of much of the potential prediction error is lying within this term (CEB 1990). Creep does not depend on the concrete strength intrinsically, but rather on the composition of the concrete. It is known that creep is increasing with increasing water-cement ratio and increasing cement content. While higher concrete strength is usually associated with lower water-cement ratio and higher cement content, the influence of the water-cement ratio is more pronounced and therefore creep is decreasing with increasing concrete strength. The established relationship represents only the observed average tendency in the available experimental data which is marked with significant scatter.

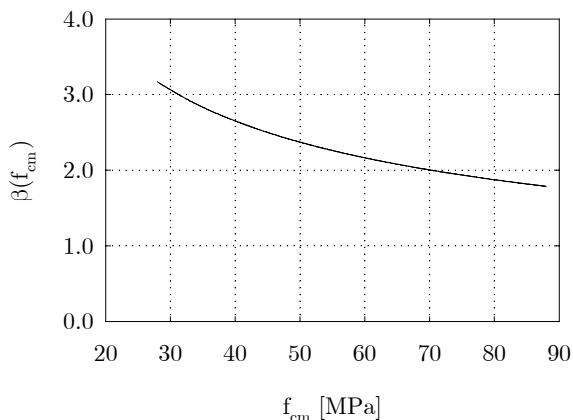


Figure 3.3 Influence of the concrete strength on the creep coefficient

Figure 3.4 illustrates the influence of the concrete age at loading on the notional creep coefficient. The hyperbolic function (*vide* Eq.(3.13)) gives a good estimation for the effect of age even for very high ages at loading provided that no significant moisture loss occurs in the concrete prior to loading (CEB 1990). This condition is true for bulk concrete members in humid environment. Whereas the model may overestimate creep in thin members exposed to dry environment if loading takes place long after drying begins. This deficiency could be eliminated only if total creep was separated into basic and drying creep components.

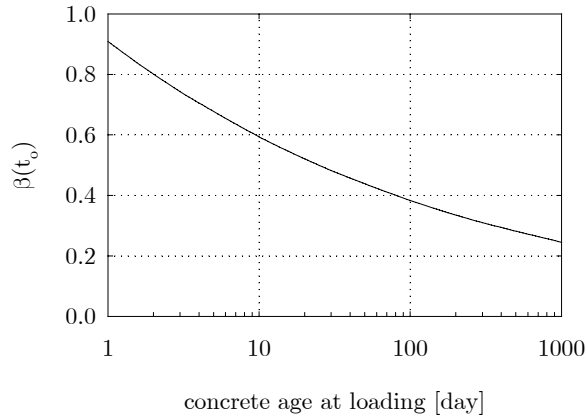


Figure 3.4 Influence of the concrete age at loading on the creep coefficient

The development of creep with time is illustrated in Figure 3.5 according to Eq. (3.14). The development is delayed with the increasing size of the structural member and the increasing relative humidity while a limiting curve exists.

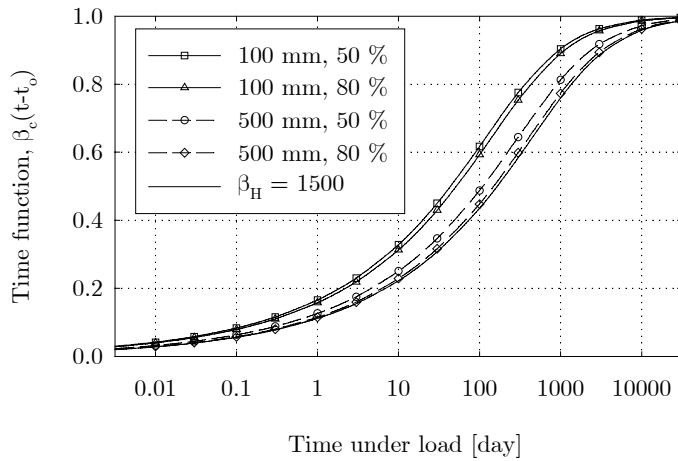


Figure 3.5 Time dependency function for creep

### 3.2.2.2 Shrinkage

The shrinkage strain (or swelling) is calculated as

$$\varepsilon_{cs}(t, t_s) = \varepsilon_{cso} \cdot \beta_s(t - t_s) \quad (3.16)$$

where

- $\varepsilon_{cso}$  is the notional shrinkage coefficient,
- $\beta_s$  is the time function to describe the development of shrinkage with time,
- $t_s$  is the age of concrete when drying begins [day].

The notional shrinkage coefficient can be estimated from

$$\varepsilon_{cso} = \varepsilon_s(f_{cm}) \cdot \beta_{RH} \quad (3.17)$$

with

$$\varepsilon_s(f_{cm}) = \left[ 160 + 10\beta_{sc}(9 - f_{cm}/10) \right] \cdot 10^{-6} \quad (3.18)$$

and

$$\beta_{RH} = \begin{cases} -1.55 \cdot \left[ 1 - \left( \frac{RH}{100} \right)^3 \right] & \text{for } 40\% \leq RH < 99\% \\ +0.25 & \text{for } RH \geq 99\% \end{cases} \quad (3.19)$$

where

- $f_{cm}$  is the mean compressive strength of concrete at the age of 28 days [MPa],
- $RH$  is the relative humidity of the ambient environment [%],
- $\beta_{sc}$  is a coefficient which depends on the cement type, 4 for slowly hardening cement, 5 for normal and rapid hardening cement and 8 for rapid hardening high strength cement.

The development of shrinkage with time is given by

$$\beta_s(t - t_s) = \left[ \frac{t - t_s}{350(h/100)^2 + t - t_s} \right]^{0.5} \quad (3.20)$$

where

- $h$  is the notional size of the structural member [mm].

The time dependency function is in agreement with the fundamental principle of the diffusion theory. The drying time required to reach a certain degree of average drying over the cross-section is increasing linearly with the square of the notional size. Also its value is approaching a final asymptotic value.

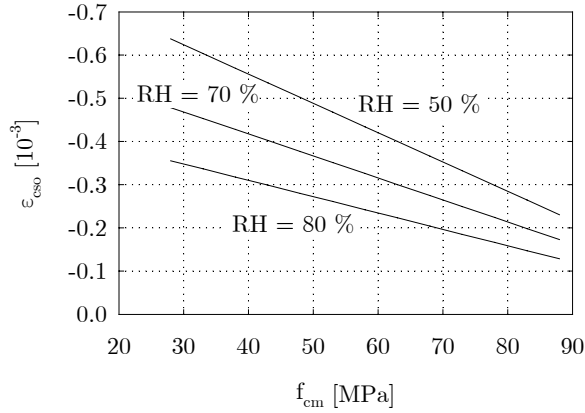


Figure 3.6 Notional shrinkage coefficient

Figure 3.6 illustrates the influence of the concrete strength and the relative humidity on the notional shrinkage coefficient. Similar to creep, shrinkage does not depend on the concrete strength *per se*, but rather on the water-cement ratio and cement content. But the indirect relationship through these parameters offers a convenient and practical way to estimate shrinkage from the concrete strength.

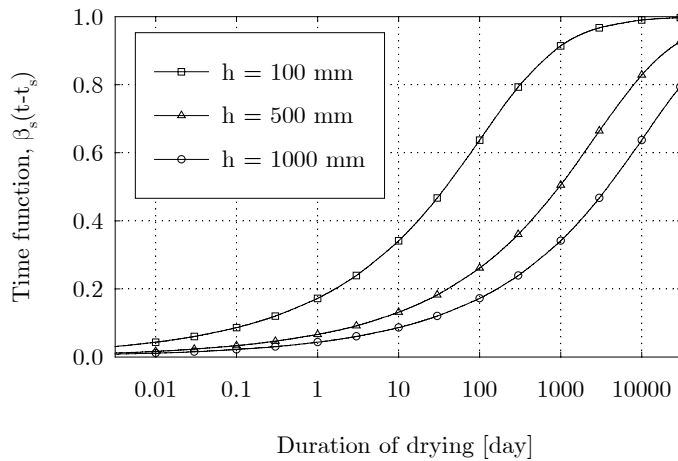


Figure 3.7 Time function for shrinkage development

Figure 3.7 shows the time dependency function for shrinkage with the influence of the element size. The curves well illustrate that the final value of shrinkage is not reached even after long duration of drying (70 years) in thick sections. The assumption that a final value for shrinkage exists and it is independent of the member size is most certainly theoretically

correct. However, if the full development may take centuries in bulk members it is reasonable to assume, from a practical perspective, that the “final” value of shrinkage does depend on the element size. It also has to be noted that due to the little information which exists on shrinkage in large members after long duration of drying, the time dependency function according to Eq. (3.20) is uncertain for elements with notional size larger than 500 mm (CEB 1991).

### 3.2.2.3 Temperature effects

The influence of mean temperature other than 20° C can be taken into account. With the decreasing temperature both the notional creep coefficient and the notional shrinkage coefficient are decreasing and their development with time are decelerated. Since the annual average temperature varies from 5° C to 10° C in the coastal areas of Norway, the temperature influence on creep and shrinkage should be considered.

The formulas presented here are meant to take into account the effect of constant temperature differing from 20° C.

The effect of temperature on the elastic modulus at the age of 28 days is estimated as

$$E_c(T) = E_c(1.06 - 0.003 \cdot T) \quad (3.21)$$

where

$T$  is the temperature [°C],

$E_c$  is the modulus of elasticity at the temperature of 20°C according to Eq. (3.2).

The effect of elevated or reduced temperature on the aging parameters such as the elastic modulus,  $E_c(t)$  and the aging coefficient for creep,  $\beta(t_o)$  is taken into account by adjusting the concrete age according to the following formula

$$t_T = \sum_{i=1}^n \Delta t_i \cdot \exp\left[\frac{4000}{273 + T(\Delta t_i)} - 13.65\right] \quad (3.22)$$

where

$t_T$  is the temperature adjusted concrete age which replaces  $t$  in Eq. (3.6) and Eq. (3.13) [day],

$T(\Delta t_i)$  is the temperature during the time period  $\Delta t_i$  [°C],

$\Delta t_i$  is the number of days where temperature  $T$  prevails.

When only constant temperature is considered, Eq. (3.22) can be written in a simpler form as follows

$$t_T = t \cdot \exp - \left[ \frac{4000}{273 + T} - 13.65 \right] \quad (3.23)$$

The effect of temperature on the creep coefficient is taken into account by replacing  $\phi_{RH}$  in Eq. (3.10) with

$$\phi_{RH,T} = \phi_T + (\phi_{RH} - 1) \cdot \phi_T^{1,2} \quad (3.24)$$

where

$$\phi_T = \exp[0.015(T - 20)] \quad (3.25)$$

and

$\phi_{RH}$  is calculated according to Eq. (3.11).

It can be seen in Eq. (3.24) that the first term expresses the influence of temperature on basic creep while the second term does so on drying creep. Figure 3.8 illustrates the temperature influence on the notional creep coefficient. The creep coefficient at 5° C is about 20-22 % lower than at 20° C in the range of the relative humidity of 60-90 %.

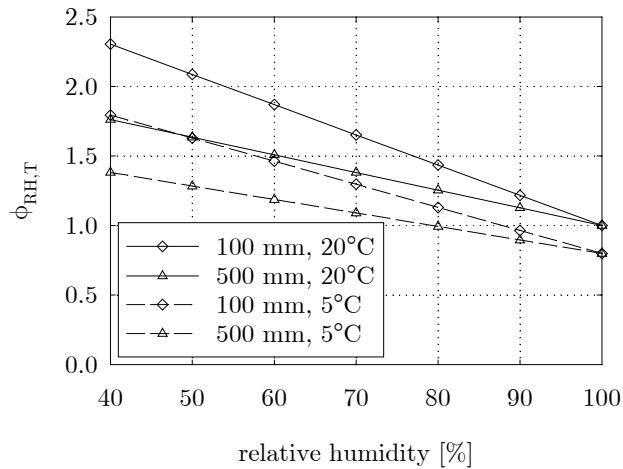


Figure 3.8 Influence of temperature on the notional creep coefficient

The temperature influence on the time dependency function is taken into account by replacing  $\beta_H$  in Eq. (3.14) with

$$\beta_{H,T} = \beta_H \cdot \exp[1500/(273 + T) - 5.12] \quad (3.26)$$

where

$\beta_H$  is calculated according to Eq. (3.15).

The effect of temperature on the notional shrinkage coefficient is taken into account by replacing  $\beta_{RH}$  in Eq. (3.17) with

$$\beta_{RH,T} = \beta_{RH} \cdot \left[ 1 + \left( \frac{8}{103 - RH} \right) \cdot \left( \frac{T - 20}{40} \right) \right] \quad (3.27)$$

where

$\beta_{RH}$  is calculated according to Eq. (3.19).

According to the formula the notional shrinkage coefficient is reduced by 6 % at temperature 10° C and by 9 % at temperature 5° C on a relative humidity of 70 %. The reduction is 9 % and 13 % respectively on a relative humidity of 80 %. The reduction is stated in comparison to temperature 20° C.

To consider the effect of temperature on the time development of shrinkage, the time development function given in Eq. (3.20) is replaced by

$$\beta_s(t - t_s) = \left[ \frac{t - t_s}{350(h/100)^2 \cdot \exp[-0.06(T - 20)] + t - t_s} \right]^{0.5} \quad (3.28)$$

### 3.2.3 The 1999 update of the CEB-FIP Model Code 1990

The models were published in the *fib* Bulletin «*Structural Concrete*» (*fib* 1999). The primary intention with the update was to improve the prediction models for high strength concrete and further extend the validity of the models to high performance concrete.

The updated creep model was in fact first published in Eurocode 2 (CEN 1999). It is closely related to the model in the CEB-FIP Model Code 1990, but three strength dependent coefficients were introduced into the original model. In this thesis the model is referred to as MC90(99) model.

The shrinkage model represents a major change. The total shrinkage is subdivided into the autogenous shrinkage component and the drying shrinkage component.



### 3.2.3.1 Creep

The extended model is valid for both normal strength concrete and high performance concrete up to a concrete cylinder strength of 110 MPa. Three coefficients were introduced into the MC 90 model. The coefficients are functions of the mean concrete strength and they are written as

$$\alpha_1 = \left( \frac{35}{f_{cm}} \right)^{0.7} \quad \alpha_2 = \left( \frac{35}{f_{cm}} \right)^{0.2} \quad \alpha_3 = \left( \frac{35}{f_{cm}} \right)^{0.5} \quad (3.29a,b,c)$$

Coefficients  $\alpha_1$  and  $\alpha_2$  are meant to adjust the notional creep coefficient through the  $\phi_{RH}$  term. Coefficient  $\alpha_2$  can be considered as the adjusting factor for basic creep while the product of  $\alpha_1$  and  $\alpha_2$  is the adjusting factor for drying creep. Eq. (3.30) is replacing Eq. (3.11) in the MC90 model.

$$\phi_{RH} = \left[ 1 + \frac{1 - RH/100}{0.46(h/100)^{1/3}} \cdot \alpha_1 \right] \cdot \alpha_2 \quad (3.30)$$

Coefficient  $\alpha_3$  is meant to be the adjustment for the time dependency function. Eq. (3.31) replaces Eq. (3.15).

$$\beta_H = 150 \left\{ 1 + \left( 1.2 \frac{RH}{100} \right)^{18} \right\} \frac{h}{100} + 250 \alpha_3 \leq 1500 \alpha_3 \quad (3.31)$$

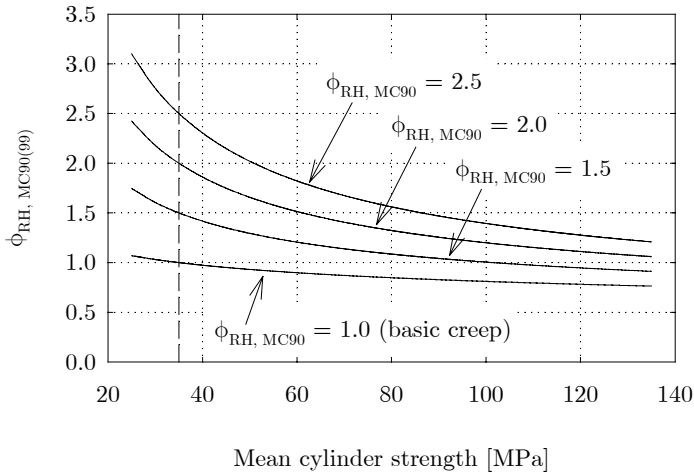


Figure 3.9 Adjustment on the notional creep coefficient (through the  $\phi_{RH}$  term)

In Figure 3.9 the adjustment on the notional creep coefficient is illustrated. It is seen that the change is rather significant for concrete with very high strength. In the range which is relevant for the current investigation (*i.e.* RH = 60-90 %, h = 350-750 mm), the reduction is

11-18 % for concrete with a mean cylinder strength of 55 MPa and 15-23 % for concrete with a mean cylinder strength of 65 MPa as compared to MC90.

The effect on the time dependency function is moderate. With increasing concrete strength, the development of creep with time slightly accelerates.

### 3.2.3.2 Shrinkage

In the MC90(99) model the total shrinkage is subdivided into the autogenous shrinkage component and the drying shrinkage component. With this approach it was possible to formulate a model which is valid for both normal strength concrete and high performance concrete up to a strength of 120 MPa.

The total shrinkage strain is calculated as

$$\varepsilon_{cs}(t, t_s) = \varepsilon_{cas}(t) + \varepsilon_{cds}(t, t_s) \quad (3.32)$$

with

$$\varepsilon_{cas}(t) = \varepsilon_{caso}(f_{cm}) \cdot \beta_{as}(t) \quad (3.33)$$

and

$$\varepsilon_{cds}(t, t_s) = \varepsilon_{cdso}(f_{cm}) \cdot \beta_{RH}(RH) \cdot \beta_{ds}(t - t_s) \quad (3.34)$$

where

- $\varepsilon_{cs}(t, t_s)$  is the total shrinkage strain at time  $t$ ,
- $\varepsilon_{cas}(t)$  is the autogenous shrinkage strain at time  $t$ ,
- $\varepsilon_{cds}(t, t_s)$  is the drying shrinkage strain at time  $t$ ,
- $\varepsilon_{caso}(f_{cm})$  is the notional autogenous shrinkage coefficient (*vide* Eq. (3.35)),
- $\beta_{as}(t)$  is the time development function for autogenous shrinkage, (*vide* Eq. (3.36)),
- $\varepsilon_{cdso}(f_{cm})$  is the notional drying shrinkage coefficient (*vide* Eq. (3.37)),
- $\beta_{RH}(RH)$  is the coefficient taking into account the effect of relative humidity on drying shrinkage (*vide* Eq. (3.38)),
- $\beta_{ds}(t - t_s)$  is the time development function for drying shrinkage, (*vide* Eq. (3.39)),
- $t$  is the concrete age [day],
- $t_s$  is the age of concrete when drying begins [day],
- $t - t_s$  is the duration of drying [day].

The formulations for estimating the autogenous shrinkage are written as

$$\varepsilon_{caso}(f_{cm}) = -\alpha_{as} \left( \frac{f_{cm}/10}{6 + f_{cm}/10} \right)^{2.5} \cdot 10^{-6} \quad (3.35)$$

$$\beta_{as}(t) = 1 - \exp(-0.2 \cdot t^{0.5}) \quad (3.36)$$

where

- $f_{cm}$  is the mean compressive strength [MPa],  
 $\alpha_{as}$  is a coefficient which depends on the cement type, 800 for slowly hardening cement, 700 for normal and rapidly hardening cement and 600 for rapidly hardening high strength cement.

The formulations for estimating the drying shrinkage are written as

$$\varepsilon_{cdso}(f_{cm}) = \left[ (220 + 110 \cdot \alpha_{ds1}) \cdot \exp\left(-\alpha_{ds2} \cdot \frac{f_{cm}}{10}\right) \right] \cdot 10^{-6} \quad (3.37)$$

$$\beta_{RH}(RH) = \begin{cases} -1.55 \cdot \left[ 1 - \left( \frac{RH}{100} \right)^3 \right] & \text{for } RH < 99\% \cdot \beta_{s1} \\ +0.25 & \text{for } RH \geq 99\% \cdot \beta_{s1} \end{cases} \quad (3.38)$$

$$\beta_{ds}(t - t_s) = \left[ \frac{t - t_s}{350(h/100)^2 + t - t_s} \right]^{0.5} \quad (3.39)$$

with

$$\beta_{s1} = \left( \frac{35}{f_{cm}} \right)^{0.1} \quad (3.40)$$

where

- $f_{cm}$  is the mean compressive strength [MPa],  
 $RH$  is the relative humidity of the ambient environment [%],  
 $h$  is the notional size of the member [mm],  
 $\alpha_{ds1}$  is a coefficient which depends on the cement type, 3 for slowly hardening cement, 4 for normal and rapidly hardening cement and 6 for rapidly hardening high strength cement,  
 $\alpha_{ds2}$  is a coefficient which depends on the cement type, 0.13 for slowly hardening cement, 0.11 for normal and rapidly hardening cement and 0.12 for rapidly hardening high strength cement.

The  $\beta_{s1}$  coefficient in Eq. (3.38) is meant to take into account that in higher concrete grades swelling already occurs at lower relative humidity because of the preceding reduction of the internal relative humidity due to self-desiccation.

### 3.2.4 Norwegian Standard (NS 3473)

The creep and shrinkage prediction models are published in the Norwegian Standard 3473, section A.9.3.2 (NS 3473 1998). The models are similar to the models of the CEB-FIP Model Code 1990 having the same parameters; concrete strength, notional size of the structural member, relative humidity, concrete age at loading and duration of loading and duration of drying respectively. In the shrinkage model, however, neither the concrete composition nor the concrete strength is taken into account. The final shrinkage strain for a given relative humidity is defined as an average value. A validity range, however, is given with respect to the water content. The model applies to concrete with water content of 155 to 175 l/m<sup>3</sup>. The final shrinkage strain has to be reduced by 25 % below that range and has to be increased by 25 % above that range.

### 3.2.5 B3 model

The complete description of the B3 creep and shrinkage model can be found in (Bazant and Baweja 1995). An important feature of the B3 creep model is that the compliance function is decomposed into the instantaneous response, the compliance function for basic creep and the additional compliance function for drying creep.

The creep compliance is written as

$$J(t, t_0) = \frac{1}{E_o} + C_o(t, t_0) + C_d(t, t_0, t_s) \quad (3.41)$$

where

- $E_o$  is the so-called asymptotic modulus,
- $C_o(t, t_0)$  is the compliance function for basic creep,
- $C_d(t, t_0, t_s)$  is the compliance function for drying creep.

The instantaneous response is defined with the so-called asymptotic modulus,  $E_o$  which is not the same as the conventional static modulus. The asymptotic modulus is an empirical parameter and considered age independent. Its value is higher than the real elastic modulus and it can be estimated roughly as  $E_o \cong 1.5E$ . According to Bazant, it is more convenient to use the asymptotic modulus because concrete exhibits pronounced creep even after very short duration of loading.

Unlike in the MC90 model, the creep compliance in the B3 creep model is not approaching a final value but it is increasing indefinitely with time. The compliance function for drying

creep possesses a final value because it is related to the moisture exchange between the concrete and the ambient environment and that process possesses an equilibrium state.

The B3 model takes into account the influence of the material composition directly. Besides model parameters which are considered in previously reviewed models, the cement content, the water-cement ratio, the aggregate-cement ratio and the water content are taken into account.

The B3 model is considered as a rather sophisticated model but somewhat cumbersome due to the parameters which are not necessarily available for the design engineer in the design phase. The model also requires an excessive amount of computational work, however, that can be easily computerised for both analytical or numerical purposes. In fact the description of the model includes a rate-type formulation for the compliance function for basic creep.

### 3.2.6 Uncertainty in creep and shrinkage prediction

An important but often overlooked property of creep and shrinkage prediction models is the expected error of the prediction. Creep and shrinkage are among the most uncertain mechanical properties of concrete. The theoretical models only predict the mean tendencies based on observations in available experimental data. In any particular prediction the effect of a certain parameter may be overestimated or may be underestimated.

The creep compliance and the shrinkage strain should therefore be considered as statistical variables. Accordingly, the measure of dispersion is an important parameter in addition to the mean. The dispersion is characterised with the coefficient of variation for the prediction. The reported coefficient of variation for the CEB-FIP Model Code 1990 and the B3 creep and shrinkage models are shown in Table 3.2. It should be noted that smaller coefficient of variation does not necessarily mean that the model is more accurate than the other and vice versa as it depends also on the range of the experimental data upon which the model was developed and adjusted and hence the coefficient of variation was computed.

Table 3.2 Coefficient of variation\* [%]

Model	Creep compliance	Shrinkage strain
CEB-FIP Model Code 1990	20	35
Bazant's B3 model	23	34

\*(CEB 1991) and (Bazant and Baweja 1995)

The values of the coefficient of variation in Table 3.2 concern the mean coefficient of variation calculated on the basis of all included experiments and over the entire duration of loading or drying. It characterises the average error in the prediction method. The numerical

procedure of the statistical evaluation is described in the CEB Bulletin «*Evaluation of the Time Dependent Behaviour of Concrete*» (CEB 1990).

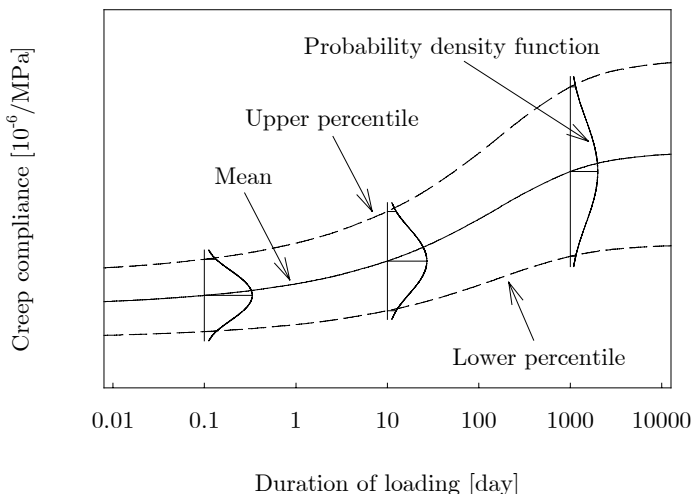


Figure 3.10 Statistical variation in the creep compliance

Figure 3.10 illustrates the statistical variation in the creep compliance with the estimated mean curve and the curves representing the estimated upper and lower percentile. If the curves represent the 2.5 % and 97.5 % percentile that means that the probability is 95 % that the observed value will fall between those curves (dashed lines). The stochastic aspects of deformation prediction and a probabilistic structural analysis are discussed in Chapter 10.

### 3.2.7 Creep and shrinkage models in comparison

The reviewed models are compared under a few characteristic sets of conditions in a parametric study. The comparison for creep is primarily relevant between the CEB-FIP Model Code 1990 and the B3 model. The MC90(99) and the Norwegian Standard are closely related to the formulations of MC90.

The general observation is that the models can be found in reasonable agreement when the parameters are in the range which is typical for an experimental setup in a laboratory. It seems evident that the availability of sufficient experimental data within that range provides a more solid basis for adjusting the theoretical models and the degree of uncertainty is smaller. On the other hand, the difference among the models can be rather significant when they are applied under conditions where availability of experimental data is obviously limited and the prediction inevitably has an extrapolative nature. Such conditions are high concrete strength, drying in large members and long duration of loading.

The effect of high strength is illustrated on the top diagrams in Figure 3.11. The curves exhibit good agreement for normal strength concrete but the difference rises significantly for high strength concrete.

The difference after long time is significant when drying in large member is concerned (*vide* middle diagram on right in Figure 3.11). The long-time difference is somewhat smaller when the humidity is higher and the structural member is smaller.

The B3 model is generally in agreement with the other models up to 100-1000 days of loading. For longer duration of loading the difference is increasing considerably as creep is increasing indefinitely according to the B3 model while the other creep curves are approaching a final value.

Figure 3.12 compares creep curves with different concrete ages at loading under conditions similar to those for the investigated bridges. It is seen that the variation in the concrete age at loading has a more pronounced influence on creep according to the B3 model.

Predicted shrinkage curves are compared in Figure 3.13. Considerable difference is seen for high strength concrete between the MC90(99) model which takes into account autogenous shrinkage in a separate term and the other models which considers shrinkage as a mechanism primary driven by external drying. The difference increases as drying shrinkage becomes less significant in magnitude and its time development is decelerated (*i.e.* large member in humid environment).

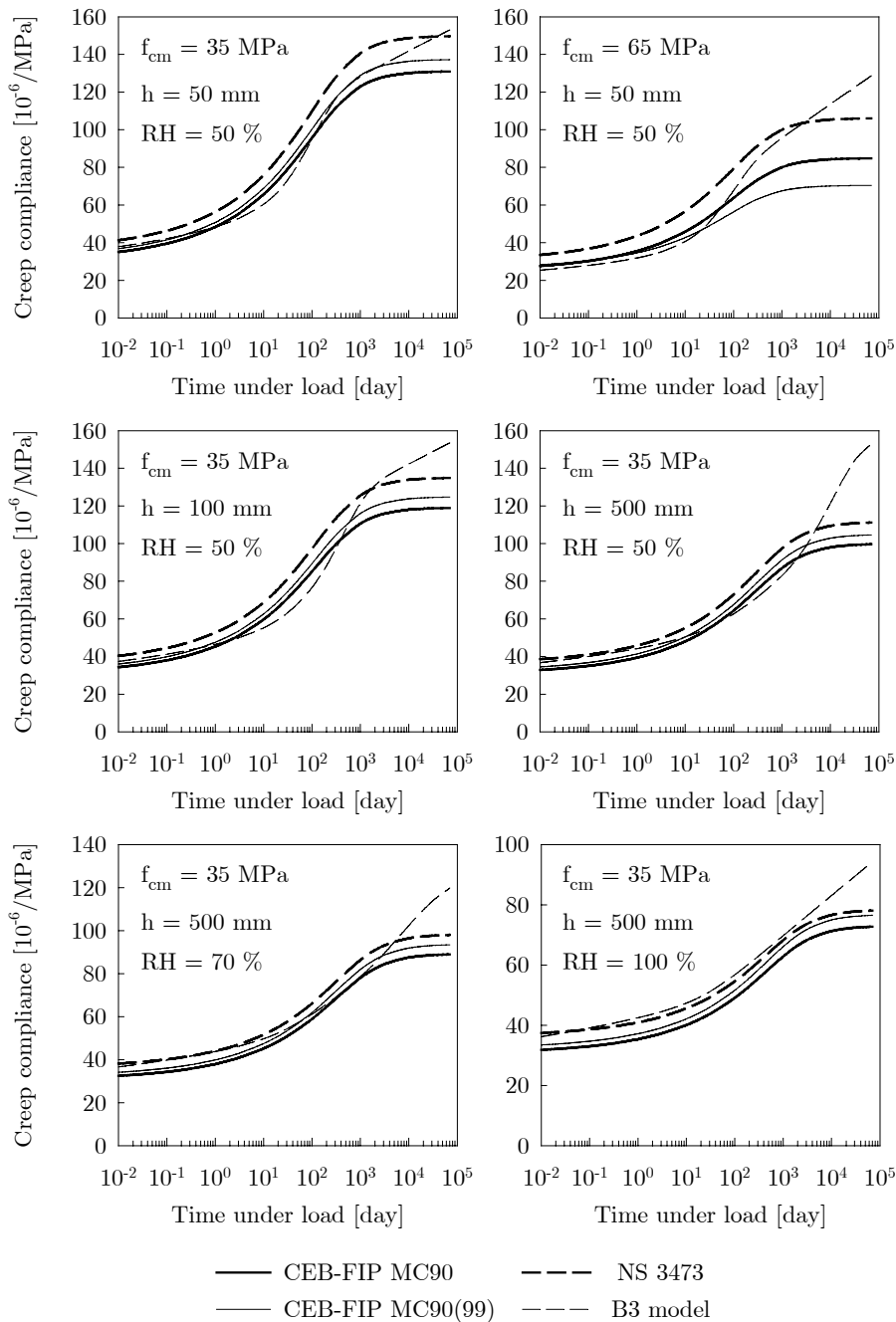


Figure 3.11 Creep compliance given by different models ( $t_0 = 28$  day)



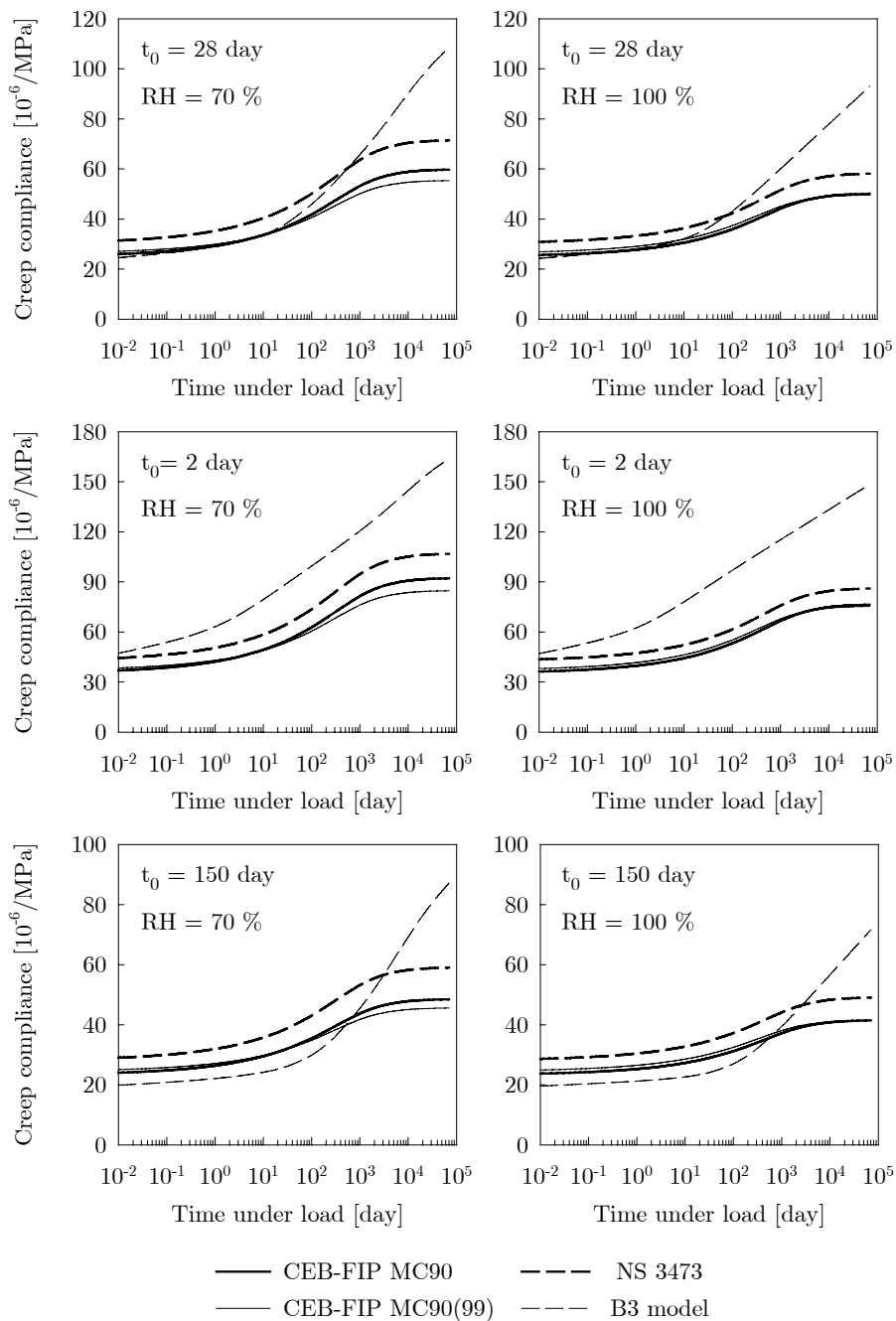


Figure 3.12 Creep compliance given by different models ( $h = 500$  mm,  $f_{cm} = 65$  MPa)

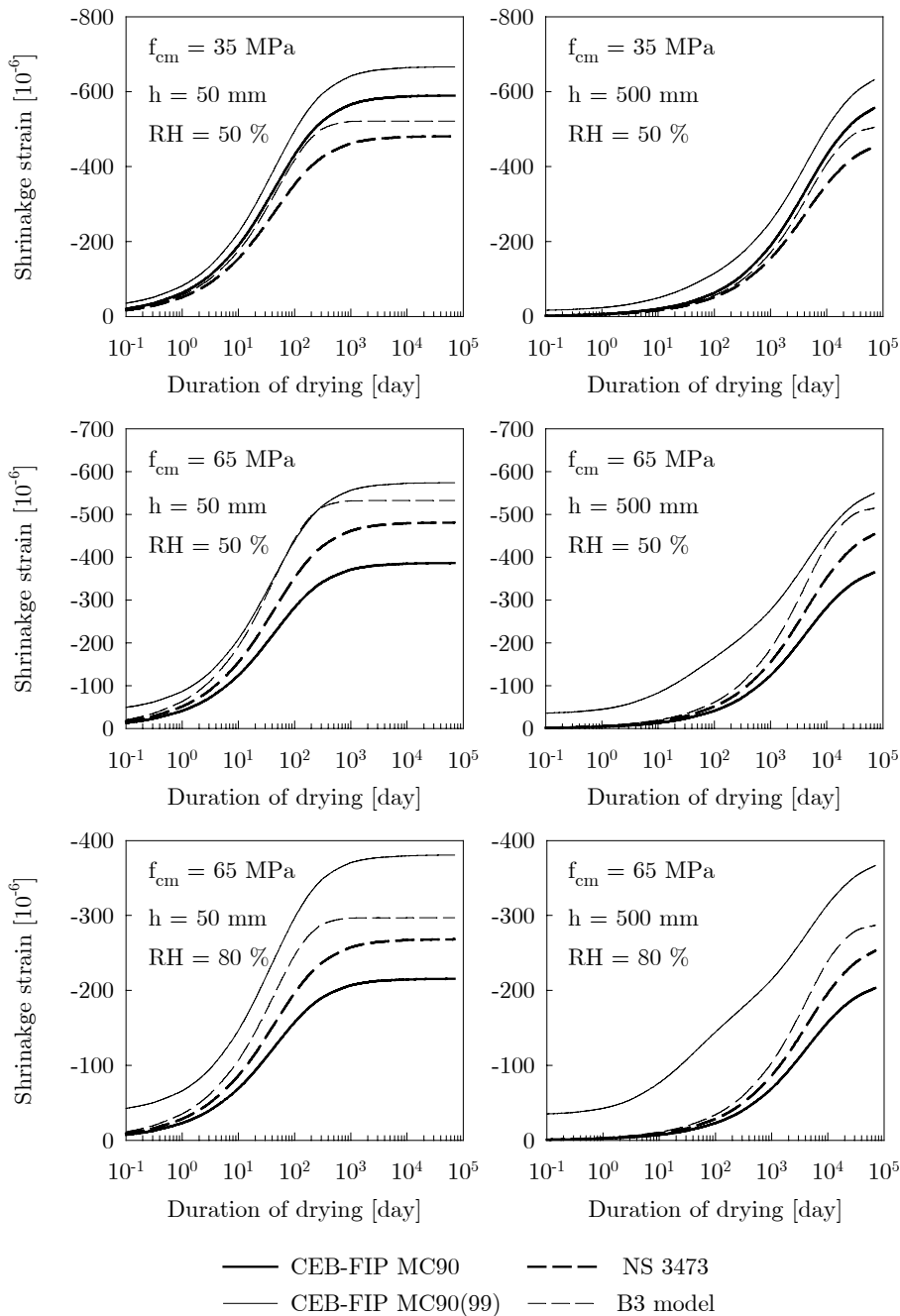


Figure 3.13 Shrinkage development given by different models

The MC90(99) shrinkage model is demonstrated in Figure 3.14. The drying and the autogenous shrinkage components are shown separately for normal strength concrete and for high-performance concrete under conditions similar to the investigated bridges. It is interesting that the total shrinkage after 70 years for HPC is almost as large as for the NSC.

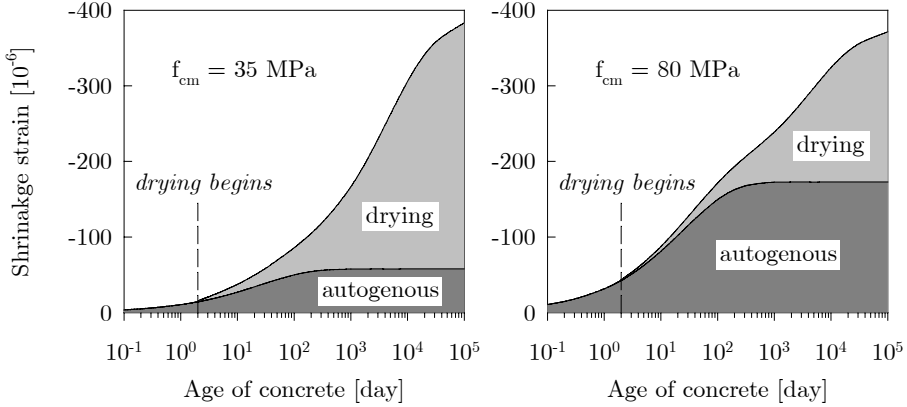


Figure 3.14 Autogenous shrinkage and drying shrinkage components in NSC and HPC as given by the MC90(99) model (large member in humid environment,  $h = 500$  mm,  $RH = 80$  %)

### 3.3 Material model for reinforcing and prestressing steel

The tensile stress-strain relationship can be approximated by a bilinear diagram for the reinforcing steel and by a multilinear diagram for the prestressing steel as illustrated in Figure 3.15. The hardening diagram for the prestressing steel is specified by the plastic strain values and the corresponding stress values at the given points. The reinforcing steel is assumed to follow a symmetrical stress-strain relationship in compression.

The notations in the diagrams are

- $f_{yk}$  is the characteristic yield stress for the reinforcing steel,
- $E_s$  is the elastic modulus for the reinforcing steel,  $E_s = 200 \text{ GPa}$ ,
- $f_{ptk}$  is the characteristic tensile strength for the prestressing steel,
- $\varepsilon_{pu}$  is the total elongation at the maximum stress and may be taken as  $\varepsilon_{pu} = 35\%$ ,
- $E_p$  is the elastic modulus for the prestressing steel,  $E_p = 195 \text{ GPa}$ .

The  $0.9 f_{ptk}$  stress is defined as the corresponding stress at a plastic deformation of 2 %.

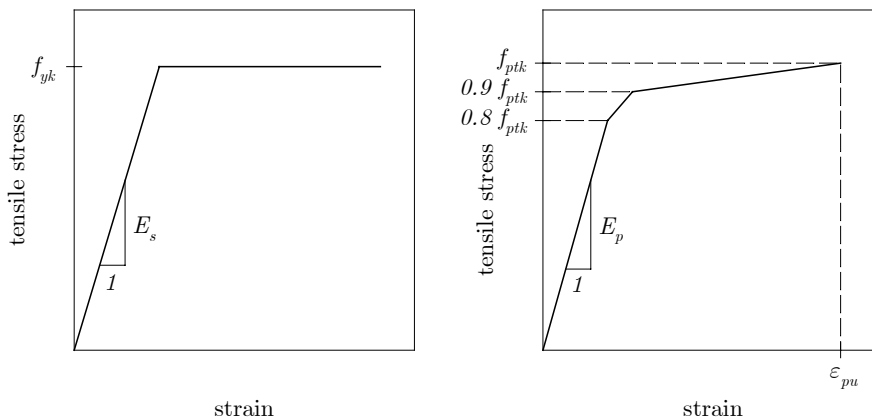


Figure 3.15 Idealised stress-strain diagram for reinforcing steel (left) and prestressing steel (right)

The characteristic values of the material parameters are used in the absence of the mean values.

Relaxation properties of the prestressing steel is taken into account according to the CEB-FIP Model Code 1990. The relaxation loss is specified at 1000 hours for initial stresses equal to 0.6, 0.7 and 0.8 of the rupture stress. The loss of prestress is 4, 8 and 12 % respectively, for strands with normal relaxation characteristics, «Class 1» and 1, 2 and 5 % for strands with improved relaxation characteristics, «Class 2».

To estimate relaxation at time other than 1000 hours, the following formula can be used

$$\rho(t) = \rho_{1000} \left( \frac{t}{1000} \right)^k \quad (3.42)$$

where

$t$  is the time [hour],

$\rho(t)$  is the relaxation loss after time  $t$  [%],

$\rho_{1000}$  is the relaxation after 1000 hours [%],

$k$  can be determined from laboratory test as  $k \approx \log(\rho_{1000}/\rho_{100})$ .

In the absence of more exact information the value of  $k$  can be taken as 0.12 for Class 1 strands and 0.19 for Class 2 strands.

It is important that when the actual initial stress level in the strand is determined the applied prestress is reduced by instantaneous prestress losses of other kind.

Computation of the effective prestress in the tendons is discussed together with the geometrical model for the prestressing tendons in Chapter 7.



## Chapter 4

# Lightweight Aggregate Concrete

*The creep and shrinkage properties of lightweight aggregate concrete are discussed in this chapter. The recent advancement in theoretical modelling is reviewed. Experimental results from NTNU and SINTEF are studied. The experimental data is evaluated in comparison with the current formulations of the extended CEB-FIP Model Code 1990.*

### 4.1 Introduction

Lightweight aggregate concrete (LWAC) is a relatively new material. Considerable effort has been made for the past 15 years to gain knowledge on the creep and shrinkage characteristics of LWAC and to update existing design codes. Nevertheless still very few long-term creep and shrinkage tests have been carried out. Due to the little amount of experimental evidence, the concluding remarks and indications and correctness of existing prediction formulas are often controversial. Further tests are necessary before information will allow clear conclusions.

Current extensions to design codes recommend multiplying the elastic modulus and the notional creep coefficient given for normal concrete of the same strength with factors which are functions of the oven-dry density of the lightweight aggregate. The shrinkage strain is estimated with the model given for normal concrete but the notional shrinkage coefficient is multiplied with a fixed value. On the other hand the same time-dependency functions are used for both creep and shrinkage as for normal concrete. It is now well recognised that the development of drying is significantly delayed in LWAC.

Smeplass (2001) concluded that LWAC dries out very slowly due to the low permeability of high strength binders preferred in LWAC and the high moisture content.

Test results in the EuroLightCon program (Hynne 2000) suggest that lightweight aggregates with capacity of high water absorption are acting like internal water reservoirs in the concrete, also reducing the rate of drying in the early period. At later ages a reverse tendency is observed.

With the different time-dependency of drying, not only the correctness of applying the same time-dependency function is questionable but the correctness of the recommended multiplying factors for the final values of creep and shrinkage as well. In the evaluation of experimental information, the final value of creep and the final value of shrinkage are estimated based on the extrapolation of short-term observed data applying the same time-dependency function as for normal concrete. In the Lettkon project, Maage and Olsen (2000) compared observed creep data resulted from 18 month long tests with extrapolated creep curves based on earlier three month long or shorter tests and concluded that estimating the final creep on the basis of short term test results has a tendency toward underestimating creep.

Walraven (2000) presented a review on some of the theoretical arguments and experimental work on creep and shrinkage in LWAC in connection with a status report of the revision of EC-2. He concluded that the existing experimental data does not allow definite conclusion on creep. He suggested that the specific creep of LWAC should be considered the same as of NWC and the same formulas should be used. The final drying shrinkage in LWAC with a characteristic cylinder strength of 20 MPa or higher – as stated in EC-2 – should be taken as 1.2 times the final drying shrinkage in NWC. On the other hand, autogenous shrinkage in LWAC with aggregate particles saturated with water does not increase with the increasing strength to the same extent as it is observed in NWC. The supply of water from the aggregate to the microstructure of the cement paste prevents a significant drop in the moisture content and thus reduces autogenous shrinkage.

Hynne (2000) summarized test results from six experimental programs on creep and shrinkage of LWAC which were carried out at NTNU and SINTEF between 1987 and 1999. The experimental results are utilised in this chapter. The available data is rather limited and heterogeneous and considerable scatter is observed at least as far as the current modelling approach is concerned. The effect of delayed drying is apparent on shrinkage and creep in specimens exposed to drying. The experimental results are compared with the theoretical model of the extended version of the CEB-FIP Model Code 1990.



## 4.2 Prediction models for creep and shrinkage in LWAC

The recommended extension to the CEB-FIP Model Code 1990 (*fib* 2000b) does not contain explicit formulations for creep and shrinkage due to the lack of sufficient experimental evidence. Only the observed tendencies on the available data are commented.

The Eurocode 2 and the Norwegian Standard specify multiplying factors for the elastic modulus and the notional creep coefficient. The Eurocode 2 also contains recommendation for shrinkage.

### 4.2.1 Modulus of elasticity

The modulus of elasticity for LWAC can be assumed equal to the value of normal density concrete of same strength multiplied by a factor which is given as function of the oven-dry density of the LWAC. Table 4.1 shows the multiplying factor as given in the extension to the CEB-FIP Model Code 1990, Eurocode 2 and the Norwegian Standard. The multiplying factors apply to the respective formulas for the elastic modulus of normal concrete given in Chapter 3.

### 4.2.2 Creep

The creep coefficient for LWAC can be assumed equal to the value of normal density concrete of same strength multiplied by the factor which is given as function of the oven-dry density of the LWAC. The multiplying factors are shown in Table 4.1 for the CEB-FIP Model Code 1990, Eurocode 2 and the Norwegian Standard. Since the extension to the CEB-FIP Model Code 1990 does not provide formulation for the multiplying factor of the creep coefficient, the formula in the table is derived from the comment which states that the specific creep of LWAC is about 20 % higher than that of NWC, the strength being the same.

Table 4.1 Multiplying factors for the elastic modulus,  $\eta_E$  and creep coefficient,  $\eta_\phi$

Design code	$\eta_E$	$\eta_\phi$	
CEB-FIP MC 90	$(\rho/2200)^2$	$1.2 (\rho/2200)^2$	
Eurocode 2	$(\rho/2400)^2$	$\rho > 1800 \text{ kg/m}^3$	$(\rho/2400)^2$
		$\rho < 1500 \text{ kg/m}^3$	$1.3 (\rho/2400)^2$
linear interpolation for intermediate values			
NS 3473 (1998)	$(\rho/2200)^2$	$\rho > 1800 \text{ kg/m}^3$	$(\rho/2200)^2$
		$\rho < 1500 \text{ kg/m}^3$	$1.3 (\rho/2200)^2$
linear interpolation for intermediate values			

$\rho$  is the oven-dry density of concrete

### 4.2.3 Shrinkage

The extension to the CEB-FIP Model Code 1990 states that the final shrinkage strain of LWAC is equal to that of NWC multiplied by a factor of 1.0 to 1.5.

According to Eurocode 2, the final drying shrinkage for LWAC may be estimated as equal to the value of normal density concrete of same strength multiplied by 1.2 for strength classes LC20 and higher. For strength classes below LC20, the multiplying factor is 1.5. The formulation for autogenous shrinkage of NWC can be used only when no supply of water from the aggregate to the drying microstructure is possible. Otherwise the autogenous shrinkage is considerably less in LWAC.

The Norwegian Standard does not contain information with respect to shrinkage of LWAC.

## 4.3 Experimental results in comparison with theoretical models

Experimental results are evaluated and compared to predicted values which were calculated according to the extended CEB-FIP Model Code 1990. The experiments used in this study were carried out in the past 15 years at SINTEF and NTNU. Description of the six experimental programs and the results are summarised in a EuroLightCon project report (Hynne 2000). Table 4.2 shows the basic properties of the concrete mixes and the use of the test results in the current study with respect to the modulus of elasticity, creep and shrinkage.

The creep data from the A92123 test program is included in the study but treated separately from the other series. The stress to strength ratio at those tests are higher than 0.4. Above that load level the stress-strain relationship is non-linear, thus the theory of linear viscoelasticity can not be used. Although non-linear creep is not within the scope of this work, these results are believed to be relevant to a certain extent.

Table 4.2 Experimental programs and their use in the current study

Test program	$f_{cm}$ [MPa]	$\rho$ [kg/m <sup>3</sup> ]		E	C	S
A97836	29 - 44	1300 - 1390	sealed, unsealed	+	+	+
A92029	46 - 56	1580 - 1700	unsealed	+	+	+
A99746	51 - 66	1640 - 1800	sealed, unsealed	+	+	+
A88011	60 - 63	1800 - 1830	sealed	+	+	
A92123	67 - 79	1810 - 1850	unsealed	+	*	
A93080	53	1760	sealed	+		

E - elastic modulus, C - creep, S - shrinkage

\* Not included in the overall statistical evaluation (see explanation in text above table).

The length of the tests vary from 3 months to 1 year. One test program (A99746) was specifically aiming to obtain creep data over a longer period of time. That program furnished results for a load duration of 1.5 year.

#### 4.3.1 Modulus of elasticity

Calculated and measured elastic moduli are compared in Figure 4.1. In addition to the experiments referred in Table 4.2, the values from Støvset Bridge and Stolma Bridge are included in the diagram. They are in good agreement with the tendency observed in the experimental results. While the agreement between the measurement and the theoretical formula is good for lower values of the elastic modulus, the formula has a tendency toward overestimating the elastic modulus for LWAC with higher values. These are typically the types of concrete with higher density and higher strength.

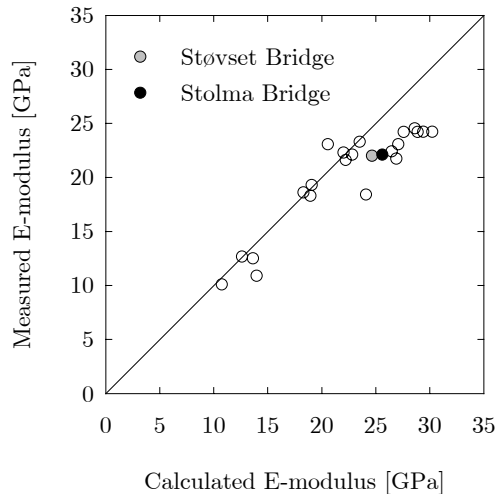


Figure 4.1 Comparison between calculated and measured modulus of elasticity of LWAC

The relationships are elaborated in Figure 4.2. It is seen that in a relatively narrow range of density (1780-1850 kg/m<sup>3</sup>) there are concrete specimens with a wide range of strength (53-79 MPa). The theoretical formula for the elastic modulus is a product of two terms, one considering the influence of the concrete strength and the other considering the influence of the density. According to the formulation the elastic modulus is increasing on the power of 1/3 with the strength and quadratically with the density. The predicted values for the elastic moduli follow the variation in strength accordingly. But it is observed that the measured values are influenced by the variation of the strength to a lesser extent than predicted.

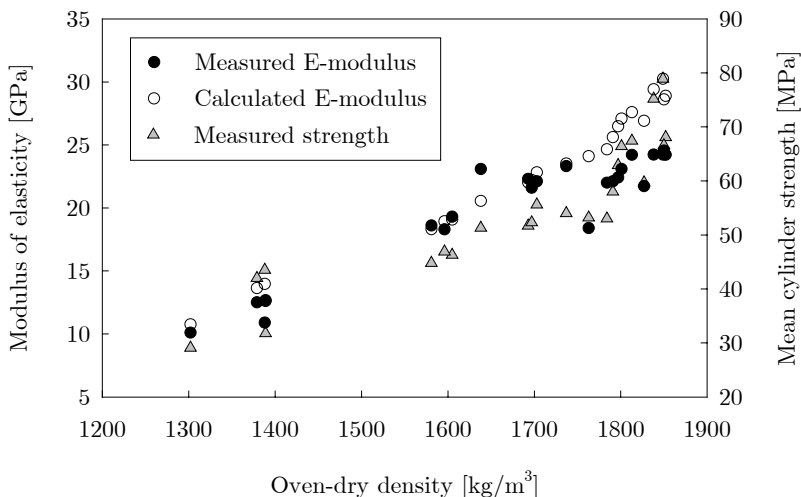


Figure 4.2 Measured and calculated elastic modulus and measured strength

### 4.3.2 Creep

Measured and calculated values of the creep compliance are compared in Figure 4.3 for each test program separately. The diagram shows the mean coefficient of variation for the prediction. It characterises the mean error of the prediction for the entire duration of loading. The mean coefficient of variation was computed according to the procedure described in (CEB 1990). The equations are presented in Appendix A.

The theoretical prediction for the sealed specimens were calculated under the assumption that the insulation is perfect and no external drying takes place.

Two tests series, A92029 and A99746 have a considerably large average coefficient of variation for the prediction, 51.6 % and 45.0 % respectively. In the former series, it is a result of systematic, large overestimation while the intrinsic scatter of the data points is relatively small. It should be noted that the average relative humidity for that series was about 40 % or slightly below. As the relative humidity of 40 % is the lower limit for the validity range of the theoretical model, the soundness of the prediction is questionable. Moreover the variation of the relative humidity during the tests was significant, it varied between 20 % and 67 %. The other two series, A97836 and A88011 have smaller average coefficient of variation, 17.7 % and 16.0 % respectively. For comparison, the reported coefficient of variation for the prediction method in the CEB-FIP Model Code 1990 is 20.4 % for normal density concrete (CEB 1990).

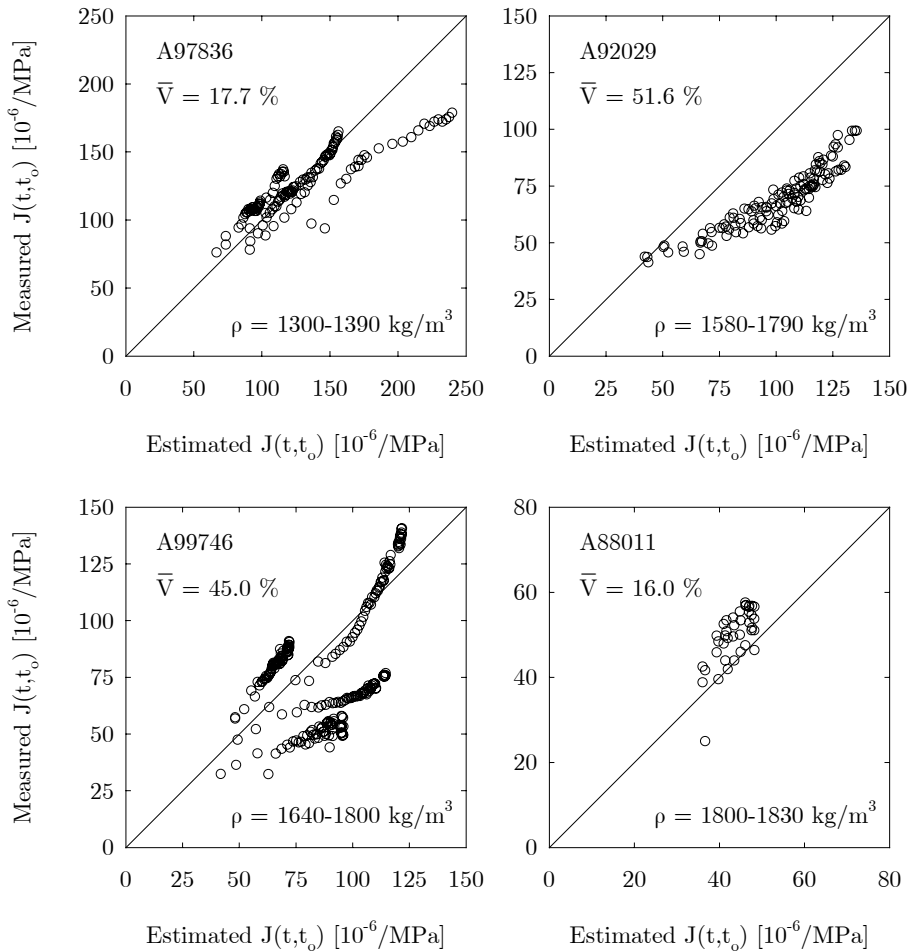


Figure 4.3 Comparison between estimated and measured values of the creep compliance

Certain tendencies are apparent when the experimental data is separated into experiments on sealed and unsealed specimens. The relation of measured creep to the prediction is shown accordingly in Figure 4.4. Under laboratory conditions the unsealed specimens are exposed to a dry ambient environment. The prediction is observed overestimating creep particularly in the early period of loading and drying. However, a tendency is seen in some of the experiments that the measured creep compliance increases more rapidly after a longer period of time than the predicted creep compliance does. In other experiments (*e.g.* typical for the A92029 series) the observed creep rate become similar to the prediction after an initial period of slower than predicted creep development. In conclusion, even if creep is overestimated on average (*vide* statistic in Table 4.3) over the limited duration of loading of

the available data, the tendency shows that after a longer period of time creep may increase at a higher rate and the final value of creep may be equal to predicted value or may exceed that. The delayed creep development is most certainly due to the initially slower drying process in lightweight aggregate concrete as that is suggested by several researchers (*vide* subsection 4.1).

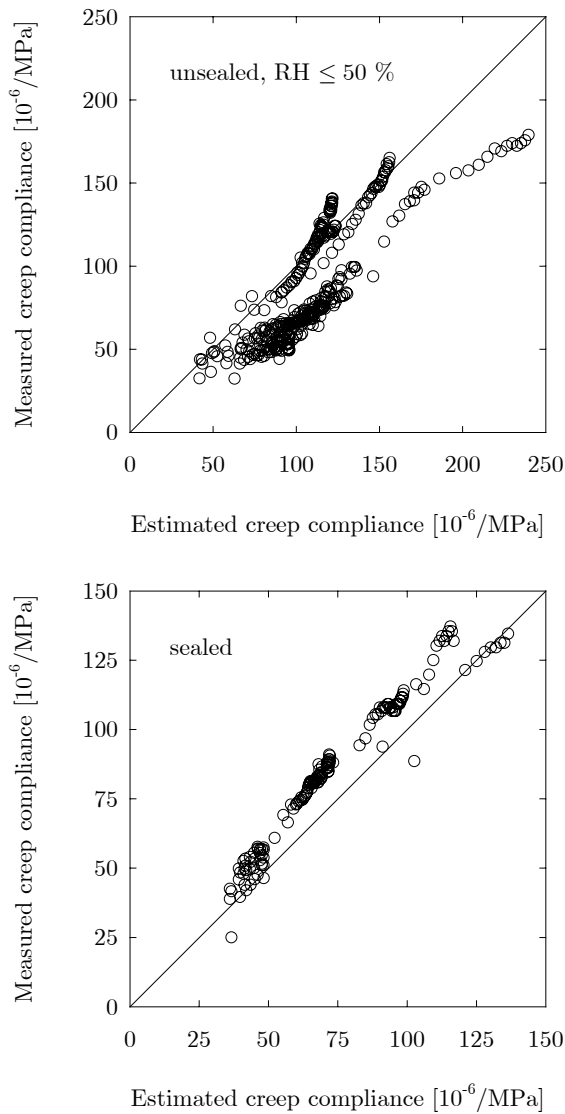


Figure 4.4 Comparison between estimated and measured values of the creep compliance in the unsealed specimens (above) and the sealed specimens (below)

The tendency is well illustrated in Figure 4.5 which shows the creep development for a long-term experiment with a load duration of 530 days. The unsealed and sealed specimens are made from the same concrete mix and subjected to the same load level. In the unsealed specimen the creep rate is lower than predicted in the early period of loading followed by a reverse tendency later. The creep rate in the sealed specimen is well estimated by the theoretical models. In fact the slightly higher observed creep rate may be the result of imperfect sealing.

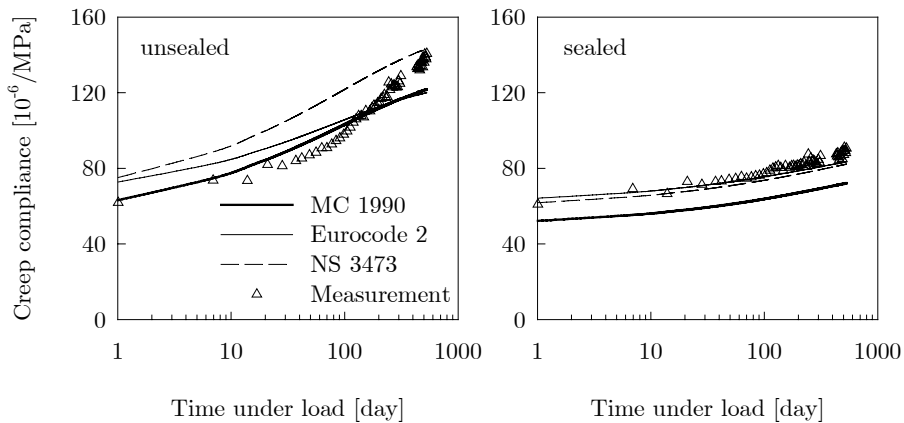


Figure 4.5 Creep in unsealed and sealed specimens in comparison with theoretical curves

Creep in the sealed specimens are somewhat underestimated by the MC90 model, although the creep rate on average does not deviate from the prediction (*vide* bottom diagram in Figure 4.4).

The statistical evaluation of the prediction method in relation to the experimental data is summarised in Table 4.3. The average deviation is the average of the mean percentage deviation of the predicted creep curves from the measured curves. It is calculated over the entire duration of loading. Negative value indicates systematic underestimation while positive value indicates systematic overestimation. The computation formulas can be found in Appendix A.

Table 4.3 Statistical evaluation of the prediction given by the MC90 model

	overall	unsealed	sealed
Coefficient of variation [%]	36.1	44.4	14.8
Average deviation [%]	17.2	34.3	-10.6

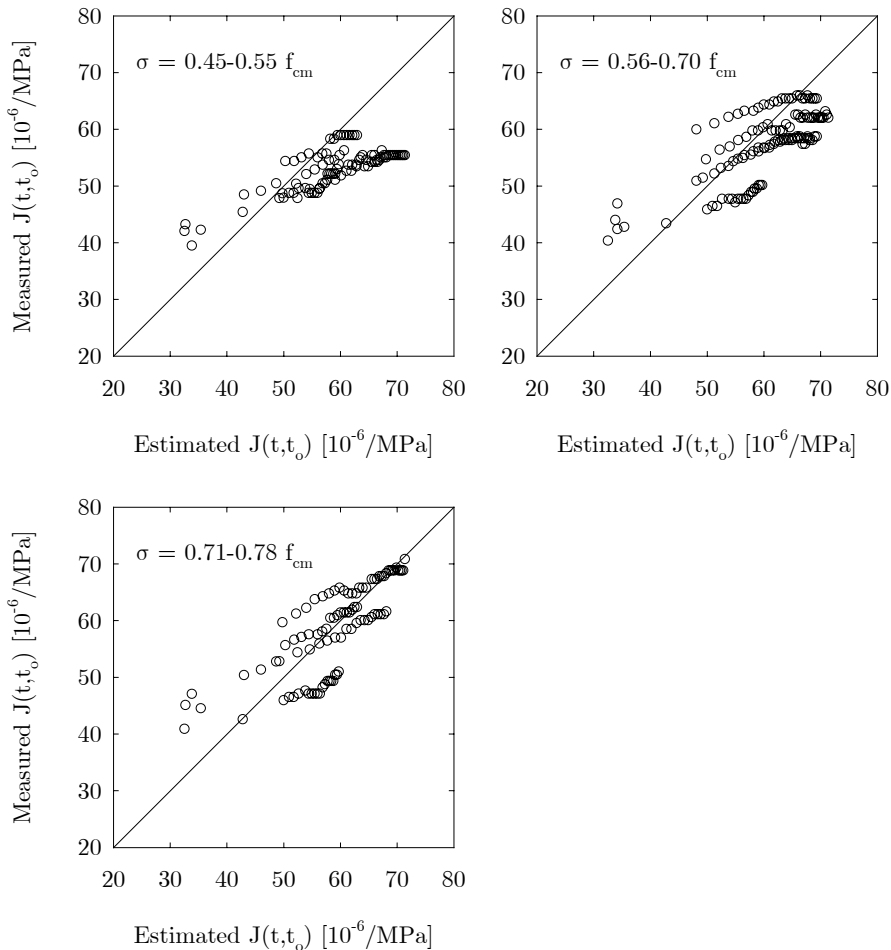


Figure 4.6 Observed creep at high stress level as compared to prediction by linear model

Experimental results from the A92123 test program are shown in comparison with the prediction model in Figure 4.6. The experiments are separated according to the load level. They were all carried out at a load level higher than 40 % percent of the mean cylinder strength, thus they are presumably influenced by non-linearity. The prediction was made by the linear creep model. That may explain the higher observed initial deformation. The creep development, however, is significantly slower than predicted. That is in accordance with the previous observations. The specimens were unsealed and exposed to a relative humidity of 50 %. The load durations were relatively short, it varied between 40 and 70 days. The non-linear influence is appreciable when the three diagrams are compared. As the load level is increasing the ratio of the observed creep to predicted creep is somewhat increasing.



### 4.3.3 Shrinkage

The influence of delayed drying which was observed on drying creep is more apparent on shrinkage. The tendency is characteristic for all test series shown in Figure 4.7. The theoretical predictions were made according to the MC 90 model given for normal weight concrete. The extension to MC 90 indicates that shrinkage of LWAC may exceed that of NWC by up to 50 %. The fourth diagram shows all the experiments together and contains a second data set where the estimated notional shrinkage coefficient given by the MC90 model is multiplied by 1.5. While the shrinkage strain is well overestimated on average over the duration of the experiments, the observed tendency suggests that the final shrinkage may be even higher than the increased prediction values.

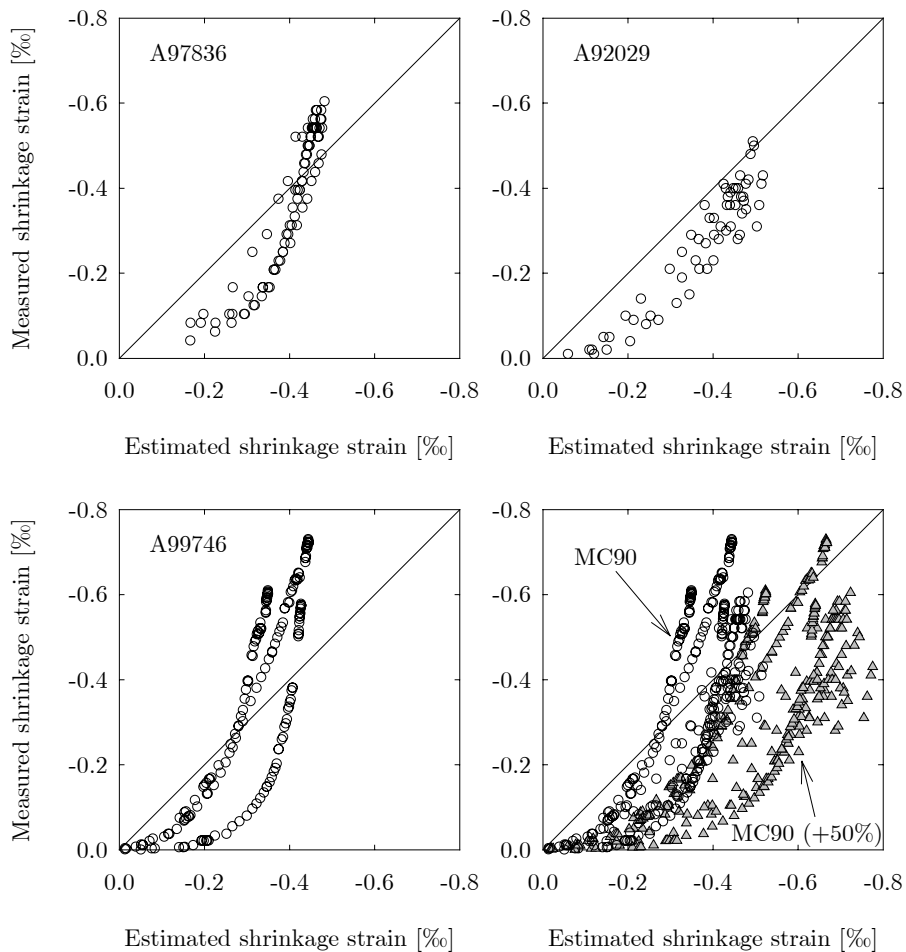


Figure 4.7 Comparison between estimated and measured values of the shrinkage strain

## 4.4 Conclusions

The elastic modulus was found overestimated by the extended MC 90 formula for high strength lightweight aggregate concrete. The observed difference is 12-18 % for concrete with mean cylinder strength of 53-67 MPa and oven-dry density of 1800 kg/m<sup>3</sup> and 17-25 % for concrete with mean cylinder strength of 60-79 MPa and oven-dry density of 1850 kg/m<sup>3</sup>. The elastic modulus was seen less influenced by the higher strength than it is expressed by the theoretical formula. In lower strength classes the formula was reasonably accurate.

Modelling creep and shrinkage development in lightweight aggregate concrete apparently requires a more sophisticated approach than simply adjusting the notional creep and shrinkage coefficient in the models that have been developed for normal density concrete. The drying process is seen considerably slower in the early period of drying which may be followed by a reverse tendency at later times. Consequently estimating the final value of creep and shrinkage by extrapolation based on short-term test data and with the time-dependency function of the normal density concrete may be false. Sufficient amount of *long-term* experimental information is necessary before clearer conclusions can be drawn. Experiments with a loading or drying duration of only a few months are inadequate and can be misleading.

As far as the available experiential data is concerned, the observed tendency indicates that the final specific creep of LWAC may be higher than that of NWC by 20 % (*c.f. fib 2000b*) or even more. The final value of shrinkage of LWAC is also seen to be considerably higher than that of NWC.

## Chapter 5

# Experimental Results on High Strength Concrete

*Experimental results on creep and shrinkage in high strength concrete and high performance concrete are discussed. The experiments were carried out at SINTEF in Norway in 1987-90 and at the Lund University in Sweden in 1991-96. The experimental data is evaluated in comparison with theoretical models.*

### 5.1 Introduction

It is generally acknowledged that the creep coefficient, as well as the specific creep, is decreasing with the increasing concrete strength. Drying shrinkage is also decreasing with higher strength. These tendencies are reflected by traditional prediction models which have been developed primary for normal strength concrete (NSC). However, it is recognised that those models do not take into account the particular characteristics of high strength concrete (HSC) and high performance concrete (HPC). The progress made in recent years in experimental work and development of new theoretical models is significant. The existing experimental data on long-term creep and shrinkage in HSC and HPC, however, is still limited.

Early experimental results on high strength concrete subjected to long-term sustained loads indicated that creep is considerably smaller in HSC than in NSC (Ngab *et al.* 1981 and Smadi *et al.* 1987), even to a larger extent than it was assumed based on tendencies observed in test results on concrete of lower strengths. Figure 5.1 shows the creep coefficient observed in low, medium and high strength concrete under identical conditions. It is seen that the influence of the strength on the creep coefficient is more pronounced than it is estimated by the CEB-FIP MC90 formula (*vide* Eq. 3.12). The European specification EC2 (ENV 1999) adopted the CEB-FIP MC90 creep model but it was adjusted in order to extend the validity

of the model to high performance concrete up to a strength of 110 MPa. The adjusted model was later included in the 1999 extension of the CEB-FIP Model Code 1990 (fib 1999). The model was reviewed in Chapter 3.

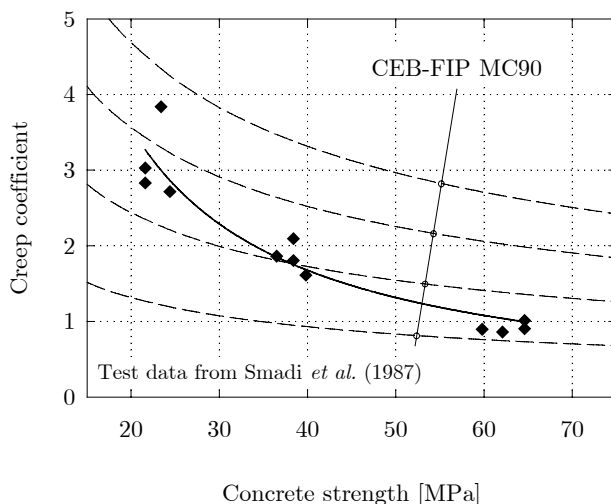


Figure 5.1 Strength dependency of the creep coefficient according to the experimental results from Smadi *et al.* (1987) and the CEB-FIP Model Code 1990

Shrinkage is commonly associated with the moisture loss in the concrete due to external drying. The meaning of shrinkage, however, is more general and it refers to the volume change in the unloaded concrete at constant temperature irrespective of the mechanisms involved. Besides drying shrinkage there are other types of shrinkage. For ordinary concrete it is reasonable to assume that external drying is the primary and in fact the only driving force behind shrinkage because the other types of shrinkage are considerably smaller in magnitude. On the other hand, autogenous shrinkage becomes more significant with the increasing strength due to the decreasing water to binder ratio which accompanies the higher strength. In high performance concrete autogenous shrinkage is a very significant component of the total shrinkage. It is therefore believed that traditional shrinkage models which considers only the drying mechanism underestimate total shrinkage for concrete of higher strength. That can be particularly significant in bulk concrete where the drying process is very slow. Whereas autogenous shrinkage is not influenced by external drying, it is uniform across the element and its magnitude is the same irrespective of the element size.

In the 1999 extension of the CEB-FIP Model Code 1990 (fib 1999) a new shrinkage model was presented where total shrinkage is subdivided into the drying shrinkage and the autogenous shrinkage component. With such an approach it was possible to formulate a

prediction model which can be used for both normal concrete and high performance concrete up to a strength of 120 MPa. The model was reviewed in Chapter 3.

In Norway long-term creep and shrinkage tests were carried out on high strength concrete at SINTEF (Tomaszewicz 1988 and 1993). The experimental results are used in this chapter to evaluate the theoretical material models. Also the experimental results on long-term creep from Persson (1998) are utilised here.

## 5.2 Experimental results from SINTEF

The test programs were part of a joint research project with the objective to study the general behaviour of HSC. The tests which are utilised here were executed in two phases, the first phase in 1987-88 and the second phase in 1989-90. Both test programs concerned also high strength lightweight aggregate concrete. Those test results were discussed in Chapter 4.

### 5.2.1 Description of the experiments

The first phase involved five test series. The specimens were cylinders with diameter of 100 mm and height of 300 mm. They were stored in water at a temperature of 20 °C until the start of loading. The specimens were unsealed. During the tests the temperature and the relative humidity was stable at 20 °C and 50 %, respectively. Further test parameters specific to the series are summarised in Table 5.1.

Table 5.1 Test data, Phase 1 (Tomaszewicz 1988)

Series no.	$f_{c,cyl100/300}$ [MPa]	concrete age at loading [day]	load duration [day]	load levels $\sigma/f_c$
1	48.3	127	49	0.48, 0.66, 0.78
2	79.6	176	67	0.36, 0.51, 0.69
3	76.8	48	28	0.49, 0.58, 0.75
4	102.4	231	70	0.45, 0.73
5	94.8	28	54	0.51
5R*	99.4	34	48	0.69, 0.72

\* replacement for series no. 5 due to failure of the original specimens

The second phase involved four test series. The specimens were cylinders with diameter of 100 mm and height of 300 mm. They were stored in water at a temperature of 20 °C until the start of loading. The tests involved sealed and unsealed specimens. During the tests the temperature was 20 °C and the relative humidity was 50 %. Further test parameters specific to the series are summaries in Table 5.2.

Table 5.2 Test data, Phase 2 (Tomaszewicz 1993)

Series no.	$f_{c,cyl100/300}$ [MPa]	concrete age at loading [day]	load duration [day]	load level $\sigma/f_c$	condition
1	69.4	43	34	0.50	sealed, unsealed
2	69.4	98	31	0.45	sealed, unsealed
3	76.0	34	88	0.50	sealed
4	77.5	38	65	0.46	sealed

Phase 2 involved test series on elevated temperature at 50 °C, but these series are not included here because of their little relevance to this study.

Load levels varied from 0.36 to as high as 0.78. Typically they were above 0.40-0.45 which value is considered the stress-strain proportionality limit for ordinary concrete with respect to both elastic and creep deformation. Deformation at such high load level is, in some degree, out of the scope of the current study. It is, however, believed that it is reasonable to consider these test results here as useful information can be derived.

To take into account the nonlinearity of creep in the calculation, the creep coefficient was adjusted according to the formula recommended in the CEB-FIP Model Code 1990. Nonlinearity in the instantaneous deformation was not considered. The nonlinear notional creep coefficient is defined for load levels between 0.40 and 0.60 as

$$\phi_{o,k} = \phi_o \cdot \exp[1.5(k_\sigma - 0.4)] \quad (5.1)$$

where

- $\phi_{o,k}$  is the nonlinear notional creep coefficient,
- $\phi_o$  is the linear notional creep coefficient, *vide* Eq. (3.10),
- $k_\sigma$  is the load level (stress to strength ratio).

While the above formula is used for the calculation, a few comments should be made concerning the effect of high load level on the instantaneous and the creep deformation. Based on experimental studies Ngab (1981) and Smadi (1987) indicated that the stress-creep proportionality limit in HSC is significantly higher than in NSC. They found the proportionality limit as 0.70 and 0.65, respectively. Evaluating the test results from Phase 1 Tomaszewicz (1988) found that the MC90 formula (*vide* Eq. (5.1)) overestimates the nonlinear influence in high strength concrete. Better agreement was established with the test results when the formula was modified as

$$\phi_{o,k} = \phi_o \cdot \exp\left[\frac{35}{f_{cm}}(k_\sigma - 0.4)\right] \quad (5.2)$$

The above formula considers the influence of the concrete strength on the magnitude of the nonlinear effect on creep.

Smadi (1987) found that also the stress-total strain proportionality limit is higher in high strength concrete than in ordinary concrete.

## 5.2.2 Elastic modulus

The measured elastic moduli are compared to the prediction formulae given in MC90 and the Norwegian Standard in Figure 5.2. In addition to the experimental results the elastic moduli measured on samples taken from Støvset Bridge and Stolma Bridge are shown. The measured values for the bridges show good consistency with the experimental values.

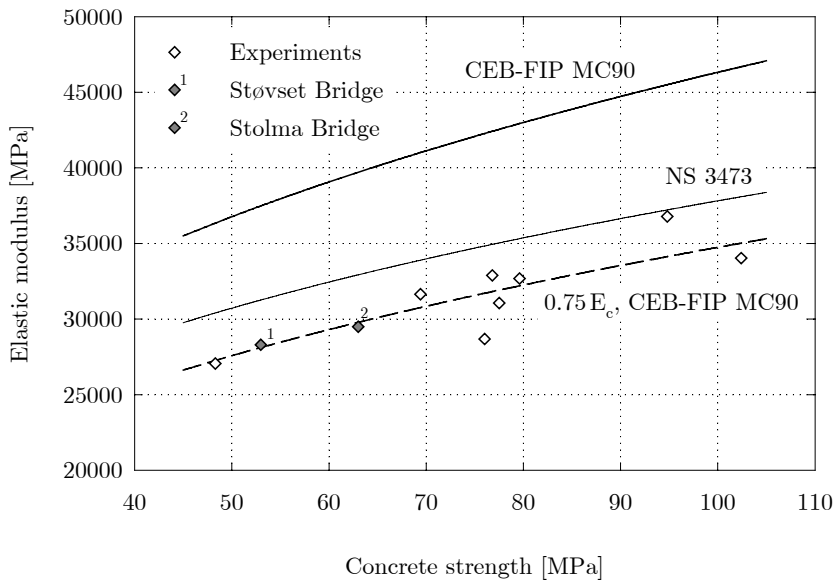


Figure 5.2 Measured elastic modulus in comparison with theoretical formulas

The measured values are seen 25 % lower on average than they are estimated by the MC90 formula. The large deviation is primary the result of the type of the aggregate. The aggregate which is typically used in Norway is softer than it is presumed by the MC90 formula.

### 5.2.3 Creep

In Figure 5.3 and Figure 5.4 the measured responses are compared with the predicted values as given by the MC90 and the MC90(99) models. The diagrams show the instantaneous responses and the total responses at the end of the loading period.

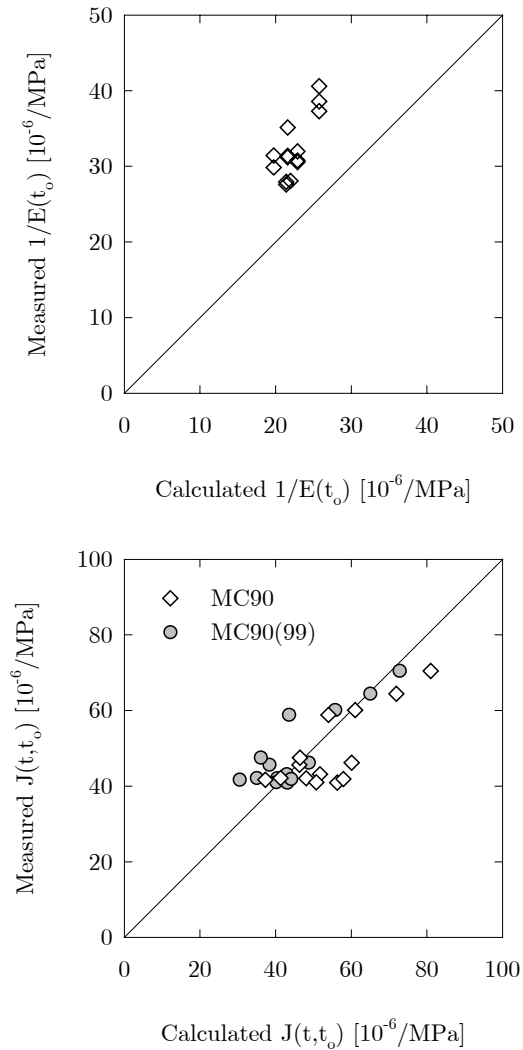


Figure 5.3 Measured deformation responses are compared with the calculated values at time zero (above) and at the end of the loading period (below), test results from Phase 1

The instantaneous deformation is underestimated by the theoretical formula as that was foreseen from the test results on the elastic modulus. While the measured elastic moduli



were found 25 % lower than predicted, the reciprocal of the instantaneous responses are 28 % lower on average than predicted. The difference may be attributed to the non-linearity due to the high load levels. For the instantaneous deformation only one set of data points is seen because the prediction formula for the elastic modulus is the same in the 1999 version of the Model Code.

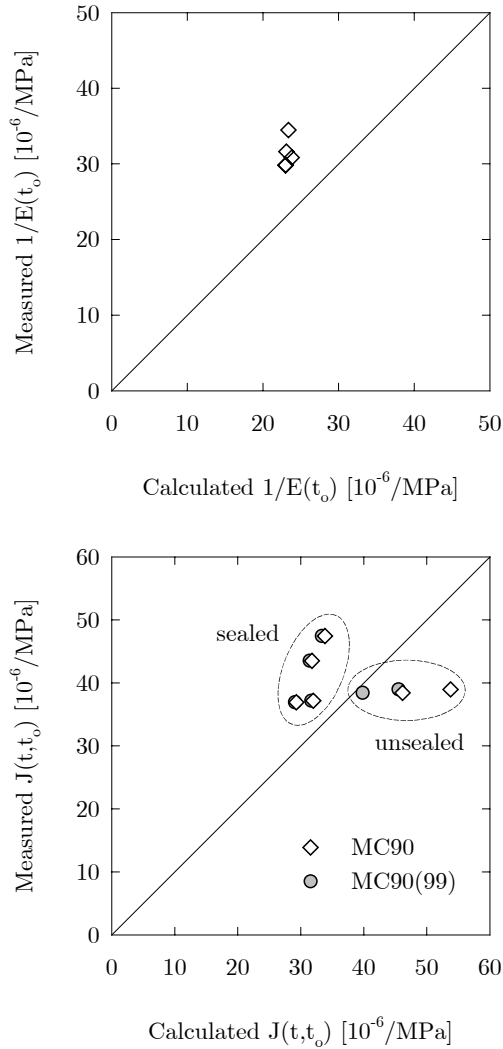


Figure 5.4 Measured deformation responses are compared with the calculated values at time zero (above) and at the end of the loading period (below), test results from Phase 2

The total stress dependent deformation at the end of the loading period is slightly overestimated on average by the MC90 model and slightly underestimated on average by the MC90(99) model. The mean coefficient of variation for the predictions are 22 % and 16 %, respectively.

In the calculation the creep coefficient was increased by an average of 30 percent according to Eq. (5.1) due to the high load level.

### 5.2.4 Shrinkage

The measured shrinkage strain in the unsealed specimens are shown in Figure 5.5 in comparison with the predictions given by the theoretical models. The scatter of the data points is large but the improvement in the prediction by the MC90(99) model is clearly visible. The mean coefficient of variation for the MC90 prediction is 43 % with a significant systematic underestimation. The mean coefficient of variation for the MC90(99) prediction is 25 %, but the average tendency is good.

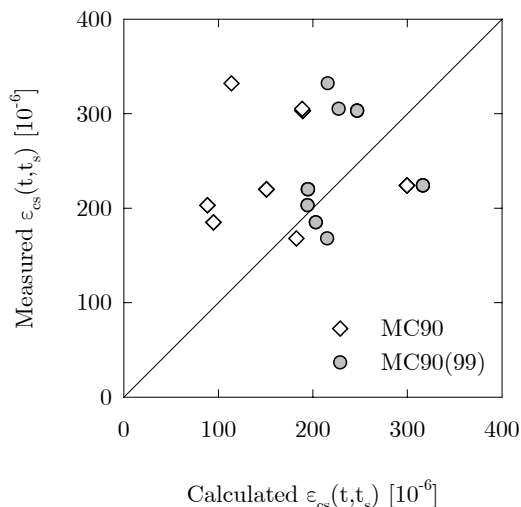


Figure 5.5 The measured shrinkage strain at the end of the drying period as compared to the predictions

### 5.3 Experimental results from Persson

The long-term creep tests were carried out by Persson (1998) at the Lund University in Sweden as part an extensive experimental and numerical study on deformations of high performance concrete.

### 5.3.1 Description of the experiments

Eight concrete mixes were involved in the tests. Four tests were carried out on each concrete mix. A sealed and an unsealed specimens were tested with a concrete age at loading of 2 days and also a sealed and an unsealed specimens were tested with a concrete age at loading of 28 days. The load level was 0.42. Identical test series were carried out with the same arrangements at the load level of 0.84 but those results are not discussed here. The specimens were cylinders with diameter of 55.5 mm and height of 200 mm. The tests were performed at temperature of 20 °C and relative humidity of 55 %. The load duration varied from 1070 days to 1690 days. Table 5.3 shows the concrete strength for the concrete mixes. The strength was tested on 100 mm cubes at the age of 28 days.

Table 5.3 Concrete strength

Mix no.	$f_{c,cube100}$ [MPa]	$f_{c,cyl150/300}$ [MPa]
1	89	66
2	105	77
3	95	70
4	101	74
5	121	89
6	126	93
7	122	90
8	129	95

For the calculation the concrete strength determined on 100 mm cube had to be transformed into an equivalent 150/300 cylinder strength. The transformation was made according to Eq. (5.5) which relationship was established from Eq. (5.3) (Morabito *et al.* 2000) and Eq. (5.4) (ENV 206 1990).

$$f_{c,cube150} = 0.916 f_{c,cube100} \quad (5.3)$$

$$f_{c,cyl160/320} = 0.805 f_{c,cube150} \quad (5.4)$$

Since the dimensions of the 160/320 cylinder do not differ much from the dimensions of the 150/300 cylinder, equivalency between the strength of the two cylinders is assumed.

$$f_{c,cyl150/300} \simeq 0.74 f_{c,cube100} \quad (5.5)$$

### 5.3.2 Experimental creep data in comparison with theoretical models

The large number of test series enabled a sound statistical assessment of the test results. The experimental results are examined in comparison with three models. The models are the CEB-FIP Model Code 1990, the 1999 version of the Model Code and the creep model in the Norwegian Standard. A fourth calculation was made which followed the lines of the CEB-FIP Model Code 1990 but the elastic modulus was multiplied by 0.75. It is meant to consider a potentially lower elastic modulus as it was found in the Norwegian experiments (*vide* Figure 5.2). The type of the aggregate is different here, thus the multiplying factor of 0.75 should not be seen as the probable factor concerning the influence of the aggregate stiffness on the elastic modulus but rather an assumed lower limit. The 25 % lower elastic modulus consequently results in a 33 % higher creep compliance.

The creep in the sealed specimens were calculated under the assumption that the insulation is perfect and no moisture exchange takes place with the ambient environment.

Figure 5.6 shows the measured values of the creep compliance in comparison with the predicted values. The corresponding statistical measures are shown in Table 5.4. A tendency toward underestimation is observed in case of the MC90 model. That is interesting in view of the fact that the MC90 model is believed to overestimate creep for concretes of higher strength. The underestimation by the MC90(99) model is consequently even larger in magnitude, however, the model furnished the smallest intrinsic scatter.

Table 5.4 Statistical evaluation of the predictions<sup>1</sup>

	Mean coefficient of variation for the prediction[%]			
	<i>Average deviation* [%]</i>			
	MC90	MC90(99)	NS 3473	MC90(0.75E)
Total creep	22.3	30.7	36.9	41.4
(unsealed spec.)	-6.4	-25.7	17.9	24.7
Basic creep	25.2	27.2	16.9	17.4
(sealed spec.)	-20.3	-22.4	-5.7	6.3
Overall	23.8	29.0	28.7	31.7
	-13.4	-24.0	6.1	15.5

\*negative value indicates underestimation, positive value indicates overestimation

<sup>1</sup> The mean coefficient of variation for the prediction characterises the mean error over the entire duration of loading. It is the most relevant statistical measure for the prediction. The average deviation is the average of the percentage difference of the predicted value from the observed value in all data points. Consequently the average deviation is calculated here for the entire load duration. High negative value of this measure indicates systematic underestimation by the theoretical model and high positive value indicates systematic overestimation. The calculation formulas can be found in Appendix A.

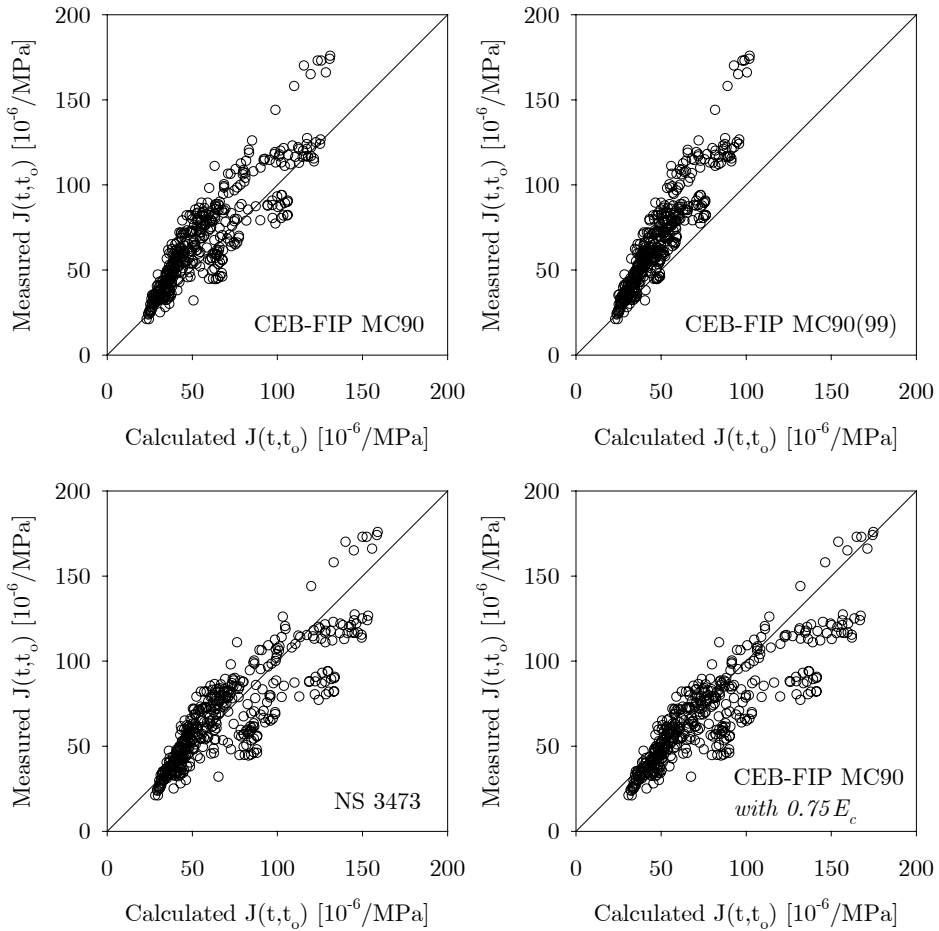


Figure 5.6 Experimental values of the creep compliance in comparison with theoretical models (all data points from the 32 test series are included in the diagrams) (Persson 1998)

The model in the Norwegian Standard and the MC90 model with the lowered elastic modulus (MC90(0.75E)) overestimated the observed creep values. The NS model has a low average deviation which indicates a good overall tendency, however, the mean error has the same magnitude as the other models. It is seen that the mean error for the unsealed specimens (total creep) and sealed specimens (basic creep) significantly differ in case of these two models while the respective values for the MC90 and MC90(99) models are similar in magnitude.

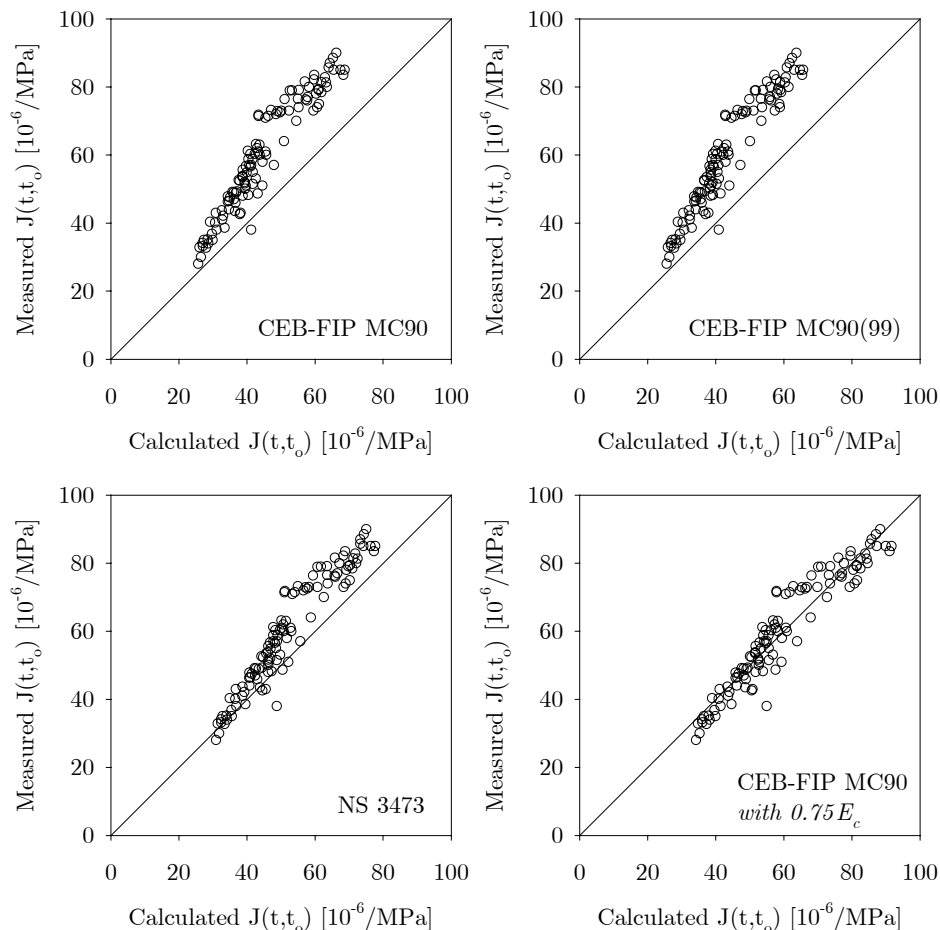


Figure 5.7 Experimental values of the creep compliance in comparison with theoretical models, sealed specimens (basic creep) with concrete strength between 66 and 77 MPa (Persson 1998)

It is also observed that the accuracy of the prediction is significantly influenced by the concrete strength for the NS model and MC90(0.75E). The eight concrete mixes can be sorted into two classes. The cylinder strength of the first four mixes vary from 66 to 77 MPa and the cylinder strength of the other four mixes vary from 89 to 95 MPa (*vide* Table 5.3).

The comparison between the experimental data and the predicted values are shown separately for the sealed and unsealed specimens and for the two concrete strength ranges (*vide* Figure 5.7, Figure 5.8, Figure 5.9 and Figure 5.10). Each diagram contains results from

eight experiments. The mean coefficient of variation for the predictions are shown accordingly in Table 5.5.

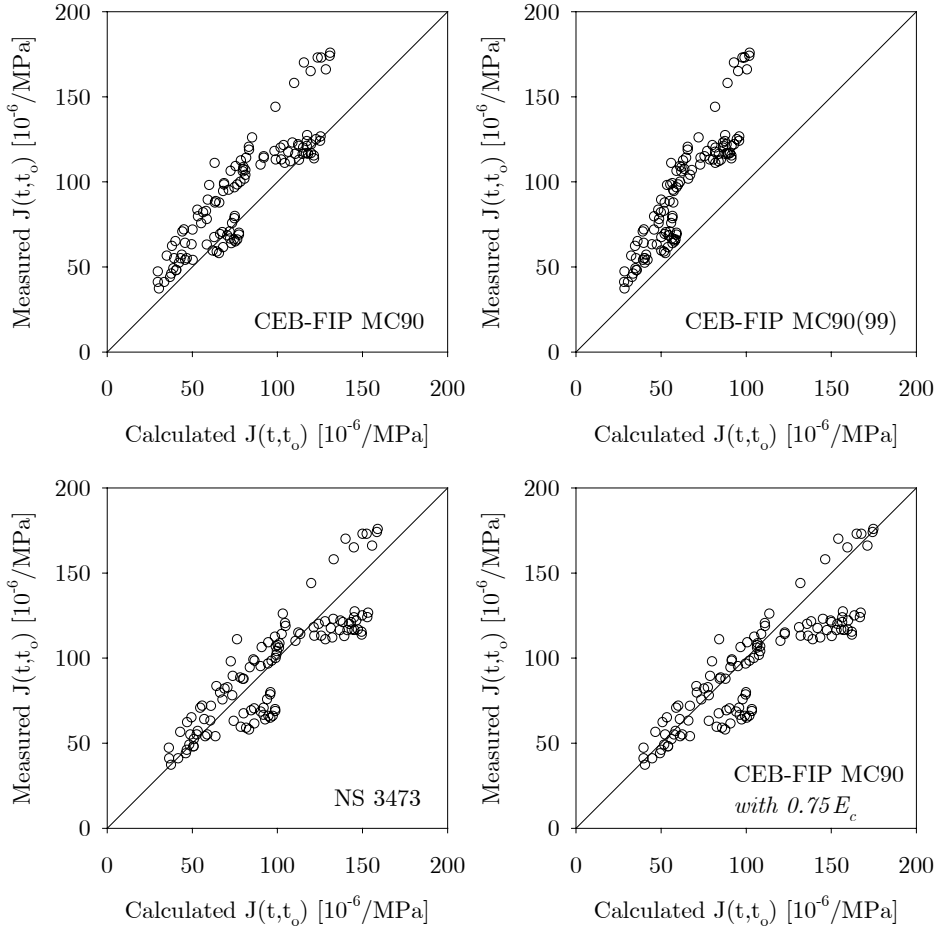


Figure 5.8 Experimental values of the creep compliance in comparison with theoretical models, unsealed specimens (total creep) with concrete strength between 66 and 77 MPa (Persson 1998)

The inherent scatter is small for the sealed specimens in the lower strength range in case of all four models. It increases for the unsealed specimens and in the higher strength range.

The models underestimate the creep deformation in the sealed specimens. The underestimation is particularly significant in the higher strength range.

The prediction error is the smallest for the NS model with the exception of the unsealed specimens in the higher strength range.

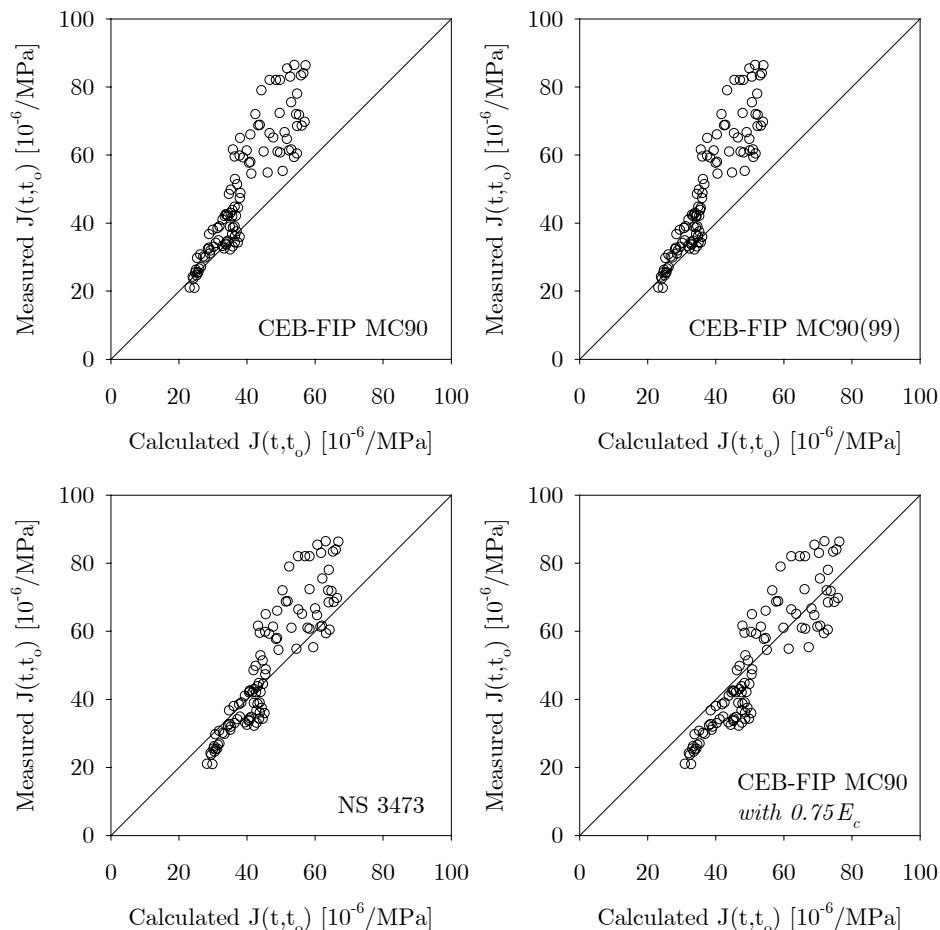


Figure 5.9 Experimental values of the creep compliance in comparison with theoretical models, sealed specimens (basic creep) with concrete strength between 89 and 95 MPa (Persson 1998)

Table 5.5 Mean coefficient of variation for the predictions

$f_{c,cyl}$ [MPa]		MC90	MC90(99)	NS 3473	MC90(0.75E)
66 - 77	basic creep	27.1	29.3	15.2	8.4
	total creep	21.7	35.5	21.2	25.3
89 - 95	basic creep	23.1	24.9	18.5	23.1
	total creep	22.8	25.0	47.7	52.7
Overall		23.8	29.0	28.7	31.7



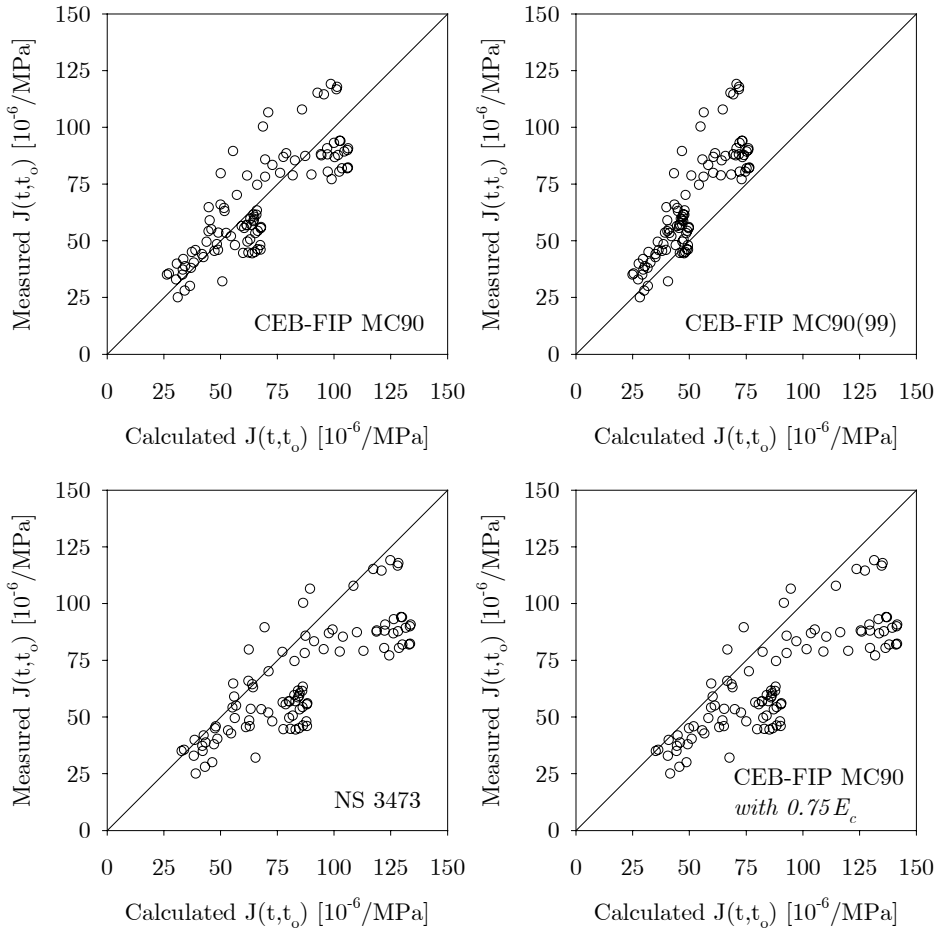


Figure 5.10 Experimental values of the creep compliance in comparison with theoretical models, unsealed specimens (total creep) with concrete strength between 89 and 95 MPa (Persson 1998)

## 5.4 Conclusions

Based on the results of the experimental programs carried out in Norway, the following conclusions can be made.

The elastic modulus is seen 25 % lower than estimated by the MC90 formula. The same relationship was found in the concrete samples taken from Stolma Bridge and Støvset Bridge. The deviation is the result of the lower stiffness aggregate which is typically used in Norway.

The shrinkage strain is underestimated by the MC90 model in concretes of higher strength. The prediction is significantly improved in the MC90(99) model which takes into account the larger autogenous shrinkage component which accompanies the higher strength. Nevertheless the mean observed error of the prediction is significant.

The predicted creep is seen in reasonable agreement with the experiments. However, it is difficult to draw conclusions due to the significant uncertainty about the nonlinear influence due to the high load levels.

Concerning the creep experiments carried out by Persson, the observed long-term deformations were found higher than predicted by the MC90 model. Since the MC90(99) model gives smaller creep deformation in HSC and HPC, the error was found even larger for the MC90(99) model.

## Chapter 6

# Mathematical Modelling of Viscoelasticity

*The chapter reviews the mathematical modelling of the viscoelastic material behaviour of concrete. A rate-type solution algorithm suitable for robust numerical computations is described. The solution method is based on the Maxwell and Kelvin Chain models. Finally the procedure used to determine the chain parameters from creep and relaxation curves are presented.*

### 6.1 Introduction

To calculate the strain response to a certain stress history or the stress response to a certain strain history one can use the classical Riemann integral equations if the stress or strain history is known *a priori* and they are expressed as continuous functions<sup>1</sup>.

$$\varepsilon(t) = \int_0^t J(t, \tau) \bar{C} \dot{\sigma}(\tau) d\tau \quad (6.1)$$

$$\sigma(t) = \int_0^t R(t, \tau) \bar{D} \dot{\varepsilon}(\tau) d\tau \quad (6.2)$$

The principle of superposition constitutes the fundamental basis for the integral equations. The principle is equivalent to the hypothesis of linearity in the stress-strain relation. The principle of superposition was first proposed by Boltzmann in 1876 and extended to aging materials by Volterra in 1913. A historical review on the superposition principle of strains was given by Bazant (1986).

---

<sup>1</sup> To admit discontinuous stress or strain history the Riemann integral must be replaced by Stieltjes integral.

For general structural computations, however, the stress or strain history is not known beforehand. Therefore a step-by-step solution algorithm must be implemented where the computation is discretised by finite time increments. The integral formulations then are replaced by finite sums. Such a formulation, however, has the inconvenient feature that the strain (or stress) increment at any new time step is calculated as a function of the entire previous stress (or strain) history. This makes the formulation impractical for large computations because the entire stress (or strain) history must be stored for each computational point and an excessively long sums of strain (or stress) values must be computed at each time step. That would require large storage capacity and long computational time to an unreasonable extent.

A different formulation is preferable where the stress increment at a new time step can be calculated from the strain increment and a finite number of *state variables*, all of which are known at the beginning of the time step. The relaxation function has to be rewritten in a form which enables to formulate such an algorithm. If the viscoelastic behaviour is described by the creep function, a similar fashion has to be followed but the constitutive relation also has to be rewritten in a way that the stress increment is expressed as the function of the strain increment (de Borst and van den Boogaard 1994). This is necessary because the displacements are the basic variables in the finite element method.

The relaxation and creep functions are rewritten as sums of real exponential functions (the equations will be explained later in the chapter):

$$R(t, \tau) = \sum_{\alpha=0}^n E_{\alpha}(\tau) e^{-\frac{t-\tau}{\lambda_{\alpha}}} \quad (6.3)$$

$$J(t, \tau) = \sum_{\alpha=0}^n \frac{1}{E_{\alpha}(\tau)} \left( 1 - e^{-\frac{t-\tau}{\lambda_{\alpha}}} \right) \quad (6.4)$$

From a mathematical perspective Eq. (6.3) and Eq. (6.4) are the approximation of the relaxation and creep function with Dirichlet series. From a physical perspective they can be interpreted as the governing equations of the Maxwell and the Kelvin Chain models.

## 6.2 Viscoelastic models

Rheological models can be constructed by combining theoretical bodies with ideal rheological properties. To set up models for linear viscoelastic behaviour the ideal bodies are the Hookean solid body (*i.e.* perfect linear elasticity) and the Newtonian liquid body (*i.e.* perfect linear viscosity). The idealised deformations are represented by a spring and a dashpot respectively.

Rheological models consisting of springs and dashpots are not intended to capture the physical mechanisms of the viscoelastic behaviour of concrete on a microscopic level. This approach is largely empirical and it is simply to approximate the overall deformation pattern of concrete by assigning specific parts of overall deformation to given components of the model. They represent physical properties of continua and they can be interpreted from a macroscopic point of view only.

### 6.2.1 Basic viscoelastic models

There are two basic models, known as the Maxwell element and Kelvin element<sup>1</sup>. In the Maxwell element a spring and a dashpot are connected in series while in the Kelvin element a spring and a dashpot are connected in parallel. Neither of the two basic models on its own is capable of describing sufficiently every aspects of the viscoelastic behaviour of concrete. But they are the fundamental components of more complex models. An isolated spring or dashpot can be considered as a degenerate form of either the Maxwell or the Kelvin element. The two most important models are the Maxwell Chain model where finite number of Maxwell elements are connected in parallel and the Kelvin Chain model where finite number of Kelvin elements are connected in series. As the Maxwell and the Kelvin elements are the basic components of the chain models, their behaviour is examined first.

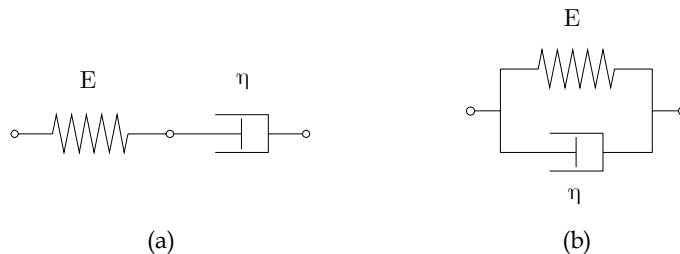


Figure 6.1 (a) Maxwell element and (b) Kelvin element

The spring and the dashpot are in series in the Maxwell element. Consequently the stress is the same in both bodies while the total strain is the sum of the strains in each. (It would be more precise to talk in terms of forces and displacements but the spring and the dashpot are imaginary bodies representing the same continuum, *i.e.* they coexist within the same geometrical dimensions.)

$$\sigma = \sigma^{spring} = \sigma^{dashpot} \quad (6.5)$$

$$\varepsilon = \varepsilon^{spring} + \varepsilon^{dashpot} \quad (6.6)$$

<sup>1</sup> The models are named after Scottish scientists, J.C. Maxwell and W.T. Kelvin (later Lord Kelvin).

Hence the governing differential equation is written as

$$\frac{d\varepsilon}{dt} = \frac{1}{E} \frac{d\sigma}{dt} + \frac{1}{\eta} \sigma \tag{6.7}$$

where

$E$  is the elastic modulus of the spring,

$\eta$  is the viscosity of the dashpot.

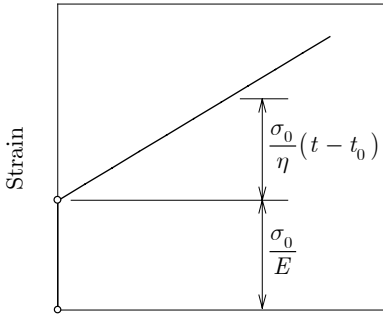
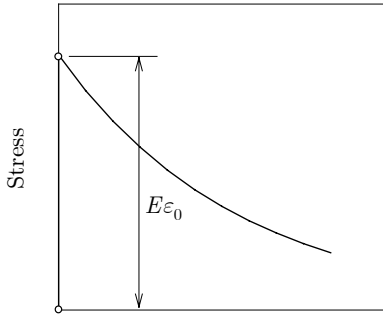
Creep	Relaxation
$\frac{d\sigma}{dt} = 0 \quad \sigma = \sigma_o$	$\frac{d\varepsilon}{dt} = 0 \quad \varepsilon = \varepsilon_o$
Differential equation $\frac{d\varepsilon}{dt} = \frac{1}{\eta} \sigma_o$	Differential equation $\frac{1}{E} \frac{d\sigma}{dt} + \frac{1}{\eta} \sigma = 0$
Boundary condition $t = t_o \quad \varepsilon = \varepsilon_o = \frac{\sigma_o}{E}$	Boundary condition $t = t_o \quad \sigma = \sigma_o = E\varepsilon_o$
Solution $\varepsilon = \sigma_o \left( \frac{1}{E} + \frac{1}{\eta} (t - t_o) \right) \tag{6.8}$	Solution $\sigma = E\varepsilon_o e^{-\frac{E}{\eta} (t - t_o)} \tag{6.9}$
	

Figure 6.2 Maxwell element in creep and relaxation

Figure 6.2 shows the behaviour of the Maxwell element in creep and relaxation. Under constant stress (creep) the strain is increasing infinitely at a constant rate after the

instantaneous deformation. Therefore it essentially represents a liquid. If the stress were removed at time  $t^*$  the elastic strain would recover instantly while no recovery of the viscous strain would take place. The strain would remain constant at a value of  $\sigma_o / \eta (t^* - t_o)$  for non-ageing materials. Apparently the Maxwell element captures the main characteristics of creep rather poorly. As for relaxation the behaviour of the Maxwell element is more realistic. If the element is subjected to a constant strain the stress is decreasing exponentially being divided in its value by  $e$  per unit value of the relaxation time ( $E / \eta$ ). The relaxation is complete after infinitely long time.

The spring and the dashpot are in parallel in the Kelvin element. Consequently the strain is the same in both bodies while the total stress is the sum of the stresses in each.

$$\varepsilon = \varepsilon^{spring} = \varepsilon^{dashpot} \quad (6.10)$$

$$\sigma = \sigma^{spring} + \sigma^{dashpot} \quad (6.11)$$

The governing differential equation is written as

$$\sigma = E\varepsilon + \eta \frac{d\varepsilon}{dt} \quad (6.12)$$

Figure 6.3 shows the behaviour of the Kelvin element in creep and relaxation. Under constant stress the strain is increasing with time exponentially without instantaneous deformation. The strain is approaching a final asymptotic value of  $\sigma_o / E$ . This is equal to the instantaneous deformation of the spring on its own. Initially the dashpot is carrying the entire load but with time that is transferred to the spring at a decreasing rate. After an infinitely long time the spring will carry the entire load. If the load were removed at time  $t^*$  the strain would recover exponentially. The recovery would be complete after an infinitely long time. The recovery regime can be described with the following function:

$$\varepsilon = K(t^*) e^{-\frac{E}{\eta}(t-t_o)} \quad (6.13)$$

where the value of  $K(t^*)$  can be determined from the condition that the strain is equal at  $t = t^*$  from Eq. (6.13) and (6.15). For non-ageing materials that is

$$K(t^*) = \frac{\sigma_o}{E} \left( e^{\frac{E}{\eta}(t^*-t_o)} - 1 \right) \quad (6.14)$$

Thus, the Kelvin element can describe creep considerably well but on its own it does not represent the elastic deformation. On the other hand the Kelvin element is not capable of describing relaxation. If constant load is applied on a Kelvin element for a certain period of time the strain develops according to Eq. (6.15). If then the strain is fixed and the external load is removed at time  $t_o$ , the stress instantaneously drops to  $E\varepsilon_o$  which is the stress in the

spring at that point of time and remains constant afterwards (*vide* diagrams on the right in Figure 6.3).

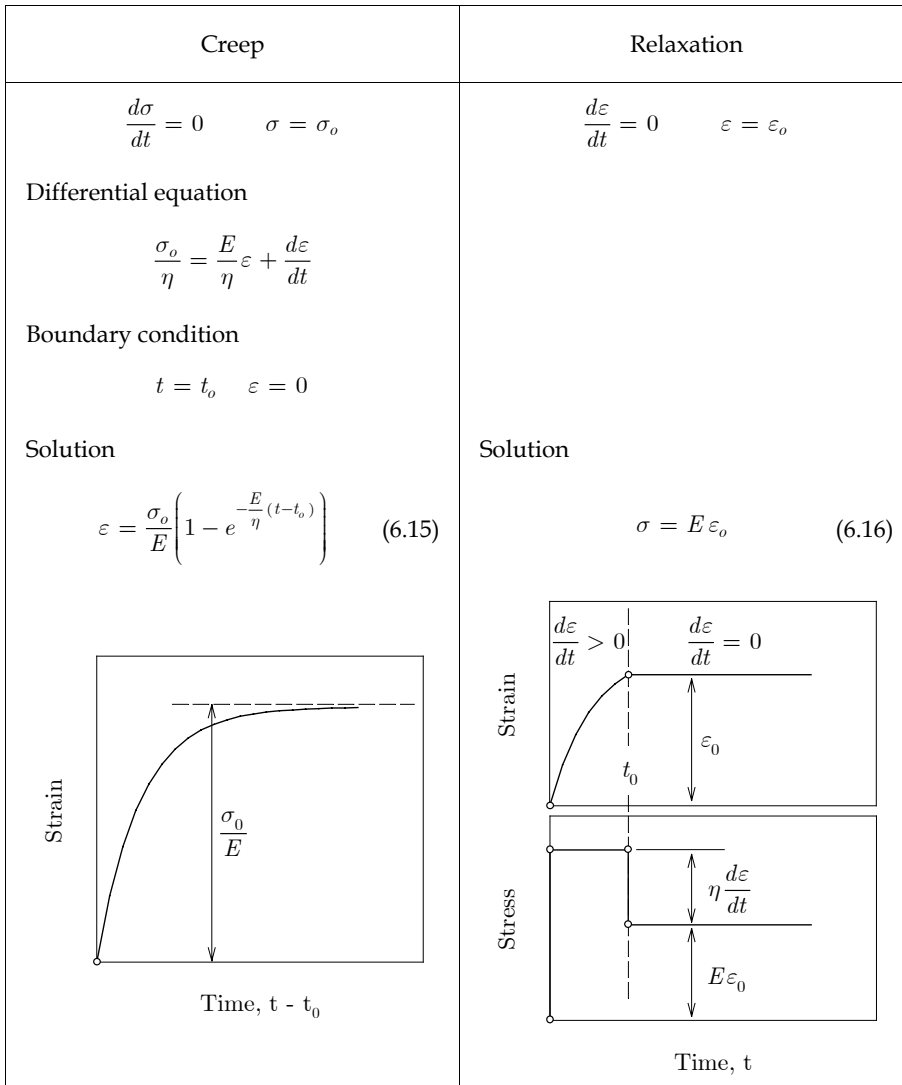


Figure 6.3 Kelvin element in creep and relaxation

### 6.2.2 Maxwell and Kelvin Chain models

Whereas neither a simple Maxwell element nor a Kelvin element is able to properly model all aspects of the viscoelastic behaviour, the more complex Maxwell and Kelvin Chain models can approximate the real deformation pattern with sufficient accuracy. The success



of the good approximation depends on the ability of certain components of the model to approximate certain parts of the overall deformation pattern.

In the Maxwell Chain model finite number of Maxwell elements are connected in parallel (*vide* Figure 6.4). The first element ( $\alpha = 0$ ) is a spring with no dashpot and can be considered as a degenerated Maxwell element<sup>1</sup>. The strain is equal in each element while the total stress is the sum of the stresses in the individual elements. Utilising Eq. (6.9) the relaxation function can be written as

$$R(t, \tau) = E_o(\tau) + \sum_{\alpha=1}^n E_{\alpha}(\tau) e^{-\frac{t-\tau}{\lambda_{\alpha}}} \quad (6.17)$$

where  $\tau$  is the age of the concrete at loading and  $\lambda_{\alpha}$  is the relaxation time of the  $\alpha$  th element which is defined as

$$\lambda_{\alpha} = \frac{\eta_{\alpha}}{E_{\alpha}} \quad (6.18)$$

Ageing is introduced in Eq. (6.17). The stiffness of the springs,  $E_{\alpha}$  are age-dependent while the relaxation times,  $\lambda_{\alpha}$  are constant values. It means that the development of the viscosity of the dashpot and the stiffness of the spring with age follow the same time function, so their proportion,  $E_{\alpha} / \eta_{\alpha}$  remains constant.

In the Kelvin Chain model a finite number of Kelvin elements are connected in series (*vide* Figure 6.5). The first element ( $\alpha = 0$ ) is a spring with no dashpot and can be regarded as a degenerated Kelvin element<sup>2</sup>. The stress is equal in each element while the total strain is the sum of the strains in the individual elements. Utilising Eq. (6.15) the creep function can be written as

$$J(t, \tau) = \frac{1}{E_o(\tau)} + \sum_{\alpha=1}^n \frac{1}{E_{\alpha}(\tau)} \left( 1 - e^{-\frac{t-\tau}{\lambda_{\alpha}}} \right) \quad (6.19)$$

where  $\lambda_{\alpha}$  is the retardation time of the  $\alpha$  th element and can be calculated as Eq. (6.18).

It is generally considered that the Maxwell Chain model is better suited for relaxation dominated problems while the Kelvin Chain model is better suited for creep dominated problems. That is because the former is based on the relaxation function while the latter is based on the creep function. Practically both models are equally capable of representing the viscoelastic behaviour of concrete.

---

<sup>1</sup> As an alternative approach it can be considered as a regular Maxwell element with a sufficiently long relaxation time, min. 1000 times longer than the longest load duration.

<sup>2</sup> Along the same analogy as for the Maxwell model, the single spring can alternatively be considered as a regular Kelvin element with the viscosity of the dashpot being equal to zero.

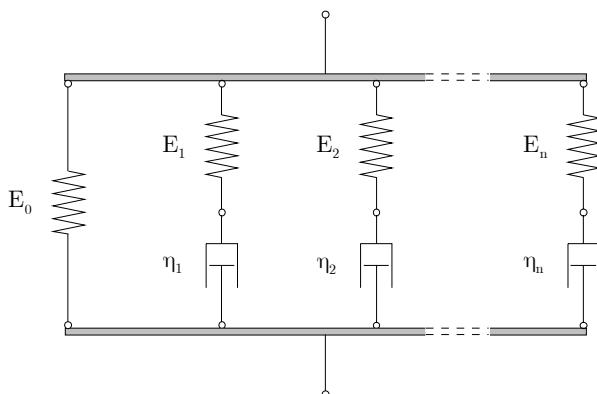


Figure 6.4 Maxwell Chain model

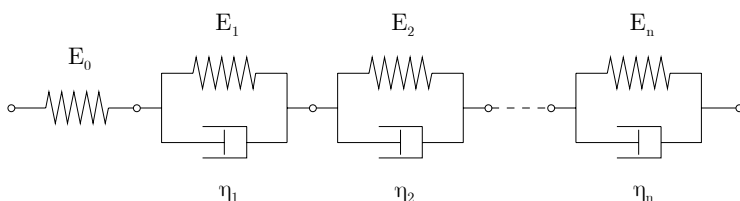


Figure 6.5 Kelvin Chain model

### 6.3 Rate-type constitutive relations

With the relaxation and creep functions now being written as sums of real exponential functions (*vide* Eq. (6.17) and Eq. (6.19)) rate-type constitutive equations can be formulated. The rate-type formulation has the advantage that there is no need to keep and evaluate information from all the previous time steps but the relationship between the stress and strain increment over a time step can be expressed with a finite number of state variables which are all known at the beginning of the time step.

#### 6.3.1 Formulation with the relaxation function

The formulation with the relaxation function (Maxwell Chain model) is rather straightforward. If Eq. (6.17) is substituted into Eq. (6.2) for time  $t$  and  $t + \Delta t$  and it is assumed that nothing has happened until  $t = 0$ , the stresses are written as

$$\sigma(t) = \bar{D} \int_0^t E_o(\tau) \dot{\epsilon} d\tau + \bar{D} \sum_{\alpha=1}^n \int_0^t E_{\alpha}(\tau) e^{-\frac{t-\tau}{\lambda_{\alpha}}} \dot{\epsilon} d\tau \quad (6.20)$$

$$\sigma(t + \Delta t) = \bar{D} \int_0^{t+\Delta t} E_o(\tau) \dot{\epsilon} d\tau + \bar{D} \sum_{\alpha=1}^n \int_0^{t+\Delta t} E_{\alpha}(\tau) e^{-\frac{t+\Delta t-\tau}{\lambda_{\alpha}}} \dot{\epsilon} d\tau \quad (6.21)$$

where  $\bar{D}$  is a dimensionless matrix that relates the multiaxial deformation state to the one-dimensional relaxation function with the Poisson's ratio (e.g. de Borst 1991).

The stress increment is calculated by subtracting Eq. (6.20) from Eq. (6.21). The integrals from 0 to  $t + \Delta t$  can be split into a part from 0 to  $t$  and a part from  $t$  to  $t + \Delta t$ . It is assumed that the strain rate is constant from  $t$  to  $t + \Delta t$  and also the values of  $E_{\alpha}(\tau)$  are taken as constant values,  $E_{\alpha}(\hat{t})$  from  $t$  to  $t + \Delta t$  with  $\hat{t}$  as a sampling point, usually halfway the time increment. With these simplifications the integral can be elaborated analytically which gives

$$\Delta\sigma = \bar{D} E_o(\hat{t}) \Delta\varepsilon + \sum_{\alpha=1}^n \left( 1 - e^{-\frac{\Delta t}{\lambda_{\alpha}}} \right) \left( \frac{E_{\alpha}(\hat{t}) \lambda_{\alpha}}{\Delta t} \bar{D} \Delta\varepsilon - \sigma_{\alpha}(t) \right) \quad (6.22)$$

where  $\sigma_{\alpha}(t)$  is the partial stress in the  $\alpha$  th element of the Maxwell Chain and it is a state variable.

$$\sigma_{\alpha}(t) = \bar{D} \int_0^t E_{\alpha}(\tau) e^{-\frac{t-\tau}{\lambda_{\alpha}}} \dot{\varepsilon} d\tau \quad (6.23)$$

The values of  $\sigma_{\alpha}(t)$  are known at the beginning of the time step (for  $\alpha = 0$  that is not needed to calculate the stress increment).

### 6.3.2 Formulation with the creep function

If it is assumed that nothing has happened until  $t = 0$ , the stain increment from  $t$  to  $t + \Delta t$  is written as

$$\begin{aligned} \Delta\varepsilon = \int_0^t (J(t + \Delta t, \tau) - J(t, \tau)) \bar{C} \dot{\sigma}(\tau) d\tau \\ + \int_t^{t+\Delta t} J(t + \Delta t, \tau) \bar{C} \dot{\sigma}(\tau) d\tau \end{aligned} \quad (6.24)$$

where  $\bar{C}$  is a dimensionless matrix that relates the multiaxial stress state to the one-dimensional creep function with the Poisson's ratio.

In order to attain a constitutive relation which is suitable for implementation in a displacement based finite element method, Eq. (6.24) has to be rearranged such way that the stress increment is expressed as a function the strain increment and stress history (de Borst and van den Boogaard 1994). It is assumed that the strain rate is constant over the time increment. Also  $E_{\alpha}(\tau)$  is taken as a constant from  $t$  to  $t + \Delta t$  which equals to its value at time  $\hat{t}$  according to mid-point rule. With  $\bar{D} = \bar{C}^{-1}$  then the stress increment is written as

$$\Delta\sigma = \tilde{E}(\hat{t})\bar{D}\Delta\varepsilon + \tilde{\sigma}(t) \quad (6.25)$$

with

$$\frac{1}{\tilde{E}(\hat{t})} = \frac{1}{\Delta t} \int_t^{t+\Delta t} J(t + \Delta t, \tau) d\tau \quad (6.26)$$

and

$$\tilde{\sigma}(t) = -\tilde{E}(\hat{t}) \int_0^t (J(t + \Delta t, \tau) - J(t, \tau)) \dot{\sigma}(\tau) d\tau \quad (6.27)$$

If Eq. (6.19) is substituted in Eq. (6.26) and (6.27) and again the mid-point rule is applied for  $E_{\alpha}(\tau)$ , the resulting integrals can be integrated analytically which yields

$$\frac{1}{\tilde{E}(\hat{t})} = \frac{1}{E_o(\hat{t})} + \sum_{\alpha=1}^n \frac{1}{E_{\alpha}(\hat{t})} \left( 1 - \frac{\lambda_{\alpha}}{\Delta t} \left( 1 - e^{-\frac{\Delta t}{\lambda_{\alpha}}} \right) \right) \quad (6.28)$$

and

$$\tilde{\sigma}(t) = -\tilde{E}(\hat{t}) \sum_{\alpha=1}^n \left( 1 - e^{-\frac{\Delta t}{\lambda_{\alpha}}} \right) \tilde{\varepsilon}_{\alpha}(t) \quad (6.29)$$

with

$$\tilde{\varepsilon}_{\alpha}(t) = \int_0^t \frac{1}{E_{\alpha}(\tau)} e^{-\frac{t-\tau}{\lambda_{\alpha}}} \dot{\sigma}(\tau) d\tau \quad (6.30)$$

The value of  $\tilde{\varepsilon}_{\alpha}(t)$  is known at the start of the time increment. Its value at the start of the next time increment is calculated as follows

$$\tilde{\varepsilon}_{\alpha}(t + \Delta t) = e^{-\frac{\Delta t}{\lambda_{\alpha}}} \tilde{\varepsilon}_{\alpha}(t) + \frac{\lambda_{\alpha} \Delta \sigma}{E_{\alpha}(\hat{t}) \Delta t} \left( 1 - e^{-\frac{\Delta t}{\lambda_{\alpha}}} \right) \quad (6.31)$$

With Eq. (6.28) and (6.29), the stress increment in Eq. (6.25) is expressed as function of the strain increment and a finite number of state variables all of which are known at the start of the time increment.

## 6.4 Determination of the chain parameters

The starting point to set up the material model for a time-dependent numerical analysis is the creep compliance which can be taken either from a theoretical model (*e.g.* CEB-FIP

Model Code 1990) or from experiments. In rarer instances the relaxation function is available. Parameters of the Kelvin Chain model is determined based on the creep curves while the parameters of the Maxwell Chain model is determined based on the relaxation curves. If the Maxwell Chain model is of interest but the creep compliance is available, the creep curves have to be transformed into relaxation curves (e.g. Bazant and Wu 1974).

### 6.4.1 Curve fitting

The stiffness of the degenerated element (*i.e.* single spring) can be determined directly for both chain models. In the Maxwell Chain model,  $E_o(\tau)$  is equal to the asymptotic final value of the relaxation curve while in the Kelvin Chain model,  $E_o(\tau)$  is equal to the value of the compliance function at time zero. Furthermore, in the Maxwell model, the sum of the elastic moduli,  $\sum_{\alpha=0}^n E_{\alpha}(\tau)$  is equal to the value of the relaxation function at time zero while in the Kelvin model, the sum of the reciprocal values of the elastic moduli,  $\sum_{\alpha=0}^n \frac{1}{E_{\alpha}(\tau)}$  is equal to the asymptotic final value of the creep compliance<sup>1</sup>.

The elastic moduli for the other chain elements and the relaxation or retardation times then are obtained by a nonlinear least square method (DIANA 1999) minimising the sum of the quadratic differences between the theoretical curve,  $f$  and the approximating curve  $f'$  at  $n$  number of discrete sampling load durations.

$$\delta = \sum_{i=1}^n (f_i - f'_i)^2 \quad (6.32)$$

It is recommended to choose the sampling points distributed uniformly on the logarithmic time scale.

### 6.4.2 Ageing chain

For ageing materials like concrete, the viscoelastic behaviour can be represented by not a single creep curve but a series of creep curves in order to take into account the effect of ageing. Accordingly an ageing chain model is defined by many sets of chain parameters. The relaxation or retardation times remain fixed while the elastic moduli are determined at a number of sampling loading ages. The elastic moduli at intermediate loading ages (*i.e.* other than the sample loading ages) are then calculated by multi-linear interpolation. There are two methods to determine the elastic moduli of the chain model for different sampling loading ages.

---

<sup>1</sup> There are creep models which do not possess a final asymptotic value (e.g. Bazant's B3 model). The Kelvin Chain model can still provide a good approximation for this kind of creep development pattern but strictly on the domain of fitting with respect to the load duration. In that case the sum of the reciprocal stiffnesses does not have a real physical meaning or significance.

The *scaled fit method* is normally suitable for creep curves only and therefore it is used for the Kelvin Chain model. The creep curve with a loading age of 28 days is used as a base curve and for that the elastic moduli are determined by curve fitting. For all the other sampling loading ages the elastic moduli are scaled based on the base curve. Creep models usually specify an ageing coefficient for the instantaneous response,  $\beta_E(\tau)$  and a different ageing coefficient for the time-dependent response,  $\beta_\phi(\tau)$ .

$$J(t, \tau) = \frac{1}{\beta_E(\tau)} \frac{1}{E_c(\tau = 28)} + \frac{1}{\beta_\phi(\tau)} \frac{\phi(t, \tau = 28)}{E_c(\tau = 28)} \quad (6.33)$$

Accordingly the elastic moduli are scaled with  $\beta_E(\tau)$  for the single spring and with  $\beta_\phi(\tau)$  for all the other elements ( $\alpha \geq 1$ ).

$$E_o(\tau) = \beta_E(\tau) \cdot E_o(\tau = 28) \quad (6.34)$$

$$E_\alpha(\tau) = \beta_\phi(\tau) \cdot E_\alpha(\tau = 28) \quad (6.35)$$

Since relaxation curves are normally not scalable the same way as creep curves, the scaled fit method is not applicable for the Maxwell model. Instead, each set of elastic moduli with different loading ages are determined by an independent curve fit. The relaxation times are determined at the first curve fit and then they remain fixed upon the subsequent fits. This method - the so-called *multiple fits method* - can also work with creep curves.

## Chapter 7

### Numerical Model and Simulation

*The finite element model and simulation used for the time-dependent deformation analysis of segmentally cast concrete cantilever bridges are described. Some critical aspects of the beam model are studied in order to verify its performance. The calculation procedure for the effective prestressing force is presented. The simulation of the segmental construction method for cantilever bridges is also discussed.*

#### 7.1 Introduction

Deformation analysis in segmentally built concrete cantilever bridges is a considerably complex problem irrespective of the difficulties with creep and shrinkage prediction. The general notion applies, *videlicet* it is relatively easy to give a safe limit with a considerable safety margin where the structure will not fail but the *actual behaviour* of the structure is only known by the structure itself.

The finite element models which are used throughout this study are based on a two-dimensional beam model. Shear deformation and the additional element stiffness from the conventional reinforcement are taken into account. The prestressing tendons are modelled according to their actual layout and the variation of the effective prestressing force along the tendons axis and with time is considered. The segmental construction procedure is simulated with phased structural analysis.

In this chapter the geometrical model and the time-dependent phased structural analysis is discussed. The material models and their mathematical formulation were discussed earlier.

The finite element calculations are carried out with general purpose finite element program system DIANA (DIANA R7.2 1999).

## 7.2 Geometrical model

### 7.2.1 Two dimensional beam model

The numerical analyses are carried on two dimensional models consisting of beam elements. The symmetry in both geometry and loading across the vertical median in the cross-section is utilized. The subdivision of the model into beam elements corresponds to the subdivision of the superstructure into segments. Each element represents one segment. This is not only convenient for specifying the geometrical dimensions but it is essential for the simulation of the segmental construction process as well.

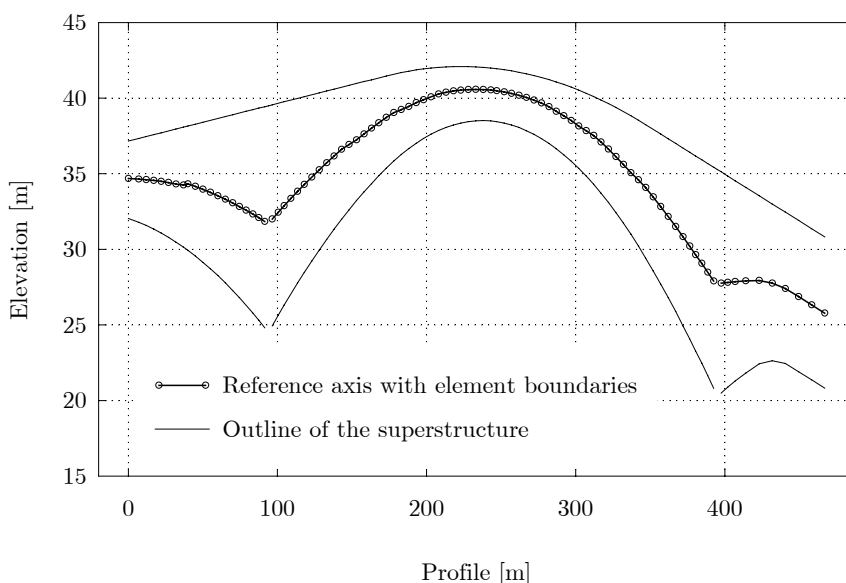


Figure 7.1 Subdivision of the superstructure into beam elements, Stolma Bridge

#### 7.2.1.1 Equivalent cross-section

The box-girder cross-section is converted into an equivalent I-shape. The I-shape consists of three rectangle zones: the upper slab, the web and the lower slab. The conversion is made based on the condition that, for both the upper and the lower slabs separately, the position of the horizontal neutral axis, the respective central moment of inertia and the area of the cross-section remain the same as those of the original shape<sup>1</sup>. For a fixed neutral axis there are two free variables (height and width of the rectangle) and two conditions (area and moment of inertia), thus the dimensions can be determined exactly. The bottom edge of the

<sup>1</sup> Since the model is only two dimensional the moment of inertia over the vertical axis and the polar moment of inertia are not of interest.



resulted equivalent rectangle of the upper slab most certainly does not coincide with the upper edge of the web. Therefore a certain area from the upper slab above the web is counted into the area of the web. Since it is necessary to know this area in order to calculate the equivalent rectangle of the upper slab but it is not known beforehand, the calculation involves an iterative procedure. The procedure is the same for the lower slab but there a certain area from the web above the lower slab is counted into the area of the slab. The thickness of the web is simply the sum of that of the walls of the box-girder since they have regular rectangular form.

The columns, column foundations and caissons are modelled with rectangular or box shape cross-sections. Where the actual cross-section has a unique form, the cross-section is converted into an equivalent rectangular or box shape under similar conditions described above.

7.2.1.2 Element type

The formulation of the beam element is based on the Mindlin theory and the type of the element is referred to as *Mindlin beam* (e.g. Cook 1989). The advantage of the Mindlin beam is that, unlike the classical beam element, it takes shear deformation into account. This implies that the Bernoulli hypothesis is abandoned. The plane initially normal to the midsurface remains plane but not necessary normal. Consequently the normal strain varies linearly over the depth while the transverse shear strain is forced to be constant.

The elements are two-dimensional, 3-node beam elements based on an isoparametric formulation (e.g. Zienkiewicz 1971). The basic variables are the translations and rotation in the element plane. The local axes in the first node of the element serve to describe the direction of the displacement degrees of freedom in all nodes (*vide* Figure 7.2). In the Mindlin beam element the displacements and rotations are independent and are respectively interpolated from the nodal displacements and rotations. That is necessary since the beam axis normal does no longer coincide with the cross-section plane subjected to shear deformation.

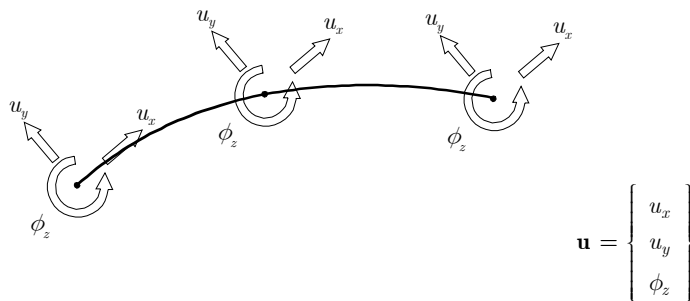


Figure 7.2 Nodal displacements in the two dimensional quadratic beam element

Although the element formulation allows to specify quadratic shape as it is illustrated in Figure 7.2 in general, the elements in the models are straight. In fact the use of higher order elements is not essential for the given problem *per se*. The element type was chosen for its other favourable properties. The curvature in the reference axis of the superstructure is small and the subdivision into elements is fine (*vide* Figure 7.1), thus assuming linearity between the element boundaries is sufficient. The coordinates of the middle element node are determined by linear interpolation between the element boundaries.

### 7.2.1.3 Numerical integration

The elements are numerically integrated along the beam axis and in the cross-section. Since it is a two-dimensional beam element, integration in the cross-section is only performed in the vertical direction. The Gauss quadrature (*e.g.* Zienkiewicz 1989) is used along the beam axis with two integration points. The Gauss quadrature is used also in the cross-section with two integration points for each quadrilateral zone of the I-section. The I-section consists of three quadrilateral zones and consequently that means six integration points in one cross-section and twelve integration points for one element (*vide* Figure 7.3).

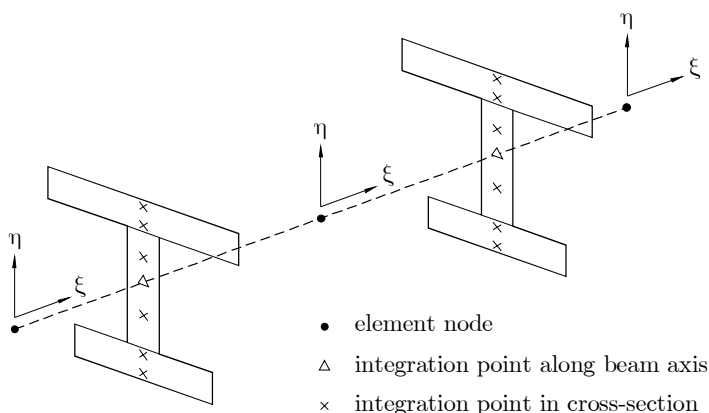


Figure 7.3 Integration scheme for the beam element

### 7.2.1.4 Reference axis

Special attention has to be paid when the reference axis of the superstructure and the respective cross-section dimensions are determined. The reference axis has a certain inclination over the horizontal. Consequently the plane of the cross-section perpendicular to the model axis is not vertical. The cross-section dimensions for the actual structure, however, are given in the vertical plane. The reference axis is not known beforehand because it is calculated from the cross-section dimensions and its absolute elevation. Therefore the reference axis and the corresponding cross-section dimensions in the normal

plane are determined by an iterative procedure: (1) as a first approximation the reference axis is calculated from the cross-section dimensions given in the vertical plane, (2) the cross-section dimensions then can be determined in the plane perpendicular to the approximate reference axis, (3) with the new cross-section dimensions, the reference axis can be recalculated, (4) the second and third steps are then repeated until the difference in the vertical coordinate of the reference axis point between two consecutive iteration steps is negligibly small. At the end of the third step the new reference axis point will be out of the original vertical plane, so it needs to be projected back to that plane. Since the inclination of the reference axis is small, two iteration steps were found sufficient in all cases.

### **7.2.2 Reinforcement and prestressing tendons**

Conventional reinforcement is taken into account in the model to consider the additional stiffness given to the structural elements. Reinforcement elements are embedded into the surrounding beam element, referred to as the *mother element*. They do not have degrees of freedom of their own. Their strains are coupled to the displacement field of the mother element. This implies perfect bond between the reinforcement and the mother element. A reinforcement element is described with the area of its cross-section and its position in the mother element. The position is specified by the eccentricities in the respective element nodes. One reinforcement bar is defined in the upper slab to account for the total amount of conventional reinforcement in the upper slab and one bar is defined in the lower slab to account for the total amount of conventional reinforcement in the lower slab.

The reinforcement elements which represent the prestressing tendons are used to define the prestressing load. They remain unbonded to their mother elements until the tendons are grouted. While they are unbonded they remain undeformed and add no stiffness to the mother elements. The prestressing tendons are modelled by series of individual segments between the beam element boundaries. The position of each segment is described with the eccentricities in the respective beam element nodes. Since the beam element has three nodes it is possible to specify linear and quadratic shape particles. The latter is particularly useful to describe sudden angle change within the element. Each series of particles represents two tendons due to the utilised symmetry in the cross-section. The computation and modelling of the effective prestressing force is discussed in subsection 7.3.

It has to be noted that although the bonded reinforcement elements are taken into account when the element stiffness is calculated, they are neglected when the element reference axis is calculated.

### **7.2.3 Verification of the *Mindlin* beam model and shear deformation**

Shear deformation is expected to play a very minor role in the total deformation. Although the height of the superstructure near the piers is large, the length to height ratio of the

completed spans are well above what is considered a practical limit for the classical beam theory<sup>1</sup>. When the cantilever is considered with only the first few segments, as that occurs during construction, the classical beam theory could not be appropriate. The deformations, however, are very small in that stage due to the very high stiffness of the partial cantilever relative to its length. Nonetheless shear deformation is taken into account in the computation with the *Mindlin beam* elements in order to improve the accuracy. To estimate the contribution from the shear deformation to the total deformation the Mindlin beam model is compared with a model consisting of classical beam elements.

A more sophisticated two-and-a-half dimensional model which consists of shell elements is included in the comparison to verify the beam model in regard to its general performance. Such a model would be unreasonably time consuming in a realistic full scale analysis due to its enormous pre-processing need and computational time requirement.

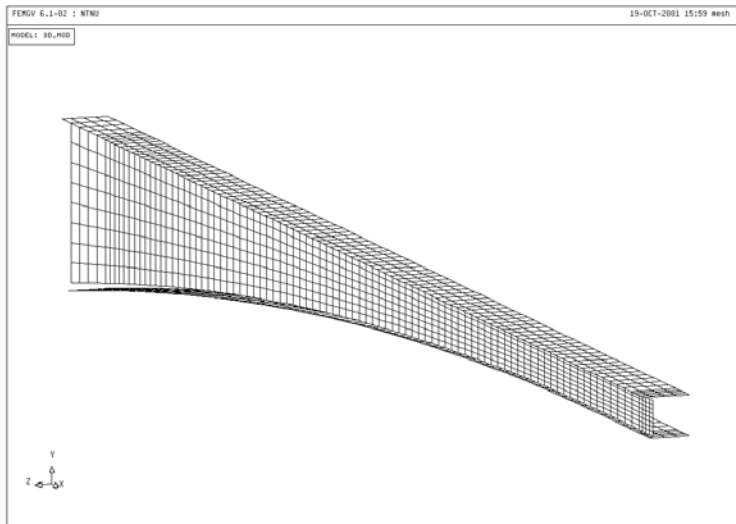


Figure 7.4 Two-and-a-half dimensional shell model<sup>2</sup>

The comparison was carried out for the selfweight only on models of a continuous single span based on a simplified geometry of Støvset Bridge. The underlying structural models are identical in all three finite element models. The support condition was taken as perfectly rigid. The investigation was made in the linear elastic state to avoid introducing effects of

---

<sup>1</sup> The height of the superstructure at the piers is 13.0 meter in Norddalsfjord Bridge, 12.0 meter in Støvset Bridge and 15.0 meter in Stolma Bridge. The corresponding length to height ratio with respect to the cantilever (i.e. half of the span) is 8.9, 9.2 and 10.0 respectively.

<sup>2</sup> A small gap can be seen between the web and the two flanges in the finite element mesh. The respective series of nodes are tied together by linear dependencies between the degrees of freedom.

non-linear behaviour. Only one half of the span is modelled utilising the symmetry. Due to the symmetry also in the cross-section, only one half of the box-girder is modelled in the 2½D shell model (*vide* Figure 7.4).

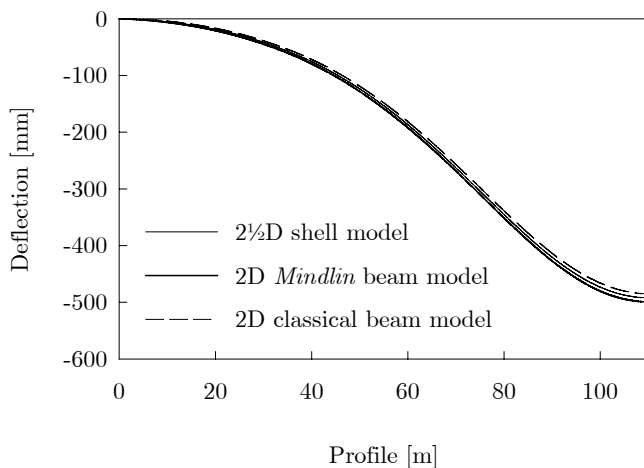


Figure 7.5 Deflection in the continuous span according to the three models

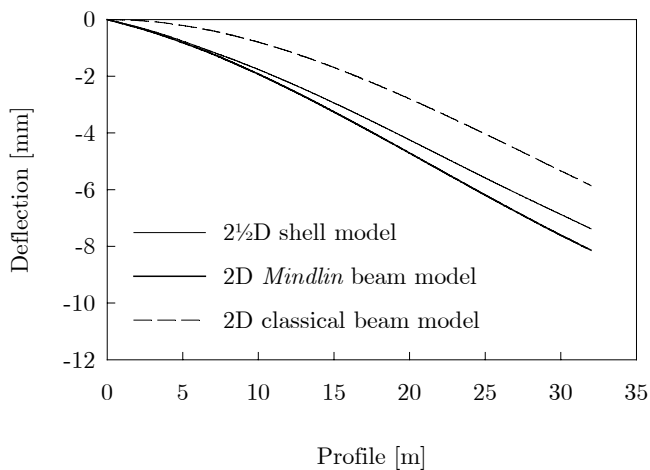


Figure 7.6 Deflection for a short cantilever

Figure 7.5 shows the deflection for the three models. The contribution from the shear deformation, indeed, was found small. Another analysis was carried out where only the first seven segments are considered in the free cantilever state. It concerns the first 32 meters of the span and the corresponding length to height ratio at the piers is 2.67. The shear

deformation is appreciable (*vide* Figure 7.6), although the deformations in general are very small. Good agreement was found between the Mindlin beam model and the two-and-a-half dimensional shell model, however, a small deviation was observed.

#### **7.2.4 Effect of non-uniform creep and shrinkage over the cross-section**

The development of creep and shrinkage are significantly affected by the dimensions of the structural member through drying. To characterise the average size of the cross-section of an arbitrary shape the parameter *notional size* is used. In the beam model the notional size is associated with the entire box-girder as an average value for the cross-section. Therefore creep and shrinkage properties are considered identical in any point of a given cross-section. The different thickness of individual parts of the box-girder, however, results in different creep and shrinkage properties within the box-girder. The non-uniform creep and shrinkage development has influence on the global deformation of the superstructure. The magnitude of this influence is determined in this section.

The investigation is carried out on the same two-and-a-half dimensional shell model which was described in the previous section (*vide* Figure 7.4). In first case the same notional size is assigned to all elements within the same cross-section which is characteristic for the box-girder as an average. In general these values are used for the beam model. In the second case the notional size is determined separately for the upper slab, the web and the lower slab.

The comparative analysis is carried out on a single phase analysis on the continuous span (*i.e.* the entire span is activated in a single step) with an initial concrete age of 28 days and on a realistic phased analysis which includes the simulation of the construction process as well.

The thickness of the lower slab is considerably larger than the thickness of the upper slab apart from a certain length around the middle section. Consequently the creep and shrinkage development in the lower slab is slower than in the upper slab. According to the CEB-FIP MC90 creep model the notional size has influence on both the notional creep coefficient (*i.e.* the final value of creep) and on the creep time dependency function. Whereas shrinkage is influenced by the notional size through its time dependency function only and the theoretical final shrinkage strain is the same irrespective of the geometrical dimensions. Since the cross-sections are in the state of combined axial compression and bending, it is expected that faster creep and shrinkage development in the upper slab and the slower development in the lower slab result in a relative upward bending as compared to the situation where the creep and shrinkage properties are uniform over the cross-section. In other words the non-uniform creep and shrinkage properties result in somewhat smaller deflection than the uniform properties.

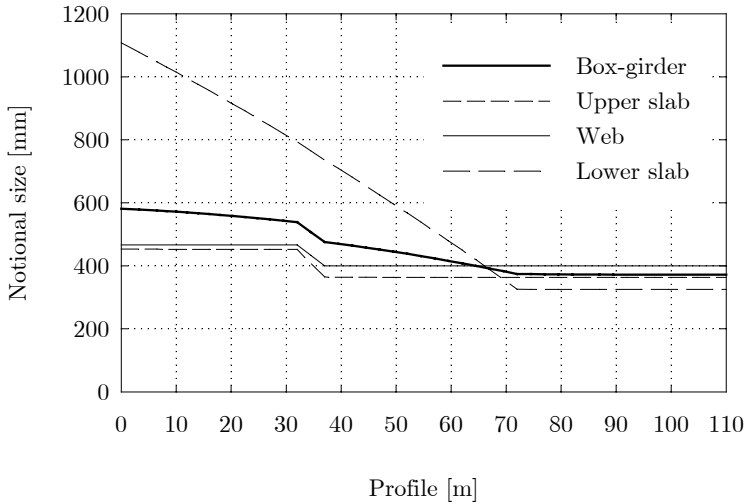


Figure 7.7 Notional size for the entire box-girder and for the individual parts separately (shown for one half of the main span of Støvset Bridge)

The notional size for the box-girder or for individual parts of the box-girder is calculated based on the recommendation of the Norwegian Standard (NS 3473), *i.e.* taking into account the inner perimeter of the box-girder with a multiplier of 0.5 (*vide* Eq. (7.1)). This is meant to consider that the inner surface is not in direct contact with the ambient environment and less affected by drying. This approach is taken in the absence of more accurate information.

$$h = \frac{2 \cdot A}{u_{outer} + 0.5 \cdot u_{inner}} \quad (7.1)$$

where

- $A$  is the area of the member,
- $u_{outer}$  is the outer perimeter of the member,
- $u_{inner}$  is the inner perimeter of the member.

The notional size for the entire box-girder and for its individual parts separately are shown in Figure 7.7. The values are calculated based on the actual geometry of the main span of Støvset Bridge. The notional size at the pier is 1100 mm for the lower slab and 450 mm for upper slab whereas 580 mm for the entire box-girder as an average. For these values the creep functions are shown in Figure 7.8 for the concrete age of 28 days at loading under the conditions that the relative humidity is 70 % and temperature is 10 °C. Figure 7.9 shows the shrinkage development under the same conditions.

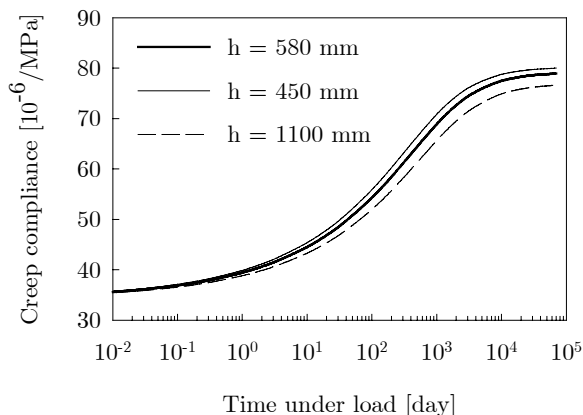


Figure 7.8 Creep compliance with different notional sizes

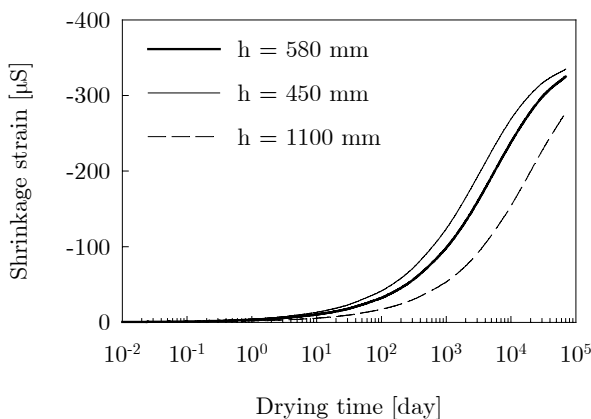


Figure 7.9 Shrinkage strain with different notional sizes

The difference in the shrinkage strain is considerable. Although theoretically the shrinkage strain is approaching the same final value irrespective of the notional size, the time dependency is significantly influenced by the geometrical dimension. The drying time which it takes to reach a certain level of average shrinkage across the thickness of the slab is quadratically increasing with the increasing notional size. In bulk concrete the drying process is slow and even after 70 years significant difference is seen in Figure 7.9 between the shrinkage strain in the lower and upper slab. In fact actual shrinkage in bulk concrete may be smaller. The prediction formula is rather uncertain for large concrete members as little information exists in that regard (CEB 1991).



The difference between the creep compliance and the shrinkage strain in the lower slab and those on the upper slab are shown in Figure 7.10. The difference in the creep compliance is increasing until about 1000 days and then decreasing while approaching a certain final value. The difference in the shrinkage strain is increasing until about 10000 days and then decreasing while approaching zero.

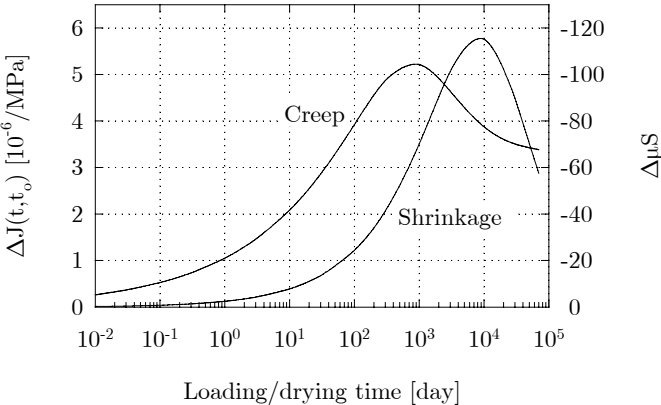


Figure 7.10 Difference in the creep compliance and the shrinkage strain between the lower slab and the upper slab of the box-girder

One has to keep in mind that the differences in the creep and shrinkage curves between the lower and the upper slabs shown in Figure 7.8, Figure 7.9 and Figure 7.10 concern the largest difference at the pier only, thus they are not characteristic for the entire span. The magnitude of the differences are decreasing as the thickness of lower slab is gradually decreasing (*vide* Figure 7.7).

The computed deflections obtained by the single phase analysis are shown in Figure 7.11. The instantaneous deflection curve is evidently identical for the model with the uniform creep and shrinkage properties and the model with the non-uniform creep and shrinkage properties. As it was expected the non-uniform properties resulted in slightly smaller deflection after long time (70 years). The difference at mid-span is 21 mm, that is about 2.5 % of the total deflection. The difference was found not higher than 4 % at any point of the span.

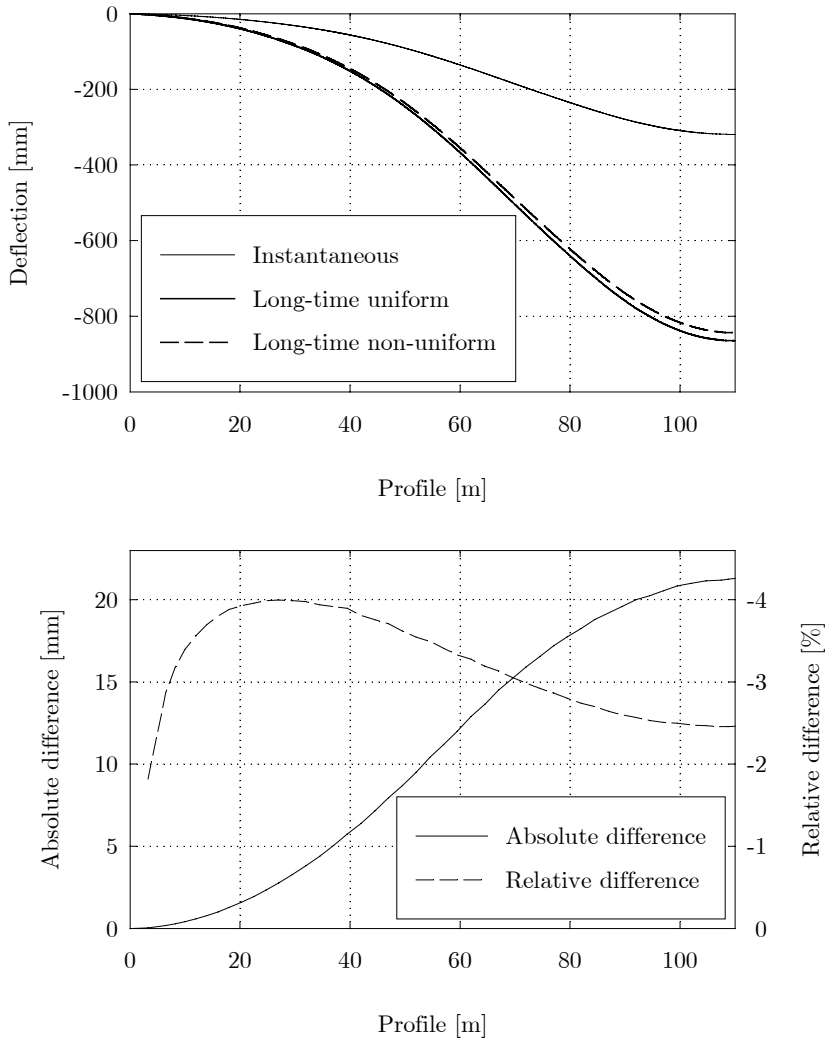


Figure 7.11 Instantaneous and long-time deflection obtained by the single phase analysis (above) and the long-time difference after 70 years as a result of the non-uniform creep and shrinkage properties within the cross-section (below)

The single phase analysis was carried out to estimate the magnitude of the difference between the two modelling approaches on a simpler and more apparent model. The second comparative analysis is carried out with a realistic phased analysis which includes the simulation of the segmentwise construction process as well. The concept of the phased structural analysis is discussed later in subsection 7.4.

The computed deflection curves are shown in Figure 7.12 in three stages: (1) prior to the casting of the last segment and connection of the cantilevers, (2) after the bridge is fully completed (*i.e.* non structural parts of the bridge are also in place and (3) after 70 years of service.

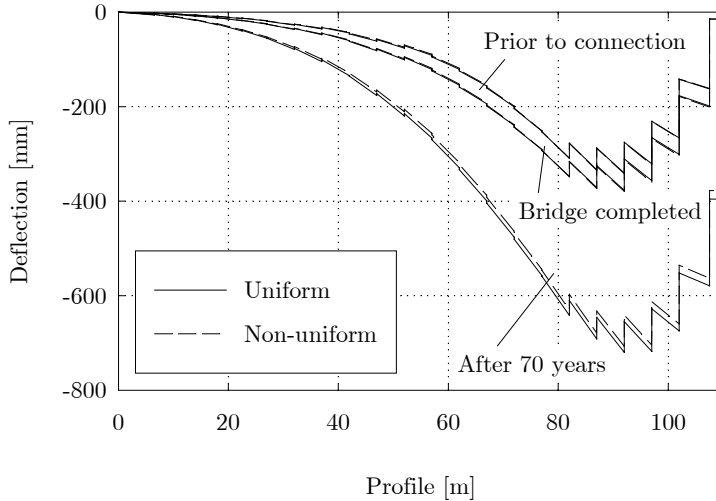


Figure 7.12 Deflections obtained by the uniform and non-uniform cross-section properties

The differences between the models are highlighted in Figure 7.13. The long-time deflection after 70 years is 18 mm smaller at mid-span with the non-uniform properties which is about 4.6 % of the total deflection. The same figures are 13 mm and 1.8 % for the maximum deflection at the profile of 92 m. The difference prior to the connection of the cantilevers is negligible.

In conclusion it can be said that the global deformations in the construction period is practically not affected by the non-uniform creep and shrinkage development within the box-girder. The long-time deflection is overestimated to a small extent by the assumed uniformity which exists in the beam model, but the difference is small. It is not the magnitude which could raise concern about the validity of the model which assumes uniformity.

It should be mentioned that it is still possible to take into account the non-uniformity of creep and shrinkage properties with certain beam elements as well. Since the elements are numerically integrated over their cross-section with a separate integration for each zone, different material properties can be defined to each zone within the same cross-section. The current study does not concern this type of beam element.

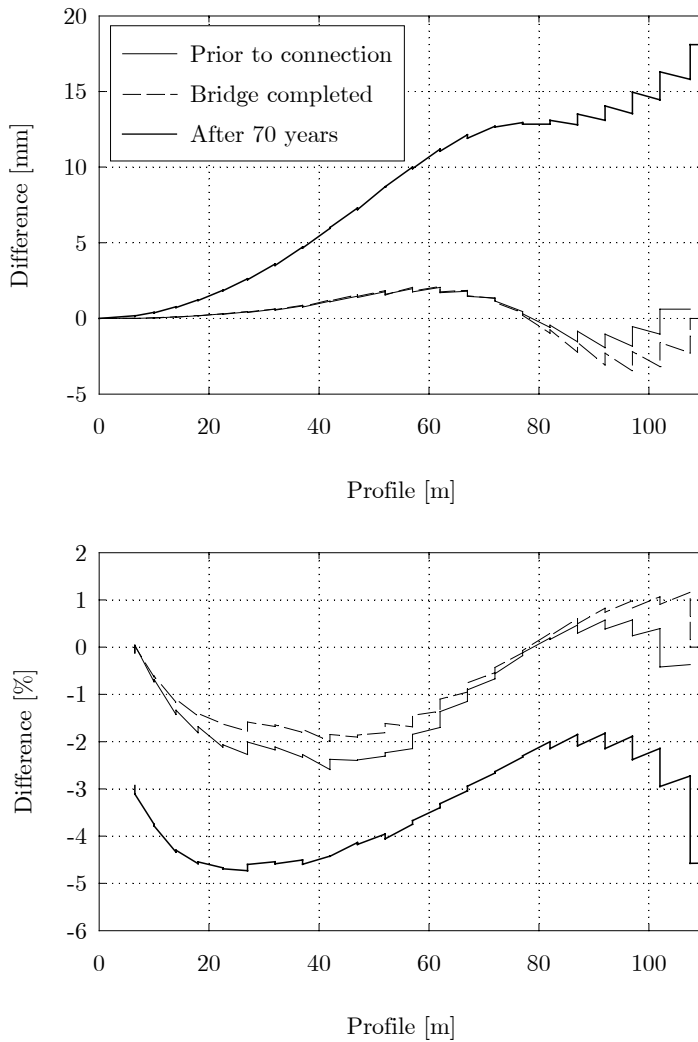


Figure 7.13 The excess vertical deformation due to the non-uniformity of the creep and shrinkage properties within the box-girder as compared to the model which assumes uniformity

### 7.3 Modelling the effective prestressing force

The prestressing force in the tendon varies along the tendon axis and with time. In post-tensioned systems the initial prestressing force applied at the anchor is reduced by prestress losses resulted from friction, anchor slip, steel relaxation and shortening of the concrete element due to elastic, creep and shrinkage deformation.

Estimating the prestress losses along the tendon axis and its variation with time is one of the significant uncertainties in the analysis. The total deflection is basically the sum of two large opposite distributions (*i.e.* selfweight and prestressing). A small deviation in either of them may result in a large deviation in their sum. Those physical mechanisms and properties which are responsible for the prestress losses are associated with a certain degree of uncertainty. The variation in deformations due to variation in the effective prestressing force is discussed in Chapter 9.

Distinction should be made in post-tensioned systems between bonded and unbonded tendons. In bonded post-tensioned construction the ducts are grouted after stressing the tendons. The bonded tendons become integral part of the structure. Unbonded tendons are, on the other hand, tied to the structure only at the anchors. Between the anchorage points the tendon may move relative to the surrounding structural element. Also in bonded post-tensioned systems the tendon is acting as an unbonded tendon until the grouting takes place. In segmental bridge construction all the tendons are typically grouted in one phase only after the entire span is completed and all the tendons are in place.

The same terms, *bonded* and *unbonded* tendon have to be introduced from the finite element model point of view. It has to be emphasised that the behaviour described with the term *unbonded* is somewhat different from the real physical behaviour described in the previous paragraph, nevertheless it is closely related. The bonded reinforcement element is perfectly embedded into its mother element. It adds additional stiffness to the mother element and its deformations are derived from the displacement field of the mother element. The unbonded reinforcement element is not tied to its mother element in any way. The reinforcement element remains undeformed and adds no stiffness to the mother element. Since the unbonded reinforcement element remains undeformed the prestress remains the same as specified initially irrespective of the deformations of the mother element.

Reinforcement elements which are initially specified as unbonded in the model can be changed to bonded in a later phase of the analysis. The respective attributes then change accordingly.

### **7.3.1 Friction and anchor slip**

When the tendon is stressed at the anchor point a certain amount of the applied force is dissipated due to friction forces acting between the tendon and the duct. Frictional losses can be distinguished as curvature and the wobble frictional losses. The curvature frictional loss results from the intentional angle change in the tendon profile. The wobble frictional loss is the result of the unintentional variation of the tendon axis from its intended profile. The force in the tendon at any given point along its axis can be estimated by the Coulomb friction model (*i.e.* Collins and Mitchell 1991).

$$P(x) = P_o \cdot e^{-(\mu\alpha + Kx)} \quad (7.2)$$

where

- $P(x)$  is the tendon force at a distance of  $x$  from the anchor along the tendon axis,
- $P_o$  is the applied prestressing force at the anchor,
- $\mu$  is the Coulomb friction coefficient,
- $\alpha$  is the total intended, cumulative angle change over the length of  $x$  [rad],
- $K$  is the wobble friction coefficient [1/m].

The values of  $\mu$  and  $K$  vary appreciably depending on the construction method and the materials. The value of  $K$  also depends on the quality of workmanship. If more accurate values are not available (e.g. from previous experience) the CEB-FIP Model Code 1990 (CEB 1991) recommends the use of 0.20 for  $\mu$  and 0.001-0.002 per meter for  $K$  for strands in metal sheathing<sup>1</sup>. The ACI recommendation (ACI 1988) is 0.15-0.25 for  $\mu$  and 0.0016-0.0066 per meter for  $K$  for strands in flexible metal sheathing. The value of the wobble friction coefficient can be higher in segmentally constructed structures due to the additional wobble effect at the location of the segment interfaces. A study of a variety of tendons in eight segmentally constructed bridges resulted in a mean  $\mu$  of 0.36 and a mean  $K$  of 0.003 per meter (Collins and Mitchell 1991).

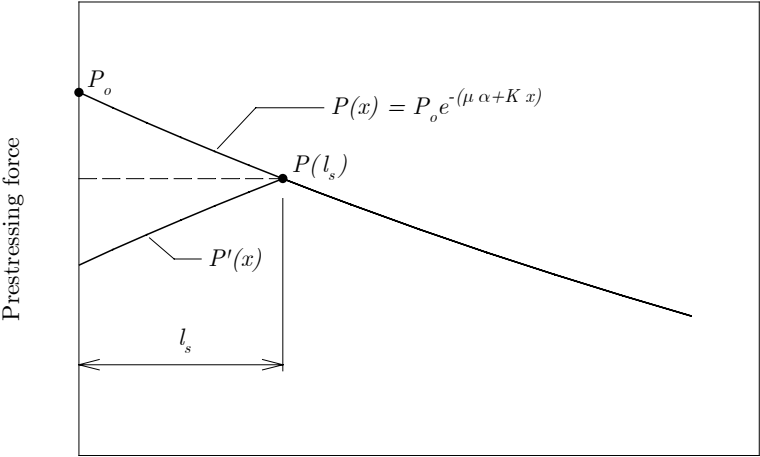
In the current numerical models the Coulomb friction coefficient is considered with a value of 0.20 and the wobble friction coefficient is considered with a value of 0.002 per meter. These numbers are based on the recommendation of the bridge designers.

When the prestressing force is transferred to the anchorage device in post-tensioned system, an inward movement of the tendon occurs as the anchor wedge seats itself and the anchorage device deforms under stress. Only a certain length of the tendon is affected by this so-called anchor slip as frictional force now work against this movement. The stress loss due to the anchor slip decreases with the increasing distance from the anchor and vanishes after that certain length. The value of the anchor slip,  $s$  depends on the type of the anchorage. The typical value varies around 2-4 mm. In the current models it is taken with a value of 3 mm.

The calculation method which is used here assumes that the tendon forces before and after the stress loss from the anchor slip are symmetrical over the horizontal line which goes through the point  $P(l_s)$ , beyond which the force is not affected by the anchor slip (*vide* Figure 7.14). The length which is affected by the anchor slip is denoted by  $l_s$  and  $P(l_s)$  is the force in the tendon at that distance from the anchor.

---

<sup>1</sup> In fact in the CEB-FIP Model Code 1990,  $K$  is expressed as  $0.005-0.01\mu$  per meter.



Tendon profile,  $x$

Figure 7.14 Influence of the anchor slip on the effective prestressing force

The anchor slip,  $s$  is equal to the total shortening of the tendon over the length of  $l_s$  as expressed by Eq. (7.3).

$$s = \frac{1}{E_p A_p} \int_0^{l_s} (P(x) - P'(x)) dx \tag{7.3}$$

which then is written due to the assumed symmetry as

$$s = \frac{1}{E_p A_p} 2 \int_0^{l_s} (P(x) - P(l_s)) dx \tag{7.4}$$

The unknown length of  $l_s$  can be determined by a trial and error method. After it is determined the effective prestressing force can be calculated over the  $l_s$  length as

$$P'(x) = 2P(l_s) - P(x) \tag{7.5}$$

Beyond the length of  $l_s$  anchor slip has no influence, thus Eq. (7.2) is used.

Eq. (7.3) assumes that the force reduction in the tendon is linearly proportional to the anchor slip. This is reasonable because anchor slip is technically a deloading process.

In certain cases anchor slip affects the force in the tendon along its entire length. This may happen if the tendon is short, the cumulative angle change is small and/or the friction is low. For the bridges involved in this study calculation indicated that the tendons for the first

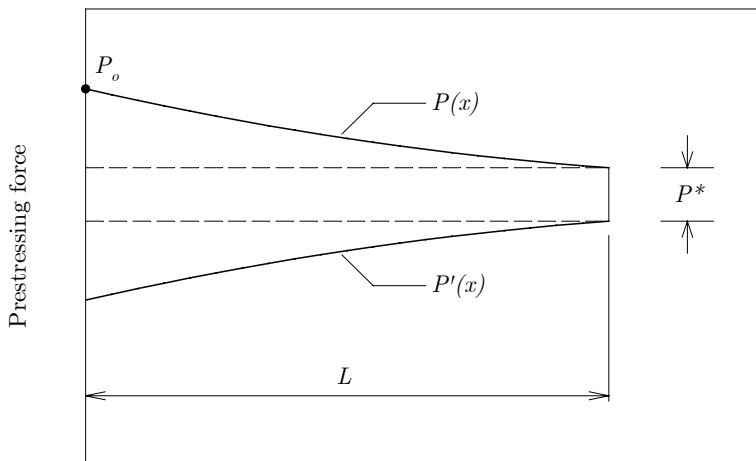
two or three segments were affected this way. If  $l_s$  obtained by Eq. (7.4) is longer than the actual length of the tendon, Eq. (7.6) replaces Eq. (7.4).

$$s = \frac{1}{E_p A_p} \left( 2 \int_0^L (P(x) - P(L)) dx + L \cdot P^* \right) \tag{7.6}$$

where  $L$  is the length of the tendon.

The unknown parameter now is  $P^*$  (vide Figure 7.15) which can be easily determined from Eq. (7.6). Then the effective prestressing force can be calculated as follows

$$P'(x) = 2P(L) - P(x) - P^* \tag{7.7}$$



Tendon profile,  $x$

Figure 7.15 Calculation of the effective prestressing force when the entire length of the tendon is affected by the anchor slip

It is common practise to apply the initial prestressing force at both anchors in very long tendons in order to minimise the frictional losses in the tendon. The effective prestressing force can be obtained by calculating the prestressing force for both ends independently according to Eq. (7.2)-(7.5) and taking the higher value of the two curves in each point as it is illustrated in Figure 7.16.



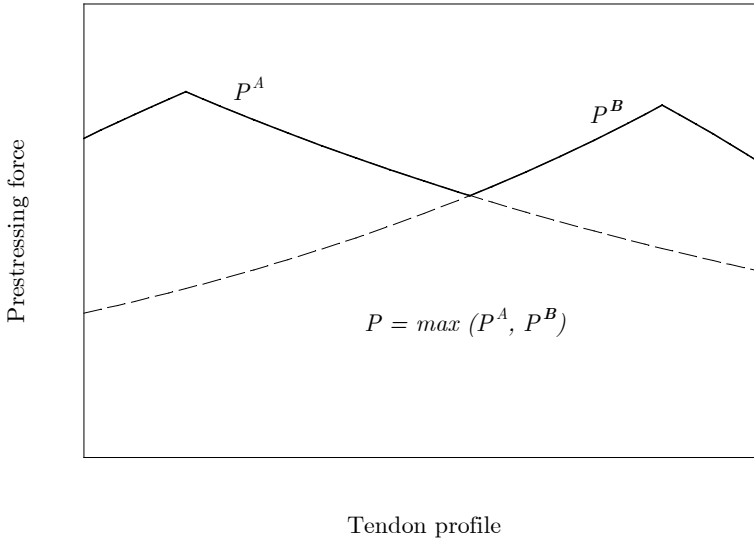


Figure 7.16 Calculation of the effective prestressing force when the tendon is stressed at both anchors

### 7.3.2 Relaxation

The material model for steel relaxation was discussed in Chapter 3. The prestress losses resulted from relaxation are taken into account in the numerical models by reducing the applied prestressing force in discrete time steps through the construction period. The further relaxation which occurs after the structure is completed is considered with one value and it equals to the relaxation after 10 years as obtained by the relaxation model. This “manual” approach is necessitated by the fact that no visco-elastic or rather visco-elasto-plastic material model is available for reinforcement elements in the given finite element program system. The reason that relaxation for the completed structure is considered with one constant value and not taken gradually in time steps like in the construction period is that the prestressing force in the reinforcement elements can no longer be redefined after the reinforcement elements are bonded. A bonded reinforcement element becomes integral part of the structure and their stresses and strains are derived from the displacement field of the mother element.

According to the relaxation model in the CEB-FIP Model Code 1990, the estimated relaxation after 10 years is 4.7 % if the relaxation after 1000 hours is taken as 2 % (for strands with improved relaxation characteristics at an initial stress level of 0.7). The estimated relaxation after 1 year and 30 years are then -1.7 % and +1.1 % respectively as compared to relaxation after 10 years.

### 7.3.3 Shortening of the concrete member

The concrete element which embeds the prestressing tendon is subjected to shortening due to elastic, creep and shrinkage deformations. Depending on the structure, the type of the prestressing system, the construction method and the restraint conditions, the deformations of the embedding element influence the force in the tendon.

If the tendons were all tensioned simultaneously in post-tensioned construction there would be no losses of prestress due to elastic shortening. For a segmentally cast concrete cantilever bridge that is not the case. Not only the tendons are tensioned sequentially within one segment but as the cantilever is being erected segment-by-segment the tendons are installed accordingly. The prestress from the subsequent tendons results in elastic deformation in the already existing segments and hence further prestress reduction in the already existing tendons.

The concrete elements are further shortened by creep and shrinkage which triggers further reduction in the prestressing force.

When the reinforcement elements which represent the prestressing tendons are bonded to their respective mother element, the strains and stresses in the reinforcement element are calculated from the displacement field of the embedding element. It implies that the stress reduction is automatically takes place as the concrete element deforms.

On the other hand the tendons remain unbonded through the construction stages and accordingly they are set in the model as unbonded. From the model point of view that also implies that the tendon remains undeformed and the initial prestressing force is not affected by either the deformations of the mother element or the deformations of the global structure. In reality, even if the tendons are unbonded they are tied to the structure at the anchorage points and to some extent along their axis by frictional forces. The prestress losses from the shortening of the concrete segments which occur while the tendons are unbonded are taken into account manually by reducing the applied initial force in discrete time steps. These time steps naturally correspond with the construction of the segments.

## 7.4 Modelling the segmental construction

The construction history has a determinative influence on the deformations. Therefore it is important to simulate the segmentwise construction procedure according to its actual chronology. The numerical method which is used through this study can be described as a time-dependent phased structural analysis.

Phased analysis is a series of quasi independent calculation phases. Each phase in the series is a complete nonlinear time-dependent finite element analysis. The connection between the sequential phases are established by transferring the values of the variables. The obtained

results in one phase are transferred to the subsequent phase as initial values. The incremental results of each phase following from the incremental effective loads are superimposed on the results of the previous phase. Between the calculation phases the structural system can be changed; elements can be added or removed and boundary conditions and constraints can be modified. New loads can be added or existing ones can be removed. Whenever a new node is activated for the first time its displacements are zero.

The entire simulation of the bridge is divided into calculation phases according to the segmental cantilevering chronology. One calculation phase normally simulates one construction cycle, *i.e.* the construction of one segment (or one segment per cantilever if those are constructed simultaneously). This gives a typical of 30-40 analysis phases for a full simulation.

In the first analysis phase the model is initialised only with the elements representing the foundations, the columns and the first pair of segments. The elements are activated with their respective concrete age. In each subsequent phase the new elements which represent the new segments are activated. Also the corresponding reinforcement and prestressing tendons are activated. A typical calculation phase covers a time period of one week as the cantilevering is progressing in one week long cycles. In the last phase the entire bridge model is active and the phase spans the service life of the bridge. The time period is subdivided into time increments which are uniform on the logarithmic time scale. Eventually the entire construction process and the service life of the bridge with a consistent time scale is built up from individual calculation phases. For the contraction period the simulation is virtually the projection of the construction stages into calculation phases.

Each calculation phase involves a basically identical series of events as those occur in reality in one construction cycle. At the starting point of the phase the new element which was "built" in the previous phase is now active and so are the corresponding prestressing tendons with the prestress applied. After a time step of one day the load system which represents the travelling formwork is moved forward to its subsequent position. That is the time when the position of the formwork is actually set according to the prescribed over-height curve. After a time step of six days the calculation phase is terminated and the new element with the corresponding tendons appears in the model at the beginning of the next phase.

If the actual construction is halted for any reason (*e.g.* holidays), additional time steps are inserted into the phase. Elements which represent the temporarily columns or other temporarily structural elements are activated and deactivated according to their presence in the actual structure. Boundary conditions are modified accordingly.

Due to the nature of the segmentwise construction procedure the deformation diagrams have discontinuities at the segment borders (*vide* Figure 7.17). When a new segment is built

it has zero deformation at time zero and before loading irrespective of the deformations of the already existing neighbouring segment(s). This corresponds to the situation in reality that the formwork for the subsequently cast segment is set at the prescribed elevation when the existing part of the cantilever has already undergone deformations. The deformation diagrams for segmentally built spans can be interpreted properly as diagrams showing the deformation of individual segments rather than the deformation of the span as a whole.

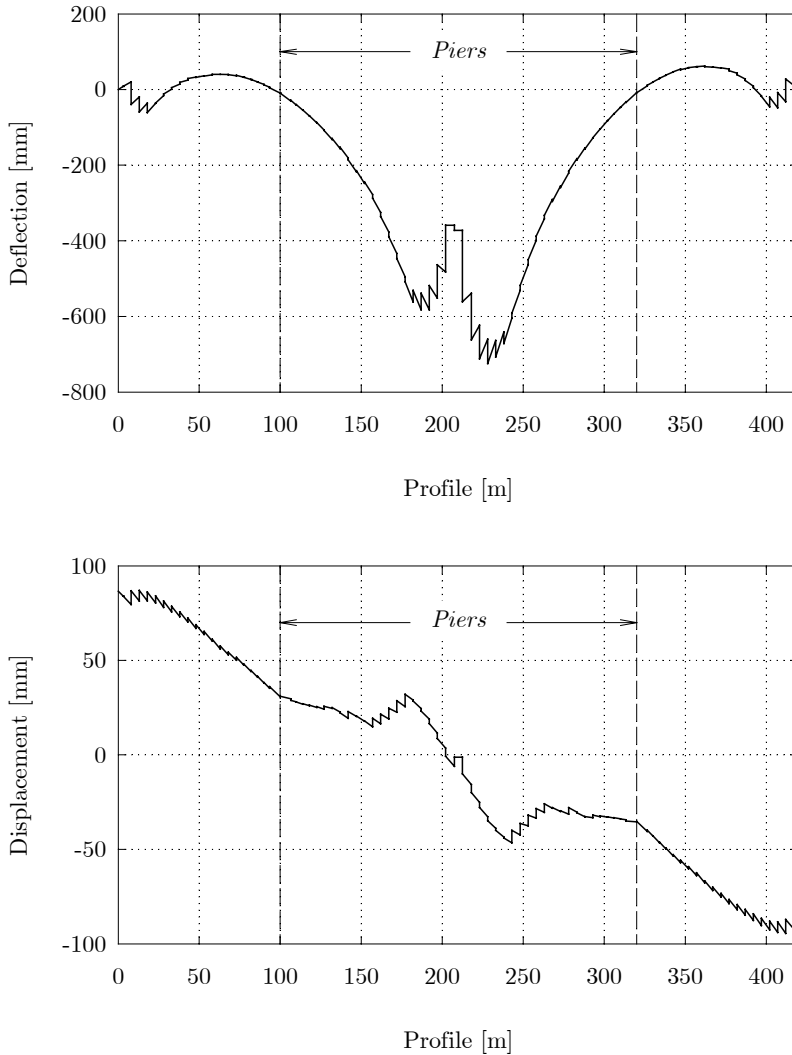


Figure 7.17 Long-time deflection (above) and horizontal displacement (below) of the superstructure

The long-time deflection curve determines the precamber curve (or over-height curve) for the construction. The precamber curve is the long-time deflection curve with opposite sign. It shows the necessary over-height for each segment over its design elevation where the formwork has to be positioned.

It was indicated that the weight of the travelling formwork is taken into account in the simulation. The realistic modelling of the formwork operation is important because it has a significant influence on the total deformations. The formwork typically weights around 500-900 kN which may be more than the weight of the segments themselves in the middle section of the span. Since the formwork is already on the cantilever, a new segment is affected by the weight of the formwork only as it is moving forward, *i.e.* the arm of force with respect to the pier is increasing. On the other hand that segment is fully affected by the removal of the formwork when the span is completed. That is why the influence of the weight of the formwork on the deflections has a net result which seems more of a deloading than a loading (*c.f.* positive deflection values in the main span shown in Figure 7.18). The deflection curve from the formwork is not symmetrical since the cantilevering procedure for the span is not symmetrical. In fact the difference in the total long-time deflection between the two cantilevers of the main span (*vide* Figure 7.17) is the result of that.

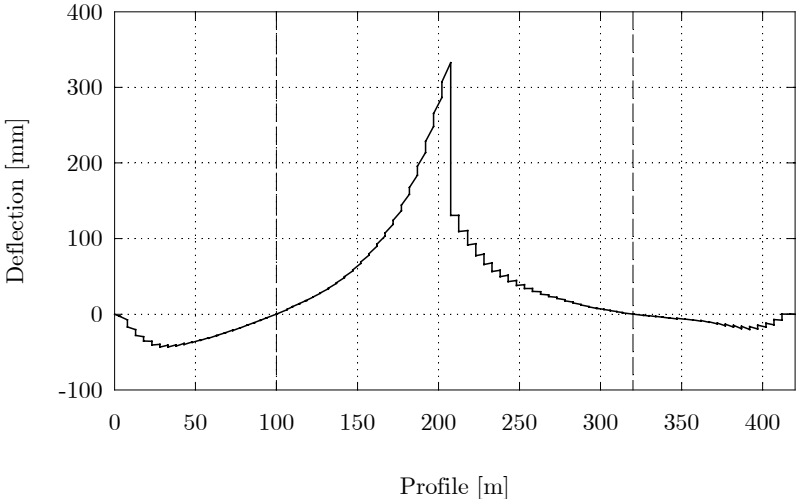


Figure 7.18 Long-time deflection of the superstructure from the weight of the travelling formwork



## Chapter 8

# Long-term Monitoring of Deformations

*The database on the observed deformations in Norddalsfjord Bridge, Støvset Bridge and Stolma bridge is the core component of the study. The chapter reviews the methods of deformation monitoring and the content of the database.*

### 8.1 Introduction

Long-term monitoring of deformations in concrete cantilever bridges is important in order to gain information on deformation development in these structures. The benefits are multifold. The measurements are used to verify the design calculation and to assess the state of the structure during its service life. The gained information can also be used to improve the theoretical models and the design procedure for future bridges. While various experiments can provide useful background and support information, monitoring the actual bridges is the only way to obtain direct knowledge on deformation development in these structures. Long-term deformation monitoring should be a standard procedure for any substantial concrete bridge as the status and value of the structure justifies the relative low extra cost and effort.

A database on observed deformations in the three investigated bridges was established within the current study. The substantial part of the data for Norddalsfjord Bridge and Støvset Bridge was available at the beginning of the study and that was completed with measurements during the study period up to the end of 2001. That means that the available data now covers 14 years and 8 years of the service life of Norddalsfjord Bridge and Støvset Bridge respectively. Stolma Bridge is relatively young, the measurement covers 3 years from the completion of the bridge.

Long-term deformation monitoring was implemented through strain and deflection measurements. The established database contains deflection measurements for Støvset Bridge and Stolma Bridge and deflection and strain measurements for Norddalsfjord Bridge. Deformation control during the construction period of the bridges were carried out by deflection measurements.

## 8.2 Methods of monitoring

### 8.2.1 Deformation control in the construction period

Strict control of deflections during the construction is crucial for the cantilevering method. In each construction stage the elevation of the entire existing span is measured by levelling including the forward tip of the travelling formwork. The measurement takes place after the prestressing force is applied in the tendons of the new segment and the formwork is moved to its subsequent position. That is the point when the travelling formwork is adjusted on the elevation prescribed by the precamber. The precamber is the designed elevation of the span plus the necessary over-height. The latter is determined from the expected long-term deflection.

The measured elevation of each existing segment in each construction stage is recorded in a pyramid-like diagram. The pyramid form is resulted as the data is recorded in rows and the length of the rows are gradually increasing at both ends as the length of the balanced cantilevers are increasing segment by segment. The diagram includes the theoretical expected value, the observed value and the difference between the two values.

In some cases the measurements are carried out also after the new segment is cast but before the prestressing tendons are installed and the formwork is moved. These additional measurements provide extra control.

Deflection measurements in the construction period are always carried out irrespective of further intentions of long-term monitoring.

### 8.2.2 Long-term monitoring of the deflection by levelling

The simplest and most reliable way to monitor the deflection of the superstructure is measuring the elevation of the deck by means of levelling on a regular basis. Such measurements do not require special instrumentation. The measurements can be easily integrated into the framework of the bridge inspection plan.

Deflection is a characteristic of the global structural behaviour of the bridge. It is the direct measure of the state of the bridge concerning deformations. On the other hand it is hardly possible to pinpoint the exact reason for an observed deviation from the expected theoretical deflection based on the deflection measurements alone.



It is favourable that the long-term deflection measurements are carried out as continuation of the measurements made during construction. The database on the measurements made during construction and the database on the long-term measurements should be coupled and managed as a coherent database. The author has experienced in case of all three investigated bridges that no connections were originally established between the reference points used for levelling in the construction stages and the reference points used for long-term measurements on the completed structure. In the absence of this information the two databases can not be coupled which renders the long-term measurements less valuable. The reference points in the construction stages are normally the upper point of deck slab in the centreline of the box-girder at the segment boundaries. When the bridge is completed those points are covered by the asphalt layer. The long-term measurements are taken either on the concrete parapet or on bolts. The exact difference between the corresponding points are often not known. For future bridges attention should be paid to document the elevation difference between the reference points.

### **8.2.3 Strain measurements**

Strain measurements are carried out with strain gauges which are normally welded to the reinforcing steel. The strain gauge is essentially a vibrating wire load cell. The sensor element is a stainless steel tube with a central steel wire clamped to the tube at both ends. The strain in the reinforcing steel is picked up by the wire in the steel tube. The exciter makes the wire oscillate and the pickup element measures and records the resonant frequency. The strain is the function of the resonant frequency measured in the wire.

Strain is a measure of local behaviour concerning deformations. The advantage of strain measurements over deflection measurements is that the strain in a given point of the structure is not effected by local structural effects occurring elsewhere in the structure as much as deflection. Consequently the observed data is the less disturbed which provides a more solid basis for evaluation with respect to creep and shrinkage.

On the other hand strain gauges are often found unreliable for long-term monitoring. The gauges may exceed their measurement range, may cease to operate due to technical malfunctions or may furnish incorrect readings. Since strain is a local measure the strain measurement may be affected by local material inhomogeneity and consequently the measured value may not be representative. Therefore strain measurements have to be evaluated with great caution and reservation.

## **8.3 Long-term deformations in the investigated bridges**

In this subsection mainly the available long-term measurements are reviewed. The measurements carried out in the construction phases are documented for all three bridges

which database is more or less complete. These measurements are presented and evaluated in comparison with the theoretical calculations in Chapter 9 in addition to the long-term measurements.

### 8.3.1 Norddalsfjord Bridge

Norddalsfjord Bridge was instrumented with strain gauges in the piers and in the superstructure. The primary objective with the instrumentation was to monitor the deformations during the construction phases in order to control the safety of the bridge and to verify the design calculations (Fergestad and Naess 1987). The majority of the strain gauges have remained operational and have continued to furnish reasonable readings.

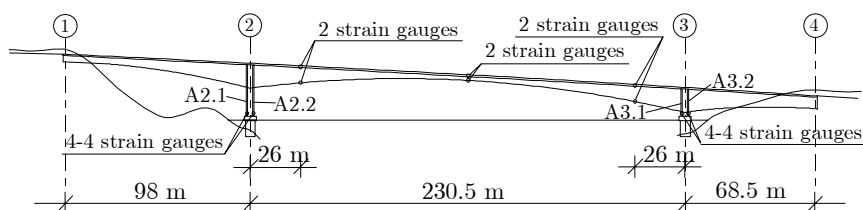


Figure 8.1 Position of the strain gauges

The twin wall piers were instrumented with four gauges in each wall. One gauge was placed in each quarter of the wall, 1.5 meter above the upper plane of the foundation. The average strain in the pier walls shown in Figure 8.2 are the average of the four measurements (or the average of the measurements by those gauges which have remained operational).

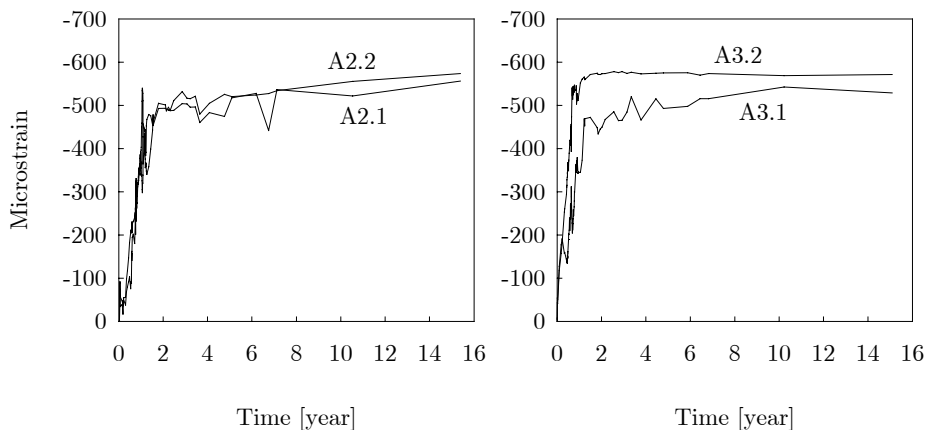


Figure 8.2 Average observed strain in the twin wall piers, Norddalsfjord Bridge

The measurements are shown from the moment the strain gauges were mounted and the pier section was cast. It means that the first 18 months covers the construction period for the pier walls in A2.1 and A2.2 while the same period is 15 months for the pier walls in A3.1 and A3.2.

It is seen that the average strain in the twin walls in A2 are almost the same while the strain in the twin walls in A3 are somewhat different. The reason is most likely that the superstructure around A2 was constructed more or less in a balanced double cantilever. Whereas the superstructure around A3 is rather asymmetric and the wall next to the side span ballast (in A3.2) was more loaded during construction than the wall next to the main span.

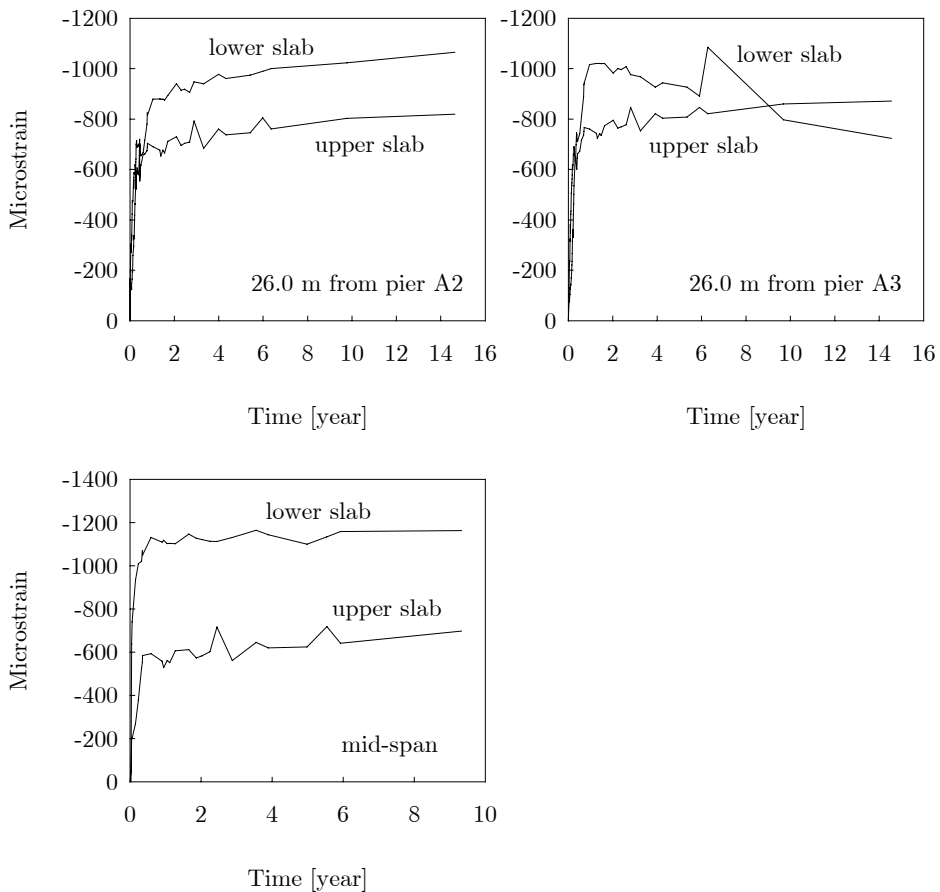


Figure 8.3 Observed strain in the superstructure, Norddalsfjord Bridge

The superstructure in the main span was instrumented in three sections with two strain gauges in each, one gauge in the upper slab and one gauge in the lower slab. The sections are situated at 26.0 meter from A2, at mid-span and at 26.0 meter from A3 (*vide* Figure 8.1). Figure 8.3 shows the measured strains in the superstructure. The measurements are shown from the moment the strain gauges were mounted and the respective segments were cast. No reasonable explanation was found why the strain in the lower slab near A3 has been seen decreasing, it is assumed that the gauge has been malfunctioning.

However the deflection in the completed bridge was not regularly monitored through its life span, two measurements took place in 2001 in addition to the two measurements which were done soon after the bridge was completed in 1987. The results of the levelling are shown in Figure 8.4 with the first measurement being the reference. The elevation of the bridge deck over the design elevation is shown in Figure 8.5 together with precamber curve. The precamber curve has a high value over the abutment in A1 (*vide* Figure 8.1) because the superstructure was jacked down in A1 prior to the continuity in the main span was established. It is seen that the elevation of the deck after 14 years is still well above the design elevation. However, the precamber was set significantly higher than it would follow from the expected long-term deflection.

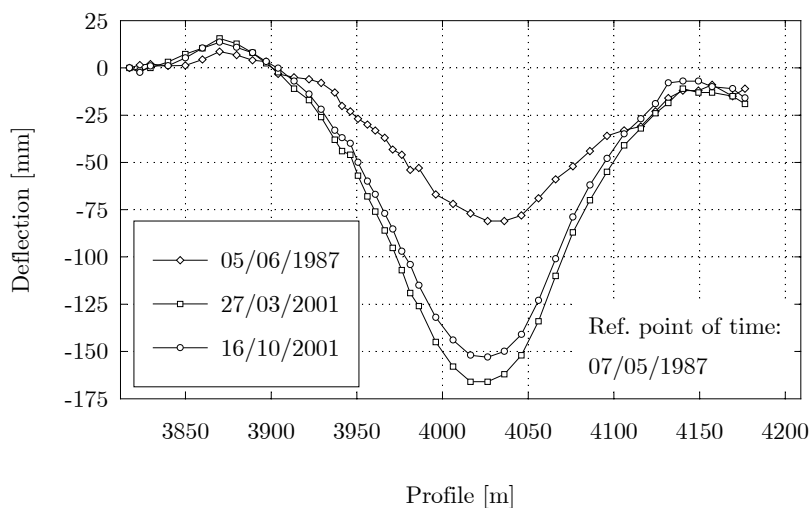


Figure 8.4 Deflection of the superstructure, Norddalsfjord Bridge

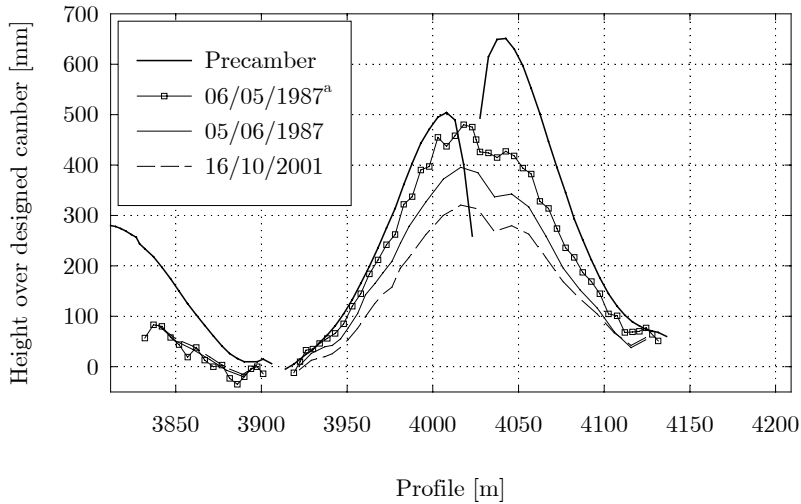


Figure 8.5 Height of the bridge deck over the design camber, Norddalsfjord Bridge (mid-span at 4025.25 m); <sup>a</sup> prior to the asphalt layer was placed

### 8.3.2 Støvset Bridge

The deflection in the superstructure of Støvset Bridge has been monitored on a regular basis. The first measurement on the completed bridge took place five months after the bridge was completed. Now one measurement is carried out in each year. The relative deflections are shown in Figure 8.6 where the first measurement is used as the reference.

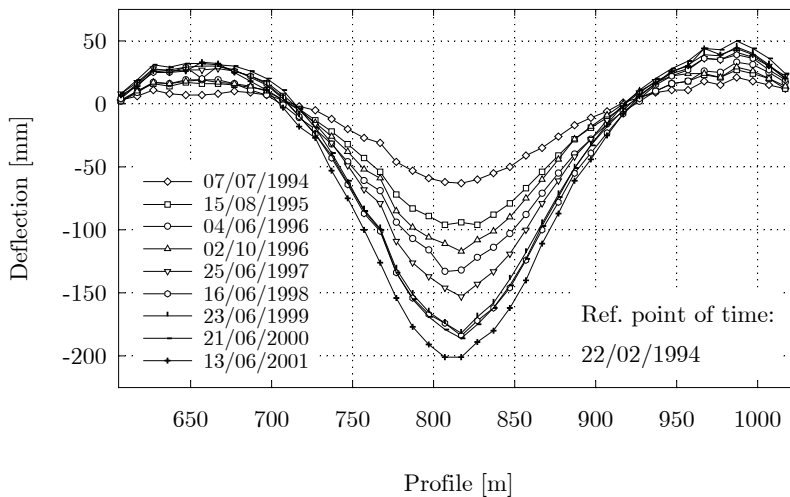


Figure 8.6 Deflection of the superstructure, Støvset Bridge

The development of the relative deflection at mid-span (at profile 815.5 m) is shown in Figure 8.7.

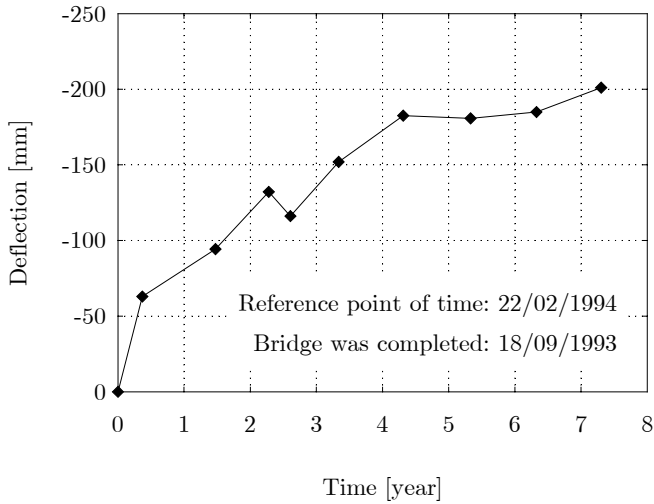


Figure 8.7 Deflection at mid-span, Støvset Bridge

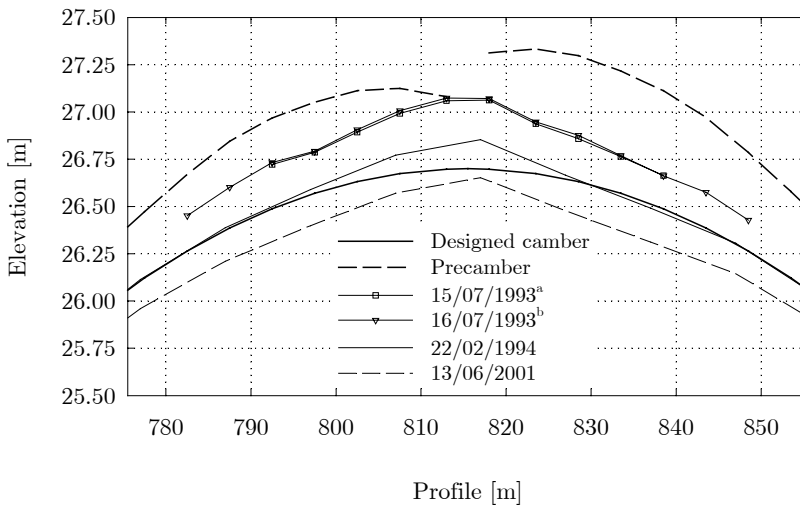


Figure 8.8 Elevation of the middle section of the central span, Støvset Bridge (mid-span at 815.5 m); <sup>a</sup> after the cantilevers are connected and the formwork is removed, <sup>b</sup> after the continuity tendons are prestressed

The elevation of the bridge deck around the middle section of the central span is shown in Figure 8.8. It is seen that the bridge deck now, eight years after the bridge was completed, is below the design elevation. The first measurement on the completed structure, just five months after the completion, indicated that the deck, apart from a short section around the mid-span, reached its design elevation. A partial explanation is suggested by the two measurements carried out in the last phase of the construction. It is seen in the diagram that the prestressing by the continuity tendons did not uplift the superstructure around the mid-span as it was expected. The design calculation figured the uplift at mid-span being equal to 125 mm whereas the observed uplift was only 11 mm. It can partially be explained with lower effective prestressing force in the continuity tendons as result of excess frictional prestress loss in the rugged and angular joint of the cantilevers. Besides it has to be mentioned that the author's calculation figured only a 51 mm uplift in contrast to 125 mm.

### 8.3.3 Stolma Bridge

Stolma Bridge has been monitored by levelling. So far four measurements took place on the completed bridge in addition to the measurements carried out during the construction phases. The first measurement took place right after the completion of the bridge. The results of the measurements are shown in Figure 8.9 with the first measurement being the reference.

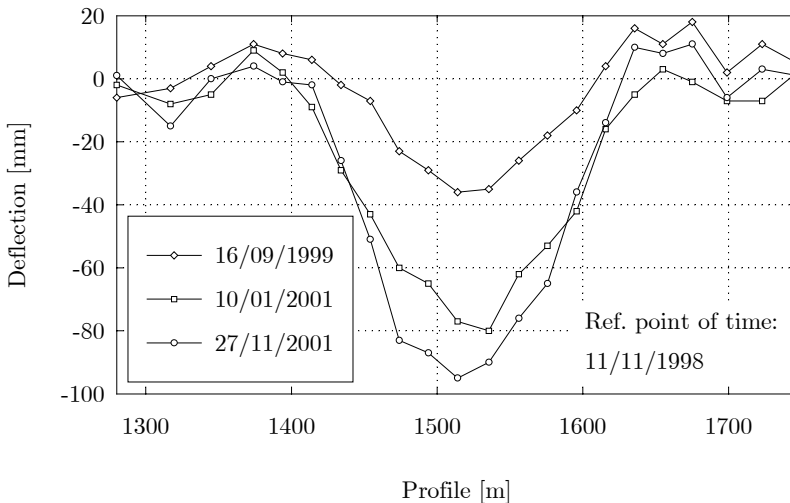


Figure 8.9 Deflection of the superstructure, Stolma Bridge

Figure 8.10 shows the over-height of the bridge deck on the design camber. The theoretical precamber shown in the diagram was slightly corrected during the erection of the cantilevers because the observed deflections in the last few segments were somewhat

smaller than predicted. The small deviation from the expected deflection did not constitute a significant problem. The right cantilever of the main span was built with an eight segment lag behind the left cantilever which offered enough room for correction. Eventually the two cantilevers met within a height difference of 10 mm which was rather satisfactory (Rosseland and Thorsen 2000). Small deviation from the intended elevation is not much of a problem in a high camber as the primary importance is to achieve a smooth curvature.

The relative deflection at mid-span in the first three years was 92 mm and the over-height is now 290 mm.

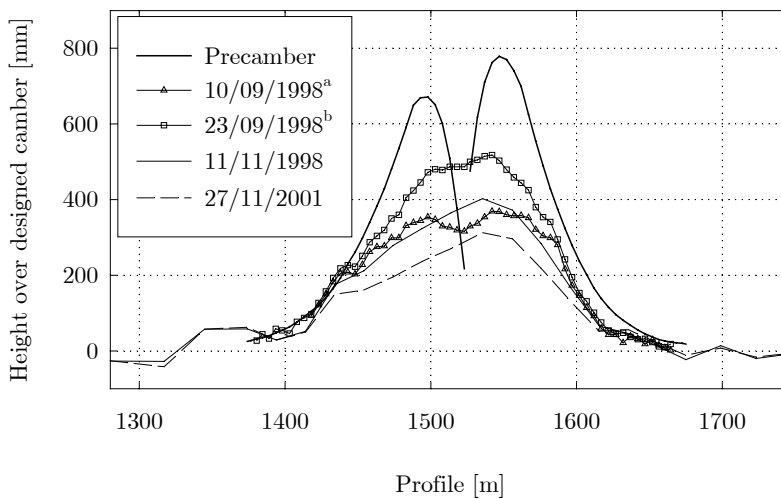


Figure 8.10 Height of the bridge deck over the design elevation, Stolma Bridge (mid-span at 1524.5 m); <sup>a</sup> after the cantilevers are connected, <sup>b</sup> after the formwork is removed and the continuity tendons are prestressed



## Chapter 9

### Numerical Studies

*The three investigated bridges are analysed and the calculated results are presented. The calculation is compared with the measurements. A sensitivity study is carried out to determine the influence of variation in creep, shrinkage and prestressing on the deflections. Further sensitivity investigations are made concerning the environmental parameters and the long-term deformation characteristics of LWAC.*

#### 9.1 Introduction

The calculated deformation responses of the three investigated bridges are presented in this chapter. The results are evaluated in comparison with the measured deformations. The numerical analyses were carried out with finite element program system DIANA Release 7.2 (DIANA 1999). The numerical model and simulation used for the analysis of the bridges were discussed earlier in the thesis. The mathematical algorithm of the rate-type constitutive model for aging viscoelasticity was described in Chapter 6 while the finite element model and the numerical simulation was described in Chapter 7. The bridges were introduced in Chapter 2.

In the first part of the chapter, the measured deformations are compared with the theoretical values calculated with the creep and shrinkage models of the CEB-FIP Model Code 1990 (CEB 1991). The viscoelastic model in the numerical analyses is the Kelvin chain model. For Støvset Bridge and Stolma Bridge, the elastic modulus of both the normal density concrete and the lightweight aggregate concrete were taken from laboratory tests. For Norddalsfjord Bridge, test result was not available. The elastic modulus was estimated as 75 % of the value given by the MC90 formula, in accordance with the observed tendency in high strength concrete in Norway (*vide* subsection 5.2.2). The creep coefficient and the shrinkage strain of

the lightweight aggregate concrete was assumed the same as those of normal density concrete of the same strength.

The calculated responses in this part of the thesis are considered as deterministic values while it is acknowledged that predictions based on theoretical models are marked with considerable statistical uncertainty. To study the effect of the variation in the model parameters, various sensitivity analyses were carried out. The effect of variation in creep, shrinkage and the effective prestressing force on the deflection was determined in all three bridges. Then, the influence of potential estimation error in the average relative humidity and temperature was considered in the analysis of Støvset Bridge.

It was concluded in Chapter 4 that the particular characteristics of creep and shrinkage in lightweight aggregate concrete is not well understood yet and the existing theoretical formulations are considered controversial. The influence of potential prediction error in that regard was studied for Støvset Bridge.

Finally, the CEB-FIP Model Code 1990 and the Bazant's B3 model are compared for Støvset Bridge. The latter model normally produces considerably higher long-term creep (*vide* Figure 3.12).

## 9.2 Norddalsfjord Bridge

Norddalsfjord Bridge is rather special in the sense that there is a large vertical drop in the elevation of the deck between the two ends of the bridge (*vide* Figure 2.3). Under such precondition in the geometry, the camber in deck is very small which allows little tolerance for excess deflection.

The calculated deflection of the superstructure is shown in Figure 9.1 in three characteristic points of time: (1) prior to the last segment is cast at mid-span and the cantilevers are connected, (2) after the bridge is entirely completed and ready for opening for traffic and (3) after 70 years of service. Deformations after 70 years can be considered as the final value of the deformations, at least for models like the CEB-FIP Model Code 1990 where a theoretical final, asymptotic value of creep exists. Either way, the deformation gradient is very small after that period of time and the 70 years of age is a reasonable reference time. This is the most important curve of the three because it is necessary for determining the precamber of the superstructure, *i.e.* the required over-height for each individual segment in the construction phase. The precamber is determined as the final deflection curve taken with opposite sign and usually further raised by a reasonable additional over-height. The latter provides a safety margin in case the calculation underestimates the long-term deflection.

The 200 mm deflection at the abutment in A1 comes from jacking down the superstructure in order to stabilise the twin wall pier in A2 before continuity of the span was established.

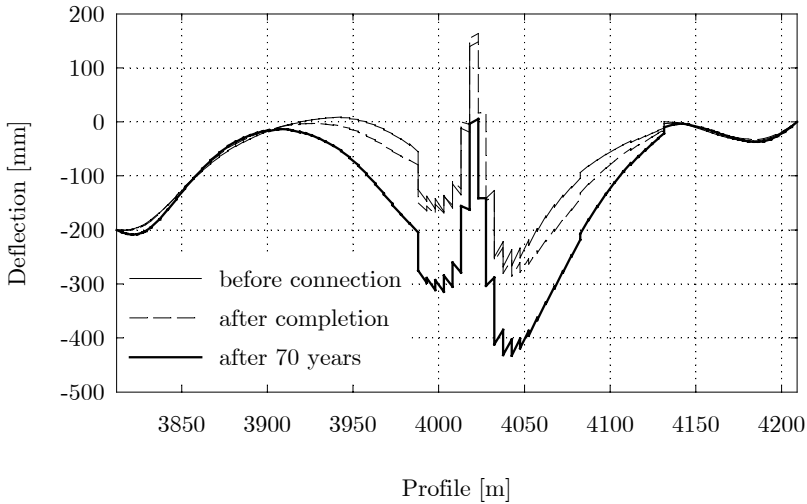


Figure 9.1 Deflection of the superstructure, Norddalsfjord Bridge (piers are at 3910.0 m and 4140.5 m)

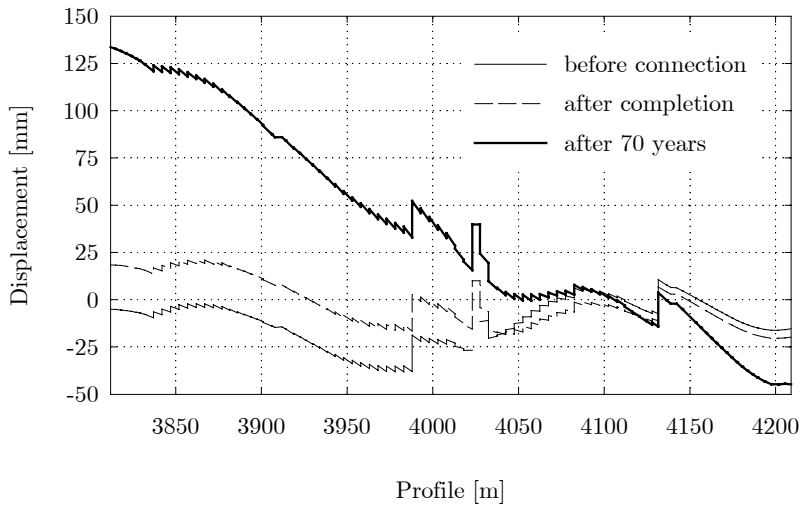


Figure 9.2 Horizontal displacement of the superstructure, Norddalsfjord Bridge (the values apply for the reference line of the superstructure), (piers are at 3910.0 m and 4140.5 m)

The horizontal displacement of the superstructure is shown in Figure 9.2 in the reference line of the box-girder. Virtually the entire horizontal movement is handled by the left pier in A2 since the right pier in A3 has no flexibility due to its small height. Therefore the movement in A2 is significant, the long-term static displacement alone is 86 mm. The

advantage of the twin wall pier design is its capacity to cope with large horizontal movements. When joining the cantilevers at mid-span by simple articulation was abandoned long time ago due to its many disadvantages in structural performance, the possibility of expansion joint went as well. The piers had to be made flexible enough to overcome the problem.

The calculated development of strains are compared with the measurements in Figure 9.4 and Figure 9.5. The position of the strain gauges are shown in Figure 9.3 (also *vide* subsection 8.3.1).

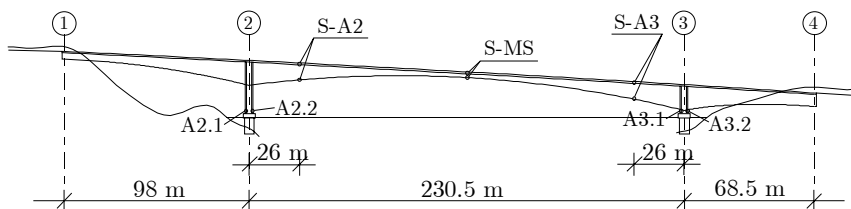


Figure 9.3 Position of the strain gauges in Norddalsfjord Bridge

The starting point of the diagrams correspond to the moment when the strain gauges were mounted and the corresponding sections were cast. In the calculation the annual average relative humidity and temperature were set equal to 75 % and 10° C, respectively. The comparison for the pier walls shows that the long-term strain was overestimated. In fact very little long-term strain is seen in the measurements.

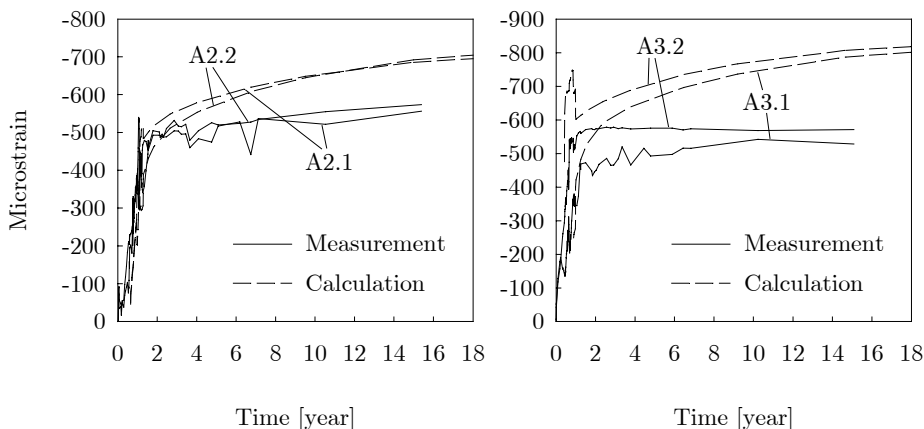


Figure 9.4 Calculated and measured strain in the twin wall piers, Norddalsfjord Bridge

The calculation shows reasonably good agreement with the measurements in the superstructure near the piers, particularly for S-A2 (*vide* Figure 9.3). The strain gauge in the lower slab in S-A3 is most certainly malfunctioning. The calculated strains at mid-span (S-MS) show good agreement with the measurements as far as the short-time responses are concerned. The observed long-time strain, however, is somewhat higher in the prestressed lower slab than it was calculated. The strain development at mid-span is very sensitive to variations in the construction schedule and the quality of the joint.

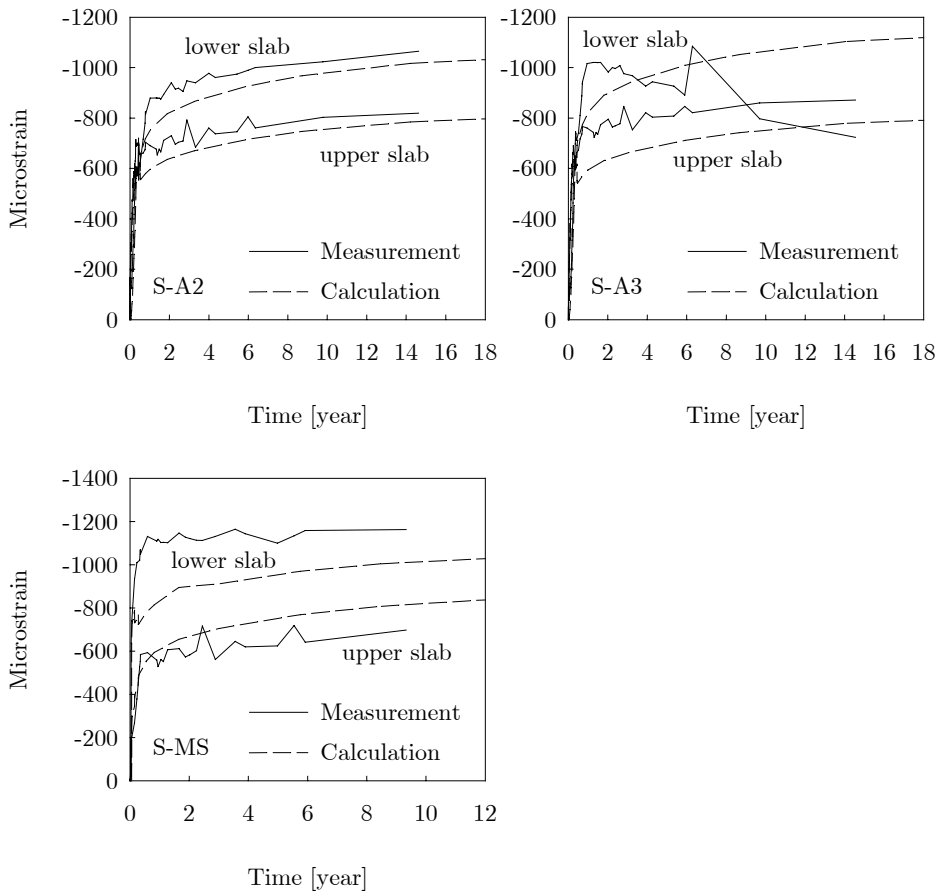


Figure 9.5 Calculated and measured strain in the superstructure, Norddalsfjord Bridge

The deflection at mid-span is shown in Figure 9.6. Unfortunately no long-term measurements were made until 2001, thus the development of the deflection can not be seen. The two measurements made in 2001 indicate very good agreement. The measurement made just prior to the asphaltting is used as the reference, *i.e.* the starting point of the diagram.

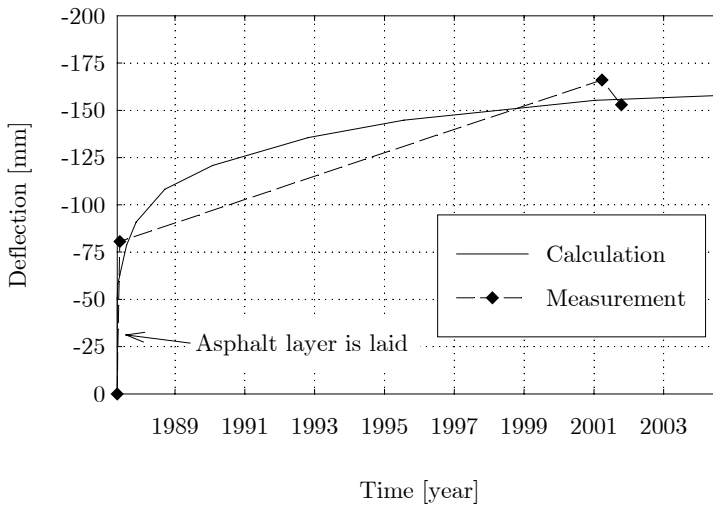


Figure 9.6 Deflection at mid-span, Norddalsfjord Bridge (the starting point of the diagram is measurement made before the asphalt layer is laid)

The measured and calculated deflections in the construction phase are shown for two segments in Figure 9.8. The position of the segments are illustrated in Figure 9.7 with their front profile where the measurements were taken.

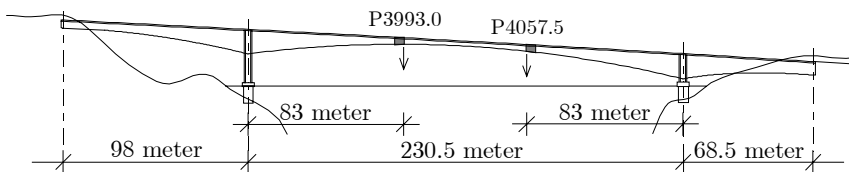


Figure 9.7 Position of the profile 3993.0 m and 4057.5 m, Norddalsfjord Bridge

The deflection is shown from the stage when the respective segment was cast and prestressed and the formwork was moved to its next position. The measurements are also made in the same stage of the subsequent construction cycles. The axis is given according to the progress made in the cantilevering, instead of the time. The deflection is seen somewhat overestimated for P3993.0. The last data point corresponds to the stage prior to the formwork is removed and the superstructure is jacked down in A1. For P4057.5, the last data point shows the deflection when the formwork is moved into the position of the last segment and it is adjusted vertically.

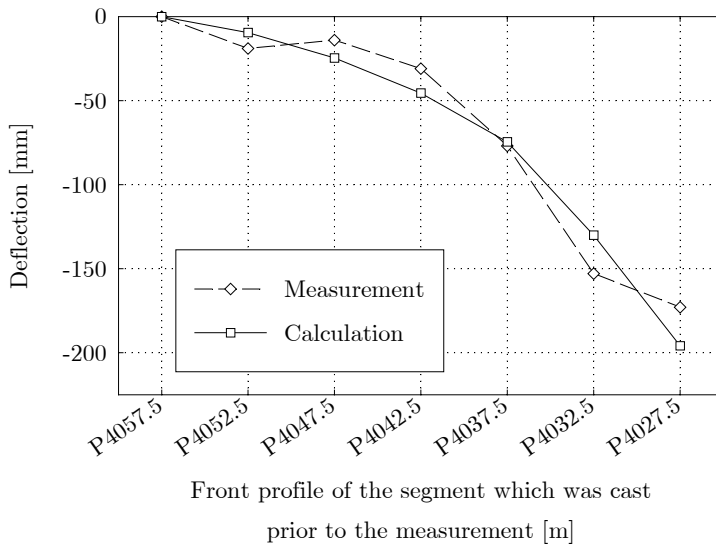
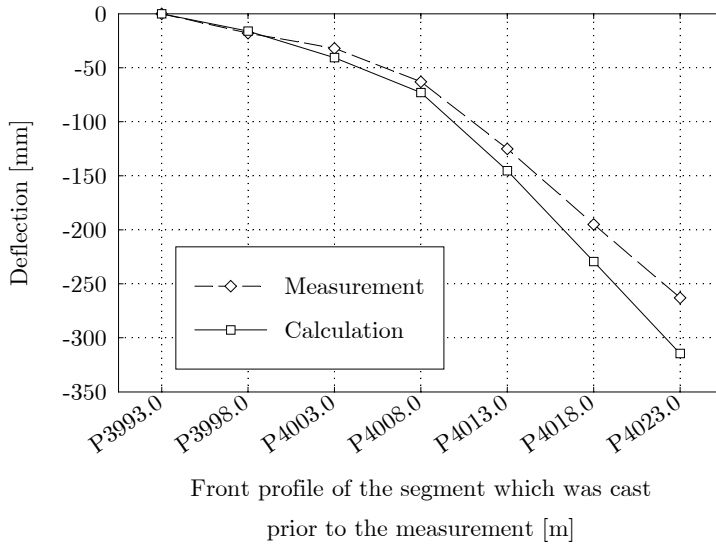


Figure 9.8 Deflection during construction at profile 3993.0 m (top diagram) and 4057.5 m (bottom diagram), Norddalsfjord Bridge (the diagrams start when the segment to profile 3993.0 m and 4057.5 m, respectively, was cast and prestressed and the formwork is moved to its subsequent position)

### 9.3 Støvset Bridge

The calculated deflection and the horizontal displacement of the superstructure are shown in Figure 9.9 and in Figure 9.10, respectively.

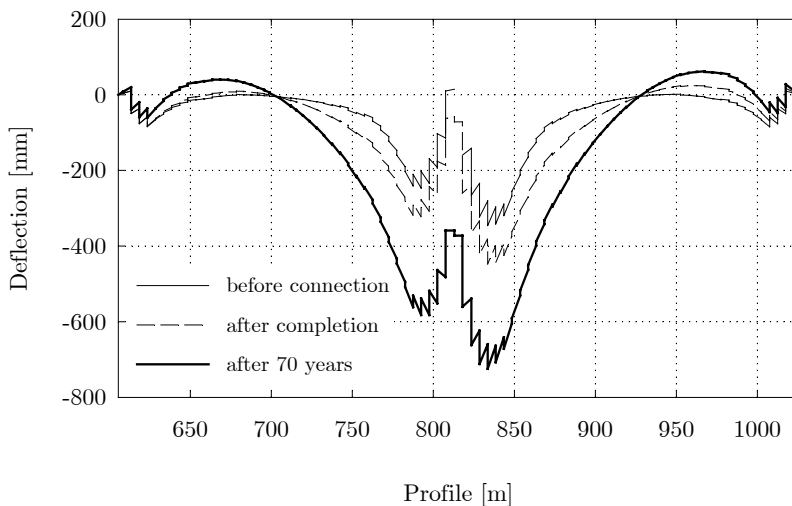


Figure 9.9 Deflection of the superstructure, Støvset Bridge (piers are at 705.5 m and 925.5 m)

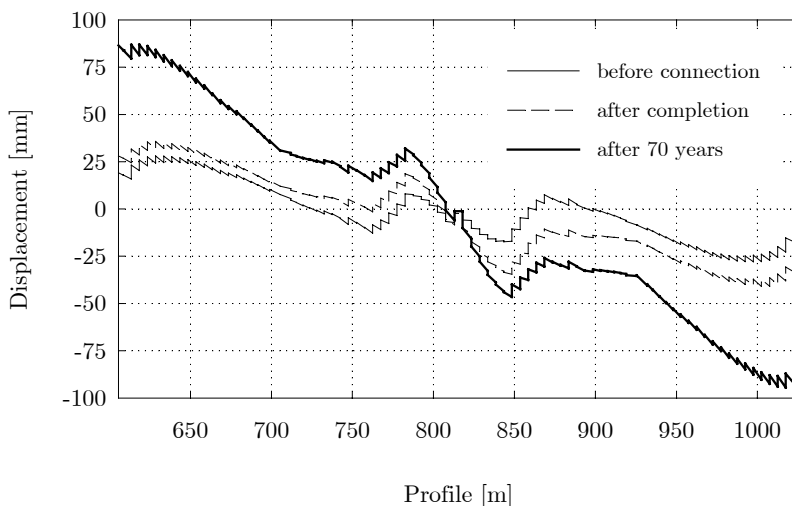


Figure 9.10 Horizontal displacement of the superstructure, Støvset Bridge (the values apply for the reference line of the superstructure), (piers are at 705.5 m and 925.5 m)



The deflection diagram indicates that the rotation at the piers are significant after 70 years which explains the relatively large deflections. The deflections are considerable larger than in the slightly longer span of Norddalsfjord Bridge (*vide* Figure 9.1) and almost as large as in the much longer span of Stolma Bridge (*vide* Figure 9.14). The horizontal displacement diagram suggests the explanation. It is seen that there are sudden changes in the gradient of the long-time curve at the piers (unlike in Norddalsfjord Bridge, *vide* Figure 9.2 and Stolma Bridge, *vide* Figure 9.15) which implies that the specific displacement is considerably smaller in the central span than in the side spans. It means that the pier walls are too rigid and they are acting as constraints on the central span. Internal tensile force is being built up in the main span as the result of long-term creep and shrinkage effects. Eventually, this tensile force is acting on the pier-heads and bending the piers toward the main span.

In the calculation the annual average relative humidity and temperature were set equal to 70 % and 10° C, respectively. The measured and calculated deflection at mid-span are compared in Figure 9.11. The reference point of the diagram is the moment when the superstructure is completed, the formwork is removed and the continuity tendons are prestressed. The small positive deflection at the beginning of the calculated diagram is coming from the partial recovery of creep deformation caused by the weight of the formwork. The agreement between calculation and measurement can be considered as reasonably good, however, moderately underestimated. The average deformation gradient within the first five years is seen higher than it was estimated.

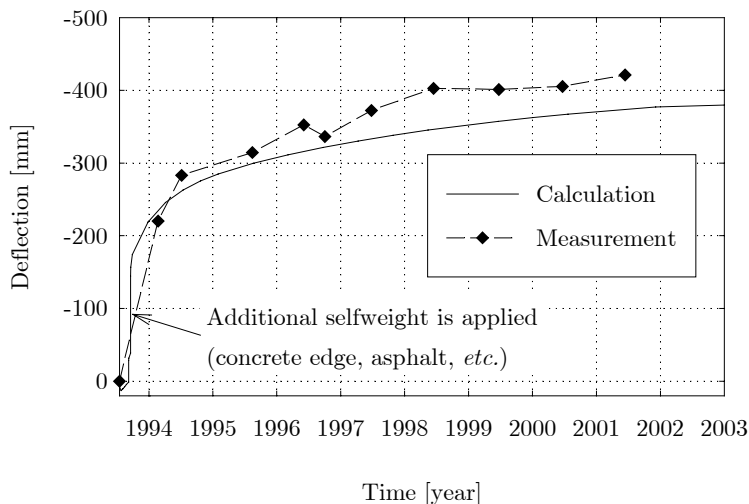


Figure 9.11 Deflection at mid-span, Støvset Bridge (the diagram starts when the span is completed and the continuity tendons are prestressed)

The deflection of the segment 3-17 at profile 838.5 m during in construction phases is shown in Figure 9.13. Figure 9.12 shows the position of the segment.

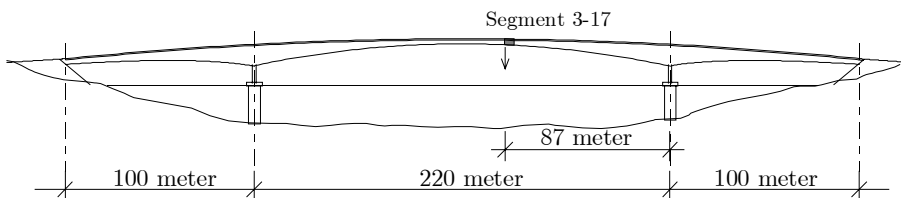


Figure 9.12 Position of the front profile of segment 3-17 (P838.5 m), Støvset Bridge

The diagram starts when the segment 3-17 was cast and prestressed and the formwork was moved to its next position. The calculated values are in close agreement with the measurements until the cantilevers are connected. The comparison is not too relevant in that stage since the elevation of the cantilever was adjusted prior to the connection. The last two data points, however, illustrate that the prestressing by the continuity tendons failed to raise the mid-span in contrast to what was expected (*vide* subsection 8.3.2).

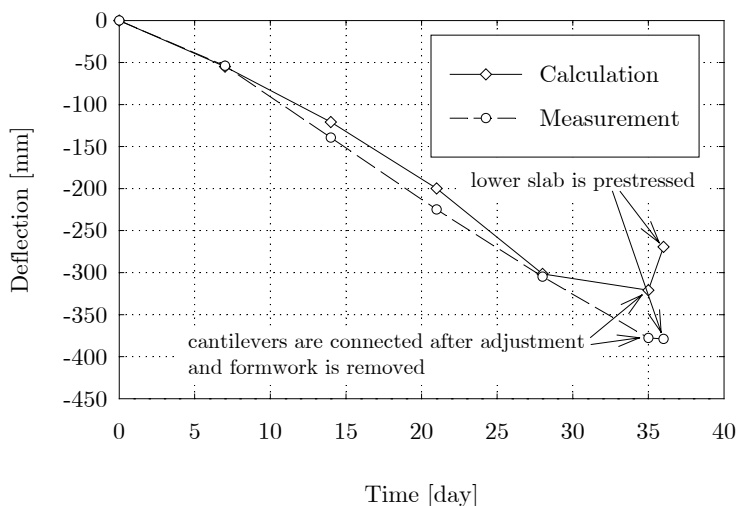


Figure 9.13 Deflection during construction at profile 838.5 m, Støvset Bridge

## 9.4 Stolma Bridge

The calculated deflection of the superstructure is shown in Figure 9.14. A few segments around mid-span are seen at a higher elevation after the bridge is completed than prior to

the last segment is cast. The reason is that the uplift resulted from the removal of the formwork and the prestressing by the continuity tendons are larger than the opposite effect from the weight of the last segment and the additional non-structural bridge parts.

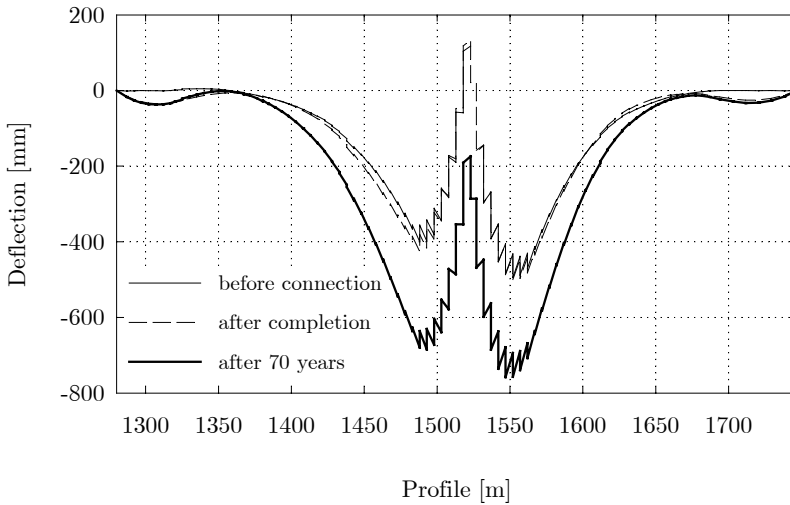


Figure 9.14 Deflection of the superstructure, Stolma Bridge (piers are at 1374 m and 1675 m)

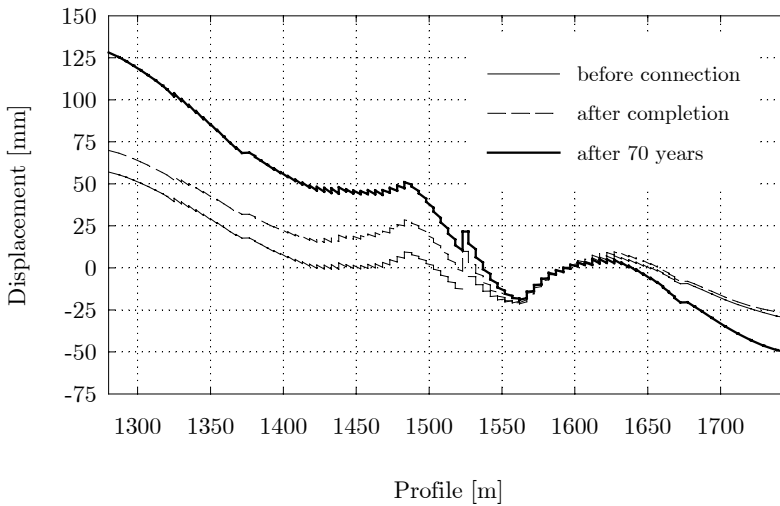


Figure 9.15 Horizontal displacement of the superstructure, Stolma Bridge (the values apply for the reference line of the superstructure), (piers are at 1374 m and 1675 m)

The calculated horizontal displacement of the superstructure is shown in Figure 9.15.

The calculated and observed deflection at mid-span are compared in Figure 9.16. The diagram starts when the formwork is removed from the completed superstructure and the lower slab is prestressed. The long-term measurements indicate smaller deflection than it was predicted by the theoretical model. In the calculation the annual average relative humidity and temperature were set equal to 80 % and 8° C, respectively.

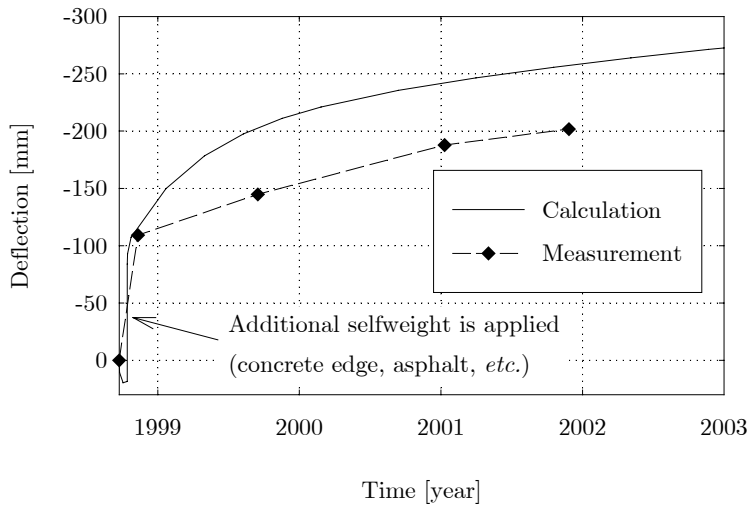


Figure 9.16 Deflection at mid-span, Stolma Bridge (the diagram starts when the span is completed and the continuity tendons are prestressed)

Figure 9.18 compares the measured and the calculated deflection in the construction phase for segment 3-25 at profile 1547 m (vide Figure 9.17).

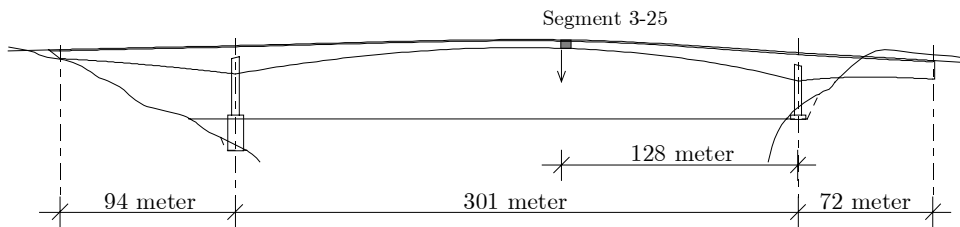


Figure 9.17 Position of the front profile of segment 3-25 (P1547 m), Stolma Bridge

Unlike previous diagrams concerning the construction stages, the diagram in Figure 9.18 starts when the formwork is set in its position for casting the 3-25 segment, *i.e.* the values include the deflection from its own selfweight and prestressing. The calculation is virtually

in perfect agreement with the measurements after the 3-25 segment and the following two segments are completed while the observed deflection is smaller in the subsequent stages.

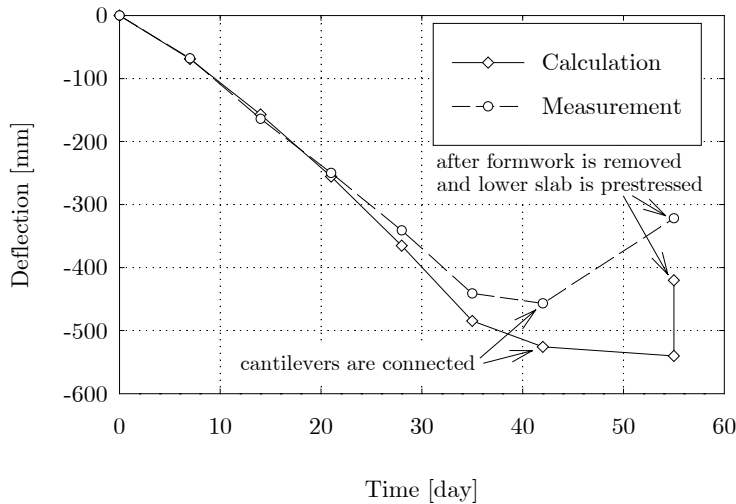


Figure 9.18 Deflection during construction at profile 1547 m, Stolma Bridge

## 9.5 Sensitivity of the deflections to variations in material models

Sensitivity of the deflections to variations in the creep coefficient, the shrinkage strain and the effective prestressing force were investigated. Two parameters were introduced into the DIANA code in order to manipulate the predefined creep and shrinkage models, a multiplier for the creep coefficient,  $\vartheta_c$  and a multiplier for the shrinkage strain,  $\vartheta_s$  (vide Eq. (9.1)).

$$\varepsilon(t) = \int_0^t \left( \frac{1}{E_c(t_o)} + \vartheta_c \cdot \frac{\phi(t, t_o)}{E_{c28}} \right) d\sigma(t_o) + \vartheta_s \cdot \varepsilon_s(t) \quad (9.1)$$

Three analyses were carried out for each bridge in addition to the original analysis: (1) the creep coefficient was increased by 30 percent,  $\vartheta_c = 1.30$ , (2) the shrinkage strain was increased by 30 percent,  $\vartheta_s = 1.30$  and (3) the effective prestressing force was reduced by 3 percent. The latter is meant to consider variation in the effective prestressing force due to various uncertainties such as that in steel relaxation, friction coefficient between the strand and the sheathing, wobble effect and anchor slip.

The variation in the deflection responses are summarised in Table 9.1. The maximum deflection prior to the cantilevers are joint, the maximum deflection after 70 years and the mid-span deflection after 70 years are shown in the table. The variation in the creep and the

shrinkage characteristics produces fairly consistent variations in the corresponding responses percentage-wise in the three bridges.

Table 9.1 Variation in the deflection responses

	original	+ 30 % creep coefficient		+ 30 % shrinkage		- 3 % eff. prestress	
	mm	mm	%	mm	%	mm	%
<b>Norddalsfjord Bridge</b>							
max. prior to connection	-268	-281	(4.6)	-268	(0.0)	-276	(2.6)
max. after 70 years	-433	-479	(10.7)	-443	(2.4)	-459	(6.0)
mid-span after 70 years	-141	-171	(21.4)	-153	(8.5)	-160	(13.5)
<b>Støvset Bridge</b>							
max. prior to connection	-346	-366	(5.7)	-346	(0.0)	-353	(2.2)
max. after 70 years	-725	-809	(11.7)	-753	(4.0)	-743	(2.5)
mid-span after 70 years	-373	-437	(17.4)	-404	(8.3)	-384	(3.1)
<b>Stolma Bridge</b>							
max. prior to connection	-495	-522	(5.5)	-495	(0.0)	-504	(1.8)
max. after 70 years	-758	-848	(11.9)	-778	(2.6)	-778	(2.7)
mid-span after 70 years	-286	-352	(23.0)	-309	(7.8)	-299	(4.4)

The number in the brackets is the percentage increment as compared to the original value.

The 30 % higher creep coefficient gives an 11-12 % larger maximum long-time deflection and a 5-6 % higher maximum deflection prior to the cantilevers are connected. The 30 % higher shrinkage strain produces a 2-4 % higher maximum long-time deflection. The shrinkage has virtually no effect on the deflections until the cantilevers are connected, because the cantilevers can move unrestrained in the horizontal direction.

## 9.6 Estimation error for the relative humidity and the temperature

The relative humidity and the temperature of the ambient environment are parameters of the material models (*vide* subsection 3.2.2). The final value of creep and shrinkage are smaller at higher relative humidity and reduced temperature. Also their development with time is decelerated at higher relative humidity and reduced temperature. Furthermore, the maturity of the concrete is reduced while the elastic modulus at given age is higher at reduced temperature.

In the calculations the relative humidity and the temperature are taken into account with their expected annual average values. These values are assumed uniform and representative

over the entire life span of the bridges. The expected annual average value of the relative humidity and the temperature can normally be estimated based on meteorological records of nearby weather observation posts. Depending on the availability of the information and local conditions, the estimated values may slightly differ from the actual values. The effect of potential error in the parameter estimation for the relative humidity and the temperature was determined for Støvset Bridge.

Along the Norwegian coast, excluding the far northern part, the annual average relative humidity varies around 70-80 % and the annual average temperature is between 5° C and 10° C. The average relative humidity is higher on the western coast (Stolma Bridge and Norddalsfjord Bridge) and lower on the northern coast (Støvset Bridge).

In the present analysis, the expected range of the variation is determined for the deflections. Figure 9.19 shows the deflection of the main span calculated with two sets of parameter values. The maximum long-time deflection is 9 % smaller at the relative humidity of 80 % and the temperature of 5° C as compared to the original calculation with the relative humidity taken as 70 % and the temperature taken as 10° C. The deflection in the construction phase is little affected. The development of the mid-span deflection is shown in Figure 9.20.

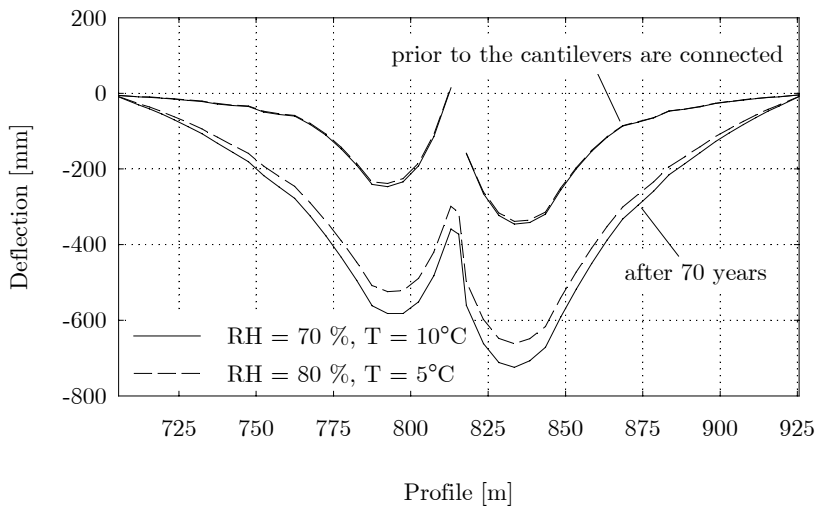


Figure 9.19 Deflection in the central span under different average environmental conditions, Støvset Bridge<sup>1</sup>

<sup>1</sup> The deflection diagram represents the same deflection as previous zigzag-like diagrams but only that value at the segment boundaries is considered which belongs to the segment built first. This is for the simpler illustration and easier comparison between curves.

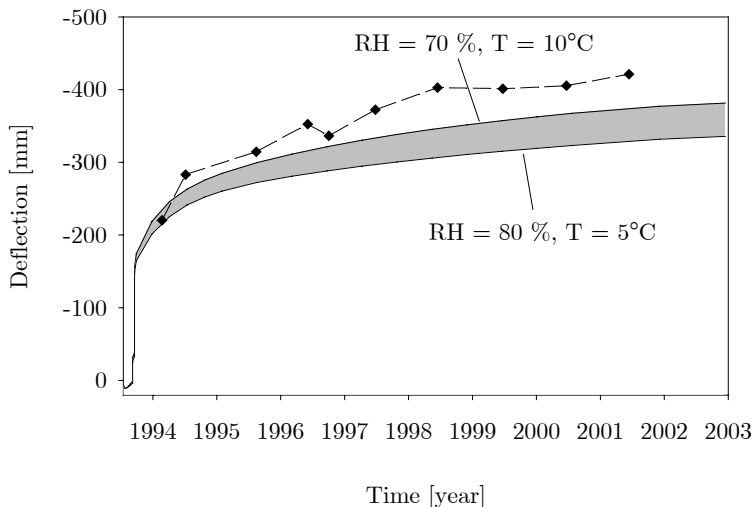


Figure 9.20 Deflection at mid-span under different environmental conditions, Støvset Bridge

## 9.7 Uncertainty in the long-term characteristics of LWAC

In previous calculations, the creep coefficient and the shrinkage strain of the lightweight aggregate concrete was assumed the same as those of normal density concrete of the same strength. Although extension to the CEB-FIP Model Code 1990 concerning LWAC (*fib* 2000b) was published recently which comments on the creep and shrinkage characteristics of LWAC but the existing theoretical formulations seem questionable (*vide* Chapter 4).

In the present approach of modelling, the creep compliance of normal weight concrete is supplemented with two reduction factors. The reduction factors are assigned to the elastic modulus and the creep coefficient (*vide* Eq. (9.2)). They are functions of the oven-dry density of the lightweight aggregate concrete. The formulations were presented in Table 4.1.

$$J(t, t_0) = \frac{1}{\eta_E \cdot E_c(t_0)} + \frac{\eta_\phi \cdot \phi(t, t_0)}{\eta_E \cdot E_{c28}} \quad (9.2)$$

In previous calculations, the elastic modulus of LWAC was taken from test results, thus the  $\eta_E$  modifying factor was intrinsically considered while, on the other hand, the creep coefficient was estimated as for NWC of the same strength. The resulted creep deformation was approximately 50 % higher than that of NWC (*vide* Eq. (9.3)).

$$\frac{1}{\eta_E} = \frac{1}{(\rho/2200)^2} = 1.52 \quad \text{where } \rho = 1784 \text{ kg/m}^3 \text{ (Støvset Bridge)} \quad (9.3)$$



In the first analysis of the present investigation, it was determined what effect it makes on the deflections if the creep deformation is considered according the LWAC extension of the CEB-FIP Model Code 1990. It suggests that the creep deformation of LWAC is 20 % higher than that of NWC, the strength being the same.

$$\frac{\eta_{\phi}}{\eta_E} = 1.2 \quad (\text{vide Eq. (9.2)}) \quad (9.4)$$

For Støvset Bridge, it implies that the creep coefficient is approximately 80 % of that of normal weight concrete.

$$\eta_{\phi} = 1.2 \eta_E = 1.2(\rho/2200)^2 \simeq 0.8 \quad \text{where} \quad \rho = 1784 \text{ kg/m}^3 \quad (9.5)$$

In the second analysis, the reduced creep coefficient was combined with a 50 % higher shrinkage strain. The LWAC extension of the CEB-FIP Model Code 1990 states the final shrinkage strain of LWAC is higher than that of NWC by up to 50 %.

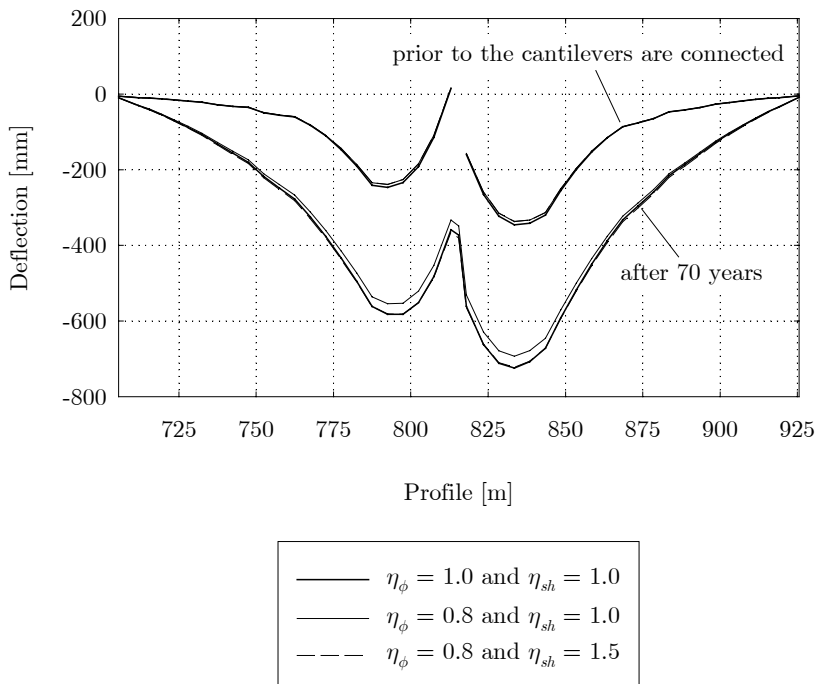


Figure 9.21 Deflection in the central span with different creep and shrinkage characteristics of LWAC, Støvset Bridge (the third curve can hardly be seen because it is in close agreement with the first curve *after 70 years*)

The deflection of the central span is shown in Figure 9.21. The reduced creep coefficient furnished 4 % lower maximum long-time deflection. The reduced creep coefficient together with the increased shrinkage strain resulted in an almost identical long-time deflection as the original calculation (for that reason the curve in the diagram can hardly be seen). The deflection in the construction phase prior to the cantilevers are joint is little affected by the reduced creep coefficient. Since shrinkage does not induce deflection in the free cantilevers, the higher shrinkage strain has no effect on the deflections in the construction stages. The development of the mid-span deflection is shown in Figure 9.22 in the three cases.

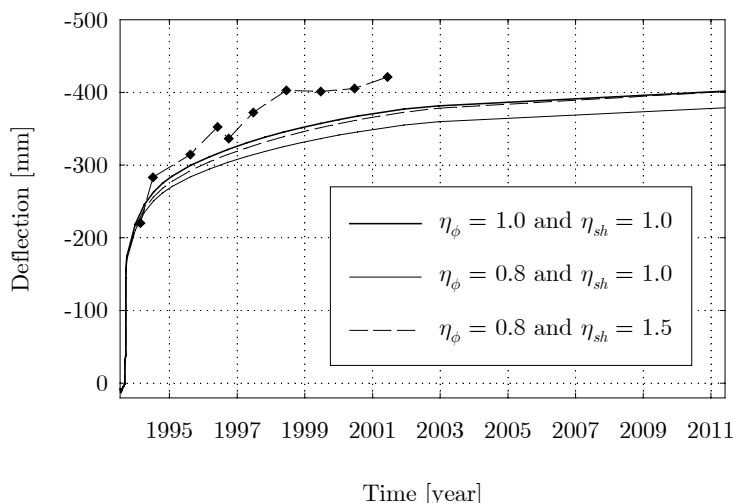


Figure 9.22 Deflection at mid-span with different creep and shrinkage characteristics of LWAC, Støvset Bridge

### 9.8 Calculated deflection, MC90 versus B3 model

Different creep and shrinkage models were compared in subsection 3.2.7. The predicted creep and shrinkage curves showed significant differences in many cases. Deviation from the CEB-FIP Model Code 1990 was particularly large for the creep compliance given by Bazant’s B3 model. The objective of the present investigation was to determine the magnitude of the difference in the actual deformation responses of a segmentally built cantilever bridge and eventually to see the consequences of the model choice, as far as these two widely recognised but characteristically different models are concerned.

Støvset Bridge was used again in the comparative study. The numerical model with the MC90 material models was the same as in previous analyses. The creep compliance was approximated with the Kelvin Chain model. The B3 model, on the other hand, was

approximated with the Maxwell Chain model. The chain parameters in the latter case were determined by the RELAX program (Jonasson and Westman 1999). Since the Maxwell Chain is based on the relaxation function, the creep functions had to be converted into relaxation functions. The RELAX program uses an algorithm for that purpose which was proposed by Bazant and Ashgari (1974).

The temperature was set equal to 20° C in both analyses because no formulation for temperature other than 20° C was given for the drying creep component and shrinkage in the B3 model (Bazant and Baweja 1995).

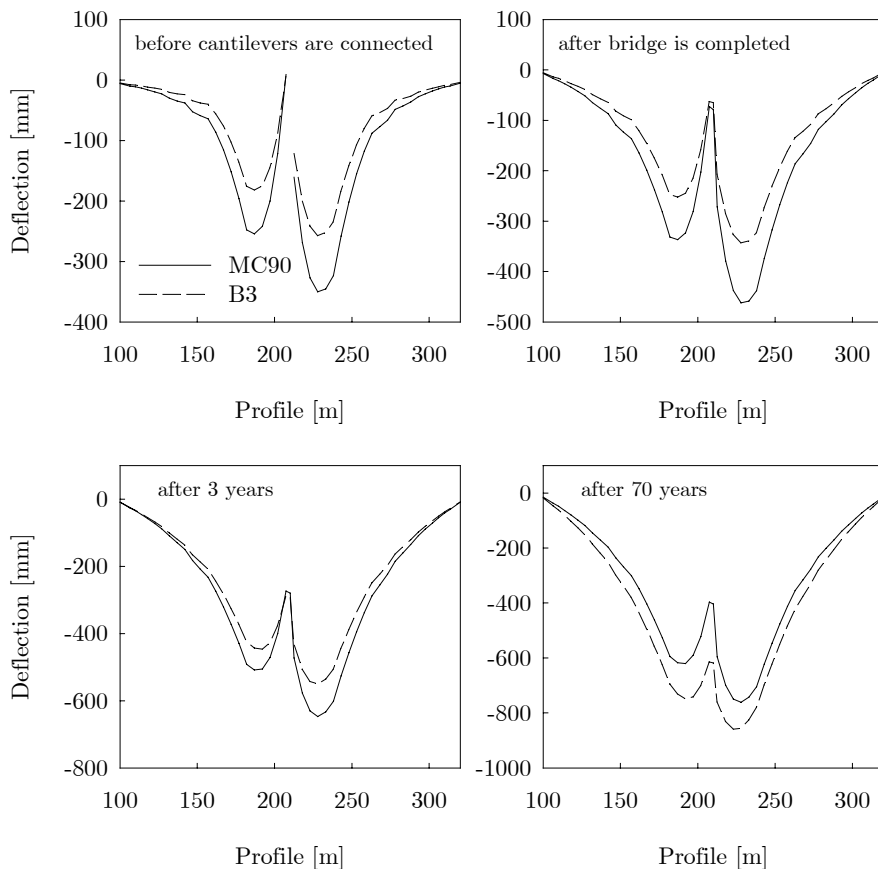


Figure 9.23 Calculated deflection in the central span in four stages as given by the CEB-FIP Model Code 1990 and the B3 model

The calculated deflection in the central span is shown in Figure 9.23 in four stages. The development of the deflection is shown at mid-span in Figure 9.24. The short-time deformation is significantly smaller with the B3 model. However, the deformation gradient

after a short period of time is higher. While the deflection according to the MC90 model is approaching a final value, the B3 curve has an almost constant gradient on the logarithmic scale after about 1000 days. Eventually the deflection after 70 years is significantly larger with the B3 model. The smaller calculated short-time deformation given by the B3 model is in agreement with what was observed in Figure 3.12. The initial response was considerably lower than estimated by other models when the concrete age at loading was higher than 28 days.

The measurements are seen in better agreement with the MC90 model. The estimated deflection is slightly higher than in previous analyses with the MC90 model because of the higher temperature taken in the calculation.

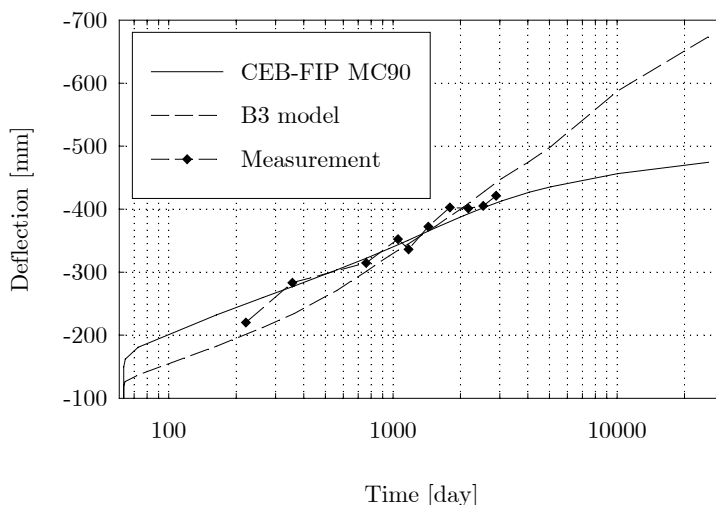


Figure 9.24 Development of the deflection at mid-span as given by the CEB-FIP Model Code 1990 and the B3 model in comparison with the measurements

### 9.9 Concluding remarks

Various calculated deformation responses were compared with the measurements in three bridges. While moderate differences were observed in most cases, no clear overall tendency toward under- or overestimation was found. The predicted long-term deflection in Norddalsfjord Bridge was in good agreement with the measured values while the long-term deflection was slightly underestimated in Støvset Bridge and overestimated in Stolma Bridge.

The three bridges are the same type of structure built with the same construction method and exposed to similar environmental conditions. The numerical model for all three bridges

were set up along the lines of the very same principles using the same material models. It is difficult to pinpoint the precise reason for the prediction error in any particular case. In the light of the general uncertainty associated with long-term creep and shrinkage prediction in concrete it has to be acknowledged that prediction errors can not be eliminated entirely. While numerical methods reached the level of sophistication where the most complex problems can be addressed effectively, the statistical uncertainty in the long-term material models are significant and the room for improvement is very limited in that regard (CEB 1990). In the next chapter the statistical variation in the material models and various model parameters are taken into account in a probabilistic model in order to estimate the statistical properties of the deformations.

In a sensitivity study, the effect of variation in the creep coefficient, shrinkage strain and the effective prestressing force was studied. The resulted relative variation in the deflections was very similar in the three bridges as far as the variation in creep and shrinkage is concerned. The effect of variation in the prestressing force evidently depends on in what degree the permanent loads are compensated by the prestressing.

The sensitivity of the deflections of Støvset Bridge to variations in the creep and shrinkage characteristics of lightweight aggregate concrete was studied. Using the same creep coefficient for LWAC as for NWC results in an approximately 50 % higher creep deformation as compared to NWC<sup>1</sup>. Whereas the extension to MC90 (*fib* 2000b) suggests to reduce the creep coefficient so the resulted creep deformation is only 20 % higher. On the other hand, the experimental results in Chapter 4 indicated that long-term creep in LWAC might be higher by more than 20 %. Nevertheless the variation in the deflections was found small between these two values.

The CEB-FIP Model Code 1990 and the B3 model were compared in the analysis of Støvset Bridge. The prediction by the MC90 model showed somewhat better agreement with the long-term measurements.

---

<sup>1</sup> The 50 % applies for Støvset Bridge. The number is different for concretes with different density.



## Chapter 10

# Probabilistic Deformation Modelling

*The stochastic aspects of deformation prediction are studied. Statistical variation in the creep and shrinkage models and the model parameters are considered. A Monte Carlo simulation is carried out to estimate the statistical properties of structural responses of Støvset Bridge. Practical aspects of the Monte Carlo simulation are discussed.*

### 10.1 Introduction

Creep and shrinkage are the most uncertain mechanical properties of concrete. The stochastic aspects of these physical phenomena therefore should be taken into account in structural analysis and design. Structural responses were treated as deterministic values so far in the study, although it was acknowledged that the prediction models are marked with a certain degree of statistical variation. Deformations should rather be considered as statistical variables and the deformations calculated by theoretical models have to be seen as expectation values. Material and environmental parameters were also taken into account with their expected mean value but in reality they are also subjected to statistical variation and prediction errors.

Deformation problem is generally a Service Limit State issue and as such it usually needs to be considered with the expectation value of the parameters on both the action and the structural resistance sides. This approach is sufficient for structures which are not sensitive to deformations, like short-span concrete bridges, reinforced concrete beams, frames and slabs of ordinary structures. Slender and long span concrete girder bridges built with the cast-in-place segmental construction method in free cantilevers are creep and shrinkage sensitive structures. Even if the safety against collapse is not threatened (*e.g.* as in long-time creep buckling of thin concrete shells) excessive deformations may compromise the

service-life and state of the bridge or compromise the smooth connection of the cantilevers in the construction phase. It is therefore important to consider the stochastic aspects of long-term deformation prediction in the analysis of deformation sensitive structures. The structure should be designed for response values representing a certain confidence limit rather than the expectation value in order to minimise the risk of intolerable deformations (Bazant and Baweja 1995).

In this chapter the following issues are addressed: (1) characterise the level of uncertainty in the prediction of deformations in concrete cantilever bridges, (2) define design criteria for concrete cantilever bridges concerning deformations, (3) identify the critical statistical variables and estimate their statistical properties, (4) introduce method for probabilistic deformation analysis and (5) determine the expected variation of the deformations and estimate the confidence interval of given probability. The probabilistic analysis was implemented in a Monte Carlo simulation using an advanced sampling method known as the Latin hypercube sampling. The method is demonstrated in the statistical analysis of Støvset Bridge.

## 10.2 Statistical properties and definitions

Statistical measures and definitions are reviewed for later reference. The measures are used to estimate population properties from random samples (*e.g.* Kottogoda and Rosso 1997). Special considerations which are specific to the Latin hypercube sampling are discussed later in subsection 10.4.

### 10.2.1 Arithmetic mean

The arithmetic mean is a measure of central tendency for roughly symmetric distributions (*e.g.* normal distribution). It is denoted by  $M$  when computed in a sample.

$$M = \bar{x} = \frac{\sum x}{n} \tag{10.1}$$

where  $n$  is the sample size.

The sample mean,  $M$  is not the theoretical true mean. The true mean is the property of the population and it is denoted by  $\mu$ . In many cases of practical interest the true mean is not known. One purpose of a statistical analysis is to estimate the true mean. The sample mean is the estimator of the theoretical true mean.

### 10.2.2 Standard deviation, variance and coefficient of variation

The standard deviation is the measure of the dispersion representing the degree of variability in a phenomenon and also indicating the precision of the data. Similarly to the



arithmetic mean, the standard deviation in most practical cases is calculated in a sample and can be considered as the estimator of the theoretical true standard deviation,  $\sigma$ . The sample standard deviation is denoted by  $S$  and can be calculated from the following formula:

$$S = \sqrt{\frac{n \sum x^2 - (\sum x)^2}{n^2}} \quad (10.2)$$

Statistic  $S$  is a biased estimate of the standard deviation, however. It consistently over or underestimates the standard deviation in the long run. The most commonly used formula for computing standard deviation in a sample is

$$\hat{S} = \sqrt{\frac{n \sum x^2 - (\sum x)^2}{n(n-1)}} \quad (10.3)$$

Statistic  $\hat{S}$  is referred to as the unbiased estimate of the standard deviation. From this point forward in this subsection the sample standard deviation will be denoted by  $S$  irrespective of being a biased or unbiased estimate.

Variance is an equivalent statistical measure to standard deviation. The standard deviation is the square root of the variance. Variance is reflecting more of its signification as being the second central moment of the statistical variable. From the practical perspective standard deviation is a more useful measure of spread because it has the same unit as the mean.

The standard deviation is a measure of absolute variation. It measures the actual amount of variation and depends on the scale of the data. It is favourable to use a measure of relative variation (*e.g.* to compare the variation in several sets of data). The relative variation can be measured by the coefficient of variation denoted by  $V$ . It gives the standard deviation in percentage of the mean.

$$V = \frac{S}{M} \cdot 100 \quad (10.4)$$

### 10.2.3 Standard error of the mean and the standard deviation

The standard error of a statistic is the standard deviation of the sampling distribution of that statistic. Standard errors reflect how much sampling fluctuation a statistic will show. They depend on the size of the sample. Larger sample size yields smaller standard error.

The standard error of the mean is the standard deviation of the sampling distribution of the mean. It measures the reliability of the sample mean as the estimate of the theoretical true mean. The standard error of the mean can be estimated from the standard deviation of the original distribution and the sample size on which the mean is computed.

$$S_M = \frac{S}{\sqrt{n}} \quad (10.5)$$

The standard error of the standard deviation can also be estimated from the standard deviation of the original distribution and the sample size.

$$S_S = \frac{0.71 S}{\sqrt{n}} \quad (10.6)$$

### 10.2.4 Confidence limit

The confidence limits are the bounding values of the confidence interval, which interval contains the statistical variable with a certain probability. In many cases of practical interest in the engineering field the 95 % confidence interval is applied. It means that the probability is 95 % that the statistical variable will fall within the confidence interval. When the confidence interval is bounded by a lower and an upper limit value (*i.e.* lower and upper percentile) it is referred to as a two-sided confidence interval. In many cases, however, the nature of the problem requires only a lower or an upper limit and consequently it is referred to as a one-sided confidence interval (*e.g.* the characteristic value of the concrete strength is the confidence limit of a lower-bounded one-sided confidence interval).

Confidence limits denoted by  $C$  can be defined by the number of standard deviations they are above or below the mean value. The number of standard deviations depends on the required degree of confidence and the type of the distribution.

Throughout the study it is assumed that model parameters (*i.e.* the input of the numerical analysis) are following roughly normal distribution. As for the structural responses (*i.e.* the outcome of the numerical analysis) the situation is less straightforward. One may assume normal distribution also for the responses (Bazant and Baweja 1995) and assume that the theoretical true standard deviation has been obtained by the stochastic analysis (*i.e.* the standard deviation is *known* and not *estimated*). The confidence limits then can be obtained by the so-called  $z$ -values. For the two-sided 95 % confidence interval those are

$$C_{0.95} = M \pm 1.960 S \quad (10.7)$$

and for the one-sided 95 % confidence interval (lower or upper respectively)

$$\begin{aligned} C_{0.95} &= M - 1.645 S \\ C_{0.95} &= M + 1.645 S \end{aligned} \quad (10.8a,b)$$

Even if it is assumed that a statistical variable follows normal distribution, it has to be taken into account that the sample standard deviation may deviate from the theoretical true standard deviation with a certain error. It is certainly important in case of small samples. It

may be desirable to abandon normal distribution and use  $t$ -distribution instead. By definition, whenever the standard deviation is *estimated* based on a sample taken from a normal population, the  $t$ -distribution should be used instead of the normal distribution. The  $t$ -distribution furnishes somewhat broader confidence interval to account for the potential error in the estimated sample standard deviation. The so-called  $t$ -values would replace the  $z$ -values in Eq. (10.7) and Eq. (10.8a,b). The  $t$ -values - unlike the  $z$ -values - are functions of the sample size as well. When the sample size is increasing the  $t$ -values are approaching the respective  $z$ -values. From a practical point of view the standard normal distribution provides a good approximation to the  $t$ -distribution for a sample size of 30 or more. This number and the  $t$ -values are valid for random samples.

When a proper sampling method is used the potential error in the statistical estimator can be reduced. The normal distribution may not need to be abandoned even if the sample size is smaller than 30. Evidently an important concern with a robust stochastic structural analysis is to keep the number of computer runs as small as possible due to the enormous amount of computational work. Latin hypercube sampling (McKay *et al.* 1979) which method will be used for the Monte Carlo simulation furnishes significantly more accurate estimators than simple random sampling with the number of computer runs being the same. In other words, the same accuracy can be reached with less number of computer runs. In the present investigation the calculated standard deviation will be treated as the true value (Bazant and Baweja 1995).

The 95 % confidence limits for the sample mean can be obtained when Eq. (10.5) is substituted to Eq. (10.7).

$$C_{0.95} = M \pm \frac{1.960 \cdot S}{\sqrt{n}} \quad (10.9)$$

### 10.2.5 Pearson Product Moment Correlation

The correlation between two variables reflects the degree to which the variables are related. The most common measure of correlation is the Pearson Product Moment Correlation (Pearson's correlation for short). Pearson's correlation reflects the degree of linear relationship between two variables. It is a dimensionless index that ranges from -1 to +1 inclusive. A correlation of +1 means perfect positive linear relationship between two variables, -1 means perfect negative linear relationship and 0 means that there is no linear relationship. However the latter does not mean that there is no relationship at all (e.g. non-linear relationship). When computed in a sample it is denoted by  $r$ . A commonly used formulation to calculate Pearson's correlation is shown below where  $x$  and  $y$  are two variables.

$$r = \frac{n(\sum xy) - (\sum x)(\sum y)}{\sqrt{[n\sum x^2 - (\sum x)^2][n\sum y^2 - (\sum y)^2]}} \quad (10.10)$$

The correlation is often characterised by the square of the correlation coefficient. It is referred to as the r-squared value and denoted by  $r^2$ . It gives the proportion of the variation in  $y$  attributable to the variation in  $x$ .

### 10.3 Design criteria concerning deformations in concrete bridges

The purpose of the probabilistic deformation analysis is to enable a structural design where the risk that intolerable deformations will occur can be minimised.

Two types of situations have to be distinguished. In most cases the issue is to set a maximum limit value for a certain deflection or displacement. In that case the procedure is rather straightforward. The structure can be designed to the deformation response which represents the confidence limit of a one-sided confidence interval of given probability. For example, to design the structure for the deformation response representing the confidence limit of the 95 % one-sided confidence interval means that if 20 identical bridges were built and subjected to identical conditions only one would suffer intolerable deflections statistically. Whereas the design for the mean response means that 10 bridges out of the 20 would exhibit intolerable deflections. The left diagram in Figure 10.1 illustrates a one-sided confidence interval and the confidence limits.

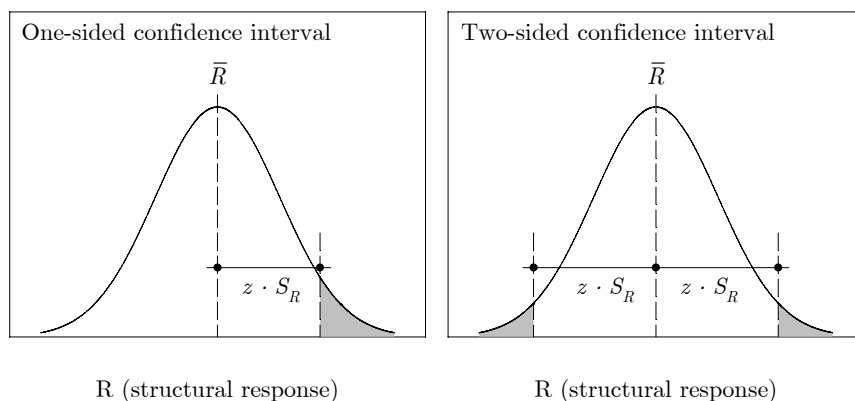


Figure 10.1 One-sided and two-sided confidence interval

There are problems, however, where a deviation in either way from the expected theoretical mean value may have negative effect on the structure or the construction process. In those cases it is necessary to consider both a lower and an upper limit for a certain deformation

response. The structure can be designed to the expectation value of the deformation response but an interval should be considered within that the variation of that deformation response is still tolerable. The right diagram in Figure 10.1 illustrates a two-sided confidence interval where the unfavourable range is cut off on both the lower and upper tails. A typical example of such situation is the construction process. The two cantilevers have to meet in the middle and there is a very small room for a vertical deviation between the tip of the two cantilevers. With the probabilistic analysis it is possible to estimate the expected range of the deviation of given probability and consider the necessary measures (*i.e.* possibility for additional prestressing, extra counterweight ballast, vertical jacking at the abutments).

Since both types of the situations exist within the same structure the design can not be broken down into individual problems considered and treated separately. It has to be a progressive refinement of the design.

## 10.4 Monte Carlo simulation for probabilistic deformation analysis

### 10.4.1 Introduction

Simulation techniques which involve random variables are referred to as Monte Carlo simulations<sup>1</sup> (or Monte Carlo methods). Monte Carlo simulations are used in various disciplines of engineering, science and economics. The term *simulation* can generally be defined as replicating real world systems or phenomena based on numerical or physical models. To analyse engineering systems with numerical simulation has become increasingly popular with the enormous increase in computational power of digital computers.

Monte Carlo simulation involves applying random sets of system parameter values. The response of the system for a given set of system parameter values is then obtained by the numerical model. The process is deterministic for a given set of input values. After repeating the simulation with several sets of randomly generated system parameter values, the statistical properties of the response values and their sensitivity to variations in the system parameters can be assessed. A fundamental issue in the simulation is to identify the critical system parameters and to determine their statistical properties. An other important part of the analysis is the sampling method which is used to randomly generate the sets of values for the system variables.

Mathematicians consider Monte Carlo methods as the very last resort to find solution to a problem because of the undesirable random aspects involved. Engineering, on the other hand, is more application-oriented and favours Monte Carlo methods because of its

---

<sup>1</sup> The term *Monte Carlo* was allegedly first used by Hungarian-born American mathematician John von Neumann who pioneered the development of *Monte Carlo methods* in connection with his work at Los Alamos during World War II (Hammersley and Handscomb 1964).

robustness and capability to address the most complex engineering problems (Hammersley and Handscomb 1964). In fact Monte Carlo methods have no alternative for the analysis of engineering systems where the system parameters are statistical variables and the system behaviour can not be described – for either theoretical or practical reasons – in an analytical form.

In this study a Monte Carlo simulation is carried out with the objective to estimate the statistical properties of various structural responses in Støvset Bridge. Eventually the confidence limit of the responses is determined. The Monte Carlo simulation consists of three main parts: (1) sampling the system parameters, (2) performing a series of deterministic structural analyses and (3) statistical assessment of the response values. (1) and (3) are implemented in a spreadsheet application. The deterministic structural analyses are carried out with DIANA using the same deterministic model which was used in previous numerical studies.

#### **10.4.2 System parameters and their statistical properties**

The success of the Monte Carlo simulation significantly depends on the identification of the critical model parameters which need to be considered as statistical variables and the determination of their statistical properties. The latter can be based on either existing information or assumption. In the present study six model parameters are considered as statistical variables and accordingly six uncertainty factors,  $\Psi_1, \Psi_2, \dots, \Psi_6$  are introduced into the numerical model. The first two uncertainty factors are meant to consider the potential prediction error in the creep and shrinkage models while other three uncertainty factors are assigned to model parameters such as concrete strength, relative humidity and temperature (Bazant and Baweja 1995) to take into account the statistical variation and estimation error. The sixth uncertainty factor is assigned to the effective prestressing force. The uncertainty factors are assumed to follow normal distribution with the mean value of one.

##### *10.4.2.1 Creep coefficient*

The highest degree of uncertainty undoubtedly lies in the prediction of the creep compliance. The coefficient of variation associated with the model is the inherent property of the prediction model as well as the prediction itself. Creep prediction models usually report the coefficient of variation for the creep compliance which is 20 % for the CEB-FIP Model Code 1990 (CEB 1991).

Specifying the coefficient of variation for the creep compliance function is in agreement with the widely acknowledged principle that creep models should specify the creep compliance function rather than the creep coefficient alone. It seems therefore an obvious step to assign the uncertainty factor to the creep function. Two concerns, however, arise which explains

why the modulus of elasticity and the creep coefficient are treated separately in the current simulation as far as the statistical analysis is concerned.

To obtain the value of the modulus of elasticity for the numerical analysis is more deterministic than to obtain the creep function. In most cases of practical interest, like in the present analysis, the value of the modulus of elasticity is available from laboratory test, thus it represents a significantly smaller uncertainty. The statistical variation in the elastic modulus therefore is taken into account only to the extent as it varies as the result of the statistical variation in the compressive strength (*vide* subsection 10.4.2.3).

On the other hand, in most practical cases the total stress-dependent deformation is important and the separation into instantaneous and creep components remains an academic question. However, the situation is somewhat different for segmentally cast bridges. A segment which is built in a later stage does not “feel” the instantaneous deformation in the already existing part of the cantilever which takes place before the segment is built but it does “feel” that part of their creep deformation which occurs after the segment is built. Obviously, later a segment is built, more pronounced this effect is (*e.g.* in case of Støvset Bridge, the long-time deflection in the mid-segment is more than five times the deflection which occurs when the bridge is completed but the estimated average creep coefficient is only around 1.3). In short, segments towards the mid-span are influenced by creep to a larger extent. Along with the first argument this implies that they are also more sensitive in relative terms.

The uncertainty factor is assigned to the creep coefficient as follows

$$J(t, t_0) = \frac{1}{E_c(t_0)} + \Psi_1 \frac{\phi(t, t_0)}{E_{c28}} \quad (10.11)$$

Since the coefficient of variation is reported for the compliance function and not for the creep coefficient it needs to be converted. The conversion is made under the condition that the obtained coefficient of variation for the creep coefficient will furnish approximately identical variation in the long-time values of the creep compliance<sup>1</sup> (*vide* Figure 10.2).

$$V(\Psi_1) = V(\phi) = V(J) \frac{1 + \phi}{\phi} \quad (10.12)$$

---

<sup>1</sup> This is only a rough estimate. It neglects the part of the variation in the creep compliance which is attributable to the variation in the elastic modulus. This has to be taken in the absence of more accurate reported information.

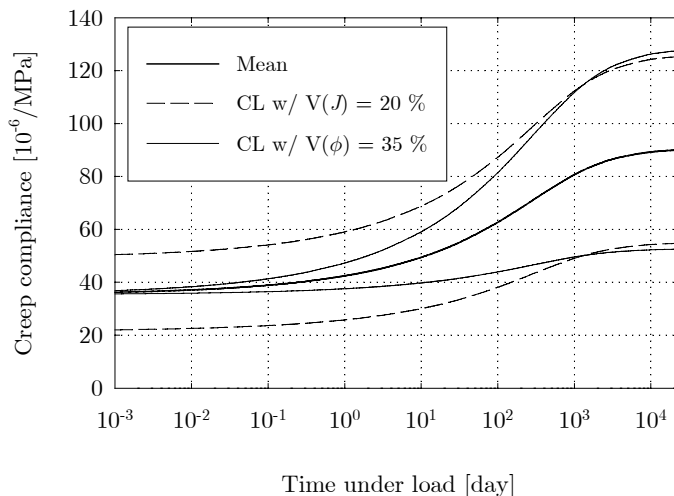


Figure 10.2 Confidence intervals for the creep compliance

If the coefficient of variation of 20 % for the creep compliance and the estimated average value of the creep coefficient of 1.33 are substituted to Eq. (10.12), the estimate for the coefficient of variation for the creep coefficient is obtained as

$$V(\Psi_1) = 35\% \quad (10.13)$$

In the absence of more accurate information the coefficient of variation for creep in lightweight aggregate concrete is assumed to be the same as in normal weight concrete.

#### 10.4.2.2 Shrinkage

The reported coefficient of variation of the shrinkage model in the CEB-FIP Model Code 1990 is

$$V(\Psi_2) = 35\% \quad (10.14)$$

#### 10.4.2.3 Concrete strength

The concrete strength is influencing both the creep coefficient and the modulus of elasticity. Bazant and Baweja (1995) suggests to consider the statistical variation of the concrete strength with a coefficient of variation of 15 %. In high strength concrete the relative variation can be expected to be lower. Measurements on concrete samples in connection with the investigated bridges gave an estimate of 7 %. It is also likely that the effect of the statistical variation is somewhat levelled off on the overall basis in a large-scale structure. If no test data is available prior to the analysis a higher value is reasonable though to take into



account a potential estimation error of the mean. The coefficient of variation of the concrete strength in the current analysis is taken as

$$V(\Psi_3) = 10\% \quad \text{for} \quad f_{cm} \Rightarrow \Psi_3 \cdot f_{cm} \quad (10.15)$$

The dependency of the modulus of elasticity on the concrete strength is considered with the formula derived from Eq. (3.2):

$$E_{c28}(f_{cm}) = \bar{E}_{c28} \left( \frac{f_{cm}}{\bar{f}_{cm}} \right)^{1/3} \quad (10.16)$$

where  $\bar{E}_{c28}$  and  $\bar{f}_{cm}$  are the mean values of the measured modulus of elasticity and the corresponding concrete strength.

#### 10.4.2.4 Relative humidity of the ambient environment and temperature

Relative humidity and temperature are parameters which are varying not only randomly but they also follow a relatively well-definable fluctuation pattern on seasonal and daily basis. It is practically impossible to follow this kind of fluctuation in a large-scale analysis. It is sufficient to consider the relative humidity and the temperature with their annual average and assign the uncertainty factors to these values. The coefficients of variation are estimated as

$$V(\Psi_4) = 15\% \quad \text{for} \quad RH \Rightarrow \Psi_4 \cdot RH \quad (10.17)$$

$$V(\Psi_5) = 15\% \quad \text{for} \quad T \Rightarrow \Psi_5 \cdot T \quad (10.18)$$

Under the assumption of normal distribution with a mean of 70 % and coefficient of variation of 15 %, the upper tail of the probability density function of the relative humidity falls above 100 %. Naturally this is inadmissible. Abandoning the normal distribution would, however, complicate the analysis. Since only 0.2 % of the area under the probability density function falls above 100 %, it is reasonable to simply cut off the upper tail above 100 %. The remedy to this problem is discussed in more detail in the discussion of the sampling method (*vide* subsection 10.4.3).

#### 10.4.2.5 Effective prestressing force

The total deflection is basically the sum of two large but opposite deflections resulted from the selfweight and the prestressing. Even a small variation in the effective prestressing force may result in a considerable variation in the total deformation. All the uncertain properties involved in the prediction of the effective prestressing force (curvature friction, wobble friction, anchor slip and relaxation) are taken into account with one uncertainty factor which is directly assigned to the effective prestressing force. Assuming that the effective

prestressing force can be estimated within  $\pm 5\%$  with a probability of 0.95, the coefficient of variation is estimated as (c.f.  $p = 0.95 \Rightarrow 1.645 \cdot 0.03 \approx 0.05$ )

$$V(\Psi_6) = 3\% \quad \text{for} \quad P_{eff} \Rightarrow \Psi_6 \cdot P_{eff} \quad (10.19)$$

### 10.4.3 Latin hypercube sampling

Latin hypercube sampling was suggested by McKay *et al.* (1979). It is a refinement of stratified sampling. The idea of Latin hypercube sampling is to partition the domain of each statistical variable  $\theta_i$  into  $N$  intervals  $\Delta\theta_i^k$  ( $k = 1, 2, \dots, N$ ) of equal probability  $1/N$ . The number of intervals  $N$  is chosen to be the same as the number of samples being taken (i.e. number of computer runs). From each interval the parameter value is sampled once and only once.

If the number of intervals,  $N$  is large the parameter value needs not to be sampled randomly within the interval but may be taken at the centroid of the intervals (*vide* Figure 10.3). The sampled value  $\theta_i^k$  for a randomly selected  $k$  value is obtained by solving the following equation:

$$F_i(\theta_i^k) = (k - 1/2)/N \quad (10.20)$$

where  $F_i(\theta_i)$  is the cumulative distribution function of  $\theta_i$ .

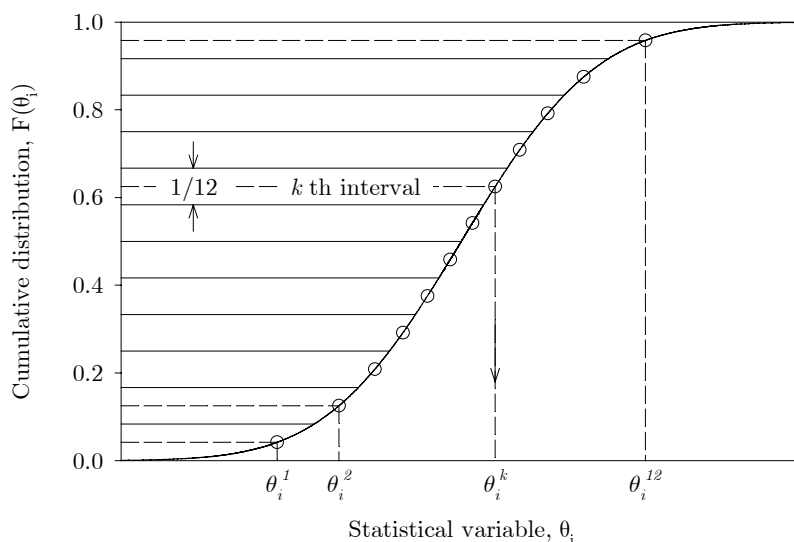


Figure 10.3 Partitioning the range of the statistical variable into twelve intervals

The advantage of Latin hypercube sampling over earlier sampling methods is that the number of computer runs can be reduced considerably to achieve the same level of accuracy, particularly when the number of the statistical variables,  $n$  is large.

McKay *et al.* (1979) and later Stein (1987) proved that Latin hypercube sampling is superior to simple random sampling and stratified sampling with respect to the precision of the estimators provided that the response is a monotonic function of the parameters,  $\theta_1, \theta_2, \dots, \theta_n$ . This condition is normally true for the effects of creep and shrinkage and the effects responsible for the stress losses in the prestressing tendon. In both works the theoretical conclusions were verified by numerical experiments. McKay *et al.* (1979) compared Latin hypercube sampling with simple random sampling and stratified sampling<sup>1</sup> while Stein (1987) compared Latin hypercube sampling with simple random sampling<sup>2</sup>. In both cases Latin hypercube sampling clearly demonstrated superiority.

In the structural engineering field Bazant and Liu (1985) used Latin hypercube sampling to study creep and shrinkage effects in simple concrete beams and frames. They compared Latin hypercube sampling with two-point estimates of probability moments and concluded that the number of analysis runs needed to reach the same accuracy as with two-point estimates is about twice the number of the system parameters, *i.e.*  $2n$ . For the method of two-point estimates of probability moments the number of computer runs is fixed as  $2^n$ . As the number of system parameters is increasing the reduction in the necessary number of computer runs becomes significant.

While it is normally sufficient to choose the number of computer runs to be equal to the number of random variables,  $N = n$ , the improvement on accuracy can be appreciable (Bazant and Liu 1985) if the number of computer runs is twice the number of the random variables,  $N = 2n$ .

In the current investigation the number of computer runs were chosen to be  $N = 12$  for the  $n = 6$  random variables. For each random variable  $\theta_i$  a randomly generated permutation of the integers  $1, 2, \dots, N$  was assigned,  $r_i^1, r_i^2, \dots, r_i^N$  (*vide* Table 10.1). The integer  $r_i^j$  indicates that the value of the random variable  $\theta_i$  is sampled at the centroid of the interval  $k = r_i^j$  for the  $j$ th computer run (*e.g.* for the second computer run, the random variable  $\theta_1$  which is assigned to the creep coefficient is sampled from the 6th interval,  $\theta_2$  which is assigned to the shrinkage strain is sampled from the 12th interval and so on).

Random permutations of integers were obtained by generating  $N$  number of uniformly distributed random numbers for each random variable  $\theta_i$  and obtaining  $r_i^j$  as the rank of the random number within the array. Random number generators may be found in various computer applications and subroutine libraries.

---

<sup>1</sup> simulation of reactor safety

<sup>2</sup> simulation of the performance of a printer actuator

Table 10.1 Randomly generated permutations of the integers 1,2,...,12

Run	$\theta_1$	$\theta_2$	$\theta_3$	$\theta_4$	$\theta_5$	$\theta_6$
1	8	8	2	7	10	10
2	6	12	5	2	4	3
3	11	10	6	8	3	7
4	10	3	3	1	7	11
5	1	2	10	3	12	8
6	5	11	11	6	1	6
7	4	1	9	9	11	1
8	3	9	1	12	2	2
9	12	6	7	10	6	5
10	9	7	8	5	8	4
11	2	4	4	4	9	12
12	7	5	12	11	5	9

Table 10.2 shows the parameter values at the centroid of the intervals while Table 10.3 shows the sets of system variable values for each computer run.

Table 10.2 Parameter values at the centroid of the intervals

$k$	$F(\theta_i^k)$	$\theta_1$	$\theta_2$	$\theta_3$	$\theta_4$	$\theta_5$	$\theta_6$	
		$\Psi_1$	$\Psi_2$	$\Psi_3 f_{cm}$	$\Psi_4 RH$	$\Psi_5 T$	$\Psi_6$	
		-	-	MPa	%	°C	-	
		$\mu$	1.000	1.000	53	70	10.0	1.000
		$V$ [%]	35	35	10	15	15	3
1	0.042	0.394	0.394	44	52	7.4	0.948	
2	0.125	0.597	0.597	47	58	8.3	0.965	
3	0.208	0.716	0.716	49	61	8.8	0.976	
4	0.292	0.808	0.808	50	64	9.2	0.984	
5	0.375	0.888	0.888	51	67	9.5	0.990	
6	0.458	0.963	0.963	52	69	9.8	0.997	
7	0.542	1.037	1.037	54	71	10.2	1.003	
8	0.625	1.112	1.112	55	73	10.5	1.010	
9	0.708	1.192	1.192	56	76	10.8	1.016	
10	0.792	1.284	1.284	57	79	11.2	1.024	
11	0.875	1.403	1.403	59	82	11.7	1.035	
12	0.958	1.606	1.606	62	88	12.6	1.052	

Table 10.3 Randomly generated sets of input parameters for the computer runs

Run	$\theta_1$	$\theta_2$	$\theta_3$	$\theta_4$	$\theta_5$	$\theta_6$
	$\Psi_1$	$\Psi_2$	$\Psi_3 f_{cm}$	$\Psi_4 RH$	$\Psi_5 T$	$\Psi_6$
	-	-	MPa	%	°C	-
1	1.112	1.112	47	71	11.2	1.024
2	0.963	1.606	51	58	9.2	0.976
3	1.403	1.284	52	73	8.8	1.003
4	1.284	0.716	49	52	10.2	1.035
5	0.394	0.597	57	61	12.6	1.010
6	0.888	1.403	59	69	7.4	0.997
7	0.808	0.394	56	76	11.7	0.948
8	0.716	1.192	44	88	8.3	0.965
9	1.606	0.963	54	79	9.8	0.990
10	1.192	1.037	55	67	10.5	0.984
11	0.597	0.808	50	64	10.8	1.052
12	1.037	0.888	62	82	9.5	1.016

It has been already mentioned that assuming normal distribution for certain statistical variables may yield physically inadmissible sampled value (e.g. relative humidity can not have a higher value than 100 %). To avoid abandoning normal distribution and thus complicating the analysis unnecessarily, one can apply the following remedy. In that particular case the upper tail of the distribution function was simply cut off (*i.e.* ignored), because not only the sampled value at the centroid of the upper marginal interval fell below  $RH = 100\%$  but the area under the probability density function over  $RH = 100\%$  was only 0.2 %, hence negligible. If the area under the probability density function outside the physically admissible range is significant and particularly when the centroid of the marginal intervals would fall outside, one may cut off the tails of the distribution function outside the physically admissible range and scale up the probability density function to restore the unity of the area under the function.

#### 10.4.4 Estimating the mean and the variance

The  $N = 12$  number of computer runs furnish twelve values for structural response  $R$ . The statistical properties of the response then can be estimated as

$$M = \bar{R} = \frac{1}{N} \sum_{j=1}^N R_j \quad (10.21)$$

$$S^2 = \frac{1}{N} \sum_{j=1}^N (R_j - \bar{R})^2 \quad (10.22)$$

where  $j = 1, 2, \dots, N$  is the number of the computer runs.

The variance,  $S^2$  is not unbiased. The unbiased estimate can not be obtained by replacing  $1/N$  with  $1/(N-1)$  in Eq. (10.22) like for simple random sampling (*vide* Eq. (10.3)). In fact the bias in the Latin hypercube plan is not known. However the unbiased estimate is between those two values (McKay *et al.* 1979).

$$\frac{1}{N} \sum_{j=1}^N (R_j - \bar{R})^2 \leq E(\hat{S}^2) \leq \frac{1}{N-1} \sum_{j=1}^N (R_j - \bar{R})^2 \quad (10.23)$$

The bias in the Latin hypercube plan, however, is considered small which was confirmed by numerical examples by McKay *et al.* (1979). From a practical perspective the bias is negligible if the number of computer runs is not too small.

Three types of the structural responses of the superstructure were investigated: deflections, horizontal displacements and moments. Table 10.4, Table 10.5 and Table 10.6 summarise the statistical properties of those responses. The results of each individual computer run can be seen in Appendix C.

In the tables notation  $M^*$  is used to indicate the value of the structural response obtained by the earlier deterministic analysis. In the light of the probabilistic analysis that value can be regarded as the response to the mean value of the system variables as expressed by Eq (10.24). In a deterministic structural analysis those parameters may not be considered statistical variables but parameter estimation does involve stochastic considerations. The response values obtained by the deterministic analysis are included in the tables for reference.

$$M^* = R(\bar{\theta}_1, \bar{\theta}_2, \bar{\theta}_3, \dots, \bar{\theta}_n) \quad (10.24)$$

The results indicate that  $M^*$  is quasi equal to the mean value,  $M$  as expressed by Eq (10.25). In case of Latin hypercube sampling, the two measures would be equal by definition if the function of  $R$  was a linear combination of the random variables  $\theta_1, \theta_2, \theta_3, \dots, \theta_n$ . The expectation value of the right side of the equation,  $E(\bar{R})$  would be equal to the left side even if  $R$  included products of any two or more variables but only if the variables were mutually independent.

$$R(\bar{\theta}_1, \bar{\theta}_2, \bar{\theta}_3, \dots, \bar{\theta}_n) \cong \bar{R}(\theta_1, \theta_2, \theta_3, \dots, \theta_n) \quad (10.25)$$

All the six statistical variables in the current study are assumed mutually independent. The relationships, however, which govern the system behaviour contains non-linear functions. Nevertheless the close agreement between  $M^*$  and  $M$  indicates that the deformations depend quasi linearly on the variables, at least as far as the two dominating variables  $\theta_1$  and  $\theta_2$  (creep coefficient and shrinkage) are concerned.

Table 10.4 Statistical properties of the deflections

	$M^*$	$M$	$S$	$V$
	mm	mm	mm	%
Maximum				
before connection	-346	-345	27	8
bridge completed	-447	-446	39	9
after 70 years	-725	-722	124	17
Mid-span				
before connection / A2 side	15	14	5	33
before connection / A3 side	-160	-160	9	6
after bridge completed	-71	-71	7	10
after 70 years	-373	-371	101	27

The maximum deflection was found at profile 228.0 meter.

The values of the *mid-span deflection before the cantilevers are connected* concern the tip of the completed cantilevers prior to the closing segment is cast.

Table 10.5 Statistical properties of the horizontal displacement at the piers

	$M^*$	$M$	$S$	$V$
	mm	mm	mm	%
Pier A2				
before connection	8	8	1	14
bridge completed	12	12	3	22
after 70 years	31	30	8	26
Pier A3				
before connection	-8	-8	1	11
bridge completed	-17	-17	2	14
after 70 years	-35	-35	8	22

Displacement is calculated at the centreline of the superstructure.

In addition to the deformations, the flexure moments were investigated and it was found that their statistical variation is negligible. However, it was expected that the moments are influenced very little by the statistical variation of creep and shrinkage because the deterministic analysis already indicated that the long-term redistribution of moments is insignificant.

Table 10.6 Statistical properties of the flexural moments

	$M^*$	$M$	$S$	$V$
	MNm	MNm	MNm	%
Pier A2 / left side				
before connection	856	855	2	0
bridge completed	970	969	2	0
after 70 years	992	991	8	1
Pier A2 / right side				
before connection	862	861	2	0
bridge completed	988	988	1	0
after 70 years	1002	1001	4	0
Pier A3 / left side				
before connection	911	910	2	0
bridge completed	1018	1018	1	0
after 70 years	1019	1019	5	0
Pier A3 / right side				
before connection	903	901	2	0
bridge completed	999	999	2	0
after 70 years	1011	1010	9	1
Mid-span				
bridge completed	-55	-54	1	2
after 70 years	-62	-62	2	3

#### 10.4.5 Estimating the confidence limits

The assumption that the responses follow roughly normal distribution can be verified by normal probability plots. To develop a probability plot, the data is ranked in ascending order. The plotting positions for  $N$  samples can be obtained by the Hazen plotting position equation (Kottegoda and Rosso 1997):

$$p(i) = \frac{i - 0.5}{N} \cdot 100 \quad (10.26)$$

where  $i$  is the rank of the sample within the array.

Figure 10.4 , Figure 10.5 and Figure 10.6 show the normal probability plots for deflection and horizontal displacement values.

The fact that the response values fall roughly on a straight line in the normal probability plot indicates that the probability distribution of the response is approximately normal. Large deviations from the straight line would indicate that normal distribution is not a good



approximation. The ordinate of the straight regression line at 50 % is the mean while the slope of the regression line is the standard deviation<sup>1</sup>.

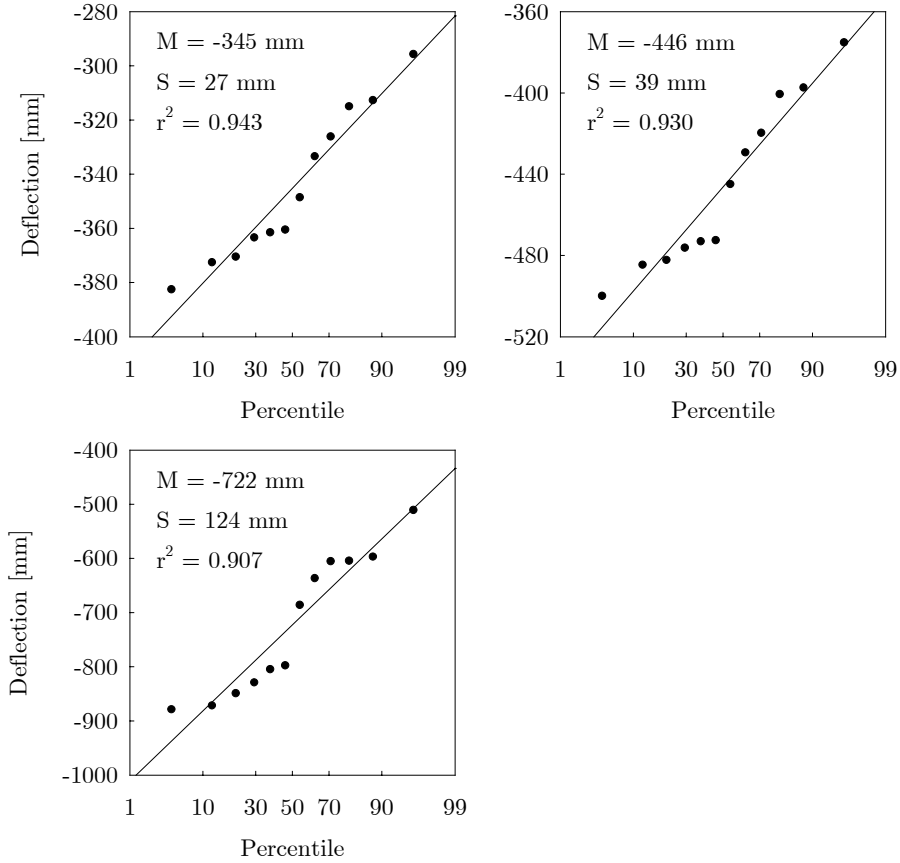


Figure 10.4 Normal probability plots of the maximum deflection (Profile 228.0 m); (a) before the cantilevers are connected, (b) after the bridge is completed and (c) after 70 years

The diagrams verify the assumption that the probability distribution of the responses are approximately normal.

<sup>1</sup> The latter becomes visible if the percentile values on the axis are substituted by the respective z-values. Then the axis has a linear scale.

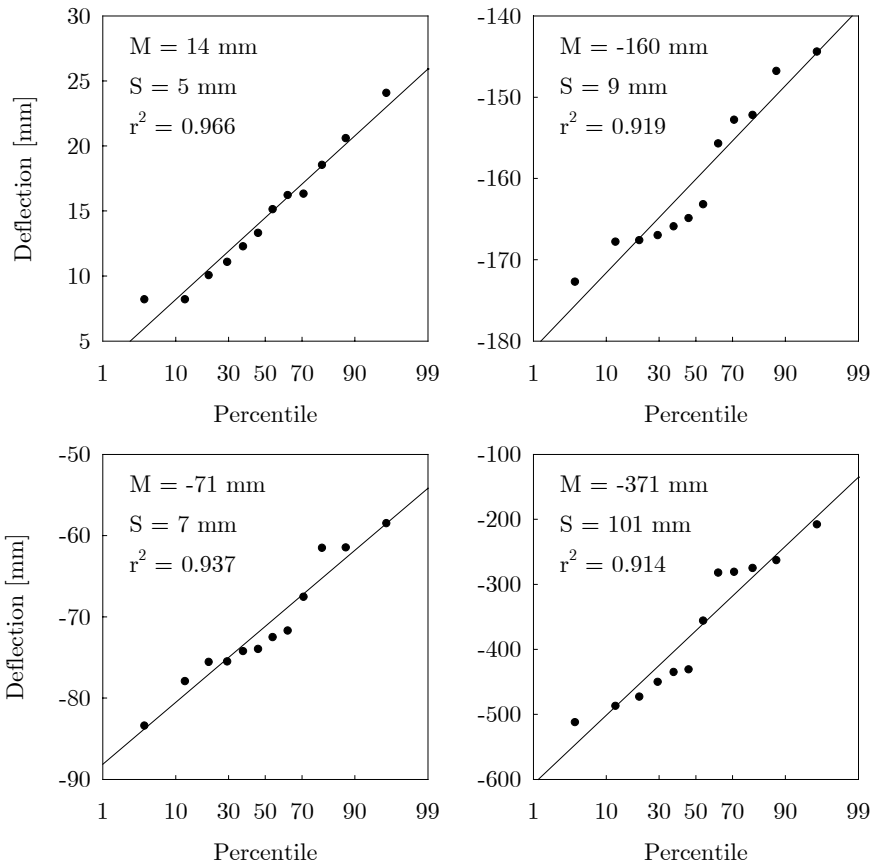


Figure 10.5 Normal probability plots of the deflection at mid-span; (a) before the cantilevers are connected, tip of the left cantilever (A2 side), (b) before the cantilevers are connected, tip of the right cantilever (A3 side), (c) after the bridge is completed and (d) after 70 years

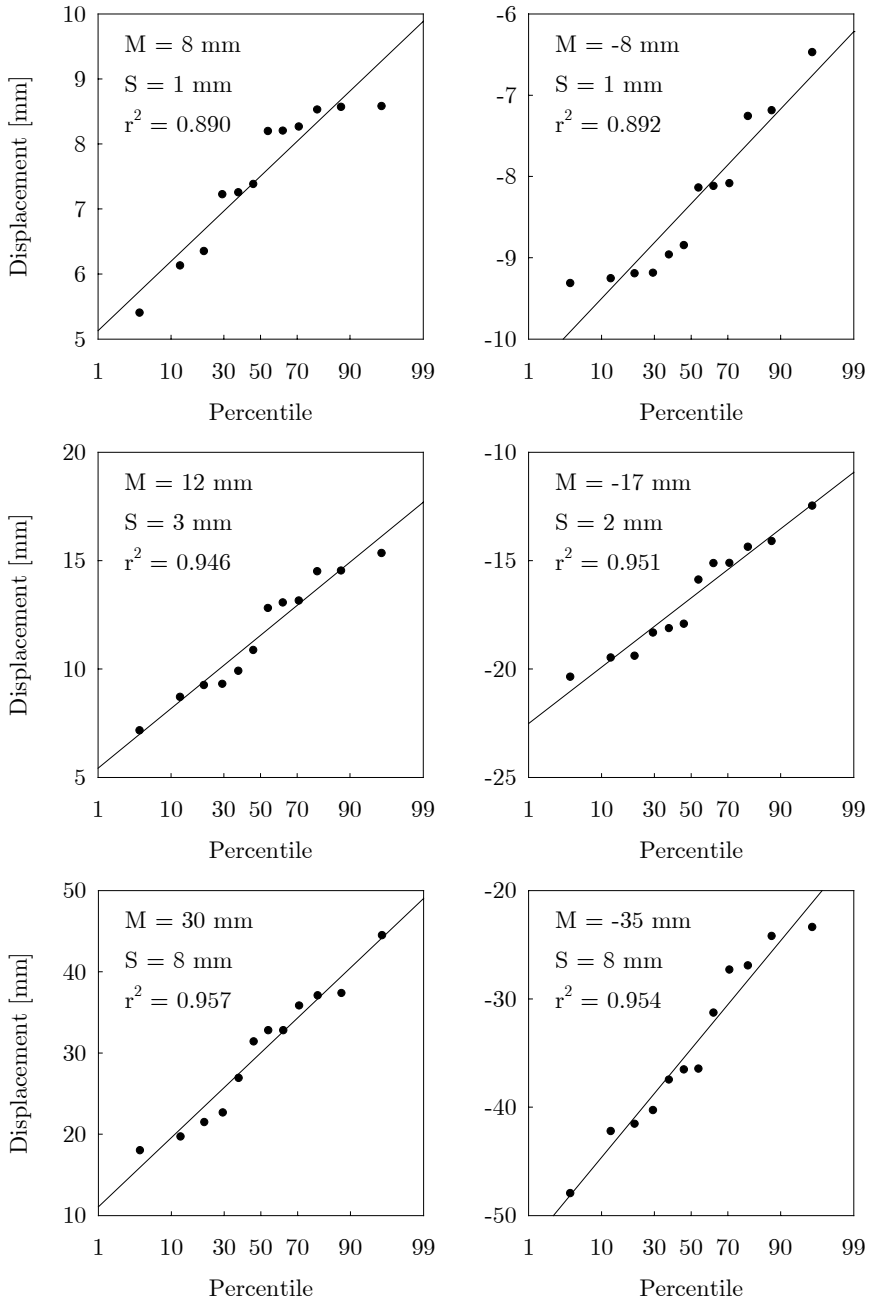


Figure 10.6 Normal probability plots of the horizontal displacement at the columns, left and right column respectively; (a,b) before the cantilevers are connected, (c,d) after the bridge is completed and (e,f) after 70 years

When the mean and the standard deviation of the responses are determined, the confidence limits can be calculated with the  $z$ -values. For the two-sided 95 % confidence interval that is

$$C_{0.95} = M \pm 1.960 S \tag{10.27}$$

and for the one-sided 95 % confidence interval

$$C_{0.95} = M - 1.645 S \tag{10.28}$$

or

$$C_{0.95} = M + 1.645 S \tag{10.29}$$

In the latter case, the nature of the problem decides whether Eq. (10.28) or Eq. (10.29) applies.

Even if the standard deviation is *estimated* and the sample size is relatively small, the  $z$ -values are used and not the  $t$ -values according to the  $t$ -distribution (*vide* subsection 10.2.4). It is allowed by the significantly more accurate statistical estimators obtained by the Latin hypercube sampling (McKay *et al.* 1979) and (Bazant and Liu 1985).

Figure 10.7 shows the mean and the confidence limit for the one-sided confidence interval for the mid-span deflection. In addition to the 95 % confidence limit, the 90 % and the 99 % confidence limits are also illustrated (the respective  $z$ -values are 1.282 and 2.326). Figure 10.8 shows the confidence limits for the long-time deflection curve of the central span.

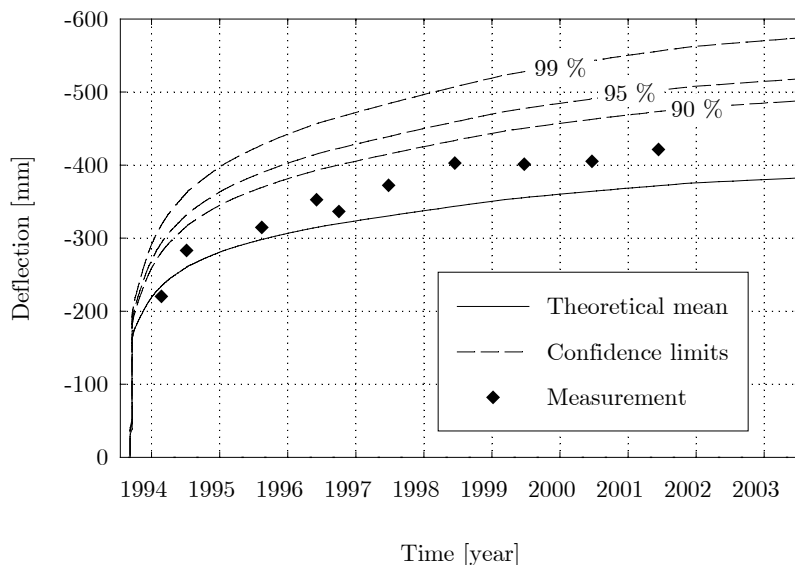


Figure 10.7 Confidence limits for the deflection at mid-span

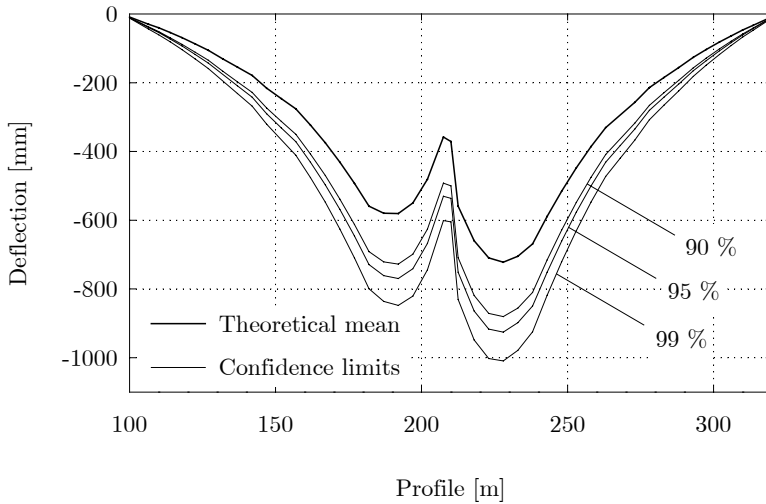


Figure 10.8 One-sided confidence interval of the deflection of the main span after 70 years

### 10.5 Simplified method

A simplified method is recommended based on the observation that the uncertainty factor for the creep coefficient is the dominant uncertainty factor for the deformation prediction in the concrete bridges. Naturally the variation in the other model variables do influence the deformations but their effect is much smaller and overwhelmed by the variation in the creep coefficient. Figure 10.9 shows strong linear correlation between the maximum long-time deflection and the value of the uncertainty factor for the creep coefficient.

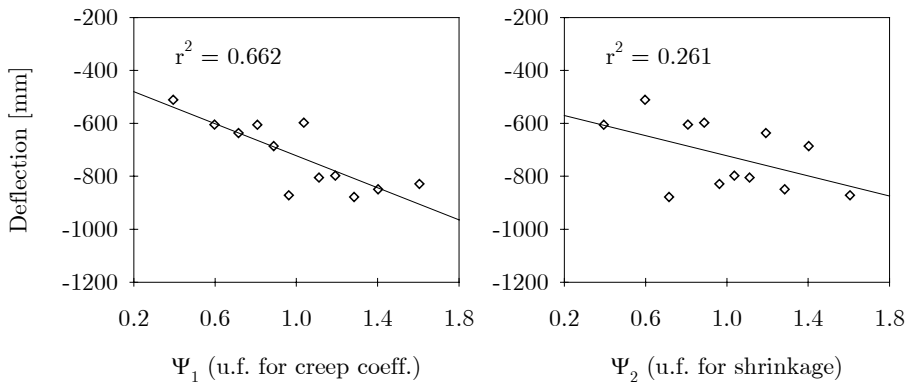


Figure 10.9 Correlation between the uncertainty factors for creep and shrinkage and the maximum long-time deflection

The same r-squared value for the other four variables are less than 0.150 which indicates very weak correlation.

In the simplified method, only one deterministic analysis has to be carried out where the uncertainty factor for the creep coefficient is taken with a value representing its 95 percentile while all the other variables are taken with their expected value.

The uncertainty factor for the creep coefficient is determined as

$$\Psi_1 = 1 + z \cdot V(\Psi_1) = 1 + 1.645 \cdot 0.35 = 1.576 \quad (10.30)$$

Figure 10.10 compares the 95 % confidence limit obtained by the Monte Carlo simulation and the simplified calculation. The diagram shows the long-time deflection in the central span of Støvset Bridge after 70 years..

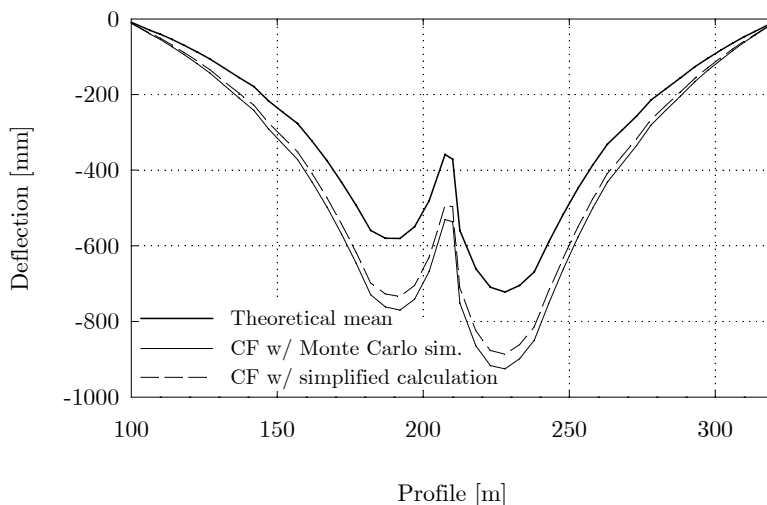


Figure 10.10 95 % confidence limit for the long-time deflection in Støvset Bridge estimated by the Monte Carlo method and the simplified calculation

## 10.6 Conclusions

The high degree of uncertainty in long-time deformation prediction in concrete bridges necessitates to take into account the statistical variation of the deformation responses. The inherent statistical uncertainty in the creep and shrinkage prediction models represent the major factor of uncertainty.

In the structural design as well as in the construction process the expected deviation from the expected theoretical mean has to be taken into consideration. The structural design

should be such which can tolerate potentially larger deflections than it was expected in the design calculation. Also the available measures in the construction process should be able to cope with potential deviation during the erection of the cantilevers with particular emphasis on the connection of the cantilevers at mid-span.

It is recognised that, while a slightly over-elevated bridge deck normally does not create any problem, if the bridge deck falls below its ideal camber it soon becomes visible. The precamber which is determined from the expected long-term deflection needs to be heightened by an excess over-height. The excess over-height can be determined from the estimated maximum variation from the mean deflection of given probability. The chosen value of the probability is a matter of design policy, *i.e.* it can be determined in accordance with the acceptable level of risk of intolerable deflections. The probability of 95 % can be considered as a reasonable value.

The probabilistic analysis can be implemented in a Monte Carlo simulation. The method is robust, however, rather time-consuming. It can be justified in the design of record span bridges. For a rough estimation of the effect of the statistical variation a simplified approach was recommended.

Deformations of Støvset Bridge was analysed with a Monte Carlo simulation. The coefficient of variation was estimated as 17 % for the maximum long-time deflection and 27 % for the mid-span deflection. The corresponding excess deflection values which represent the 95 % confidence limit are 28 % and 45 % larger than the expected values, respectively.

The statistical variation of the moments in the superstructure was found negligible. The reason is that the long-term moment redistribution in the main span is insignificant and consequently the variation in the creep and shrinkage characteristics does not influence the moments either.





## Chapter 11

### Conclusions

#### 11.1 Summary and conclusions

The thesis deals with deformation prediction in segmentally cast concrete cantilever bridges. This type of bridge has shown some propensity to develop larger deflections than they were predicted in the design calculation. Excessive deflections may lead to deterioration in aesthetic value, serviceability problems and eventually early reconstruction of the bridge. The main objective of the study was defined as to contribute to the improvement in deformation prediction in segmentally cast concrete cantilever bridges and to establish guidelines and methodology for numerical modelling.

A database on observed deformations in three modern long-span concrete cantilever bridges in Norway has been established. The bridges are Norddalsfjord Bridge in Sogn and Fjordane county, Støvset Bridge in Nordland county and Stolma Bridge in Hordaland county. The availability of such information in general is valuable for the monitored bridge as well as for the construction of future bridges. The measurements are necessary in order to verify the design assumptions and assess the state of the bridge over its life span. The obtained information can also be used to evaluate existing analysis methods and models and eventually to improve the design procedure. While monitoring is implemented in a few selected bridges, long-term deformation monitoring should be a standard requirement for every major concrete bridge. The stochastic nature of the long-term deformation characteristics of concrete is well known. Consequently the assessment of observations needs to be done on a statistical basis. It is only possible if observations from a large number of bridges are available.

A sophisticated numerical model has been created for deformation analysis. The numerical model realistically simulates the segmental construction process as well as the entire life span of the bridge. The effects of the segmentwise construction method, temporarily supports and constraints and changes in the structure system during construction are taken into account. The model also considers the different concrete age from segment to segment, the sequential application of the permanent loads and prestressing and the effect of temporary loads. The prestressing tendons are individually modelled with their true profile taking into account the variation of the effective prestressing force along the length of the tendon and with time. The finite element model consists of beam elements which are based on an advanced beam element formulation. The beam model has relatively moderate requirements for computational work which makes it suitable for large-scale practical applications. The model has been verified against a more robust two-and-a-half dimensional shell model which has confirmed the accuracy of the beam model. In particular, the effect of non-uniform creep and shrinkage characteristics across the height of the box-girder has been studied and found to be very small.

Special attention has to be paid to the constitutive model for concrete. While the methods of numerical structural analysis reached a high level of robustness and sophistication, theoretical modelling of creep and shrinkage is not as reliable as it would be necessary. It is evident that the latter constitutes the major obstacle to further improvement in deformation prediction in concrete bridges. The knowledge of concrete creep and shrinkage has been progressed significantly. The uncertainty in creep and shrinkage prediction, however, is still considerable. The large scatter and heterogeneity of existing experimental data does not allow much room for improvement.

Constitutive modelling was not among the objectives of this study *per se*. However, experimental results on lightweight aggregate concrete and high strength concrete have been evaluated in connection with existing theoretical models and the findings have been utilised. Creep and shrinkage characteristics of lightweight aggregate concrete were of particular interest due to the scarce experimental information and the current controversial theoretical formulations.

The current creep model in the extended CEB-FIP Model Code 1990 for lightweight aggregate concrete, like some of the other models, is adopting the model developed for normal density concrete and supplementing it with a reduction factor for the elastic modulus and another reduction factor for the creep coefficient. The two factors are functions of the oven-dry density of the lightweight aggregate concrete only. The experimental results, however, indicate that the drying process is considerably slower in lightweight aggregate concrete in the initial period of drying, thus the time dependency of drying creep is different than in normal density concrete. The notional creep coefficient is usually estimated by the extrapolation of short-time test data using the same time-dependency function as for normal

density concrete. Since the time dependency function is different, the procedure is questionable and so is the correctness of the reduction factor for the creep coefficient. The available experimental data suggest that long-time creep may be underestimated with the current reduction factor for the creep coefficient. The same tendency is observed in shrinkage experiments. Long-term tests indicated that shrinkage may be higher by more than 50 % as compared to normal density concrete which is considered by the present recommendation as the upper limit for shrinkage in lightweight aggregate concrete. The elastic modulus of lightweight aggregate concrete was found to be more dominantly determined by the density of the concrete and less influenced by the strength than it is assumed by the theoretical formula.

Experimental results indicated that the elastic modulus of the type of high strength concrete which is typically used for bridges in Norway is about 75 % of the value given by the CEB-FIP Model Code 1990. This has been confirmed by tests on samples which were taken from bridges. The reason for the smaller elastic modulus is probably the lower stiffness of the aggregate. The long-term experimental data on creep and the predictions by the CEB-FIP Model Code 1990 showed reasonable agreement.

Deformations of the three monitored concrete cantilever bridges have been computed. The basic material model was the CEB-FIP Model Code 1990. For Støvset Bridge and Stolma Bridge the elastic modulus for both the lightweight aggregate concrete and the normal density concrete were taken from test results. The creep coefficient and the shrinkage strain of the lightweight aggregate concrete were assumed equal to those of normal density concrete of same strength. The creep coefficient with the measured lower elastic modulus gives approximately 50 % higher creep deformation than normal density concrete. The calculated deformations have been compared with the observations. In view of the large uncertainty in deformation prediction in concrete it can be concluded that the agreement was satisfactory. While moderate differences were observed in most cases, no clear overall tendency toward under- or overestimation was found. The predicted long-time deflection in Norddalsfjord Bridge was in very good agreement with the measured values while the long-time deflection was slightly underestimated in Støvset Bridge and overestimated in Stolma Bridge. The sensitivity of the deflections to variations in creep, shrinkage and the effective prestressing force has been studied. The relative variation in the deflection responses was very similar in all three bridges as far as the variation in creep and shrinkage is concerned.

The sensitivity of the deflections in Støvset Bridge to variations in the creep and shrinkage characteristics of the lightweight aggregate concrete has been determined. In two alternative analyses the influence of the reduction factor for the creep coefficient and the effect of potentially higher shrinkage strain have been studied. The influence has been found to be very small not only during the construction period but for the long-time deflection as well.

The CEB-FIP Model Code 1990 model has been compared with Bazant's B3 model in the analysis of Støvset Bridge. The calculated deformation by the B3 model was found to be smaller in the initial period but significantly higher after 70 years. The available measurement which covers the first eight years of the service life of the bridge shows somewhat better agreement with the CEB-FIP Model Code 1990 prediction.

Finally, a robust probabilistic method has been presented where the stochastic aspects of creep and shrinkage prediction and the uncertainty in various model parameters have been considered. The objective of the probabilistic analysis is to estimate the statistical properties of the structural responses. If the statistical variation of the deflection is known, then its statistical distribution can be estimated. It is recommended to design the bridge for a deflection which represents a certain confidence limit of the long-time deflection rather than its mean value. Designing for a confidence limit (*e.g.* the 95 % confidence limit) minimises the risk that intolerable deflection will occur during the service life of the bridge. The probabilistic deformation analysis was based on a Monte Carlo simulation. The employed sampling method was the Latin Hypercube sampling which is well suited for applications in which it is important to keep the necessary number of computer runs small. An alternative, more simple approach has been presented for the estimation of the confidence limit for the deflection. Based on the fact that the statistical variation in the creep model is the dominant uncertainty factor in the analysis, the creep coefficient can be taken with its confidence limit and employed in a deterministic analysis.

### **11.2 Suggestions for further research**

This study has involved three bridges. The long-term monitoring of deformation development in these bridges should be continued. Taking into consideration the stochastic nature of long-time deformation prediction in concrete structures, it is recommended to monitor more bridges and collect the measurements in a databank. Observations made in a sufficiently large number of bridges would allow to assess the data statistically. The statistical assessment of the observations in connection with the theoretical predictions would furnish valuable information on the general tendencies in the prediction errors which would allow to further refine the theoretical models.

Deformation measurements should be accompanied by monitoring the prestressing force in a number of tendons. Depending on what portion of the permanent load is compensated by prestressing, small variation in the effective prestressing force may result in large variation in the deflection. The knowledge of the actual force in the tendons would also help to better evaluate the effects of creep and shrinkage because a significant factor of uncertainty could be eliminated.

More long-term creep and shrinkage experiments on lightweight aggregate concrete are necessary before prediction models can be improved. The existing approach should be replaced with a model which considers the particular characteristics of the lightweight aggregate concrete also in the time dependency function.



---

## References

ACI Committee 343 (1988), *Analysis and design of reinforced concrete bridge structures*, American Concrete Institute

Bazant, Z. P., principal author (1986), "Material models for structural analysis", *Creep and shrinkage of concrete: mathematical modeling*, Proceedings of the Fourth RILEM International Symposium, Evanston, IL, USA

Bazant, Z. P. and Ashgari, A. (1974), "Computation of age-dependent relaxation spectra", *Cement and Concrete Research*, Vol. 4

Bazant, Z. P. and Baweja, S. (1995), "Creep and shrinkage prediction model for analysis and design of concrete structures – B3 model", *Materials and Structures*, Vol. 28

Bazant, Z. P. and Ferretti, D. (2001), "Asymptotic temporal and spatial scaling of coupled creep, aging, diffusion and fracture processes", *Creep, shrinkage and durability mechanics of concrete and other quasi-brittle materials*, Proceedings of the Sixth International Conference ConCreep-6@MIT, Cambridge, USA, Elsevier

Bazant, Z. P. and Liu, K.-L. (1985), "Random creep and shrinkage in structures: sampling", *Journal of Structural Engineering*, Vol. 111

Bazant, Z. P., and Wittman, F. H. (1982), *Creep and shrinkage of concrete structures*, John Wiley & Sons

Bazant, Z. P. and Wu, S. T. (1974), "Rate-type creep law of aging concrete based on Maxwell chain", *Materials and Structures*, Vol. 7

Bazant, Z. P., Xi, Y.-P., Baweja, S. and Carol, I. (1993), "Preliminary guidelines and recommendation for characterizing creep and shrinkage in structural design codes", *Creep and shrinkage of concrete*, Proceedings of the Fifth International RILEM Symposium, Barcelona, Spain

*Brueckenweb.de* (2002), WWW, URL: <http://www.brueckenweb.de> (in German)

## References

---

de Borst, R. (1991), *Computational methods in non-linear solid mechanics*, Part 2: Physical non-linearity, Delft University of Technology, Delft, the Netherlands

de Borst, R., and van den Boogaard, A. H. (1994), "Finite-element modeling of deformation and cracking in early-age concrete". *Journal of Engineering Mechanics*, Vol. 120

Collins, M. P. and Mitchell, D. (1991), *Prestressed concrete structures*, Prentice Hall

Comité Euro-International du Béton (1990), *Evaluation of the time dependent behaviour of concrete*, Bulletin No.199

Comité Euro-International du Béton (1991), *CEB-FIP Model Code 1990*, Bulletin No.203

Comité Européen de Normalisation (1999), *Eurocode 2: Design of concrete structures*, European Standard, prEN 1992-1

Cook, R. D., Malkus, D. S. and Plesha, M. E. (1989), *Concepts and applications of finite element analysis*, John Wiley & Sons

DIANA User's Manual release 7.2 (1999), TNO Building and Construction Research, Division of Engineering Mechanics and Information Technology, Delft, The Netherlands

ENV 206 (1990), *Beton – Eigenschaften, Herstellung, Verarbeitung und Gütenachweis*, 3/1990 (in German)

Jonasson, J.-E. and Westman, G. (1999), *Conversion of creep data to relaxation data by the program RELAX*, IPACS Document TG 3.2/1, TU Luleå, Sweden

Favre, R., Burdet, O., Charif, H., Hassan, M. and Markey, I. (1995), *Enseignements tirés d'essais de charge et d'observations à long terme pour l'évaluation des ponts en béton et le choix de la précontrainte*, Research report for OFR, Lausanne (in French)

fédération internationale du béton (1999), *Structural concrete. Textbook on behaviour, design and performance. Updated knowledge of the CEB/FIP Model Code 1990*, Vol. 1, Bulletin No.1

fédération internationale du béton (2000a), *Guidance for good bridge design*, Bulletin No.9

fédération internationale du béton (2000b), *Lightweight aggregate concrete*, Bulletin No.8

Fergestad, S. and Naess, K. (1987), "Instrumentation and monitoring of Norddalsfjord Bridge, Norway", *Monitoring of Large Structures and Assessment of their Safety*, Report of the IABSE Colloquium in Bergamo, Italy, 1987, International Association for Bridge and Structural Engineering

Hammersley, J. M. and Handscomb, D. C. (1964), *Monte Carlo Methods*, Methuen



- Heimdal, E. (1997), *Experience with light weight aggregate concrete. Støvset Bridge*, LightCon Report 2.7, STF22 A97827, SINTEF Civil and Environmental Engineering, Department of Cement and Concrete, Norway
- Hynne, T. (2000), *Creep properties of LWAC*, EuroLightCon Document BE96-3942, Economic Design and Construction with Lightweight Aggregate Concrete, Norway
- Kanstad, T. (1990), *Nonlinear analysis considering time-dependent deformations and capacity of reinforced and prestressed concrete*, Ph.D. thesis, NTH, Trondheim, Norway
- Kanstad, T. (1993), "Deformations of segmentally cast cantilever bridges of high-strength concrete", *Creep and shrinkage of concrete*, Proceedings of the Fifth International RILEM Symposium, Barcelona, Spain
- Kottegoda, N. T. and Rosso, R. (1997), *Probability, Statistics and Reliability for Civil and Environmental Engineers*, McGraw-Hill
- Lane, D. M. (2001), *HyperStat Online Textbook*, WWW, URL: <http://www.davidmlane.com/hyperstat>
- Maage, M. and Olsen, T. O. (2000), "LETTKON. A major joint Norwegian research programme on lightweight aggregate concrete", Proceedings of the *Second International Symposium on Structural Lightweight Aggregate Concrete*, Kristiansand, Norway
- Markey, I., Fluge, F., Blankvoll, A. and Hansvold, C. (1998), "Short and long-term monitoring of Støvset Bridge" Proceedings of the *Second International Conference on Concrete under Severe Conditions*, Tromsø, Norway
- McKay, M. D., Beckman, R. J. and Conover, W. J. (1979), "A comparison of three methods for selecting values of input variables in the analysis of output from a computer code", *Technometrics*, Vol. 21
- Morabito, P., Dalmagioni, P., Hedlund, H., Lura, P., Sellevold, E., Bjøntegaard, Ø., Gram, H.-E., Jonasson, J.-E., Pellegrini, R., van Breugel, K., Gutsch, A., Kanstad, T. and Rostasy, F. (2000), *Round Robin Testing Programme. Equipment, testing methods, test results*, IPACS Report BE96-3843/2001:42-7, Lund, Sweden
- Naess, K. (1988), *Spennings- og tøyningmålingane på Norddalsfjord Bru pr. Februar 1988*, Statens Vegvesen, Sogn og Fjordane, Norway (in Norwegian)
- Ngab, A. S., Nilson, A. H. and Slate, F. O. (1981), "Shrinkage and creep of high strength concrete", *Journal of the American Concrete Institute*, Vol. 78

## References

---

NS 3473 (1998), *Concrete structures. Design rules*, Norwegian Standard, Norwegian Council for Building Standardization (NBR)

Persson, B. (1998), *Quasi-instantaneous and long-term deformations of high-performance concrete with some related properties*, Ph.D. thesis, Lund University, Lund Institute of Technology, Division of Building Materials, Lund, Sweden

Rosseland, S. and Thorsen, T. A. (2000), "The Stolma Bridge - world record in free cantilevering", *Proceedings of the Second International Symposium on Structural Lightweight Aggregate Concrete*, Kristiansand, Norway

Santos, L. O., Virtuoso, F. and Fernandes, J. A. (2001), "In situ measured creep and shrinkage of concrete bridges", *Creep, shrinkage and durability mechanics of concrete and other quasi-brittle materials*, Proceedings of the Sixth International Conference ConCreep-6@MIT, Cambridge, USA, Elsevier

Smadi, M. M., Nilson, A. H. and Slate, F. O. (1987), "Shrinkage and creep of high-, medium-, and low-strength concretes, including overloads", *American Concrete Institute Materials Journal*, Vol. 84

Smeplass, S. (2000), "Drying of lightweight aggregate concrete", *Proceedings of the Second International Symposium on Structural Lightweight Aggregate Concrete*, Kristiansand, Norway

Stein, M. (1987), "Large sample properties of simulations using Latin Hypercube sampling", *Technometrics*, Vol. 29

*structurae* (2002), International Database and Gallery of Structures, WWW, URL: <http://www.structurae.net>

Takács, P. F. and Kanstad, T. (1998), *Stolmasundet Bridge. Analysis in the service limit state*, Report, STF22 A98734, SINTEF Civil and Environmental Engineering, Department of Cement and Concrete, Norway

Tomaszewicz, A. (1988), *High strength concrete subjected to long-term sustained loads*, High strength concrete, SP1 Beams and columns, Report 1.4, STF65 F88079, SINTEF Cement and Concrete Research Institute, Norway

Tomaszewicz, A. (1993), *Creep on high strength concrete at elevated temperatures*, High strength concrete, SP1 Beams and columns, Report 1.7, STF70 A93080, SINTEF Structures and Concrete, Norway

Tsubaki, T., principal author (1986), "Probabilistic models", *Creep and shrinkage of concrete: mathematical modeling*, Proceedings of the Fourth RILEM International Symposium, Evanston, IL, USA

Vitek, J. L. (1997), "Long-term deflections of large prestressed concrete bridges", *Serviceability Models. Behaviour and modelling in serviceability limit states including repeated and sustained loads*, Progress Report, CEB Bulletin No.235

Vitek, J. L. and Kristek, V. (1999), "Deformations of prestressed concrete structures - measurement and analysis", *Structural concrete - the bridge between people*, Proceedings of the 1999 fib Symposium, Prague, Czech Republic

Walraven, J. (2000), "Design of structures with lightweight concrete: present status of revision of EC-2", Proceedings of the *Second International Symposium on Structural Lightweight Aggregate Concrete*, Kristiansand, Norway

Zienkiewicz, O. C. (1971), *The finite element method in engineering and science*, McGraw-Hill

Zienkiewicz, O. C. and Taylor, R. L. (1989), *The finite element method*, Volume 1, Basic formulation and linear problems, McGraw-Hill



## Appendix A

### Formulations for the statistical evaluation of creep and shrinkage test data

The *mean coefficient of variation for the prediction* characterises the mean error over the entire duration of loading in a series of creep experiments. It is calculated according to the following equations (CEB 1990).

The mean coefficient of variation is calculated as

$$\bar{V} = \sqrt{\frac{1}{N} \cdot \sum_{i=1}^N V_i^2}$$

where  $V_i$  is the coefficient of variation in the  $i$  th experiment. It is calculated as

$$V_i = \frac{S_i}{M_i} \cdot 100$$

with

$$M_i = \frac{1}{n} \cdot \sum_{j=1}^n J_{ij}$$

$$S_i = \sqrt{\frac{1}{n-1} \cdot \sum_{j=1}^n (\Delta J_{ij})^2}$$

where

$J_{ij}$  is the observed  $j$  th value of the creep compliance in the  $i$  th experiment,

$\Delta J_{ij}$  is the difference between the observed and predicted  $j$  th value in the  $i$  th experiment,

$n$  is the number of data points in the  $i$  th experiment,

$N$  is the number of experiments.

When only one value is considered in each experiment (*e.g.* the value of the creep compliance at the end of loading period, the mean coefficient of variation for the prediction is calculated as

$$\bar{V} = \sqrt{\frac{1}{N} \cdot \sum_{i=1}^N \left( \frac{\Delta J_i}{J_i} \right)^2}$$

The *average deviation* characterises the average tendency in the prediction. It indicates systematic over- or underestimation. Here, unlike in the (CEB 1990), every data point in the experiments are considered and consequently the average deviation is characteristic for the entire load duration.

The average deviation is calculated as

$$\bar{D} = \frac{1}{N} \sum_{i=1}^N \left( \frac{1}{n} \sum_{j=1}^n \frac{cal J_{ij} - obs J_{ij}}{obs J_{ij}} \right) \cdot 100$$

where

$cal J_{ij}$  is the predicted  $j$  th value of the creep compliance in the  $i$  th experiment,

$obs J_{ij}$  is the observed  $j$  th value of the creep compliance in the  $i$  th experiment.

High negative value of the measure indicates systematic underestimation by the theoretical model and high positive value indicates systematic overestimation.

The same formulations are used for the statistical evaluation of shrinkage test results. The shrinkage strain replaces the creep compliance in the corresponding equations.

## Appendix B

### Levelling data for Norddalsfjord Bridge

Profile [m]	Elevation of the deck [m]			
	07/05/1987	05/06/1987	27/03/2001	16/10/2001
5.3	35.027	35.027	35.027	35.027
11.4	34.748	34.749	34.746	34.745
17.5	34.448	34.450	34.448	34.449
27.8	33.916	33.917	33.919	33.917
37.9	33.366	33.367	33.373	33.371
47.9	32.806	32.810	32.816	32.816
57.9	32.314	32.323	32.330	32.328
67.9	31.835	31.842	31.848	31.846
77.1	31.412	31.416	31.420	31.420
85.1	31.052	31.055	31.054	31.055
92.0	30.738	30.735	30.736	30.738
101.3	30.297	30.292	30.286	30.290
110.1	29.886	29.880	29.869	29.872
117.1	29.569	29.561	29.543	29.547
125.1	29.193	29.180	29.155	29.160
129.4	28.997	28.977	28.953	28.960
134.2	28.773	28.750	28.727	28.733
138.7	28.569	28.542	28.512	28.519
144.1	28.322	28.292	28.254	28.262
148.7	28.097	28.074	28.021	28.030
154.2	27.850	27.813	27.764	27.773
158.9	27.635	27.592	27.540	27.550
164.2	27.393	27.347	27.286	27.296
169.1	27.166	27.112	27.047	27.062
cont.				

Appendix B

---

---

174.2	26.924	26.871	26.798	26.809
184.1	26.458	26.391	26.313	26.326
194.1	25.966	25.894	25.808	25.822
204.3	25.439	25.362	25.273	25.287
214.3	24.894	24.813	24.728	24.741
224.0	24.315	24.234	24.153	24.165
234.0	23.729	23.651	23.577	23.588
244.0	23.109	23.040	22.975	22.986
254.0	22.448	22.389	22.338	22.347
264.0	21.778	21.726	21.691	21.699
274.0	21.108	21.064	21.038	21.046
284.0	20.441	20.405	20.386	20.393
294.0	19.763	19.730	19.722	19.728
303.7	19.125	19.094	19.093	19.098
312.2	18.573	18.550	18.549	18.554
319.7	18.070	18.054	18.051	18.062
328.3	17.492	17.480	17.481	17.485
337.3	16.916	16.904	16.903	16.909
345.3	16.395	16.386	16.382	16.385
357.3	15.624	15.609	15.609	15.613
364.4	15.247	15.236	15.228	15.231

---

The position of the profile is given in the local coordinate system of the deck with the starting point being at the abutment in axis 1. The global coordinate of axis 1 is P3812.0 m.



### Levelling data for Støvset Bridge

Profile [m]	Elevation of the deck [m]					cont.
	22/02/94	07/07/94	15/08/95	04/06/96	02/10/96	
1.5	14.556	14.559	14.559	14.558	14.558	
11.5	15.196	15.202	15.206	15.205	15.206	
21.5	15.922	15.933	15.938	15.939	15.939	
31.5	16.742	16.750	16.756	16.758	16.758	
41.5	17.555	17.562	17.572	17.574	17.573	
51.5	18.347	18.354	18.363	18.366	18.366	
61.5	19.139	19.147	19.155	19.158	19.156	
71.5	19.941	19.951	19.956	19.957	19.957	
81.5	20.732	20.741	20.745	20.743	20.746	
91.5	21.527	21.534	21.538	21.534	21.537	
101.5	22.294	22.297	22.297	22.293	22.297	
111.5	23.087	23.085	23.083	23.076	23.082	
121.5	23.825	23.820	23.812	23.805	23.810	
131.5	24.493	24.481	24.471	24.461	24.467	
141.5	25.098	25.078	25.066	25.052	25.060	
151.5	25.635	25.608	25.592	25.574	25.583	
161.5	26.073	26.042	26.019	26.004	26.014	
171.5	26.428	26.382	26.356	26.334	26.343	
181.5	26.702	26.649	26.619	26.595	26.604	
191.5	26.903	26.844	26.814	26.787	26.797	
201.5	27.085	27.023	26.989	26.952	26.974	
211.5	27.167	27.104	27.073	27.035	27.050	
221.5	26.980	26.920	26.884	26.858	26.872	
231.5	26.805	26.750	26.717	26.691	26.704	
241.5	26.620	26.570	26.541	26.517	26.530	
251.5	26.329	26.288	26.262	26.241	26.254	
261.5	25.956	25.921	25.902	25.885	25.896	
271.5	25.507	25.481	25.466	25.452	25.463	
281.5	24.957	24.940	24.929	24.917	24.929	
291.5	24.324	24.313	24.305	24.296	24.306	
301.5	23.649	23.643	23.638	23.633	23.640	
311.5	22.870	22.871	22.867	22.864	22.870	
321.5	22.070	22.075	22.075	22.072	22.080	
331.5	21.303	21.312	21.313	21.313	21.320	
341.5	20.534	20.545	20.550	20.550	20.556	
351.5	19.730	19.741	19.748	19.748	19.754	
361.5	18.940	18.958	18.963	18.966	18.964	
371.5	18.154	18.169	18.175	18.179	18.175	
381.5	17.336	17.357	17.363	17.369	17.365	
391.5	16.529	16.547	16.553	16.560	16.555	
401.5	15.695	15.710	15.715	15.720	15.715	
411.5	14.879	14.891	14.891	14.896	14.893	

Appendix B

---

Profile [m]	Elevation of the deck [m]				
	25/06/97	16/06/98	23/06/99	21/06/00	13/06/01
1.5	14.564	14.560	14.561	14.564	14.563
11.5	15.213	15.211	15.212	15.215	15.210
21.5	15.950	15.947	15.949	15.953	15.948
31.5	16.768	16.767	16.769	16.771	16.767
41.5	17.582	17.584	17.584	17.587	17.581
51.5	18.374	18.367	18.377	18.379	18.380
61.5	19.167	19.169	19.169	19.170	19.171
71.5	19.967	19.967	19.968	19.971	19.966
81.5	20.754	20.754	20.753	20.758	20.750
91.5	21.544	21.543	21.542	21.547	21.538
101.5	22.301	22.299	22.298	22.305	22.291
111.5	23.083	23.077	23.077	23.083	23.069
121.5	23.809	23.801	23.801	23.806	23.798
131.5	24.462	24.450	24.452	24.454	24.440
141.5	25.049	25.034	25.035	25.037	25.023
151.5	25.567	25.548	25.551	25.55	25.535
161.5	25.994	25.972	25.974	25.973	25.947
171.5	26.319	26.294	26.297	26.294	26.274
181.5	26.576	26.548	26.551	26.547	26.525
191.5	26.766	26.736	26.738	26.734	26.712
201.5	26.939	26.911	26.911	26.906	26.884
211.5	27.014	26.983	26.985	26.981	26.966
221.5	26.837	26.808	26.811	26.805	26.791
231.5	26.672	26.643	26.647	26.643	26.625
241.5	26.501	26.474	26.481	26.476	26.458
251.5	26.229	26.205	26.211	26.206	26.189
261.5	25.877	25.856	25.861	25.859	25.845
271.5	25.446	25.429	25.435	25.433	25.420
281.5	24.915	24.902	24.906	24.906	24.896
291.5	24.296	24.285	24.291	24.291	24.280
301.5	23.636	23.626	23.631	23.633	23.624
311.5	22.869	22.862	22.865	22.869	22.862
321.5	22.079	22.074	22.077	22.081	22.076
331.5	21.321	21.318	21.319	21.323	21.319
341.5	20.558	20.556	20.559	20.562	20.560
351.5	19.758	19.757	19.761	19.764	19.760
361.5	18.976	18.976	18.979	18.984	18.984
371.5	18.189	18.189	18.192	18.197	18.193
381.5	17.377	17.375	17.381	17.386	17.380
391.5	16.566	16.565	16.569	16.573	16.568
401.5	15.725	15.722	15.726	15.731	15.725
411.5	14.901	14.898	14.899	14.903	14.899

The position of the profile is given in the local coordinate system of the deck with the starting point being at the abutment in axis 1. The global coordinate of axis 1 is P605.5 m.

### Levelling data for Stolma Bridge

Profile [m]	Elevation of the deck [m]			
	11/11/1998	16/09/1999	10/01/2001	27/11/2001
0.077	37.475	37.469	37.473	37.476
36.979	38.391	38.388	38.383	38.376
64.838	39.168	39.172	39.163	39.168
93.982	39.894	39.905	39.903	39.898
113.961	40.361	40.369	40.363	40.360
133.988	40.882	40.888	40.873	40.880
153.966	41.502	41.500	41.473	41.476
174.023	42.036	42.029	41.993	41.985
193.976	42.493	42.470	42.433	42.410
213.971	42.728	42.699	42.663	42.641
234.018	42.760	42.724	42.683	42.665
255.578	42.563	42.528	42.483	42.473
276.024	42.095	42.069	42.033	42.019
295.763	41.386	41.368	41.333	41.321
315.725	40.445	40.435	40.403	40.409
335.627	39.319	39.323	39.303	39.305
355.548	38.098	38.114	38.093	38.108
374.880	36.870	36.881	36.873	36.878
395.072	35.584	35.602	35.583	35.595
419.012	34.140	34.142	34.133	34.134
443.040	32.620	32.631	32.613	32.623
466.984	31.151	31.156	31.153	31.152

The position of the profile is given in the local coordinate system of the deck with the starting point being at the abutment in axis 1. The global coordinate of axis 1 is P1280.0 m.



## Appendix C

### Analysis results of the individual computer runs in the Monte Carlo simulation

#### Deflection

Analysis run	Deflection [mm]						
	A	B	C	D	E	F	G
1	-363	-473	-805	15	-168	-74	-435
2	-362	-476	-871	8	-166	-83	-512
3	-371	-482	-849	12	-167	-74	-473
4	-383	-500	-879	13	-173	-76	-487
5	-296	-375	-511	21	-144	-61	-208
6	-326	-420	-686	16	-153	-68	-356
7	-333	-429	-605	11	-156	-72	-263
8	-349	-445	-637	16	-165	-73	-281
9	-373	-485	-829	8	-168	-76	-450
10	-361	-473	-797	10	-163	-78	-431
11	-315	-401	-604	24	-152	-62	-282
12	-313	-397	-597	19	-147	-59	-275
Mean	-345	-446	-722	14	-160	-71	-371
Std. dev.	27	39	124	5	9	7	101

A - maximum deflection before the cantilevers are connected

B - maximum deflection after the bridge is completed

C - maximum deflection after 70 years

D - mid-span deflection before the cantilevers are connected / A2 side (tip of the cantilever)

E - mid-span deflection before the cantilevers are connected / A3 side (tip of the cantilever)

F - mid-span deflection after the bridge is completed

G - mid-span deflection after 70 years

**Horizontal displacement**

Analysis run	Displacement [mm]					
	A	B	C	D	E	F
1	7	13	36	-8	-18	-40
2	9	13	44	-9	-18	-48
3	8	15	37	-9	-19	-42
4	7	15	37	-8	-20	-42
5	6	7	20	-7	-12	-24
6	7	11	33	-8	-16	-37
7	9	10	18	-9	-15	-23
8	8	9	21	-9	-15	-27
9	9	15	31	-9	-19	-36
10	8	13	33	-9	-18	-37
11	5	9	27	-6	-14	-31
12	6	9	23	-7	-14	-27
Mean	8	12	30	-8	-17	-35
Std. dev.	1	3	8	1	2	8

A - at the pier in A2, before the cantilevers are connected

B - at the pier in A2, after the bridge is completed

C - at the pier in A2, after 70 years

E - at the pier in A3, before the cantilevers are connected

F - at the pier in A3, after the bridge is completed

G - at the pier in A3, after 70 years

**Flexural moment**

Analysis run	Flexural moment [MNm]													
	A	B	C	D	E	F	G	H	I	J	K	L	M	N
1	856	971	996	862	989	1003	911	1017	1019	903	999	1013	-55	-63
2	856	969	1004	863	989	1009	912	1018	1024	902	997	1021	-54	-65
3	856	971	992	862	989	1002	911	1018	1016	903	999	1008	-55	-63
4	857	973	992	863	990	1002	912	1017	1015	904	999	1007	-56	-63
5	856	968	991	863	987	1000	912	1020	1025	903	1001	1017	-54	-59
6	857	970	1000	864	988	1005	913	1019	1024	904	1000	1020	-55	-63
7	852	966	974	859	987	993	908	1018	1013	899	996	995	-52	-58
8	851	966	982	858	987	996	907	1019	1017	897	998	1003	-52	-59
9	852	969	983	859	989	998	908	1016	1011	899	997	998	-55	-62
10	853	968	989	860	988	1001	909	1017	1016	900	996	1006	-54	-62
11	857	971	1001	862	987	1005	911	1019	1026	904	1002	1023	-56	-62
12	854	969	989	860	987	1000	909	1019	1018	900	1000	1009	-55	-61
Mean	855	969	991	861	988	1001	910	1018	1019	901	999	1010	-54	-62
Std. dev.	2	2	8	2	1	4	2	1	5	2	2	9	1	2

- A - on the left side of the pier in A2, before the cantilevers are connected  
 B - on the left side of the pier in A2, after the bridge is completed  
 C - on the left side of the pier in A2, after 70 years  
 D - on the right side of the pier in A2, before the cantilevers are connected  
 E - on the right side of the pier in A2, after the bridge is completed  
 F - on the right side of the pier in A2, after 70 years  
 G - on the left side of the pier in A3, before the cantilevers are connected  
 H - on the left side of the pier in A3, after the bridge is completed  
 I - on the left side of the pier in A3, after 70 years  
 J - on the right side of the pier in A3, before the cantilevers are connected  
 K - on the right side of the pier in A3, after the bridge is completed  
 L - on the right side of the pier in A3, after 70 years  
 M - at mid-span, after the bridge is completed  
 N - at mid-span, after 70 years





**DEPARTMENT OF STRUCTURAL ENGINEERING  
NORWEGIAN UNIVERSITY OF SCIENCE AND TECHNOLOGY**

N-7491 TRONDHEIM, NORWAY

Telephone: +47 73 59 47 00    Telefax: +47 73 59 47 01

"Reliability Analysis of Structural Systems using Nonlinear Finite Element Methods",  
C. A. Holm, 1990:23, ISBN 82-7119-178-0.

"Uniform Stratified Flow Interaction with a Submerged Horizontal Cylinder",  
Ø. Arntsen, 1990:32, ISBN 82-7119-188-8.

"Large Displacement Analysis of Flexible and Rigid Systems Considering Displacement-Dependent Loads and Nonlinear Constraints",  
K. M. Mathisen, 1990:33, ISBN 82-7119-189-6.

"Solid Mechanics and Material Models including Large Deformations",  
E. Levold, 1990:56, ISBN 82-7119-214-0, ISSN 0802-3271.

"Inelastic Deformation Capacity of Flexurally-Loaded Aluminium Alloy Structures",  
T. Welo, 1990:62, ISBN 82-7119-220-5, ISSN 0802-3271.

"Visualization of Results from Mechanical Engineering Analysis",  
K. Aamnes, 1990:63, ISBN 82-7119-221-3, ISSN 0802-3271.

"Object-Oriented Product Modeling for Structural Design",  
S. I. Dale, 1991:6, ISBN 82-7119-258-2, ISSN 0802-3271.

"Parallel Techniques for Solving Finite Element Problems on Transputer Networks",  
T. H. Hansen, 1991:19, ISBN 82-7119-273-6, ISSN 0802-3271.

"Statistical Description and Estimation of Ocean Drift Ice Environments",  
R. Korsnes, 1991:24, ISBN 82-7119-278-7, ISSN 0802-3271.

"Turbidity Current Modelling",  
B. Brørs, 1991:38, ISBN 82-7119-293-0, ISSN 0802-3271.

"Zero-Slump Concrete: Rheology, Degree of Compaction and Strength. Effects of Fillers as Part Cement-Replacement",  
C. Sørensen, 1992:8, ISBN 82-7119-357-0, ISSN 0802-3271.

"Nonlinear Analysis of Reinforced Concrete Structures Exposed to Transient Loading",  
K. V. Høiseth, 1992:15, ISBN 82-7119-364-3, ISSN 0802-3271.

"Finite Element Formulations and Solution Algorithms for Buckling and Collapse Analysis of Thin Shells",

R. O. Bjærum, 1992:30, ISBN 82-7119-380-5, ISSN 0802-3271.

"Response Statistics of Nonlinear Dynamic Systems",

J. M. Johnsen, 1992:42, ISBN 82-7119-393-7, ISSN 0802-3271.

"Digital Models in Engineering. A Study on why and how engineers build and operate digital models for decision support",

J. Høyte, 1992:75, ISBN 82-7119-429-1, ISSN 0802-3271.

"Sparse Solution of Finite Element Equations",

A. C. Damhaug, 1992:76, ISBN 82-7119-430-5, ISSN 0802-3271.

"Some Aspects of Floating Ice Related to Sea Surface Operations in the Barents Sea",

S. Løset, 1992:95, ISBN 82-7119-452-6, ISSN 0802-3271.

"Modelling of Cyclic Plasticity with Application to Steel and Aluminium Structures",

O. S. Hopperstad, 1993:7, ISBN 82-7119-461-5, ISSN 0802-3271.

"The Free Formulation: Linear Theory and Extensions with Applications to Tetrahedral Elements with Rotational Freedoms",

G. Skeie, 1993:17, ISBN 82-7119-472-0, ISSN 0802-3271.

"Høyfast betongs motstand mot piggdekkslitasje. Analyse av resultater fra prøving i Veisliter'n",

T. Tveter, 1993:62, ISBN 82-7119-522-0, ISSN 0802-3271.

"A Nonlinear Finite Element Based on Free Formulation Theory for Analysis of Sandwich Structures",

O. Aamlid, 1993:72, ISBN 82-7119-534-4, ISSN 0802-3271.

"The Effect of Curing Temperature and Silica Fume on Chloride Migration and Pore Structure of High Strength Concrete",

C. J. Hauck, 1993:90, ISBN 82-7119-553-0, ISSN 0802-3271.

"Failure of Concrete under Compressive Strain Gradients",

G. Markeset, 1993:110, ISBN 82-7119-575-1, ISSN 0802-3271.

"An experimental study of internal tidal amphidromes in Vestfjorden",

J. H. Nilsen, 1994:39, ISBN 82-7119-640-5, ISSN 0802-3271.

"Structural analysis of oil wells with emphasis on conductor design",

H. Larsen, 1994:46, ISBN 82-7119-648-0, ISSN 0802-3271.

"Adaptive methods for non-linear finite element analysis of shell structures",

K. M. Okstad, 1994:66, ISBN 82-7119-670-7, ISSN 0802-3271.

"On constitutive modelling in nonlinear analysis of concrete structures",  
O. Fyrileiv, 1994:115, ISBN 82-7119-725-8, ISSN 0802-3271.

"Fluctuating wind load and response of a line-like engineering structure with emphasis on motion-induced wind forces",  
J. Bogunovic Jakobsen, 1995:62, ISBN 82-7119-809-2, ISSN 0802-3271.

"An experimental study of beam-columns subjected to combined torsion, bending and axial actions",  
A. Aalberg, 1995:66, ISBN 82-7119-813-0, ISSN 0802-3271.

"Scaling and cracking in unsealed freeze/thaw testing of Portland cement and silica fume concretes",  
S. Jacobsen, 1995:101, ISBN 82-7119-851-3, ISSN 0802-3271.

"Damping of water waves by submerged vegetation. A case study of laminaria hyperborea",  
A. M. Dubi, 1995:108, ISBN 82-7119-859-9, ISSN 0802-3271.

"The dynamics of a slope current in the Barents Sea",  
Sheng Li, 1995:109, ISBN 82-7119-860-2, ISSN 0802-3271.

"Modellering av delmaterialenes betydning for betongens konsistens",  
Ernst Mørtzell, 1996:12, ISBN 82-7119-894-7, ISSN 0802-3271.

"Bending of thin-walled aluminium extrusions",  
Birgit Søvik Opheim, 1996:60, ISBN 82-7119-947-1, ISSN 0802-3271.

"Material modelling of aluminium for crashworthiness analysis",  
Torodd Berstad, 1996:89, ISBN 82-7119-980-3, ISSN 0802-3271.

"Estimation of structural parameters from response measurements on submerged floating tunnels",  
Rolf Magne Larssen, 1996:119, ISBN 82-471-0014-2, ISSN 0802-3271.

"Numerical modelling of plain and reinforced concrete by damage mechanics",  
Mario A. Polanco-Loria, 1997:20, ISBN 82-471-0049-5, ISSN 0802-3271.

"Nonlinear random vibrations - numerical analysis by path integration methods",  
Vibeke Moe, 1997:26, ISBN 82-471-0056-8, ISSN 0802-3271.

"Numerical prediction of vortex-induced vibration by the finite element method",  
Joar Martin Dalheim, 1997:63, ISBN 82-471-0096-7, ISSN 0802-3271.

"Time domain calculations of buffeting response for wind sensitive structures",  
Ketil Aas-Jakobsen, 1997:148, ISBN 82-471-0189-0, ISSN 0802-3271.

"A numerical study of flow about fixed and flexibly mounted circular cylinders",  
Trond Stokka Meling, 1998:48, ISBN 82-471-0244-7, ISSN 0802-3271.

"Estimation of chloride penetration into concrete bridges in coastal areas",  
Per Egil Steen, 1998:89, ISBN 82-471-0290-0, ISSN 0802-3271.

"Stress-resultant material models for reinforced concrete plates and shells",  
Jan Arve Øverli, 1998:95, ISBN 82-471-0297-8, ISSN 0802-3271.

"Chloride binding in concrete. Effect of surrounding environment and concrete composition",  
Claus Kenneth Larsen, 1998:101, ISBN 82-471-0337-0, ISSN 0802-3271.

"Rotational capacity of aluminium alloy beams",  
Lars A. Moen, 1999:1, ISBN 82-471-0365-6, ISSN 0802-3271.

"Stretch Bending of Aluminium Extrusions",  
Arild H. Clausen, 1999:29, ISBN 82-471-0396-6, ISSN 0802-3271.

"Aluminium and Steel Beams under Concentrated Loading",  
Tore Tryland, 1999:30, ISBN 82-471-0397-4, ISSN 0802-3271.

"Engineering Models of Elastoplasticity and Fracture for Aluminium Alloys",  
Odd-Geir Lademo, 1999:39, ISBN 82-471-0406-7, ISSN 0802-3271.

"Kapasitet og duktilitet av dybelforbindelser i trekonstruksjoner",  
Jan Siem, 1999:46, ISBN 82-471-0414-8, ISSN 0802-3271.

"Etablering av distribuert ingeniørarbeid; Teknologiske og organisatoriske erfaringer fra en norsk ingeniørbedrift",  
Lars Line, 1999:52, ISBN 82-471-0420-2, ISSN 0802-3271.

"Estimation of Earthquake-Induced Response",  
Símon Ólafsson, 1999:73, ISBN 82-471-0443-1, ISSN 0802-3271.

"Coastal Concrete Bridges: Moisture State, Chloride Permeability and Aging Effects",  
Ragnhild Holen Relling, 1999:74, ISBN 82-471-0445-8, ISSN 0802-3271.

"Capacity Assessment of Titanium Pipes Subjected to Bending and External Pressure",  
Arve Bjørset, 1999:100, ISBN 82-471-0473-3, ISSN 0802-3271.

"Validation of Numerical Collapse Behaviour of Thin-Walled Corrugated Panels",  
Håvar Ilstad, 1999:101, ISBN 82-471-0474-1, ISSN 0802-3271.

"Strength and Ductility of Welded Structures in Aluminium Alloys",  
Miroslaw Matusiak, 1999:113, ISBN 82-471-0487-3, ISSN 0802-3271.

"Thermal Dilation and Autogenous Deformation as Driving Forces to Self-Induced Stresses in High Performance Concrete",  
Øyvind Bjøntegaard, 1999:121, ISBN 82-7984-002-8, ISSN 0802-3271.

"Some Aspects of Ski Base Sliding Friction and Ski Base Structure",  
Dag Anders Moldestad, 1999:137, ISBN 82-7984-019-2, ISSN 0802-3271.

"Electrode reactions and corrosion resistance for steel in mortar and concrete",  
Roy Antonsen, 2000:10, ISBN 82-7984-030-3, ISSN 0802-3271.

"Hydro-Physical Conditions in Kelp Forests and the Effect on Wave Damping and Dune Erosion. A case study on Laminaria Hyperborea",  
Stig Magnar Løvås, 2000:28, ISBN 82-7984-050-8, ISSN 0802-3271.

"Random Vibration and the Path Integral Method",  
Christian Skaug, 2000:39, ISBN 82-7984-061-3, ISSN 0802-3271.

"Buckling and geometrical nonlinear beam-type analyses of timber structures",  
Trond Even Eggen, 2000:56, ISBN 82-7984-081-8, ISSN 0802-3271.

"Structural Crashworthiness of Aluminium Foam-Based Components",  
Arve Grønsund Hanssen, 2000:76, ISBN 82-7984-102-4, ISSN 0809-103X.

"Measurements and simulations of the consolidation in first-year sea ice ridges, and some aspects of mechanical behaviour",  
Knut V. Høyland, 2000:94, ISBN 82-7984-121-0, ISSN 0809-103X.

"Kinematics in Regular and Irregular Waves based on a Lagrangian Formulation",  
Svein Helge Gjøsvund, 2000-86, ISBN 82-7984-112-1, ISSN 0809-103X.

"Self-Induced Cracking Problems in Hardening Concrete Structures",  
Daniela Bosnjak, 2000-121, ISBN 82-7984-151-2, ISSN 0809-103X.

"Ballistic Penetration and Perforation of Steel Plates",  
Tore Børvik, 2000:124, ISBN 82-7984-154-7, ISSN 0809-103X.

"Freeze-Thaw resistance of Concrete. Effect of: Curing Conditions, Moisture Exchange and Materials",  
Terje Finnerup Rønning, 2001:14, ISBN 82-7984-165-2, ISSN 0809-103X

"Structural behaviour of post tensioned concrete structures. Flat slab. Slabs on ground",  
Steinar Trygstad, 2001:52, ISBN 82-471-5314-9, ISSN 0809-103X.

"Slipforming of Vertical Concrete Structures. Friction between concrete and slipform panel."  
Kjell Tore Fosså, 2001:61, ISBN 82-471-5325-4, ISSN 0809-103X.

"Improved Fatigue Performance of Threaded Drillstring Connections by Cold Rolling",  
Steinar Kristoffersen, 2002:11, ISBN: 82-421-5402-1, ISSN: 0809-103X.